SYNTHESIS AND CHARACTERIZATION OF NANOPHOSPHOR FOR RADIATION DETECTION AND DOSIMETRY

By

T.K.Srinivasan

(Enrollment No: PHYS02200704013)

Indira Gandhi Centre for Atomic Research
Kalpakkam

A thesis submitted to the
Board of Studies in Physical Sciences
In partial fulfillment of requirements
For the Degree of

DOCTOR OF PHILOSOPHY
of
Homi Bhabha National Institute

February 2014

Homi Bhabha National institute

Recommendations of the Viva voce Board

As members of the viva voce Board, we certify that we have read the dissertation prepared by T.K.Srinivasan entitled "**Synthesis and Characterization of Nano phosphor for Radiation Detection and Dosimetry"** and recommend that it may be accepted as fulfilling the dissertation requirement for the Degree of Doctor of Philosophy

-- Date:

Chairman-Dr. B. Venkatraman 11.09.2014

-- Date:

Convener/Guide- Dr. B.S. Panigrahi 11.09.2014

-- Date:

Member- Dr. R. Ramaseshan R. Raman 11.09.2014

-- Date:

Member- Dr. D. Ponraju D. Po 11.09.2014

-- Date:

Examiner- 11/9/14

Final approval and acceptance of the dissertation is contingent upon the candidate's submission of the final copies of the dissertation to HBNI.

Date: 11/9/2014

Place: Kalpakkam

CERTIFICATE

I hereby certify that I have read this dissertation prepared under my direction and recommend that it may be accepted as fulfilling the dissertation requirement.

Date: 11/9/2014

Place: Kalpakkam

Panigrahi

(B.S.Panigrahi)
Thesis Supervisor

STATEMENT BY AUTHOR

This dissertation has been submitted in partial fulfillment of requirements for an advanced degree at Homi Bhabha National Institute (HBNI) and is deposited in the Library to be made available to borrowers under rules of the HBNI.

Brief quotations from this dissertation are allowable without special permission, provided that accurate acknowledgement of source is made. Requests for permission for extended quotation from or reproduction of this manuscript in whole or in part may be granted by the Competent Authority of HBNI when in his or her judgment the proposed use of the material is in the interests of scholarship. In all other instances, however, permission must be obtained from the author.

(**T.K.Srinivasan**)

DECLARATION

I, T.K.Srinivasan, hereby declare that the investigations presented in the thesis have been carried out by me. The work is original and has not been submitted earlier as a whole or in part for a degree/diploma at this or any other Institution/University.

(**T.K.Srinivasan**)

Dedication

To my parents Mrs. GowriKrishnamoorthy and Mr. Krishnamoorthy and my beloved sisters T.K. Vijaya, T.K. Hema, Brother T.K. Venkatesh and S.Ramyashreefor everything in Life

ACKNOWLEDGEMENT

I sincerely thank my parents for supporting my every cause throughout my life so far. Without their love, affection and patience could not have reached this stage.

I am grateful to my present guide Dr. B.S.Panigrahi and former guide Dr A.K.Arora and co-guide Dr. B.Venkatraman for their expert guidance, encouragement and patience. My heartfelt thanks to Dr.B.S.Panigrahi for his relentless support in carrying out the experiments and preparing the write-ups.

My sincere thanks to DC members Dr. R.Ramaseshan and Dr. D.Ponraju for their help, fruitful discussions and encouraging words throughout the work.My heartfelt thanks to Dr. R.Ramaseshan for his suggestions for writing the thesis work.

I owe much to Dr. S. Kalavathi, Dr V. Sridharan , Dr. H.N. Jena and Dr.ShamimaHussain for finding out her valuable time for my discussions apart from helping in XRD measurements. I am very thankful to Dr John Philip and his persons for DLS measurements.My sincere thanks to Dr. S.Amirthapandian, Dr. R.Divakar and Dr. Arup Das Gupta allotting time for TEM measurements insipte of their busy schedules.My sincere thanks to Dr.M. Kamrudin and Dr. CittaRanjan Das, for their help in FESEM measurements. I very thankful to Dr. Tom Mathews for his encouraging words and sparing the materials when required to finish the jobs in time. My heartfelt thanks to and Dr. K. Sivasburamanian for his encouraging words, correction and fruitful discussions. I my sincere thanks to Dr. N.Raghu, Krishna Chaitanya and their group members for their help during X-ray irradiation. I am highly grateful to H.Krishnan, Shailesh Joshi and P.Ilayaraja for their help and support during synthesis, FTIR measurements and fruitful discussions. I sincerely thank JagadeeshSure for his help in writing the thesis.

My heartfelt thanks to N.Thiruavkarasu, A. Suriyanarayanan and V.R. Naganathanan during UV-Vis absorption measurements and fruitful discussions. I thank Dr. S.Sankaran and S.Annapoorani for their help during concentration measurements. My sincere thanks to Dr. SathyaPanighrahi and SimthaAcharya for their help during microscope measurements. I am extremely thankful to N. Murali, M.Kasinathan and G.M.S. Krishna Chaitanya for sparing their spectrometer rendering their helping hand during X-ray scintillation measurements. I am thankful to Dr. K.K Sathpathy, Dr. M.V.R. Prasad and K.V.Kanagasabapathy for their help in ED-XRF measurements.

My sincere thanks to Dr. N.Suryamuthy for his help in TL, PL measurements and fruitful discussions.I am grateful to Dr.R.Sarangapani and Dr. M.T. Jose for adjusting my shift timings to carry out the experiments.

I am extremely thankful to K. Shyamala Devi and SwethaSonwani for their ever ready help.

I sincerely thank Ms. Sudha Devi for the Life time measurements at SAIF IIT Chennai.

Last but not the least I thank all the JRF friends who by their presence in IGCAR motivated and geared me to run towards the finish.

I convey my sincere thanks to Dr. C.Sundar and Dr. G. Amerandra for giving me an opportunity and encouragement to carry out this study. I am thankful to Dr. S.A.V.Sathya Murthy, Director EIR&SG for his encouragement and support.

I sincerely thank Dr P.R. Vasudeva Rao, Director IGCAR and Dr. Baldev Raj, (former Director) for providing the necessary infrastructure and resources to accomplish my research work.

(T.K. Srinivasan)

Contents

Page No.

Non-stoichiometric in LaF_3:Ce

SYNOPSIS

Nano sized rare-earth phosphors doped with rare earths are being studied by many groups for their superior light emission qualities and various applications. Evolution of nanophosphor research, for the past two decades opened new avenues in developments of luminescent materials and the polymer composites for various applications. Among the rare earth compounds, nano sized rare-earth halide as host with rare-earth doped phosphors are known for their higher light output, thermal stability and density for radiation detection applications. Of all the rare earth halide compounds, Lanthanum Fluoride (LaF_3) doped with rare-earth materials are explored for its photoluminescence (PL) and scintillation abilities. This material possesses excellent photochemical stability, biocompatibility and low phonon energies which interferes least with excitation or emission energies [1-9]. Moreover, transparent polymer nanocomposites with significant luminescence efficiency and scintillation abilities also find application in the field of radiation detection [10-13]. In 2008, H.Deng.,et al reported the synthesis of ligand-capped LaF_3 nano crystals [9]. In their work, $LnVO_4$ (Ln = Ce and Nd) nanocrystals were synthesized adopting facile solvo hydrothermal route. Their work demonstrated the synthesis of efficient upconverion luminescencent nanocrystal with different shapes and their applications in optoelectronics.

In some of the studies on LaF_3:Ln with organic coating were investigated for its size control and upconversion abilities. The organic surfactants such as Glycine, Oleic acid (OA), Polyethylene glycol (PEG), Tri ethylene glycol (TEG) and chitosan were used in the synthesis. Their PL characteristics have been extensively studied [14-18]. In this work, an attempt was made to coat LaF_3:Ce with OA and also with combination of OA plus PEG and study their size, UV-Vis and PL characteristics.

It is well known that the nanoparticle synthesis and performance depend on a number of factors like concentration, temperature, reaction rate and pH of the reaction environment which can be varied to synthesize very fine sized particles. The variation of pH was applied in our synthesis experiments. R.N.Bhargav et al.,[19] has reported for the first time that the quantum efficiency of ZnS:Mn was improved by 18% with reduction in particle size between 3.5-7 nm in synthesizing in acidic environment. In another work on ZnS, demonstrated the strong influence of the pH on the particle size and luminescence efficiency [20]. In this work on ZnS nanoparticle the maximum light efficiency was obtained at a pH 5 and the corresponding particle size was found to be 2.8nm. In another interesting work the pH dependent size and PL output with ZnS nanoparticles was demonstrated [21]. The synthesis of LaF_3 compound in the acidic environment has not been reported. In this work, an attempt was made to synthesize $LaF_3:Ce^{3+}$ at different pH.

Light amplification of nanophosphor is a new interesting field. During the past decade there have been a significant number of reports on core shell structures applied to enhance the light output. Materials such as LaF_3 [17, 22] and SiO_2 [23], were attempted as a coating layer on LaF_3. SiO_2 was found to be the most effective in enhancing the photoluminescence of LaF_3:Ce by two times. In a study the $La_{0.8}F_3:Ce_{0.15},Tb_{0.05}$ as core composition produced using the hydrothermal method [24]. The work concluded that the PL emission intensity can be increased selecting a proper coating material and with proper coating thickness.

Radiation stability or hardness is primary important factor for the materials which are applied for radiation detection purposes. Many workers have carried out the effect of gamma radiation on PL characteristics on single crystalline alkali halide doped with rare earths for example, Banguru et al., in his work on gamma irradiation of $KCl:Ce^{3+}$ and $KBr:Ce^{3+}$ [25] has reported the formation of Ce^{2+} and reduction in the TL efficiency. In so far only reported the radiation stability study of LaF_3 nano crystal by Nathan.J et. al [17] have demonstrated that nanocrystals exhibited excellent radiation stability after an extended exposure of about 24 kGy with Cs-137 source. In this context, the radiation stability of the synthesized nano sized LaF_3:Ce with Cobalt-60 rays were not reported, an attempt was made to study this parameter.

The feasibility and the demonstration of the nano materials for dosimetry for measuring very high doses are reported [26, 27]. In this light the TL properties of nano LaF_3:Ce was studied and reported for the first time.

The aim of the present study is to explore the synthesis routes to obtain highly luminescent nanoparticles with narrow size distribution. In this work, we have synthesized nano sized uncoated as well as surfactant capped $LaF_3:Ce^{3+}$ through four different methods. The synthesis of organic coated $LaF_3:Ce^{3+}$ was carried out by adopting the method of F.Wang et al [7] and uncoated $LaF_3:Ce^{3+}$ by adopting the method of R.N.Bhargava et al., [19]. Their structure, particle size, UV-Vis absorption, photo luminescence behavior and Lifetime were studied. The synthesis route developed for the highly florescent uncoated $LaF_3:Ce^{3+}$ particles with narrow size distribution is first of its kind. Photo luminescence studies of $LaF_3:Ce^{3+}$ codoped with terbium (Tb^{3+}) and europium (Eu^{3+}) are also carried out using the developed route, showed high light output. The energy transfer from Ce^{3+} to Tb^{3+}codopant was observed.

Apart from this, TiO_2 has been successfully coated upon the nano sized $La_{0.40}F_3:Ce_{0.45}{}^{3+},Tb_{0.15}{}^{3+}$ matrix to obtain a core-shell structure yielding higher light output. The core-shell structure formation was confirmed with TEM images and FTIR spectra. The effect of TiO_2 coating thickness on PL intensity was studied. Scintillation under X-ray excitation was observed from the uncoated and coated $La_{0.40}F_3:Ce_{0.45}{}^{3+},Tb_{0.15}{}^{3+}$ matrices. The effect of nonstoiometry of LaF_3 on the PL was studied by varying the molar ratios of

$LaCl_3$ and NH_4F. Feasibility of using this material for radiation detection is explored. The radiation stability of organic coated and uncoated LaF_3:Ce was studied in terms of degradation the PL output. Thermoluminescence property of $LaF_3:Ce^{3+}$ was studied. The TL glow peak parameters were calculated. $LaF_3:Ce^{3+}$ and $LaF_3:Ce^{3+},Tb^{3+}$nano particles were embedded in polymer matrices by adopting a insitu polymerization procedure and their PL measurements were carried out. The feasibility of detecting X-rays using indigenously developed polymer composite was demonstrated. A brief description of the chapters is given below.

Chapter 1

This chapter provides a brief introduction about the research problem dealt in the present study. Literature survey on inorganic nanophorpor so far studied carried out and their properties are discussed. Potential applications and process of scintillation are discussed. A brief insight into the requirements of the nanophosphor and mechanism of interaction and detection of γ- radiation is discussed. Conventional methods of synthesis of luminescent nanophosphor are described. The objective and the scope of the work are highlighted in this chapter.

Chapter 2

This chapter provides a brief introduction to the size controlled synthesis of nanophosphors and the role of core-sell structure. The protocol developed for the synthesis of nano phosphor and the experimental setup are described. Major part of this chapter discusses instrumentation used for characterizing the synthesized materials such as XRD (X-ray diffraction), FESEM (Field emission scanning electron microscope), TEM (Transmission electron microscope), DLS (Dynamic light Scattering), FTIR (Fourier transformed Infrared Spectroscopy), UV-Vis absorption, Photo luminescence (PL) spectroscopy and Lifetime. The working principle of all the instruments with appropriate diagram is described. The sample preparation for the above analyses is also presented.

Chapter 3

In this chapter, the problem encountered during the synthesis of nanoparticles is addressed. Attempts are made to synthesize nanophosphor without significant agglomeration adopting four different routes. The experimental conditions were designed to prevent agglomeration of the products. The novel synthesis methods developed for synthesis of $LaF_3:Ce^{3+}$ is described.

The role of organic coating on prevention of agglomeration is discussed. Various organic materials such as Oleic acid (OA), Polyethylene glycol (PEG), were coated on $LaF_3:Ce^{3+}$ and characteristics were studied. Attempts were made for the synthesis of $LaF_3:Ce^{3+}$ with narrow particle size distribution are presented in this chapter. The rate of addition of precursor during the synthesis was optimized to prevent agglomeration. The particle size was successfully controlled by using OA as the surfactant. The UV-Vis absorption and PL emission and excitation spectra were recorded for the OA coated $LaF_3:Ce^{3+}$nanophosphor are presented.

Attempts were carried out with combination of surfactants of OA and PEG for obtaining uniform particle size. With the surfactants combination, particles with narrow size distribution in the range of 6 - 90 nm were achieved. Similar optical measurements studies were carried out with OA+PEG coated $LaF_3:Ce^{3+}$nanophosphor are presented.

An alternate method was adopted to synthesize $LaF_3:Ce^{3+}$ in acidic environment without using surfactant in order to have higher light output and simultaneously with no agglomeration. The pH of the reacting environment, that affect the nature and performance of nanoparticles was varied and optimized to synthesize very fine sized particles. The effect of particle size on the PL light output was studied. The influence of pH on particle size and PL intensity were studied. The maximum light output was obtained at a pH of 4.2 and the corresponding particle size was found to be 10.6 nm. The synthesized particles found to be highly crystalline in nature yielding significant UV absorption at energy levels of Ce^{3+} with higher PL light output than organic coated particles. Optimization of cerium concentration was studied by varying the cerium concentration between x=0.01 to 0.20 mol. It was observed that in case of OA and PEG coated particles, beyond x=.01 mol of cerium concentration the PL intensity decreases. In case of uncoated particles, the PL intensity increases with the increase in cerium concentration. In the optimized pH condition, $LaF_3:Ce^{3+}$, $LaF_3:Tb^{3+}$, $LaF_3:Ce^{3+},Tb^{3+}$, $LaF_3:Eu^{3+}$ and $LaF_3:Ce^{3+},Eu^{3+}$ were prepared and their PL output were studied. The energy transfer was observed in Ce^{3+} - Tb^{3+}doped samples, where as energy transfer was not observed in Ce^{3+}- Eu^{3+} doped samples. All the synthesized samples were characterized by using XRD, DLS, SEM, UV-ViS absorption, Photo luminescent and Life time spectroscopy.

Another novel method of synthesizing $LaF_3:Ce^{3+}$ by reacting lanthanum carbonate and hydrofluoric acid was attempted and the results of this study are also presented for the first time in this chapter.

Chapter 4

The main issue of amplification of the PL output by introducing an external shell was addressed in this chapter. This chapter provides a brief introduction to the core-shell structure so far developed with LaF_3 molecule. The effect of external shell on nanophosphor surface on amplification of PL output is discussed. Attempts were made to amplify the light output by coating TiO_2. The enhancement of PL output by coating with TiO_2 on $La_{0.4}F_3:Ce_{0.45},Tb_{0.15.}$ composite is first of its kind. TiO_2 coating on the composite was achieved by adopting a mechanical dispersion method at room temperature. Though XRD pattern did not reveal the presence of TiO_2 on the surface, the presence of coating and its thickness were confirmed using TEM, EDS and FTIR spectra. The UV-Vis absorption, the photo luminescence and Lifetime characteristics of the samples were studied. The effect coating thickness on the PL behavior was studied and reported in this chapter. Scintillation under X-ray excitation was observed with uncoated and TiO_2 coated powder products.

The effect of non-stoichiometry of LaF_3 on the PL behavior of $LaF_3:Ce^{3+}$ was studied and reported for the first time. This study demonstrates a possibility of introducing tunability by changing the stoichiometry.

Chapter 5

The radiation induced degradation of nano sized $LaF_3:Ce^{3+}$ which in turn affects their performance as a radiation detector is addressed to in this chapter. As the primary application of this material is radiation detection, it requires radiation stability with respect to the PL behavior. Prolonged exposure to radiation can degrade most of the crystalline material by creating vacancies and defects, which results in poor PL intensity. A review of literature revealed less data on the degradation effects of organic coated and uncoated LaF_3:Ce nano crystals exposed to gamma irradiation. Hence, it is important to study their radiation stability.

Oleic acid coated and uncoated $La_{0.95}F_3:Ce_{0.05}$ nano crystals were irradiated with gamma rays for various doses upto 6.19 kGy. TEM, FTIR, UV-Vis absorption and PL measurements were carried out before and after the irradiation. Reduction in UV-Vis absorption and PL intensity were observed to follow a similar decreasing trend in both coated and uncoated nanocrystals. The drastic reduction in the peak intensity at 361 nm was observed in the OA coated as a function of radiation exposure, is due to the breach at the surface coating as well as the defects formed in the material. It was observed that

$LaF_3:Ce^{3+}$ nanocrystals were found to posses better radiation stability than other reported alkali halide crystals.

Apart from the above experiments, TL measurements were carried out with OA coated $LaF_3:Ce^{3+}$ nanocrystals, after annealing. TL peak appears at 136º C, indicating dosimetriclly a useful peak. TL decay kinetics follows a second order indicating Gaussian nature of the traps formed to trap more ions, which recombine to give more light. The trap depth calculated for the main peak at 409 K using Chen's mathematical equation is 0.57 eV. The results are highly promising towards using these crystals for radiation dosimetry. Removal of OA coating after annealing / gamma irradiation was confirmed from FTIR analysis. After annealing, the PL intensity decreased to half of its original intensity. The reduction in PL intensity might be due to either diffusion of Cerium ion from the surface into the host matrix (LaF_3) or oxidation of Ce^{3+} to Ce^{4+}.

Chapter 6

This chapter discusses the preparation of polymer nano composites (PNC) using the coated as well as uncoated synthesized nanoparticles and their PL properties. Luminescent PNC materials are inexpensive and can be prepared in various shapes and sizes. In nuclear industries, these materials can find applications in sensing X- and gamma radiation.

In this chapter, embedding of Oleic acid coated and uncoated $LaF_3:Ce^{3+}$ nanoparticles in polyacrylamide (PAM) host medium and their photoluminescence characteristics are presented. The LaF_3:Ce codoped with Tb matrix- viz uncoated and TiO_2 coated particles of $La_{0.4}F_3:Ce_{0.45},Tb_{0.15}$ were embedded in polymethylmethacrylate (PMMA) matrix and their PL characteristics are presented. The TiO_2 coated $La_{0.4}F_3:Ce_{0.45},Tb_{0.15}$ embedded in PMMA shows a better performance in terms of particle distribution as well as light output. For the first time scintillation of uncoated and TiO_2 coated $La_{0.4}F_3:Ce_{0.45},Tb_{0.15}$ PMMA composite under X-ray excitation was demonstrated.

Chapter 7

This chapter summarizes highlights of the results described in each chapter. The potential application of nano sized phosphors embedded in transparent polymer composite for X-ray radiation detection is demonstrated. Nanoctystals of Lanthanum fluoride doped with cerium has been synthesized successfully through four different synthesis routes: The particle sizes of samples prepared through different synthesis routes were observed to be in the range of 6-800 nm, in the case of OA coated, 6-90 nm with OA and PEG combination, 6-30 nm obtained with pH 4.2 and 190-480 nm with HF method. A novel method of synthesizing in acidic environment was successful in yielding particles with narrow size distribution and high light output. The PL output of uncoated was the best, when compared to OA and OA+PEG coated. Though OA+PEG combination yielded particles with narrow size distribution the PL output was very less which might be due to the surface groups aiding the radiation less transfer as well as prevent the UV from reaching the Ce^{3+}. $LaF_3:Ce^{3+}$ showed emission at 305 nm when exited with 250 nm wavelength. $La_{0.4}F_3:Ce_{0.45},Tb_{0.15}$ showed emission at 305, 490,543,585 and 615 nm when exited with 262 nm wavelength. For the first time, TiO_2 coated $La_{0.4}F_3:Ce_{0.45},Tb_{0.15}$ is synthesized an its PL characteristics are reported. TEM images confirm the core-shell formation and good crystallinity of the nanocrystals. EDS confirms the elemental composition. Scintillation under X-ray excitation was observed with uncoated and TiO_2 coated powder products. It is demonstrated that there is a possibility of introducing tunability by changing the stoichiometry. Even after gamma radiation exposure with to Cobalt-60 gamma rays upto a dose of 6.1kGy, the PL profile remind unchanged and no Ce^{2+} signature is observed in PL demonstrates the radiation stability of $LaF_3:Ce^{3+}$. During gamma irradiation, a breach in the oleic acid coating was observed in the OA coated material. The TL trap depth calculated for the main peak at 409 K using Chen's mathematical equation is 0.57 eV. The results are highly promising towards using these crystals for radiation dosimetry. The effect of non-stoichiometry on photoluminescence of the material is reported for the first time.

References

[1] Sivakumar S, Diamente P R, van Veggel F C J M., J.Chem. Eur. 12 (2006), 25878.

[2] Stouwdam. J.W, Hebbink G A, Huskens J, van Veggel F C, Chem. matter 15(24) (2003) 4604.

[3] Stouwdam. J.W, van Veggel and Frank C J M, Nano Letters 2(7) (2002) 733.

[4] Wei Y, Lu F Q, Zhang X R, Chen D P. Mater. Letters 61 (2007) 1337.

[5] Sun X, Zhang Y W, Du Y P, Yan Z G, Si R, You L P, Yan C H. J.Chem.Eur. 13 (2007) 2320.

[6] Peijzel .P.S, Wegh. R.T, Meijerink. A, Holsa. J, Lamminmaki R, J. Opt. Comm. 204 (2002) 195.

[7] Wang. F, Zhang. Y, Xianping Fan and Minquan Wang, J. Mater. Chem 16 (2006) 1034

[8] Stouwdam. J and .vanVeggel. F, Nano Letters. 2 (2002) 733.

[9] Deng, H, Yang. S,.Xino. S , Gong. H.M, ,J.Chem.Soc.130 (2008) 2032.

[10] Yang. X, Dong. X, Wan. J, Guixia Liu, J. Alloys Comp 487 (2009) 298.

[11] Qu. Y , Yua. Yi, Kong. X, Sun.Y , Hong. Q.Z , Mater.Lett. 63 (2009) 1285.

[12] Sheng Dai., et al US Patent /2006 /0054863.

[13] Wayne. D., Cooke et al US Patent / US2008 /0128624.

[14] Zhou. J, Wu. Zhang. Z, Liu. W and Dang. H, Wear 249 (2001) 333

[15] Wang.J, Hu.J, Tan. D, Liu.X and Zhen.Z, J. Mater Chem. 17 (2007) 1597.

[16] Chen. Z.G, Tian. Q.W, Song.Y.L, J. Alloys and Comp. 506 (2010) 17.

[17] Nathan J. Withers, John B. Plumley, Brian A. Akins, Antonio C. Rivera, Gloria Medina, Gennady A. Smolyakov, Graham S. Timmins, Marek Osinski, Proc SPIE 75750 Z (2010)

[18] Fan yang "Synthesis, Characterization and FLouresecnce performance of $LaF_3:Ce^{3+}$ nanocrystals " Thesis University of New Mexico (2009)

[19] Bhargava. R.N and Gallagher. D, Physical Review letters 72 (1994) 3

[20] Pramod H.B, Vogel. W, Kulkarni.S.K , J. Colloid Interface Sci. 293 (2006) 437.

[21] AninditaChatterjee, AmiyaPriyam, Subhash C. Bhattacharya, Abhijit Saha, J.Colloids and Surfaces A: Physicochemical and Engineering Aspects. 297 (2007) 258.

[22] Xie. M.Y, Yu. L,.He. H and Yu. X.F, J. Solid State Chemistry 182 3 (2009) 597.

[23] Cui Kai, Gao Chao, Peng Bo, and Wei Wei, J. Nanomaterials 2010 (2010) 5

[24] Wang. Q, Yumin. Y, Ludescher. R.D, YiguangJu, J. Lumin. 130 (2010) 1076.

[25] Bangaru.S 2011. Physica B 406 (2011)159.

[26] Chander, H, J. Mater. Sci.Eng. 16 5 (2005) 113.

[27] N. Salah, P.D. Sahare, S.P. Lochab and P. Kumar, Radiat. Meas. 41(2006) 40

List of Figures

List of Tables

ABSTRACT

Lanthanum Fluoride doped with Cerium has received attention in the field of luminescence as well as radiation detection for its absorption of higher energy radiation, high light emission, and silent host lattice with low phonon energies preserving the activator site and possessing fast decay time. Nano size will add strength towards more light intensity. Nano sized LaF_3:Ce was synthesised in four different routes. Initially in order to achieve nano size, surface modification of LaF_3:Ce was carried out using Oleic acid (OA) and the combination of Polyethyelne glycol (PEG) and OA. Nano size was successfully achieved by applying surfactants but at the cost of light output. In order to achieve both nano size and higher light output, LaF_3:Ce was synthesized in acidic environment without any coating. Acidic environment yielded nano particles with very narrow size distribution. Various uncoated samples of LaF_3: Ce were synthesised with upto 45 mol%. A redshift in the PL spectra was observed at higher Ce concentration. Uncoated particles showed five distinct, clearly resolved absorption peaks at wavelengths 198, 205, 218, 234 and 247 nm. For the first time LaF_3:Ce had nano size with very narrow distribution possessing very high light output. The PL output (300 – 325 nm) of Cerium was significantly converted to a visible light (543 nm) by codoping with Terbium through Energy transfer from Cerium to Terbium. Life time of the PL emission of nano sized LaF_3:Ce was found to be 25 nsec.

TiO_2 has been successfully coated upon the nano sized $La_{0.40}F_3:Ce_{0.45}^{3+},Tb_{0.15}^{3+}$, $La_{0.55}F_3:Ce_{0.45}^{3+}$ and $La_{0.85}F_3:Tb_{0.15}^{3+}$ matrices to obtain a core-shell structure. The core-shell structure formation was confirmed with TEM images and FTIR spectra. The effect of TiO_2 coating thickness on PL intensity was studied. About 1.76 times increase in the light output (543

nm) was observed at a coating thickness of 4-6 nm. Scintillation under X-ray excitation was observed from the uncoated and coated $La_{0.40}F_3:Ce_{0.45}^{3+},Tb_{0.15}^{3+}$ matrices.

The effect of nonstoiometry of LaF_3 on the PL behaviour was studied by varying the molar ratios of $LaCl_3$ and NH_4F. Changes in the particle size as well as the PL spectra and intensity were observed due to nonstochiomety. This indicates towards a possibility of introducing tunability by changing the stoichiometry.

The radiation induced degradation of nano sized $LaF_3:Ce^{3+}$ which in turn affects their performance as a radiation detector. As the proposed primary application of this material is radiation detection, it requires radiation stability with respect to the PL behaviour. Reduction in UV-Vis absorption and PL intensity were observed to follow a similar decreasing trend in both coated and uncoated nanocrystals subsequent to γ- radiation. TL measurements were carried out on $LaF_3:Ce^{3+}$nanocrystals, after annealing. TL peak appears at 409°K (136ºC), indicating dosimetriclly a useful peak. TL decay kinetics follows a second order indicating Gaussian nature of the traps formed to trap more ions, which recombine to give more light. The trap depth was calculated for the main peak at 427 K using Chen’s equation is 0.57 eV. The results are highly promising towards using these crystals for radiation dosimetry.

The main objective of the work was achieved by preparing radiation sensitive transparent polymer nanocomposite (PNC) material. Polyacrylamide as well as Polymethylmethacrylate (PMMA). PNC materials were prepared using the coated as well as uncoated synthesized nanoparticles and their PL properties measurements were carried out. The microscopical and FESEM micrograph observations indicated an uniform particle distribution in the PNC matrix. The TiO_2 coated $La_{0.4}F_3:Ce_{0.45},Tb_{0.15}$ embedded in PMMA shows a better performance in terms of particle distribution as well as light output. For the first time, scintillation of uncoated and TiO_2 coated $La_{0.4}F_3$:$Ce_{0.45}$,$Tb_{0.15}$ PMMA composite under X-ray excitation was observed.

Chapter 1

Introduction

1.1 Luminescence

Luminescence is the most fascinating, beautiful, silent language spoken by some materials. The word “Luminescence” was first coined by Eilhardt Wiedemann [1] a German physicist in 1888 for all those phenomena of light which are not solely due to rise in temperature. This terminology originates from Latin word *lumen* which means light. Luminescence is the emission of light in the visible or near visible region as a result of excitation. The emitted wavelength in most cases is longer than the exciting wavelength. The difference in wavelength between absorption maxima and emission maxima is called Stoke’s [2] shift. Luminescence can be classified according to types of excitation sources used. Photoluminescence involves excitation by an electromagnetic radiation usually in UV or visible region. Thermo luminescence is the emission of light following application of heat. Electroluminescence occurs due to the excitation by an electric voltage, Triboluminescence is produced by mechanical energy such as grinding. Chemiluminescence is the process of light emission during chemical reaction. X-ray luminescence and Radioluminescence occur due to excitation by X-rays or γ-rays respectively.

Photoluminescence is further classified as *fluorescence* and *phosphorescence* according to the time scale of the emission. Fluorescence is a spin allowed transition which has radiative life time of approximately 10^{-7}–10^{-9} s, while the phosphorescence is a spin forbidden transition with life time of about 10^{-3}–10^{-4} s.

1.2 Photoluminescence

Photoluminescence [PL] is a phenomenon in which electronic states are excited by light energy from an external source and the de-excitation energy is released as light. PL is divided into two major types: Intrinsic and extrinsic depending on the nature of electronic transition producing it. Figure 1.1 illustrates the general photo luminescence process. The PL mechanism involves different stages such as absorption, vibrational relaxation, emission, internal conversion and inter system crossing. The absorption of UV-Vis radiation excites molecules from the ground state [S_o] to the excited states [S_1]. Absorption process is usually followed by successive vibrational relaxation (VR) of the exited molecules as well as internal conversion to lower excited states. Relaxed molecules position themselves in the first exited state can return to the ground state by emission of a photon (Fluorescence- FL) within a short time of 10^{-7}–10^{-9} s. Molecules can also relax by getting rid of the exited energy through an internal conversion radiationless process. In another way, exited molecules reach ground state via a process called intersystem crossing. In this process there is an energy transfer from exited singlet state to a triplet state. The exited molecules in this state, come back to the ground singlet energy state more slowly. This slow process of radiative transition back to the ground state is termed as Phosphorescence with a time delay of 10^{-3}–10^{-4} s.

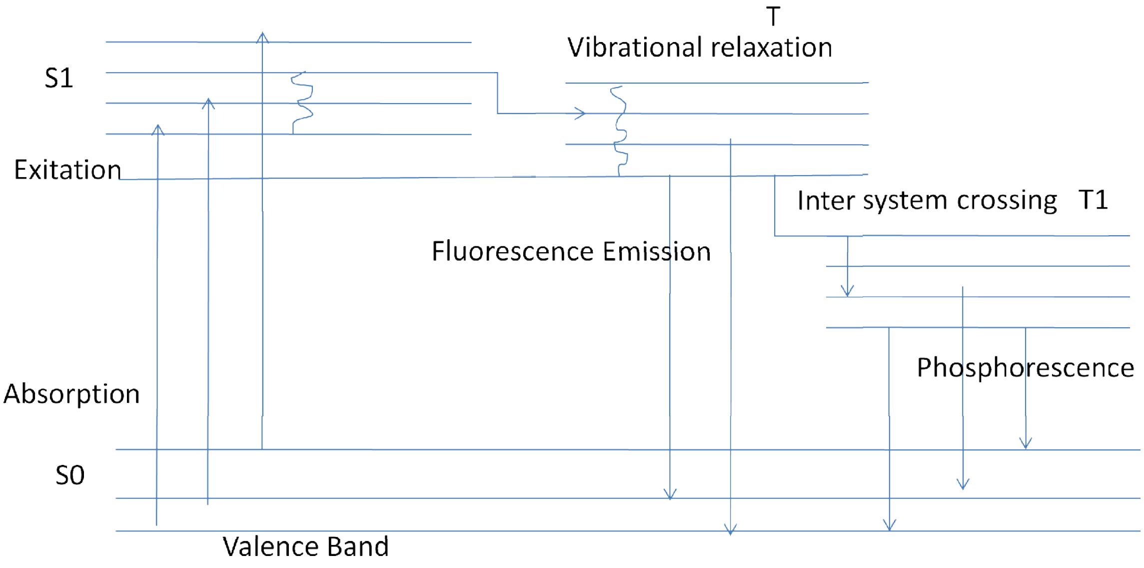

Figure 1.1 PL process

1.2.1 Intrinsic luminescence

In solids, there are three kinds of intrinsic luminescence: a) band-to-band luminescence b) exciton luminescence c) cross-luminescence.

a) Band –to –band luminescence

Light emission occurs due to recombination of electron in the valance band and hole in the conduction band. With the aid of high temperature some of semiconductors like Si, Ge and GaAs display this.

b) Exciton luminescence

Exciton is exited electron & hole pair which navigates inside crystal and emit light when they recombine. Wannier exciton and Frenkel exciton are theoretical models which predict their behavior. The Wannier exciton model express an exciton composed of an electron in the conduction band and a hole in the valence band bound together by coulomb interaction. The expansion of the wave function of the electron and hole in Wannier exciton is much larger than the lattice constant. The Frenkel exciton model is used in cases where expansion of electron and hole wave function is smaller than lattice constant or unit cell, (eg. ZnO).

c) Cross luminescence

If the light emission occurs by the recombination of an electron in the valence band with a hole created in the outer most core band then it is called as cross luminescence. Cross luminescence occurs only when the energy difference between the top of valence band and that of conduction band is smaller than the bandgap energy. This type of luminescence was first observed in BaF_2.

1.2.2 Extrinsic luminescence

Luminescence caused by intentionally incorporated impurities, mostly metallic impurities or defects is classified as extrinsic luminescence. Most of the observed type of luminescence of practical application belongs to this category. Intentionally incorporated impurities are activators and materials made luminescent in this way are called phosphors. Extrinsic luminescence in ionic crystals and semiconductors is classified into two types: unlocalized and localized. In the unlocalized type, the electrons and holes of the host lattice participate in the luminescence process, while in localized type, the luminescence excitation and emission process are confined in a localized activator center.

In semiconductors, donors and accepters act as luminescence activators. There are two types of luminescence transitions i.e. the transition of a free carrier to a bound carrier and the transition of a bound electron at a donor to a bound hole at an acceptor. These kinds of luminescence lines and bands are usually observed in semiconductor compounds such as III-V and II-VI compounds.

1.3 Nanoparticles Properties and advantages

Though voluminous works have been done in the field of luminescence since 1888, the field of study took an interesting stand – in follow-up with the famous statement quoted by Richard Feynman-“There is plenty of Room at the bottom”. The quest for smaller particles as well as the science behind these phenomenon began, this embraced the field of luminescence also, giving birth to nano sized luminescent particle in late ‘80s – a nanophosphor. “Nanophosphor” is a luminescent material the size of the crystal is being the order of nanometers. In general nano sized particles are expected to posses half of their atoms contained in top two surface layers [3], which make optical properties highly sensitive to surface morphology. As the consequence of size reduction, electron and hole [e & h] wave functions are restricted in one or more dimensions. The dimensional restriction on wave function leads to an increase in the band gap energy. Hence, the energy levels of the valance and conduction bands become more discrete than in a bulk material. Small impurities when added or removed to such nano sized material can measurably alter the energy of the band gap. The charge carriers are excited to upper energy levels by absorbing radiation as similar to an atomic excitation. The absorption and emission in a substance directly or indirectly depend upon the band structure which in turn depends upon the size of the crystal. Due to this reason, bulk band gap semiconductor, whose bandgap is in the near infrared, emits the light in the visible spectral range during deexitation. In contrast to the bulk band gap materials, the nanocrystalline materials absorb and emit shorter wavelength due to more spacing between the energy levels (ie. the larger energy gap). Less self absorption, intense emission and faster decay are the advantages.

1.4 Requirements of nanophosphors

Depending upon the application, the requirements from nanophosphor can vary. Generally, they should have one or more of the following properties: high purity; high crystallinity, small particle size; narrow particle size distribution; spherical morphology; homogenous distribution of the activator ion. The proper combination of these properties will result in a phosphor with high luminescent intensity. Some of the requirements of typical nanophosphors applied in different applications are outlined here.

1.5 Development of nanophosphor

Nanophosphor absorbs energy of electromagnetic (EM) radiation photons and converts to another photon having a different energy in electromagnetic spectra. The electromagnetic radiation emitted by the nanophosphor is usually in the visible range, but it can also be in other spectral regions such as the UV or infrared. Nanphosphor research is in the limelight since last two decades only. Devoted research is being carried out by many groups on the nano luminescent materials for their application in the energy saving fluorescent lamps with better luminescence efficiency. Moreover, attempts are being made to apply nanophosphors as high-performance novel display devices. The current status of the studies on these nanophosphors are discussed below.

Initially the nanophosphor work started with lesser bandgap compound semiconductor materials as the size of the crystals determines the bandgap energy levels, hoping the predictability and tunability of the emission. Co-precipitation technique was adopted to synthesize doped semiconductor materials that can be tuned easily. Henglien at al, [4] in early 1980's first reported the enhanced quantum properties of semiconductor nanoparticles of ZnS PbS, ZnSe and CdSe with size controlled synthesis as it involves a more sensitive size-dependent bandgap.

The predictability and the tunablility of the emission was demonstrated by R.K.Jain et al., (1983) [5] with nanoparticles of CdS and CdSe in glass samples which is impossible with the conventional bulk dielectric/semiconducting materials. A blue shift in the PL spectra was observed which is due to the discretization of energy band gap and a strong non-linear response was also evident. The first report on nanosizd ZnS luminescent material was prepared by adopting the solution co-precipitation route by Bhargava et al.,[6] in 1994. They demonstrated that with a 3.5- 7 nm particle size, 18% enhancement in the photoluminescence quantum efficiency was observed compared to its bulk counterpart. Khosravi et al.,[7] also reported upon the PL of ZnS:Mn nanoparticles synthesized by adopting the solution route. They observed that 0.12 mol of Mn was found to be the optimized dopant concentration. I.Levy et al., [8] in 1998 synthesized manganese doped Cadmium ($Cd_{1-x}Mn_x$) by adopting the reverse micelles co precipitation method that demonstrated a good PL output and size controlled synthesis to obtain particles < 5 nm. They demonstrated that as the particle size decreases the band gap increases.

Later the nanophosphor research included higher band gap oxides, halides, as well as silicates. R.Jaganathan et al.,[9] in 1996 synthesized Eu^{3+} doped Zinc Boro sulphate glasses by adopting solid state reaction at high temperature. The particle sizes were 30-50 nm emitting 612 nm (Red emission). Metallic oxide based nanophosphors were also synthesized by adopting the Sol Gel route. Qiang.Li et al., in the year 2000 [10] synthesized $Y_3Al_5O_{12}$:Ce (YAG) nanoparticles by adopting polymer network gel method. The product lattice parameter was 1.06 nm. Due to the very small size, they observed a blue shift in the PL spectra which is the effect of the increase in the crystal field. Chung.Lu and Jagannathan et al.,[11] in the year 2002 synthesized $Y_3Al_5O_{12}:Ce^{3+}$ (YAG) nanophosphor by sol-gel pyrolysis method. The particle sizes were in the range of 30-50 nm displaying very high PL intensity. Wang et al.,[13] in 2003 synthesized cubic nanocrystalline Y_2O_3:Tb phosphor by combustion technique followed by sol-gel which yielded particles with 50-70 nm size. H.X.Zhang et al.,[12] in the year 2001, synthesized Tb^{3+} as well as Eu^{3+} zinc silicate glasses at room temperature adopting a low cost sol-gel process and annealed them at 850°C. The size of the particles was in the range 40-100 nm. The product possed comparable red as well as green emitting properties useful for the CRT TV screen.

Nano sized rare-earth halides doped with other rareearths were also explored for its photo luminescence and scintillating properties simultaneously owing to its very narrow and sharp emission lines arising from the shielded f and d orbital. Surfactant capped LaF_3: was synthesized by Zhou et al., in the year 2001[14]. In the year 2002 J.W.Stoudowdam et al., [15] synthesized LaF_3 doped with (Eu^{3+},Nd^{3+} and Ho^{3+} 0.05 mol) by heating ammonium di-*n*-octadecyldithiophosphate in presence of sodium fluoride and adding lanthanum nitrate solution at 75 °C . The particles were of 5- 10 nm in size and di-*n*-octadecyldithiophosphate served as the ligand in preventing agglomeration. The emission from LaF_3:Nd were in the near infrared region which may be useful for telecommunication purposes. Wang. F et al., [15] in 2006 was the first to report successful synthesis of low temperature aqueous based water soluble LaF_3 doped with Eu^{3+}, Ce^{3+}, Tb^{3+}, and Nd^{3+} adopting co-precipitation technique. Their work resulted in the luminescence quantum yield of 16% for the synthesized $La_{0.40}$ F_3:$Ce_{0.45}$,$Tb_{0.15}$ in aqueous solution. The particle size was around 30 nm. Nanocrystals doped with different lanthanide ions showed strong luminescence in the visible (Vis) and near-infrared (NIR) spectral regions. Sun.X et al.,[17] in the year 2007 synthesized monodisperse rare-earth (RE=La to Lu, Y) fluoride and oxyfluoride nanocrystals with diverse shapes (trigonal REF_3 triangular, truncated-triangular, hexagonal, and polygonal nanoplates; orthorhombic REF_3 quadrilateral and zigzag-shaped nanoplates; cubic REOF nanopolyhedra and nanorods) from triflouro acetate precursor through controlled fluorination in oleic acid (OA)/oleylamine (OM)/1-octadecene (ODE). Jan-Xin Menga, et al., [18] in the year 2007 prepared LaF_3:Eu^{3+} nanoparticles with efficient luminescence and good crystal morphology without calcinations at high temperature. The results showed that the nanoparticles are well dispersed with a hexagonal shape and displayed excellent luminescence. The influences of reaction temperature, time and Eu^{3+} concentration on the preparation and luminescence of LaF_3:Eu^{3+} nanoparticles were also investigated. The luminescence intensity of LaF_3:Eu^{3+} nanoparticles are five times stronger than that of bulk LaF_3:Eu^{3+}. In another interesting work on luminescent hybrid material, (Yb/Eb doped nano sized Oleic acid coated LaF_3) co precipitation method was used successfully (Wang et al 2007) [19]. The OA- coated nanocrystals were nearly in spherical shape with a mean diameter of 7 nm and exhibited excellent dispersibility in common organic solvents and a PMMA matrix. The resulting nanocrystal–polymer hybrid materials exhibited strong emission around 1550 nm, when excited at 980 nm. These materials seem to be promising materials for polymer-based optical waveguide amplifiers. Deng.,*et al* [20] reported the synthesis of ligand-capped LaF_3 nano crystals. In their work, $LnVO_4$ (Ln = Ce and Nd) nanocrystals were synthesized adopting facile solvo hydrothermal route. Their work demonstrated the synthesis of efficient upconverions luminescent nanocrystal with different shapes and their applications in optoelectronics.

G. Stryganyuk et al., [21] in 2009 discussed about the bulk and nanosized difference in the photo luminescence of LaF_3:Ce doped particles. They suggested that during high temperature annealing in LaF_3:Ce , CeF_3 will be formed and the excitation spectra of CeF_3 and LaF_3 :Ce will coincide, because the saturation effect and surface losses effect are absent.. Wang et al., in the year 2009 prepared LaF_3:Eu^{3+} nanoparticles in the glycerol/water medium by adopting refluxing method. The as-prepared LaF_3:Eu^{3+} spherical nanoparticles (size was around 30 nm) were well crystallized with the hexagonal structure of bulk LaF_3. Under the UV light irradiation, the nanoparticles exhibited the characteristic emission of Eu^{3+} ions. By adopting the simple hydrothermal method. Mingzhen Yao et al., [22] in the year 2010 synthesized LaF_3:Ce^{3+-}doped nanoparticles at different temperatures in dimethyl sulfoxide (DMSO) by the chemical reaction of Lanthanum Nitrate Hydrate and Cerium Nitrate Hexa -hydrate with Ammonium Fluoride. They observed that the luminescence of the LaF_3:Ce^{3+-}doped nanoparticle powders precipitated from the DMSO solution was markedly different from that of the solution samples. The cerium emission at 310 nm was absent in solution and showed emissions from UV to blue and red depending on the reaction temperature and duration.

Along with study of nanophophors the quest for increasing the light output of the materials is also on. The results of this quest were very positive (increased light output) by synthesizing a core (Host with dopant) - shell structure comprising of the same host material or any metallic oxides). The shell structure acts a light amplifier by reducing the radiationless transfer and also participates in the energy transfer to the core. Meng-Yin Xie et al.,[23] in the year 2009 synthesized LaF_3:Ce,Tb/ LaF_3 and LaF_3:Nd / LaF_3 core shell structure through a simple solution based co precipitation technique. The core/shell nano crystals (NCs) exhibited increased emission intensity and quantum yield as compared with the bare LaF_3:Ln^{3+} nano crystals.

In the year 2010 LaF_3/ SiO_2 materials were used as shell upon LaF_3:Ce to enhance the light output.[24,25]. SiO_2 was found to be the most effective in enhancing the photoluminescence of LaF_3:Ce by two times. The fluorescence intensity of LaF_3:$Nd^{3+/}$ SiO_2 core/shell nanoparticles also had a great improvement, which can be very beneficial for applications. In the year 2011 S. Janssens et al., [26] synthesized nano sized LaF_3:Eu doped particles and demonstrated the possibility of sensitizing using TTA (Tetradecylthioacetic acid) ligand which aids in the energy transfer through the Triplelet state. Due to this ligand attachment there was an 18% increase in the PL intensity, when compared with OA capped LaF_3:Eu^{3+} nanoparticles. J.K Han et al., [27] in 2011 synthesized Y_2O_3:Eu^{3+} (core)/SiO_2 (shell) nanoparticles in the year 2011 and demonstrated enhancement of the light output. Effect of the shell thickness and PL intensity relation with it was also evolved and they concluded that a thin shell is better for amplification.

Lisha Zhang et al., [28] 2012 synthesized LaF_3:Ce,Tb nanoparticles of size 6 nm possessing high dispersability in water exhibiting strong green emission with high quantum yield of 50 % under 254 nm excitation. In another simple and easy synthesis S. G. Gaurkhede et al.,[29] in the year 2012 synthesized nanocrystals of LaF_3 doped with Nd^{3+}, Sm^{3+} by adopting a rapid solution route using domestic microwave oven at low power range. Nanocrystals were of hexagonal structure with particle size varying from 15 to 20 nm. The absorption edge in UV spectra was found to be at 250 nm (corresponding to 4.9 eV) and emission was observed in the wavelength range between 250 to 800 nm. Red emission was also reported (654 nm) for LaF_3:Nd^{3+}, Sm^{3+} nanocrystals at an excitation wavelength of 357 nm.

The quest of nanophosphors did stop with core-shell structures, but opened a new and interesting avenue called luminescent nanocomposite material. These materials are inexpensive and can be obtained in desired shapes and proposed to be applied as wave guide amplifiers in telecommunication, scinitillation, bio labeling and in vivo mapping of radiosensitive cells.

Though plenty of research is being carried out on nanophosphors as well as polymer nancomposite materials, it is yet to set its commercial foot in the market. I discuss here briefly about two interesting patents.

Sheng Dai et al., [30] in the year 2006**,** have patented upon the synthesis and performance of four nano phosphors which include CdSe/ZnS (core/shell), doped Y_2O_3, doped $LaPO_4$ and doped ZnS nano composite materials. They claim that the material was crack free composite having enhanced transparency, high intensity light emission, possess ruggedness, which can detect different ionizing radiation. Nanocomposite scintillators comprises of a fast, bright, rare-earth doped nano powder phosphor in a binder matrix that is transparent to the emission of the phosphor. Recent trend of this research is to develop a nanocomposite scintillating material which can be used for X or gamma radiation detection applications. These scintillator exhibit high quantum efficiency, good linearity of the spectral emission with respect to incident energy, posses qualities for energy spectrum measurements, posses high density, fast decay time and minimal self absorption.

In another interesting patent, D.Wayne Cooke et al., [31] in the year 2008 in their have prepared a nano composite scintillator using a rare-earth doped nanophosphor and a binder transparent to the emission. This provided a nano composite scintillator based radiation detector for γ-rays, X-rays, Protons and neutrons. They claim that these can be prepared in a wide variety of shapes and sizes using easy chemical methods and can be applied for spectrometry purposes.

As the proposed application of the study is scintillation, the material should be of higher density to attenuate the X-ray or gamma radiation and efficiently convert them to UV or visible radiation. It should also be of high crystalline in nature. The Lanthnum tri fluoride (LaF_3) posses most of the required qualities required for a good scintillator. Moreover, it is highly stable thermally and chemically stable with low vibrational energies. Cerium posseses efficient radiation absorption and fast radiative decay time (20-40 ns). Therefore Cerium-doped bulk lanthanum halide compounds are attractive for this purpose. Moreover, Cerium ion (among few lanthanide ions), has the wavelength of its first excited state higher than the 180 nm (55000 cm^{-1}) [37]. Also structurally there were no changes observed in LaF_3 matrix even when Ce^{3+} highly doped as the radius of lanthanum and cerium are slightly different.

Therefore, the motivation of this work is to develop organic coated (surface modified), uncoated and inorganic coated {with an optical amplifier (TiO_2 layer)} shell, cerium-doped lanthanum fluoride nanoparticles. Lanthanum fluoride, a chemically and thermally stable material, having a higher bandgap (10.2 eV) compared to other rare earth halide semms to be a right host matrix..

Of all the available synthesis techniques for nanophosphors, the chemical co-precipitation technique is one of the simple and easy method for obtaining highly luminescent nano material. Effective size control can be achieved by simple methodologies. Adopting such methods, high crystalline nanophosphor with core-shell structures yielding higher quantum efficiency can be easily prepared.

1.6. Inorganic based nanophosphors and their applications

1.6.1 High-energy ionizing radiation detection

High-energy ionizing radiation detection is one of the high-potential applications of nanocrystals. Nanocomposite scintillators are emerging materials which can be applied to absorb high-energy ionizing electromagnetic or charged-particle radiation and emitting at its characteristic wavelength, for radiation detection applications. These materials satisfy many of the requirements of a good scintillator: high conversion efficiency (meaning number of photons emitted per electron-volt of energy absorbed), short luminescence decay time, good energy resolution, and transparency at the wavelength of emission. Inorganic scintillaotrs are preferred over organic or plastic scintillators for their higher stopping power, since high atomic weight inorganic compounds are available with high light yield. Since some lanthanides are excellent luminescent ions, and lanthanide halides are good wide-bandgap host materials, lanthanide-doped lanthanum halide nanocrystals, are very good candidates for radiation detection applications. In the year 2014 B.Wanger et al., [32] have demonstrated the simple synthesis and effective application of nanocomposite scintillators. They have developed transparent scintillating polymer and glass-matrix containing quantum dot polymer composites, fluoride nanophosphor epoxy composites and halide nanoparticle. These materials were studied for gamma-ray spectroscopy, X-ray imaging, alpha particle and neutron detection. Scintillation was observed in all the polymer and glass matrix nanocomposite materials. Polymer nanocomposite materials with lanthanide-doped lanthanum halide nanocrystals seem to be the excellent choice in making a breakthrough in this field.

1.6.2 Nanophosphors in Solid State lighting

It is well studied and established that the size and surface chemistry affects the excitation and emission of nanocrystals due to quantum confinement effect. Smaller the particles, less is the self absorption and thus leading to intense light output satisfying the requirements of a good solid state lighting material. Furthermore, by tailoring the crystallite size, it is possible to make the materials absorb more of UV wavelength or blue LED photons (used in solid-state lighting). It is possible to synthesize nanophosphors with high quantum efficiency for solid-state lighting. The emission efficiency, insignificant emission quenching, and absence of defects and surface trap sites which cause radiation less transfer are also the important requirements for a material to be good for solid-state lighting. Nanocrystals where luminescent ions are doped in a wide-band gap host material with low phonon vibration energies proves to be attractive for solid-state lighting. Owing to the small size, the amount of scattered light is also less compared to the bulk phosphor which is an added advantage.

1.6.3 Biological fluorescent labeling

Unlike organic (dyes) luminescent materials, the inorganic materials posses high chemical and thermal stability. Inorganic nanocrystals exhibit many interesting size and shape dependent properties based on which many new potential applications can be explored   By size and composition variation of nanocrystals, the luminescence emission can be tuned from red at 6 nm to blue at 5 nm size of the same semiconductor nanocrystal. The unique photo physical properties of fluorescent nanocrystals make them very attractive firstly as biological probes for molecular recognition, fluorescent labeling of biological cells, DNA sorting, *etc.* (Parak *et al.* 2003) [33]. Other potential applications, of nanophosphors are for fabricating high quality imaging screens, solid-state lighting and display, and ionizing radiation detection

Fluorescence labeling is the process of covalently attaching a fluorescent chemical compound (fluorophore) to another molecule, such as a protein or nucleic acid. Fluorescence technique can be used to image the location of the molecule or to probe its environment. This is generally accomplished using a reactive derivative of the fluorophore that selectively binds to a functional group contained in the target molecule. The most commonly labeled molecules are antibodies, proteins, amino acids and peptides which are then used as specific probes for detection of a particular target (Rietdorf J et.al., 2005

[34]). Quantum dots potentially offer significant advantages over conventional light-emitting biological probes (Rosenthal 2001) [35], (M. Han et al.,) [36]. The nanocrystal emission is narrower and more symmetric than that of the organic dyes, potentially allowing a larger number of probes within a detectable spectral region.

Upconverting nanophosphors can be tagged to the bio molecules and can be visualized under infrared excitation. The bio-molecules absorb the heat energy and vibrate and this vibrational energy is transferred to the upconveting phosphors where this energy is converted to a visible light. This finds application in invivo organ mapping. Rare-earth halides doped with other rare earths, especially cerium- doped lanthanum fluoride with Oleic acid (hydroxyl) capping, proved to enhance the radiosensitivity of the cells owing to its high Z and human body friendly chemical nature [29, 30].

1.7 Limitation of earlier detectors and motivation

Higher energy radiation detection primarily requires materials with high density and with high quantum light output. Though there are certain semiconducator based radiation detectors such as Ge,CdTe as well as scintillators like BGO and NaI(Tl), they have certain limitations. The semiconductor detectors are expensive and crystal growth is also very difficult. Moreover liquid nitrogen cooling is essential for its good performance. Likewise BGO or NaI(Tl) are also difficult to grow. Moreover, NaI(Tl) crystal should be preserved properly as it is hygroscopic in nature.

Recent studies on rare-earth-doped heavy metal halide compounds (LaF_3) satisfy many requirements for a good radiation sensor. LaF_3 unlike NaI(Tl) is non hygroscopic and posses higher density. The high atomic weight and density can attenuate higher energy radiation efficiently, absorb and convert to UV or visible light. These studies on LaF_3 and other rare-earth based inexpensive polymer nano composite scintillating materials motivated this work. High-energy ionizing radiation detection is of particular relevance to this work. LaF_3 doped with cerium efficiently and swiftly converts the incident radiation to UV radiation. This system can be codoped with Terbium to covert the UV emission of cerium to visible green color emission. There is a very good compatibility between Ce and Tb for energy transfer from cerium to terbium is significant. Recent studies say that LaF_3 is bio- compatible and can be used as bio labels as well as upconversion phosphors. Figure 1.2 shows the history of inorganic scintillator materials studied since 1990 onwards is shown below with minor modification of figure provided by Mary Weber et al.,[38] (courtesy of Marv Weber Derenzo 2005)

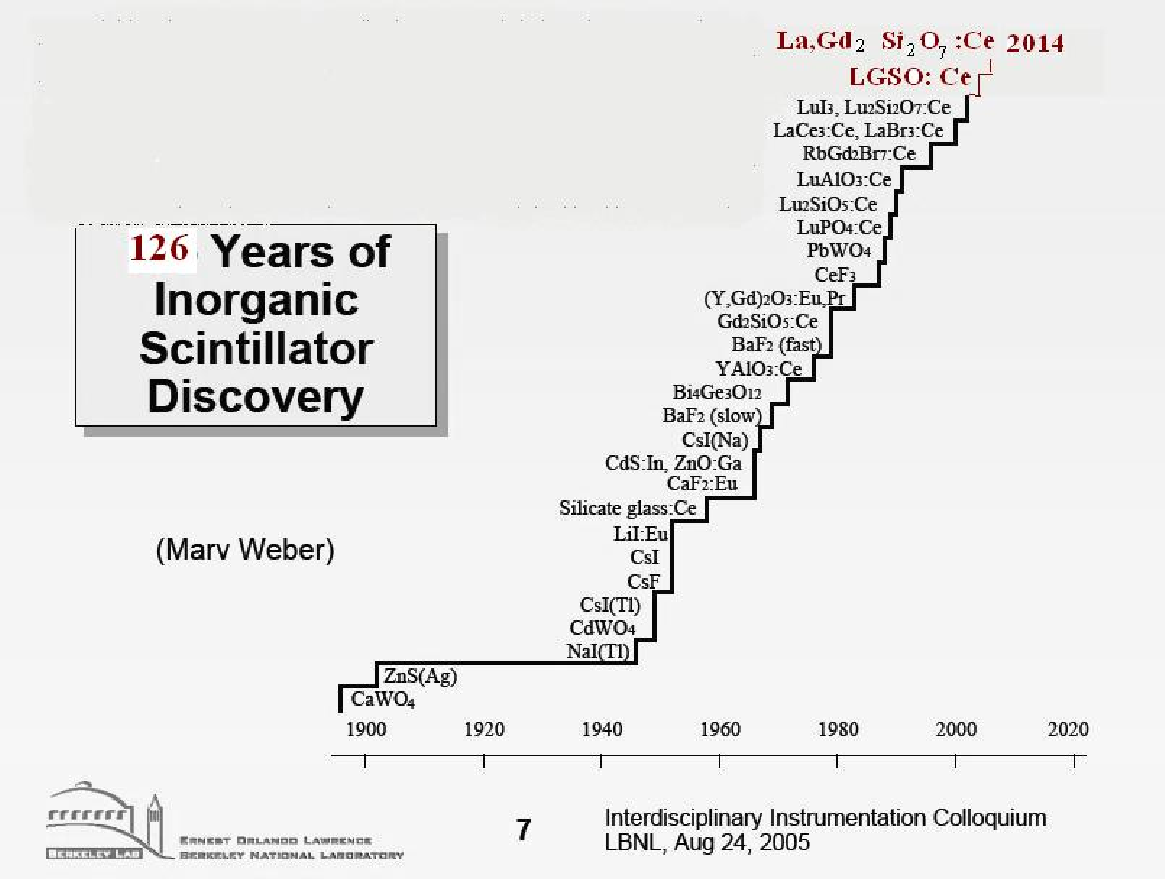

Figure 1.2 History of inorganic scintillators since 1990

1.8 Objective and scope of thesis

The motivation of this work is to obtain thermally stable LaF_3 based nanophosphor adopting different synthesis schemes schemes. The aim of the present study is to explore the different synthesis routes to obtain highly luminescent nanoparticles with narrow size distribution and demonstrate its application in the field of radiation detection. In this work, we have synthesized nano sized uncoated as well as surfactant capped $LaF_3:Ce^{3+}$ through four different methods. The synthesis of organic coated $LaF_3:Ce^{3+}$ was carried out by adopting the method of F.Wang *et al* [16] and uncoated $LaF_3:Ce^{3+}$ by adopting the method of R.N.Bhargava et al.,[6]. Their structure, particle size, UV-Vis absorption, Photo Luminescence behavior and Lifetime were studied. The synthesis route developed for the highly florescent uncoated $LaF_3:Ce^{3+}$ particles with narrow size distribution are first of its kind. For good size control, the uncoated particles were synthesized in acidic environment and its characteristics were studied. In acidic environmental synthesis, most of the time the product did not precipitate out, instead remains as very fine nano-colloidal solution. In both the uncoated and coated nanoparticle the optimum cerium concentration was determined. The PL studies were done with these colloidal samples and presented in this work. In order to shift the Cerium UV emission of 308 nm to visible range, Terbium was used as co-dopant and this was also studied systematically. The effect of thermal annealing on the uncoated particles in various atmospheres were studied and reported in this work.

Recent studies show that the core-shell structure provide good light amplification, the nano sized Lanthanum fluoride doped with cerium and co-doped with terbium was further coated with TiO_2 nano particles. The study of core-shell structure of $LaF_{3:}Ce,Tb/TiO_2$ is reported for the first time. In order to prepare nano sized cerium doped Lanthanum fluoride particles another synthesis method using Lanthanum Carbonate and hydrofluoric acid was alsoadopted. This method was very simple and easy to prepare in less time. The prepared product was characterized systematically and the results such as particle size, PL and TL performance were compared and presented here. In this method, the cerium was co-doped with europium and studied systematically.

With the nano luminescent particles obtained through all the methods the luminescent colloidal solution was utilized to fabricate transparent polymer nanocomposites. Thus obtained composite material was studied for its PL characteristics and results are presented here. The carried out work and discussions of the results are provided below chapter wise.

Chapter 2

The experimental facilities required for characterization of nanophosphors like XRD, TEM & SEM microscopy, DLS, FTIR, UV-Vis absorption, Spectrofluorometer, and thermo luminescence reader are elaborately discussed. Discussions about the methodology involved in nanoparticle synthesis and the experimental set up is also mentioned.

Chapter 3

In this chapter, the synthesis of (a) Oleic acid coated,(b) Oleic acid - Polyethylene Glycol coated and (c) uncoated , nano sized Cerium doped Lanthanum Fluoride (LaF_3:Ce) powder and its characterization are discussed. Another novel method of synthesizing LaF_3:Ce^{3+} by reacting lanthanum carbonate and hydrofluoric acid was attempted and the results of this study are also presented for the first time in this chapter. The phosphors obtained through each synthesis condition were characterized by XRD to identify the phase formation. Microstructures of these phosphors were determined by Scanning Electron Microscopy (SEM). The size distribution plot was obtained from the SEM. These samples were also examined for their luminescence properties by recording UV-Vis and Photoluminescence spectra. In addition, the molar ratio of cerium was increased and its influence on photoluminescence property is discussed. The phosphor system was codoped with Terbium and its PL properties were studied.

Chapter 4

The main issue of amplification of the PL output by introducing an external shell was addressed in this chapter. This chapter provides a brief introduction to the core-shell structure so far developed with LaF_3 molecule. The effect of external shell on nanophosphor surface on amplification of PL output is discussed. Attempts were made to amplify the light output by coating TiO_2. The enhancement of PL output by coating with TiO_2 on $La_{0.4}F_3$:$Ce_{0.45}$,$Tb_{0.15.}$ composite is first of its kind. TiO_2 coating on the composite was achieved by adopting a mechanical dispersion method at room temperature. Though XRD pattern did not reveal the presence of TiO_2 on the surface, the presence of coating and its thickness were confirmed using TEM, EDS and FTIR spectra. The UV-Vis absorption, the photo luminescence and Lifetime characteristics of the samples were studied. The effect of coating thickness on the PL behavior was studied and reported in this chapter. Scintillation under X-ray excitation was observed with uncoated and TiO_2 coated powder products.

The effect of non-stoichiometry of LaF_3 on the PL behavior of LaF_3:Ce^{3+} was studied and reported for the first time. This study demonstrates a possibility of introducing tunability by changing the stoichiometry.

Chapter 5

In this chapter, the results and discussion of radiation stability of these materials under gamma irradiation experiments are provided. The radiation induced degradation of optical properties of nano sized LaF_3:Ce^{3+} is addressed. TL measurements were carried out with OA coated LaF_3:Ce^{3+} nanocrystals, and the TL glow curve parameters were calculated.

Chapter 6

This chapter discusses the preparation of polymer nano composites (PNC) using the coated as well as uncoated synthesized nanoparticles and their PL and radio luminescence properties.

Chapter 7

This chapter summarizes highlights of the results described in each chapter.

References

[1] E. Wiedemann, Uber Fluorescenz und Phosphorescenz. Ann. der Physik 34 (1888) 446.

[2] G. Blasse, B. C. Grabmaier. Luminescent Materials, Berlin: Springer, (1994).

[3] H. Chander, Proc. of ASID ’06, 8-12 Oct, New Delhi (2006)

[4] A. Henglein, Chem. Rev. 89 (1989) 1861

[5] R.K. Jain, R.C. Lind, J. Opt. Soc. Am., 73 (1983) 647.

[6] R.N. Bhargava, D. Gallagher, X. Hong, A. Nurmikko, Phys. Rev. Lett., 72 (1994) 416.

[7] A.A. Khosravi, M. Kundu, B.A. Kuruvilla, G.S. Shekhawat, R.P. Gupta, A.K. Sharma, P.D. Vyas, S.K. Kulkarrni, Appl. Phys. Lett., 67 (1995), 2506

[8] L. Levy, D. Ingert, N. Feltin, M.P. Pileni, J. Crys. Growth., 184-185 (1998) 377.

[9] R. Jaganathan, K. Athinarayasamy, A. Mani, C.K.Jayasankar, Opt. Mater., 5 (1996) 57.

[10] Q. Li, L. Gao, D. Yan, Mater. Chem. Phy., 64 (2000) 41.

[11] Chung Hsin. Lu, Hsin-Cheng Hnog, R. Jagannathan, J. Mat. Sci. Lett., 21 (2002) 1489.

[12] H.X. Zhang, S. Buddhudu, C.H. Kam, Y. Zhou, Y.L. Lam, K.S. Wong, B.S. Ooi, S.L. Ng, W.X. QueH, X. Zhang, Mater. Chem. Phy., 68 (2001) 31.

[13] J. Wang, H. Song, B. Sun, X. Ren, B. Chen, W. Xu, Chem. Phys. Letts., 379 (2003) 507.

[14] J. Zhou, Z. Wu Zhang, W. Liu, H. Dang, Wear 249 (2001) 333.

[15] J.W. Stouwdam, van Veggel, C.J.M. Frank, Nano Letts., 2 (2002) 733.

[16] F. Wang, Y. Zhang, F. Xianping, W. Minquan, J. Mater. Chem., 16 (2006) 1034.

[17] X. Sun, Y.W. Zhang, Y.P. Du, Z.G. Yan, R. Si, L.P. You, C.H. Yan. J. Chem. Eur. 13 (2007) 2320.

[18] J-X. Menga, M-F. Zhang, Y-L. Liu, S-Q. Man, Spectrochimica Acta Part A 66 (2007) 81.

[19] J. Wang, J. Hu, D. Tang, X. Liu, Z. Zhen, J. Mater. Chem., 17 (2007) 1597.

[20] H. Deng, S. Yang, S. Xino, H.M. Gong, J. Chem. Soc.,130 (2008) 2032.

[21] G. Stryganyuk, V. Vistovskyy, V. Zakordonskyy, A. Gektin1, and A. Voloshinovskii, photon-science.desy.de/annual report/files/2009/2009774.

[22] M. Yao, A.G. Joly, W. Chen, J. Phys. Chem. C, 114 (2010) 826.

[23] M-Y. Xie, L. Yu, H. He, X-F. Yu, J. Solid State Chem., 182 (2009) 597.

[24] C. Kai, G. Chao, P. Bo, W. Wei, J. Nanomaterials 2010 (2010) 5.

[25] Q. Wang, Y. Yumin, R.D. Ludescher, Yiguang Ju, J. Lumin., 130 (2010) 1076.

[26] S. Janssens, G. Williams, D. Clarke, M. Sharp, Phys. Status. Solidi B., 248 (2010) 439.

[27] J.K. Han, G. Hirata, J. Talbot, J. McKittrick, Mater. Sci. Eng. B, 176 (2011) 436.

[28] L. Zhang, W. Li, X. Hu, Y. Peng, J. Hu, X. Kuang, L. Song, Z. Chen, Mater. Inter., 22 (2012) 488.

[29] S.G. Gaurkhede, M. M. Khandpekar, S. P. Pati, A.T. Singh, ISRN Mater. Sci. V (2012), Article ID 763048, 6; dx.doi.org/10.5402/2012/763048

[30] Sheng Dai Konxville et al Patent : US 2006/0054863 A1, March (2006).

[31] Cooke et al Patent US/2008/0128624 A1, June (2008).

[32] B. Wagner, Georgia Tech Research Institute, Nano@Tech: Jan. 14, (2014).

[33] W.J. Parak, D. Gerion, T. Pellegrino, Nanotechnology, 14 (2003) 123.

[34] J. Rietdorf, ISBN 3-540-23698-8, (2005).

[35] S. Rosenthal, Nat. Biotechnol., 19 (2001) 621.

[36] M.Y. Han, X. H. Gao, X.H. Su, S. Nie, Nat. Biotechnol., 19 (2001) 631.

[37] N.J. Withers, J.B. Plumley, B.A. Akins, A.C. Rivera, G. Medina, G.A. Smolyakov, G.S. Timmins, M. Osinski , Proc SPIE Proc. SPIE 7575, Colloidal Quantum Dots for Biomedical Applications V, 75750Z (2010); doi:10.1117/12.848944

[38] Derenzo, S. E. Interdisciplinary Instrumentation Colloquium. Berkeley: Ernest Orlando Lawrence Berkeley National Laboratory, (2005).

Chapter 2

Experimental

2.1 Nano sized LaF_3: Ln^{3+} synthesis method

Materials with nano size can be synthesized by physical techniques (Top down approach)such aspulsed laser deposition (PLD), ball milling and molecular beam epitaxy deposition as well as by adopting chemical techniques (Bottom up approach) involvingcombustion, sol-gel method, solvent-based wet chemical approach, and high & low-temperature aqueous precipitation method.

The low temperature (80°C) solution co-precipitation method was adopted throughout the work to synthesize nanosized samples have proved to yield reasonably high quality crystals. In this method, non-coordinating solvents (DM water and ethanol) were used to carry out the reaction. The precursor solutions are prepared and one precursor solution is injected slowly into to the other hot precursor solution. The nanoparticles nucleate and grow in a controlled manner and subsequently collected by centrifuging the solution after reaction is completed.

2.1.1Chemical reaction mechanism and size control

The reaction methodology suggests to add a precurcusor solution containing luminescent cations (dissolved $LaCl_3$ in DM water) to another heated precursor anionic solution (Fluoride) under constant stirring. The precursor solutions react and nucleate to form nanocyrstalline product precipitate at a temperature of 80 °C. Nanocrystal evolves after going through three stages; nucleation, growth, and Ostwald ripening (a phenomena in which smaller particles in solution dissolve and deposit on larger particles in order to reach a more thermodynamically stable state).

The important factors that influence these stages are the solute concentration and chemistry between the reactants and surfactants, temperature, and pH of the solution. I provide a brief introduction about the procedures adopted for the size controlled growth. Murray. C.B. et al., [1] in 1993 demonstrated that highly dispersed nanocrystals of CdE (E= S,Se, Te) can be obtained by rapid injection of one reactant into anotherhot precursor solution. This method involves temperature between 120 – 300°C and the particle size depends on the temperature of the mixture and the time of the reaction.In another interesting work,Gastón P. Barreto et al., [2], have demonstrated the effect of temperature (80- 140°C) on the particle size of ZnO. Microware assisted chemical method was adopted, involved variation of temperature by varying the power, which yielded smaller particles at low temperature. Along with exploration of nano synthesis by temperature variation, other ways by varying pH of the reacting environment were also attempted. The effect of pH on the crystal growth and photoluminescence at room temperature synthesis of ZnS:Pb was demonstrated by Promod.H.Dorse et al[3]. By acidifying the reacting environment ($pH < 5$), more hydrogen ions in the medium prevent the agglomeration of nucleated particles by surrounding them and repelling the neighboring particle, like the surfactant.

As the addition rate is also one of the key factors for nucleation and size control, in this work the addition of cationic solution was carried out by an automatic syringe pump. The pump has microprocessor controlled piston which pushes the 50 ml syringe to force the liquid into the reaction vessel. The flow rate and syringe volume data can be fed to the system. Throughout the work, 50 ml syringe was used and the flow rate was 50 ml/h.

In order to control the size during the synthesis, Oleic acid (OA) alone was used as surfactant material in one batch, a combination of OA and Polyethelene Glycol (PEG) was used as surfactant in another batch and acidic environment was adopted in another batch. The pH was varied by adding conc. HCl in the ammonium fluoride precursor solution that was heated first. Another novel method of synthesizing $LaF_3:Ce^{3+}$ by reacting lanthanum carbonate and hydrofluoric acid was also attempted and the results of this study are also presented for the first time.

Chemical equation

$$\mathrm{LaCl_3 + CeCl_3 + 3NH_4F \xrightarrow{OA\ /\ OA+PEG} LaF_3{:}Ce + 3\ NH_4Cl}$$ (For I and II phase of synthesis)

$\triangle$80°C

$$\mathrm{LaCl_3 + CeCl_3 + 3NH_4F \xrightarrow{Conc.HCl} LaF_3{:}Ce + 3NH_4Cl}$$ (For III phase of synthesis for co-doping $TbCl_3$ and $EuCl_3$ were also added)

$\triangle$80°C

$$\mathrm{La_2(CO_3)_3 + 6HF \longrightarrow 2LaF_3 + 3CO_2 + 3H_2O} \uparrow$$

$\triangle$ 70°C

2.1.2 Experimental setup for synthesis

The synthesis of nanocrystals by adopting the solution precipitation technique with slightly modified procedure reported by Wang.F et al., [4] was carried out in a three necked round bottom glass flask kept inside an oil bath and temperature was controlled by a microprocessor. For continuous stirring, the solution throughout the in reaction in the oil bath was kept on a magnetic stirrer with a teflon coated stirring bar in the solution. The whole setup was kept inside a fume hood. Microprocessor based condenser cooling circuit (with water) was connected with one neck of the flask and all the other necks were tightly closed. In order to inject slowly the precursor solution 2, an automated syringe pump was used. The flow rate and other specifications are fed to the system by pressing the corresponding switches. The photograph of the synthesis setup is shown in the figure 2.1. Two metal stands were used to hold the round bottom flask and the condenser unit. The chemicals required to make the precursor solutions were procured and stored in a desiccators filled with dry silica gel.The required amount of the chemicals were measured with the help of a physical balance, in small glass beaker using clean dry spatulas Rubber gloves were used as a safety precaution during handling of the chemicals. The glass vessels used for the synthesis were thoroughly cleaned with soap solutions and ordinary tap water, followed up with DM water and drying in an oven. After reaction completion, the precipitate was collected using a centrifuge. The collected precipitate was thoroughly cleaned with suitable solvents and DM water. Finally the collected wet precipitate was dried in a vacuum oven at 85 ˚C overnight. The dried precipitate was grinded using a mortar and the powder product was stored in a plastic container and labeled properly.

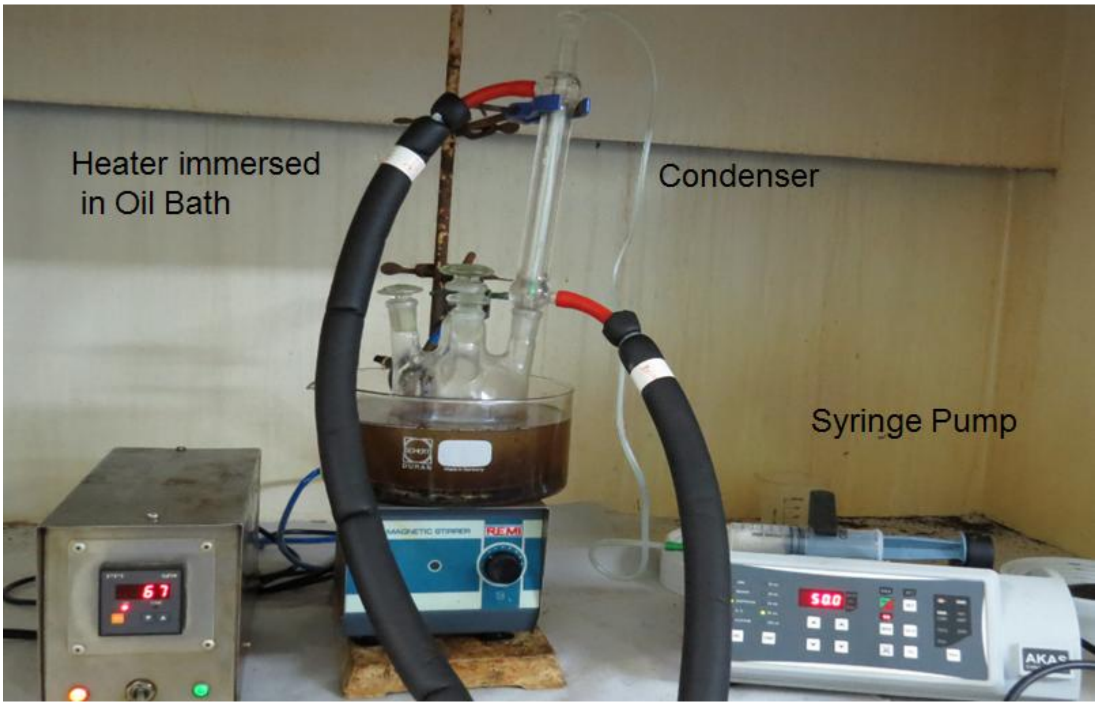

Figure 2.1 Photograph of experimental setup

2.2. Effect of surfactant / Shell on the core nanoparticles

In order to stabilize (avoid interaction with neighbor particles) the nanoparticles and at the same time amplify the light output a plain non luminescent / luminescent organic or inorganic material is used as a shell. The shell material covers the core luminescent material. The shell material mayinvolve in the excitation energy transfer mechanisms with the charge carrier clusters at trap sites originated from the activator levels and reduces the radiationless transfer. The study of the photo luminescent behavior of the core- shell structure is being carried out in the last two decades. First to study was the semiconductor as shell materials then followed up with rareearths. The three times increased light output was evidenced by Shu-Man Liu$_{a;}$et al., (2000) [5], through CdS coating upon CdSe. An effective strategy to improve the luminescence efficiency is to make core-shell structures. Stouwdam [6] and van Veggel et al., [7] in the year 2002&2004synthesized LanthanumFluoride shell on over the luminescent lanthanide ion core, which yielded higher PL intensity than the core (uncoated) material.In another demonstration of the core-shell work of Meng-Yin Xie et al., in 2009 [8] Europium doped LaF_3 core material was covered with plain LaF_3host material by a simple solution route and the quantum efficiency was increased by 27%.

In this work, we report for the first time TiO_2 used as shell material upon $La_{0.4}F_3$:$Ce_{0.45}$,$Tb_{0.15}$, by adopting a simple room temperature procedure.

2.3 Structural and compositional characterization

2.3.1 X-Ray diffraction Technique (XRD)

X-ray diffraction is used to obtain structural information about crystalline and polycrystalline solids. The inter atomic plane distance matches with the wavelengths of the X-rays, these are used to probe the materials and the interference pattern of the diffracted X-ray photons fetches the inner atomic structure. The XRD pattern is unique for each and every material. In 1912 W.L.Bragg developed a very simple relation between the position of atoms and the diffraction pattern. The path length (distance) travelled by the X-ray photon that traverses through two different atomic planes is provided by simple trigonometric relation $n\lambda=2d\ Sin\theta$; this equation related the Bragg angle θ and the atomic spacing‘d’. Then, Debye and Scherer evolved a relation between spread or the width of the diffracted peaks and the scattered angle known as “Debye Scherer” formula. It provides information about the size of the crystal. Throughout this work, structural characterization was carried out using Shimadzu (XRD-6000) as well as APD 2000PRO diffractometer equipped with a Cu K_{α}(1.5406 Å) X-ray source. The powder samples were placed in the sample holder and the scattered X-rays were scanned in 20°- 80 ˚angle. In order to cover the angle range with nominal rational speed, it takes 2 hrs. The diffracted data is processed and stored in the PC directly. STOE software was used calculate Crystallite size, lattice parameters and cell volume.

2.3.2 Scanning electron Microscopy

Scanning electron microscope is an electron microscope used to obtain high resolution images of the sample surfaces, using a highly focused energetic beam. The microscope possess an electron gun,a system to accelerate the produced electrons, a system of electromagnetic lenses to collimate and focus the beam and a detector for measuring the scattered electrons and X-rays which are generated in the process of scanning through electron matter interaction. The surface structure (morphology) of the sample is determined and imaged from the scattered electronic signals which are the sum of various components like back scattered electrons and diffracted electrons. The characteristic X-rays generated during the electron matter interaction process provides information about the elements present in the sample. The scattered electrons and the X-rays carry vital information such as the morphology, electronics density, and z of the particular analysis spot. The micrographs of as-prepared samples were observed by field emission scanning electron microscope (FESEM, ZEISS).

2.3.3 Sample preparation for FESEM

The Oleic acid coated samples were washed with acetone and dried. A very small quantity of the dried powder was dusted on top of the special carbon tape. The SEM instrument facilitates to mount six samples inside the analyzing chamber at one time. The chamber was closed tightly after sample mounting. After achieving high vacuum, the electrons generated are focused on the samples and the detector position is also focused accordingly to get a high resolution image. The detected electron signals were processed by suitable electronics and with help of the inbuilt software, the image was created and displayed on the screen. By adjusting the focus and travelling the position of the analyzing spot,the obtained highly resolution image was stored as a jpeg image.

2.3.4 TEM

The transmission electron microscope (TEM) is a sophisticated instrument used to view object's size of the order in{angstrom (10^{-10}m)}. This works on the principle as for light microscope but possess an electron source instead of light source. Electromagnetic lenses are used to focus the electron beam. The instrument requires high vacuum conditions for operation. Electron beam passes through the sample and undergoes scattering depending on the density of the material present. The transmitted electrons (unscattered) form the shadow image on the fluorescent screen. Contrast of the image varies with the density of the specimen. A photograph of the image can be obtained directly using a camera. Small amount of powder sample was dispersed in acetone, ultrsonicated for 30 mins and were transferred to a clean carbon film and was subjected to TEM analysis.

2.3.5Energy dispersive X-ray Fluorescence (ED-XRF)

Energy dispersive X-ray fluorescence technology (ED-XRF) provides one of the simplest and most accurate analytical methods for the determination of the chemical composition of many types of materials. The atoms in the sample material are excited by X-Rays emitted from the X-Ray tube. Atoms absorb or scatter the X-ray photons and also undergo photoelectric emission. In this process, X-rays are emitted from the atoms in the process of filling the vacant electronic orbitals. The unique set of energy levels, of atoms produces, the unique set of X-ray emission energies, allowingone to non-destructively measure the elemental composition of a sample. The process of emissions of characteristic

X-rays is called "X-ray Fluorescence" or XRF. Analysis using X-ray fluorescence is called "X-ray Fluorescence Spectroscopy." In most cases the innermost K and L shells are involved in XRF detection.X-Ray fluorescence signals are measured simultaneously in a fixed mounted semi-conductor detector or sealed gas-proportional counter. The instrument used for this study was EDXRF spectrometer of model EX-6600SDD supplied by Xenemetrix, Israel. The spectrometer is fitted with a side window X-ray tube (370W) that has Rhodium as anode. The power specifications of the tube are 3-60 kV; 10μA-5833μA. Selection of filters, tube voltage, sample position and current are fully customizable. The Silicon diode detector (SDD) is having energy resolution of 136eV ± 5eV at 5.9keV Mn X-ray and 10- sample turret enables keeping and analyzing 10 samples at a time. The quantitative analysis of the samples was carried out by the In-built software nEXT. As-prepared pellet sample was placed on the Mylar film and kept inside the X-ray chamber studying it.

2.4 Dynamic Light scattering (DLS)

The size of the particles in a colloidal suspension can be determined quickly by using the dynamic light scattering technique. The DLS technique is sensitive to total particle size and yields information which is weighted by the square of the particle volume. The results are generally convertedto volume or number weighting.The size distribution of nanoparticles is determined by using a Zetasizer-Nano (Malvern Instrument). It uses a He-Ne laser (4 mW, =633 nm) and avalanche photodiode detector. The Zetasizer-Nano measures the scattering information at an angle close to 180° (the detector position is at 173°).

2.5 FTIR spectroscopy

The surfactant present on the sample isconfirmed by using the Fourier Transform infrared, spectroscopy (FTIR). Photons of the infrared radiation energy region are used to probe the organic material as they are completely absorbed leading to molecular vibrations. Molecules vibrate either linearly along the chemical bond or by bending away from the equilibrium position of the bond. The FTIR spectrometer used here is a third generation IR spectrometer that incorporates advanced monochromaters, interferometers and Fourier transform of the raw data into the real spectrum. FTIR spectrometer can simultaneously collect and analyze a wide wavelength range within very short time. The spectrometer consists of a source (a heated material) which emits IR radiation, an interferometer, a sample and reference holder, an IR detector and associated electronics to convert the detected IR signal into an electrical data and displaying in the monitor. The interferometer is the heart of the FTIR instrument as this provides a relation between the difference in the intensity and the path difference between the two rays splitted by the beam splitter. FTIR instrument when used provides the IR spectrum as a plot of wave number in the X-axis vs percent transmittance in the Y-axis. Throughout the work HORIZON FTIR instrument was used to obtain the IR spectra in the transmission mode for the power samples.

Small quantity of the sample is thoroughly mixed with the KBr powder and made into a very thin transparent pellet. This pellet is mounted in the sample holder after taking the reference IR spectrum without the sample.

2.6 Optical Characterization

The general term optical characterization includes the absorption spectrum, photo luminescence emission and excitation, and life time measurement of the samples qualitatively and quantitatively. The samples are dispersed in a solvent (DM water)by ultrasonicating for 30 minutes to form a very dilute solution whichis transparent.

2.6.1 UV-Vis absorption spectroscopy

The UV-Vis absorption studies of the synthesized material were carried out using a UV-VIs absorption spectrophotometer (Shimazdu 1800 /2200 UV spectra scan). The block diagram of a spectrophotometer is shown in the figure 2.2. It is an instrument which measures the transmittance or absorbance of a sample as a function of the wavelength of electromagnetic radiation. The instrument works on the principle of Beer Lambert’s law. It consists of a radiation source either a Xenon lamp or tungsten lamp or a combination of it that emits a broad band of electromagnetic radiation, a monochormator/wavelength selector (using diffraction grating) which facilitates for the selection of the wavelength from the broad spectrum for transmitting through the sample , a sample holder (a cuvette to hold solutions and stand to fix the solid pellet sample) area , detectors (photomultiplier tubes) to collect and measure the intensity of radiation.

Each monochromatic beam in turn is split into two equal intensity beams by rotating disc device. One beam, the sample beam, passes through a small transparent container containing a solution of the compound being studied in a transparent solvent. The other beam, the reference, passes through an identical cuvette containing the solvent alone. The intensities of these light beams are then measured by electronic detectors and compared. The intensity of the reference beam, which should have suffered little or no light absorption, is defined as I_0 and the intensity of the sample beam is defined as I_S. Over a short period of time, the spectrometer automatically scans all the component wavelengths in the manner described. The ultraviolet (UV) region scanned is from 200 to 400 nm, and the visible portion is from 400 to 800 nm. If the sample compound does not absorb light of a given wavelength, $I_S = I_0$. However, if the sample compound absorbs light then $I_S < I_0$, and the difference is recorded. The instrument provides the result of the analysis as plot between the wavelength in nm on X-axis and the absorbance/transmission intensity on Y-axis.

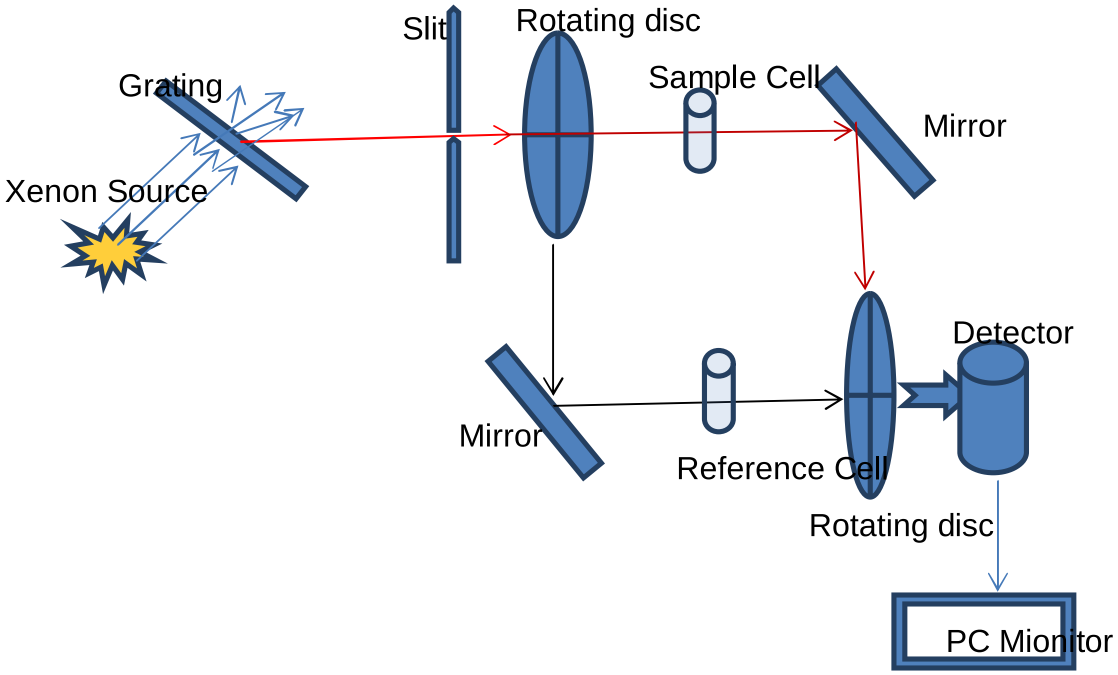

Figure 2.2 Schematic diagram of the UV-Vis absorption instrument

2.6.2 Photoluminescence spectroscopy

Photoluminescence spectroscopy is the study of the fluorescence and phosphorescence of materials by using light of various wavelengths for exciting the sample. The fluorescence spectrometer essentially consists of a radiation source emitting continuous radiation of a wide range of wavelengths. The source generally is a high pressure Xenon lamp that emits photons in the wavelength range 220-1200nm.The lamp needs continuous cooling as significant amount of heat is generated. The emitted light passes through a monochromator of wavelength selector. The selected light of a particular wavelength passes through a system of lenses and falls on the sample. The luminescent sample absorbs the radiation and gets excited and emits a light photon during de-excitation. The emitted photon is collected by the detector after getting passed through another wavelength selector and a system of optical lenses. The detector is a photomultiplier tube. With proper amplification of the electronic signal and processing, the detected information is displayed in the monitor as a plot between the wavelength in

X-axis and Photoluminescence intensity in Y-axis. Photoluminescence (PL) measurements on the nano-powder pellets were carried out using a SHIMADZU spectrophotometer [RF-5301PC] in the range of 200 – 900 nm at 1.5& 3 nm slit widths and in high/low sensitivity mode.Figure 2.3 shows the schematic diagram of the PL spectrophotometer.

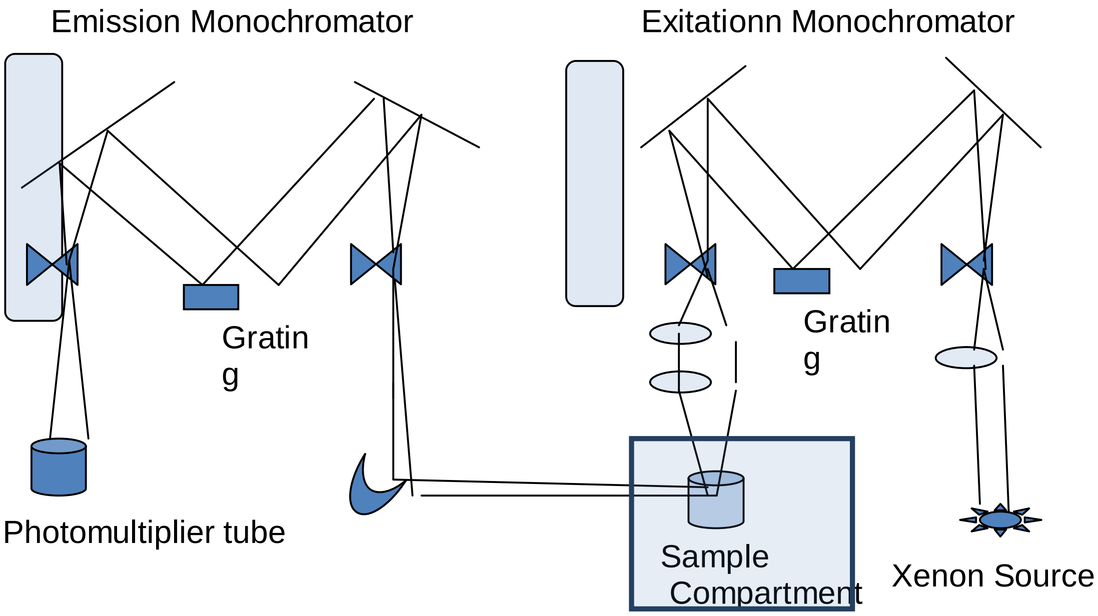

Figure 2.3 Schematic diagram of the PL spectrometer

2.6.3 Fluorescence Life time

Fluorescence life time is the average time spent by the molecule in the exited state before the emission. The emission decay is exponential which mostly follows simplefirst / second order decay kinetics. HORIBA – FluoroCube atSAIF, IIT Chennai was used to measure lifetime.The pulsed light is directed on the sample to excite the molecules into a higher energy state. The excited molecules typically decay back to their lower energy state by emitting a photon. Since the probability of decay is an exponential function of time,the observed rate of photon emission from the sample is given by: $I_r = (N_0/\tau)\ e^{-t/\tau}$ (1)

where I_r is the rate or photon (photons/s), N_0 is the number of excited atoms by the pulsed light, t is the observed time of photon emission, and τ is the characteristic decay time constant of the excited molecule. The instrument houses laser diodes which operates for picoseconds and has wavelength range from 370 nm to NIR and nanosecond LEDs with wavelength range 260 nm to NIR. The monocromator (using diffraction grating) facilitates for the selection of the wavelength from the broad spectrum and then the light is focused it on the sample. The pulsed laser light excites the sample for a very short duration of 5e-11 seconds and immediately stops. The sample de-excites by its emission. The emission light is again let through monchromators and focused on the photon detector. The output (PL intensity decay with time) of the detector is displayed on the PC monitor. The block diagram of the PL life time instrument is shownin the figure 2.4

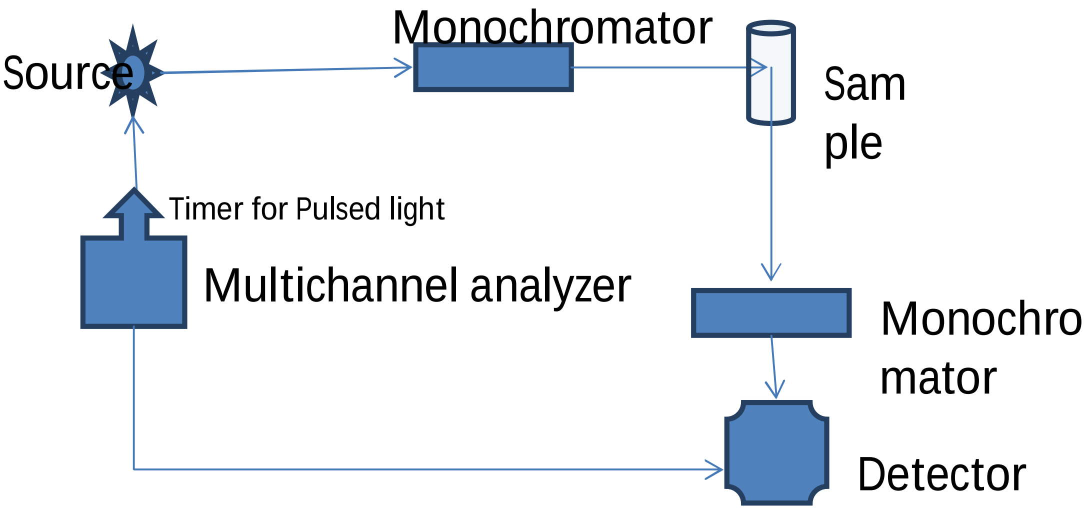

Figure 2.4 Block diagram of PL life time instrument

2.6.4 Thermolumniscent measuring set up

The instrument contains a sample holder provided with a heater at the bottom. Heating of the sample is through electrical means. The light from the sample is collected through an optical system to the photo detector.The detected signal is suitably processed and displayed as a plot between the temperature on the X-axis and TL intensity on the Y-axis. The temperature range and the heating rate can be modified using the software provided in the system. The data can be converted and stored in a .txt format. In this work thermo luminescent was studied for gamma irradiated powder samples. Around 10mg of the irradiated powder was taken and loaded in the brass holder and placed inside the reader. For beta irradiation, in housed Strotium-90 source was used for the required time through the software. The samples were heated in a series and the TL glow peak were recorded and stored.

References

[1]C.B. Murray, D.J. Norris, M.G. Bawendi, J. Am. Chem. Soc.,115 (1993) 8706.

[2]G.P. Barreto, G. Morales, M.L.L. Quintanilla, Journal of Materials, 2013 (2013), Article ID 478681, 11 pages (Hindawi Publishing Corporation).

[3]Pramod H. Borse,W. Vogel S.K. Kulkarni, J. Colloid. Interf. Sci., 293 (2006) 437.

[4]F. Wang, Y. Zhang, X. Fan, M. Wang, J. Mater. Chem.,16 (2006) 1031.

[5]S-M. Liua, H-Q. Guob, Z-H. Zhangb, R. Lib, W. Chena, Z-G. Wanga,Physica E., 8 (2000) 174.

[6]J.W. Stouwdam,F.C.J.M. van Veggel,Nano Letters,2 (2002) 733.

[7] J.W. Stouwdam, F.C.J.M. van Veggel,Langmuir,20 (2004) 11763.

[8] M-Y. Xie, L. Yu, H. He, X-F. Yu, J. Solid. State. Chem., 182 (2009) 597.

Chapter 3

Synthesis and Characterization of Cerium doped LaF_3 Nanoparticles

3.1 Synthesis of cerium doped LaF_3 nanoparticles

Nanoparticle synthesis generally goes with agglomeration due to their large surface area and chemically more active nature. This agglomeration minimizes the surface area and may affect its application. In the case of luminescence studies, the performance of the material is also dependent on the band gap energy. The agglomeration of particles resulting in bigger sized particles can lead to decreased band gap and altered luminescence properties [1]. The process of agglomeration of fine particles can happen during synthesis, subsequent drying or calcination of the synthesized product. Hence, it is vital to prevent the agglomeration at each and every step of the process till the desired product is reached.

One of the possible ways to prevent agglomeration during all the stages of synthesis is by introducing a surfactant into the system. The surfactant generally is a long chained organic material with hydrophobic and hydrophilic ends that surrounds the nucleated particle and prevent the grouping of particles by supplying charges to counter the attractive forces, which cause repulsion among them and keep them dispersed or by isolating the particles within the surfactant polymer. Depending on the polar nature of the solvent, the surfactant should be chosen. Electrostatic repulsive forces are very effective in a polar solvent, where long chained surfactant molecules through their interaction with the solvent and particle do the necessary de-agglomeration activity. Organic surfactant capped LaF_3:Ce has been extensively studied [2-5]. These Oleic acid, chitosan surfactants were often used in the synthesis of LaF_3 nanoparticles to minimize their size. The synthesis of ligand-capped LaF_3 nano crystals was first reported by Dang et al (2001) [6]. The excellent dispersibilty of Oleic acid surface modified Er,Yb doped LaF_3 molecules in common solvent and PMMA [Polymethylmetacrylate] matrix was demonstrated by Jianshe Wang et al in (2007) [7].

In this work during the first phase of the synthesis, Oleic acid (OA) was used as the surfactant to cover cerium doped Lanthanum Fluoride. It was observed that OA coated particles also agglomerated and got settled in the container with aqueous medium after sometime. Had there been no agglomeration, these particles probably could have been in the aqueous medium as colloidal particles due to their small sizes. In order to prevent the settling and form a uniform colloidal solution during synthesis, another hydrophilic organic surfactant: the Poly Ethylene Glycol (PEG) was added along with OA in the second phase of the experiment. The combination of the two surfactants resulted in good dispersibility of nanoparticles in aqueous medium. In the third phase of the experiment, synthesis of nano sized LaF_3:Ce without any organic coating was carried out in an acidic environment. The optical properties like absorption, luminescence and decay time are particle size dependent, the reaction conditions are generally varied to yield nano-particles with less agglomeration. R.N.Bhargav et al., 1994 [8] demonstrated the improved quantum efficiency of ZnS:Mn by 18% with reduction in particle size between 3.5-7 nm. A number of factors like concentration, temperature, reaction rate and pH of the reaction environment can be varied to synthesize very fine sized particles. Promod. H. Borse et al., (2005) [9] demonstrated that the ZnS particle size and its luminescence efficiency was strongly influenced by pH. The maximum light efficiency was obtained at a pH of 5 and the corresponding particle size was found to be 2.8 nm. In another interesting work Anindita Chatterjee et al.,(2006) [10] demonstrated the pH dependency of size and photoluminescence output with ZnS nanoparticles. Also WolfgangScha et al., (2009) [11] demonstrated the effect of pH on the particle size as well as on the photoluminescence. The highest quantum yield was found to be at pH 14 in their studies.

In this study, we have varied the pH during the synthesis to compare the particle sizes and luminescence from the nano particles obtained through both coated and uncoated routes.

In the fourth phase of the experiment we have synthesized LaF_3:Ce without any coating by one more new and simple method so far not reported, by reacting lanthanum carbonate with appropriate amount of hydrofluoric acid through a solution based route. The synthesized samples were characterized using XRD, DLS, SEM, UV-Vis absorption, Photoluminescence and Life time.

3.2 Experimental

High-purity $LaCl_3.7H_2O$ (99.99%), $CeCl_3.7H_2O$ (99.99%) and $NH_4F.6H_2O$ (99.99%) Ethanol, Polyethylene glycol (PEG), Oleic acid, conc. Hydrochloric acid and Hydroflouric acid (40%) were used as such without further purification. LaF_3:Ce was synthesized adopting co precipitation technique developed by Feng Wang et al., (2006) [12]. First batch of LaF_3 synthesis was carried out using Oleic acid as surfactant. Around 4g of the Oleic acid was added to 86 ml of ethanol and an alcoholic solution was prepared. Appropriate amounts of $LaCl_3$ (3.3583 g, 9.04299 millimol),$CeCl_3$ (0.16844 g, 0.4521 millimol 5%) were added in another beaker and were dissolved in 100 ml of DM water (Sol 2), and stirred well and sonicated for 30 minutes. Then NH_4F (1.00483g, 0.02128 mol) was taken in another beaker and dissolved in 10 ml of DM water. Then the alcoholic solution containing the Oleic acid was added to the ammonium fluoride solution (Sol1) and thoroughly stirred. Sol1 was transferred to the three necked flask kept inside oil bath maintained at constant temperature 80°C and stirring was continued. After 30 minutes, sol 2 was added to heated sol 1 drop wise using a syringe pump whose flow rate was set at 50 ml/h. The mixture was heated and stirred for another one hour for the reaction to be completed. A milky white precipitate was formed in the solution. After attaining room temperature, the flask was removed from the oil bath and the solution was transferred to two plastic centrifuge tubes in stages. The precipitate was collected by centrifuging the mixture at 6000 rpm for 20 minutes. The precipitate was washed with ethanol and DM water to remove the excess Oleic acid and other unreacted components. This procedure was repeated thrice. Finally, the precipitate was dried in vacuum oven at 85°C for 5 h.

In the second phase of the work, the combination of the surfactant of Oleic acid and PEG was used. This synthesis of lanthanum fluoride nanocrystals is based on a modified approach developed by Feng Wang et al (2006) by adding a combination of surfactants. Sol 1 was prepared using 1g of Oleic acid, 87 ml of ethanol and 2ml of PEG solution. Solution 2 (Sol2) was prepared in the first phase of preparation. Rest of the preparation procedure followed were the same as in the first phase of synthesis till the final dried product was obtained. $La_{1-x}F_3:Ce_x$ samples were synthesized for x=0.005, 0.01, 0.03 and 0.05.

In the third phase of the experiment, precursor solutions were prepared by using DM water alone. The pH of ammonium fluoride solution was modified to pH=4.2 by adding few ml of conc.HCl and stirred (sol 1-100 ml). Sol 2 was prepared with 50 ml of DM water, Similar first phase procedure was followed to get the product. The final dried product was obtained by following the above said procedure. Samples were synthesized at pH=4.6 and 5.6 respectively. Similarly $La_{1-x}F_3:Ce_x$ samples were synthesized for x=0.01, 0.03, 0.05, 0.1 and 0.2 at pH=4.6. At this pH precipitate product could be easily collected.

Appropriate amounts of $La_2(CO_3)_3$ (3.3583 g, 7.335 millimol), $CeCl_3$ (0.16844 g, 0.4521 millimol (5%)) were added in another beaker and were put in 10 ml of DM water and ultasonicated for 30 minutes (sol-1). Then HF (1.1002g, 22.5002 millimol) was taken in a Teflon beaker and diluted with 10 ml of DM water (sol-2). Sol-2 was heated in a water bath at 70˚C for about 30 minutes and then sol-1 was added rapidly to hot sol-2.

Reaction takes places instantaneously with effervescence and formation of water and CO_2. The mixture was stirred for 30 min at 70 ºC and then cooled to room temperature. White precipitate product was obtained after heating under IR lamp. The product was transferred to a filter paper placed on cleaning (Millipore) setup. The product was cleaned thoroughly with dil.HCl to remove the unreacted carbonate and then with DM water. The wet powder on the filter paper was transferred to glass dish and dried as said as above.

3.3 Structure and compositional characterization

3.3.1 XRD

X-ray diffraction technique and Scanning electron microscope were used to characterize the various synthesized, coated and uncoated nano particles of LaF_3:Ce. Figures 3.1 represent the XRD pattern of $LaF_3:Ce^{3+}$ obtained in all the four methods of the experiment. In figure 3.1, curve (a) represents nano sized particles coated with Oleic acid alone, (b) surfactant combination of Oleic acid and PEG, (c) without any coating at pH 4.2 and (d) by reacting lanthanum carbonate with hydrofluoric acid. Crystallite size was calculated using Scherrer formula $D=0.9\lambda/\ \beta \cos\theta$, where $\lambda=1.54184$ Å Cu (average) X-ray wavelength; β=FWHM; θ half of peak angle. The average crystallite size was calculated for (002), (110), (111), (300) and (113) distinct orientations. Curves (a) and (b) possess broad, distinct orientations with a high background pattern which are arising from the organic surfactants present on the surface of the particle. It is obvious that the XRD spectra for the first and second phase of synthesis condition resulted in nanosized crystallite, with average size around (a) 17 and (b) 12 nm respectively. Curve (c) shows well defined orientations with narrow diffraction peaks indicating a better crystalline phase formation. The average crystallite size from all the above said orientations was 29 nm. This suggests that at pH 4.2 probably better nucleation and growth of grains was possible. Curve (d) shows less intensity peaks with noisy signals which might be due to the carbonates presence. The large width of the diffraction peaks indicates the formation of the nanosized crystals. The crystallite size from all the above said orientations was 30 nm. These nanoparticles form in a hexagonal structure with lattice constants of a =7.168 Å and c = 7.3355 Å, which are consistent with the values in the database of LaF_3 (JCPDS 032-0483). Figure 3.2 shows the XRD patterns of the $La_{1-x}F_3:Ce_x$ nanoparticles (x = 0.005, 0.01, 0.03 and 0.05) synthesized using the combination of OA and PEG. Table 3.1 shows the experimentally determined lattice parameters using the (STOE) XRD software program.

Table 3.1: Lattice parameter of $La_{0.95}F_3:Ce_{0.05}$

S.No	Method	a (Å)	c (Å)
1.	OA	7.188 (2)	7.323 (3)
2.	OA+PEG	7.188 (4)	7.323 (4)
3	At pH 4,2	7.189 (2)	7.359 (3)
4	La_2CO_3 +HF	7.188 (2)	7.343 (4)

Figure 3.3 shows the XRD patterns of the $La_{1-x}F_3:Ce_x$ nanoparticles (x = 0.05) synthesized under different pH conditions. Curve (a) represents pH 4.2 (b) pH 4.6 and (c) pH 5.6. Figure 3.4 (a) shows the XRD patterns of the $La_{1-x}F_3:Ce_x$ nanoparticles (x = 0.01, 0.03, 0.05, 0.1 and 0.2) synthesized at pH=4.6. Figure 3.4(b) shows the XRD patterns of the $La_{1-x}F_3:Ce_x$ nanoparticles (x = 0.05, 0.1 and 0.2) synthesized using lanthanum carbonate and HF. Overall the XRD measurements did not indicate any shift in peak even at high dopant concentration. The uncoated samples synthesized in the acidic environment have yielded crystals with better quality when compared to the surfactant coated sample. No detectable signals of $CeCl_3$ /NH_4F/CeF_3 phases were observed.

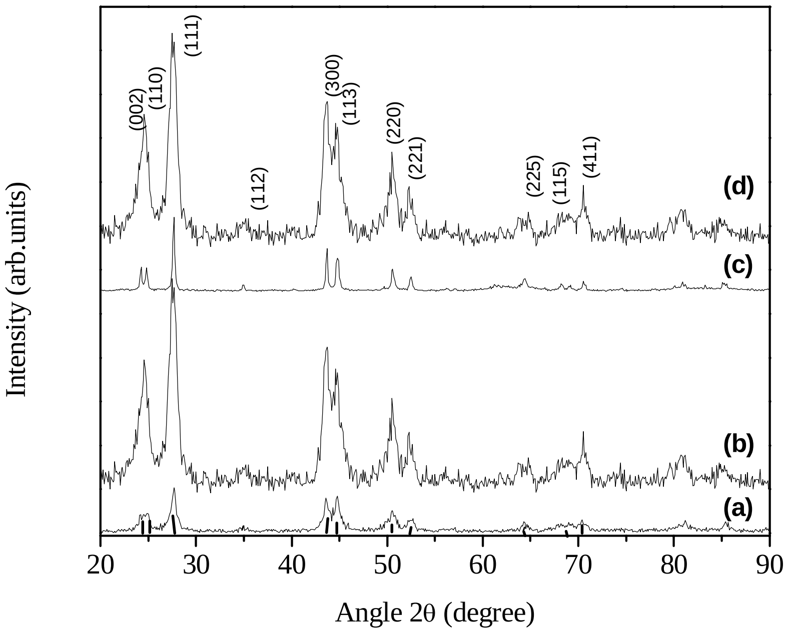

Figure 3.1 XRD pattern of $La_{0.95}F_3$:$Ce_{0.05}$ (a) nanosized particles coated with Oleic acid alone; (b) combination of Oleic acid and PEG ;(c) in acidic environment and (d) with Lanthanum carbonate and HF.

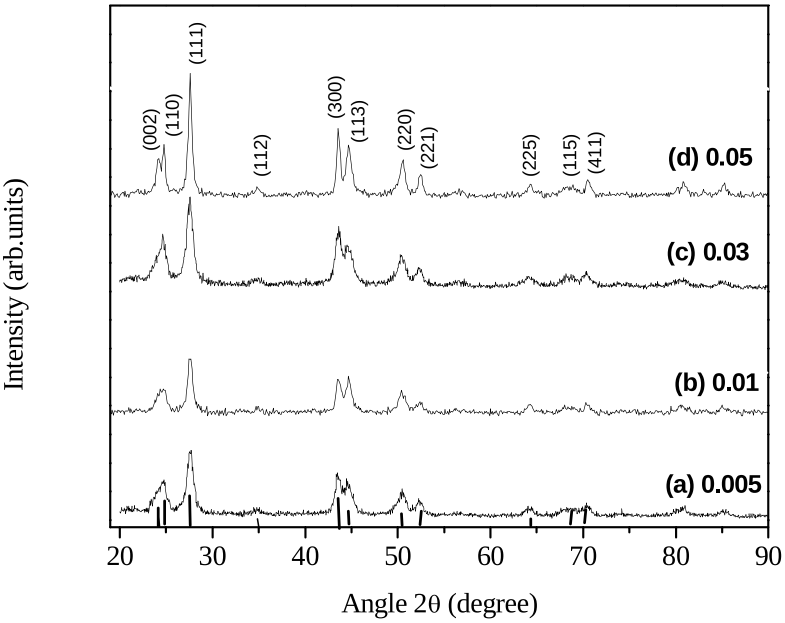

Figure 3.2 XRD pattern of the $La_{1-x}F_3$:Ce_x ,(a) x= 0.005;(b) x=0.01;(c) x=0.03 & (d) x= 0.05 synthesized with OA and PEG .

Table 3.2: Lattice parameters and cell volume of $La_{1-x}F_3$:Ce_x (OA+PEG)

S.No	**Dopant x=**	**a (Å)**	**c (Å)**	**Cell Volume (Å)^3**	**Crystallite Size (nm)**
1	0.005	7.189 (2)	7.359 (2)	328.68	19
2	1	7.186 (2)	7.349 (4)	328.64	15
3	3	7.188(2)	7.348 (3)	328.78	16
4	5	7.181 (3)	7.35 (3)	328.23	19

There was no change in the positions of diffraction peaks. This is due to the similar ionic radius of Ce^{3+} (1.034 Å) and La^{3+} (1.061 Å) and therefore, Ce^{3+} ions can substitute for La^{3+} ions in the LaF_3 crystal lattice easily without changing the crystal structure significantly [13]. Crystallite size was calculated for all 'x' values ($La_{1-x}F_3$:Ce_x) and shown in Tables 3.2, 3.3 and 3.4 along with calculated lattice parameters, cell volume and the crystallite size using the STOE XRD software program.

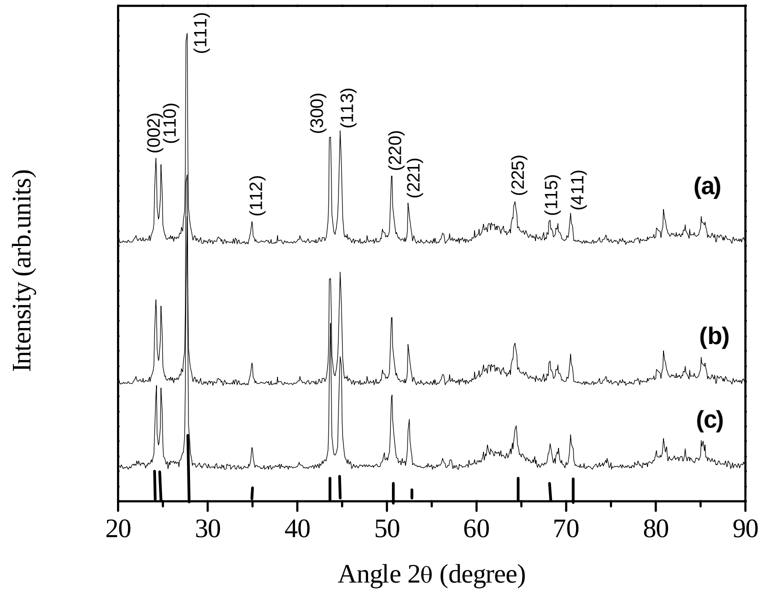

Figure 3.3 XRD pattern of the $La_{1-x}F_3$:Ce_x (x = 0.05) nanoparticles Curve (a) pH 4.2 (b) pH 4.6 and (c) pH 5.6

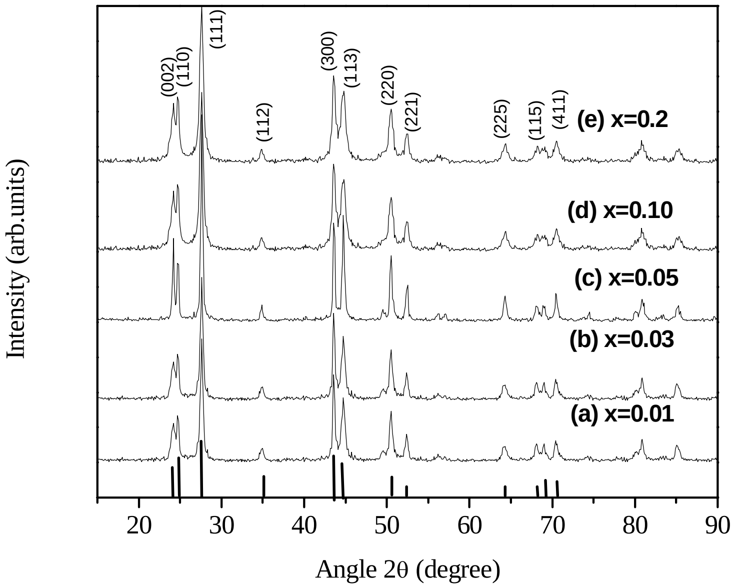

Figure 3.4(a) XRD pattern of the La$_{1-x}$F$_3$:Ce$_x$ ((a) x = 0.01;(b) x=0.03;(c) x=0.05;(d) x=0.1; and (e) x= 0.2, synthesized at pH 4.6

Table 3.3. Lattice parameter and cell volume of the La$_{1-x}$F$_3$:Ce$_x$ samples prepared at pH=4.6 environment

S.No	**Dopant X=**	**a (Å)**	**c (Å)**	**Cell Volume (Å)^3**	**Crystallite Size (nm)**
1	1	7.183 (3)	7.349 (2)	328.68	52
2	3	7.188 (2)	7.350 (3)	328.87	28
3	5	7.186 (5)	7.350 (4)	328.67	22
4	10	7.185 (2)	7.345 (4)	328.48	33
6	20	7.186 (3)	7.343 (6)	328.43	22

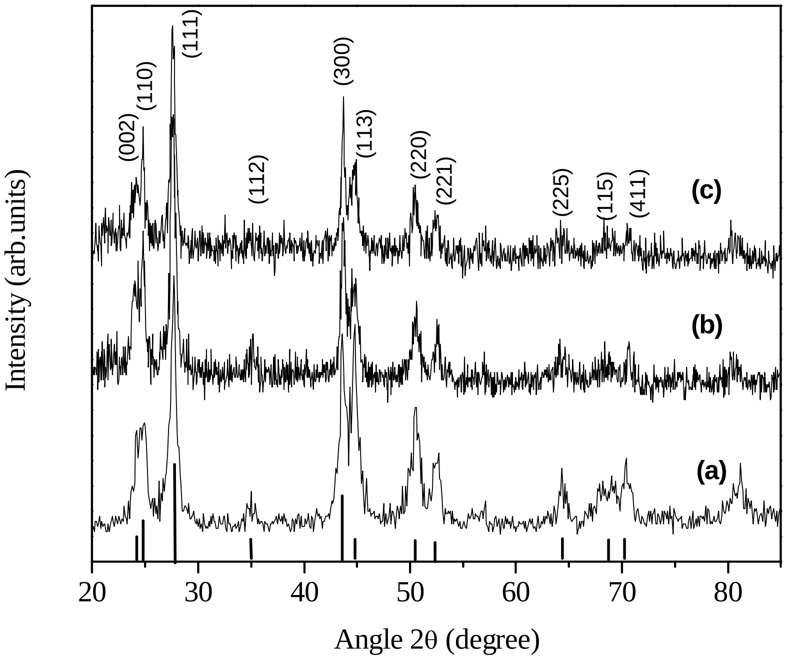

Figure 3.4(b) XRD pattern of the $La_{1-x}F_3:Ce_x$ (a) x = 0.05;(b) x=0.10 and (c) x=0.20 with HF

Table 3.4 Lattice parameter and cell volume of $La_{1-x}F_3:Ce_x$ prepared using HF method.

S.No	Dopant X=	a Å	c Å	Cell Volume $(Å)^3$	Crystallite Size (nm)
1	5	7.183 (3)	7.349 (2)	328.68	30
2	10	7.162 (6)	7.352 (6)	330.60	30
3	20	7.172 (3)	7.356 (4)	328.48	22

3.3.2 XRF elemental composition

Figure 3.5 shows the elemental presence of lanthanum and cerium in one of the $La_{0.95}F_3:Ce_{0.05}$ confirmed through the XRF experiment. Table 3.5 presents the experimentally estimated data.

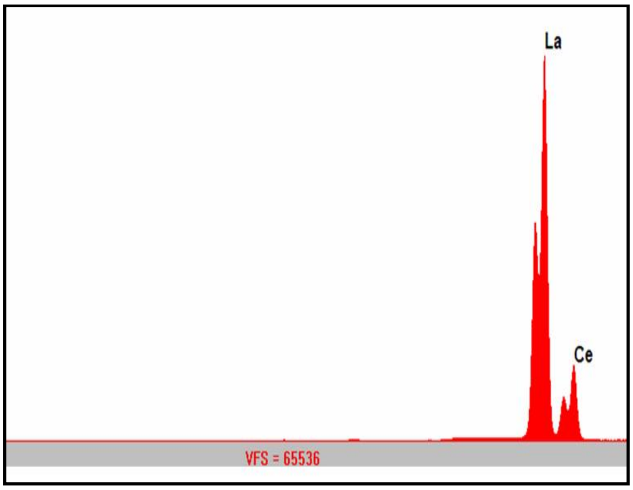

Figure 3.5 Elemental composition spectra obtained with XRF

Table 3.5 Elemental composition of $La_{0.95}F_3:Ce_{0.05}$

S.No	Element	Concentration %
1.	La	95.184 (error 0.477)
2.	Ce	4.816 (error 0.142)

3.3.3 FESEM

Figure 3.6, 3.7, 3.8 and 3.9 show the FESEM micrographs of the LaF_3:Ce particles with surfactants Oleic acid alone, OA and PEG, at pH 4.2 and synthesized using lanthanum carbonate with hydrofluoric acid respectively. In figure 3.6 the particles appear to be flattened and not of spherical shape and also were of irregular shapes. The size of the particles was ranging between 12 and 790 nm. Agglomeration of particles was clearly evident. In figure 3.7 the particles though spherical were slightly oblong in shape with the diameter ranging between 8 and 36 nm. However, some agglomeration of particles leading to bigger sized particles was also observed. The modified approach with the combination of OA and PEG yielded particles of smaller size compared to Oleic acid alone. In figure 3.8 the particles appear spherical with uniform microstructure. The image indicates absence of any hard agglomerates. It is clear from figure 3.9 that the particles are spherical in shape with uniform microstructure. However there is some agglomeration observed. In order to know about the particle size, a size distribution plot was arrived at by using the ImageJ software. Figures 3.10, 3.11, 3.12 and 3.13 show the size distribution histogram plot of the particles obtained in OA alone, OA and PEG combination, in acidic environment and lanthanum carbonate with hydrofluoric acid. With Oleic acid (Figure 3.10) bigger sized agglomerated particles were seen. The particles were in wide range from 12- 790 nm with maximum number of particles of 167 nm sized. With Oleic acid and PEG combination as surfactant (Figure 3.11) the particles had narrow distribution between 6- 30 nm respectively. The maximum number of particles were seen having size around 12-15 nm. Few agglomerated particles were also present. Figure 3.12 for the sample prepared in acid environment without any surfactant shows that the particle sizes were between 6-55 nm and the maximum number of particles had a size of 22 nm. Figure 3.13 shows the particle nature synthesized by the method using lanthanum carbonate with hydrofluoric acid. The particles possessed an average particle size of 68±19 nm, The FESEM results has brought out the fact that with oleic acid alone, indeed the agglomeration is significant. The particle sizes in cases of combined surfactants (Oleic acid and PEG) or no surfactants (acidic environment alone) were nearly same or comparable.

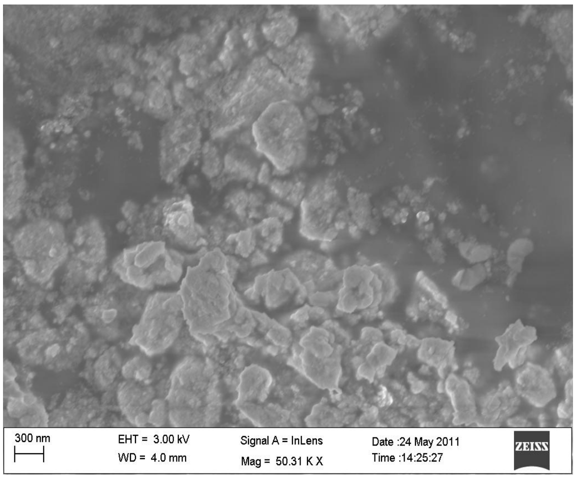

Figure 3.6 FESEM image of the Oleic acid coated particles

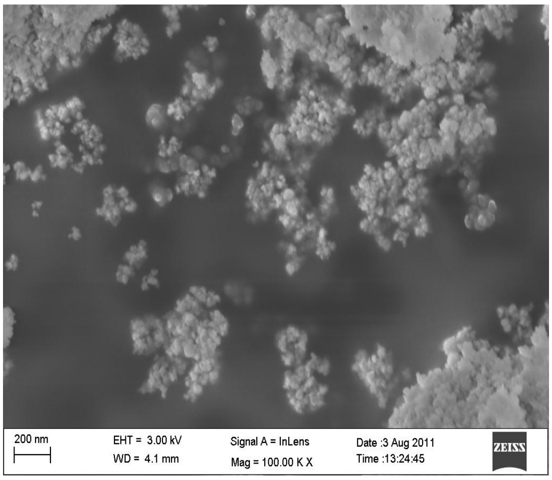

Figure 3.7 FESEM image of the Oleic acid and PEG coated particles

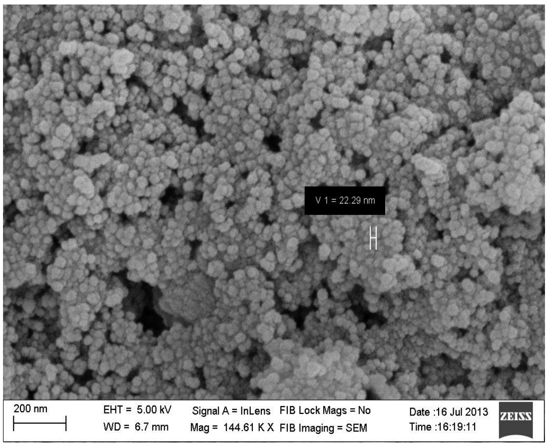

Figure 3.8 – FESEM image of the uncoated Particles synthesized at pH 4.2

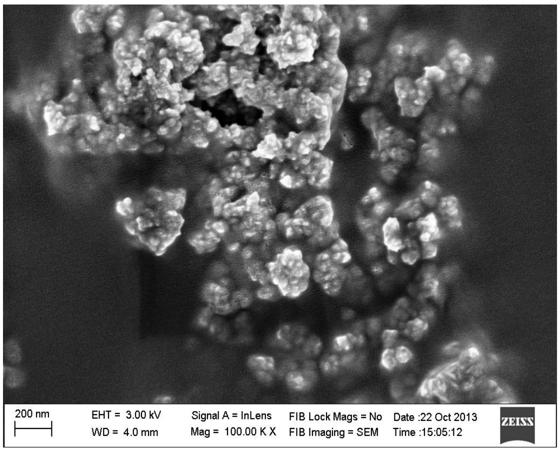

Figure 3.9 - FESEM image of uncoated particles Synthesized by reacting lanthanum carbonate with Hydrofluoric acid

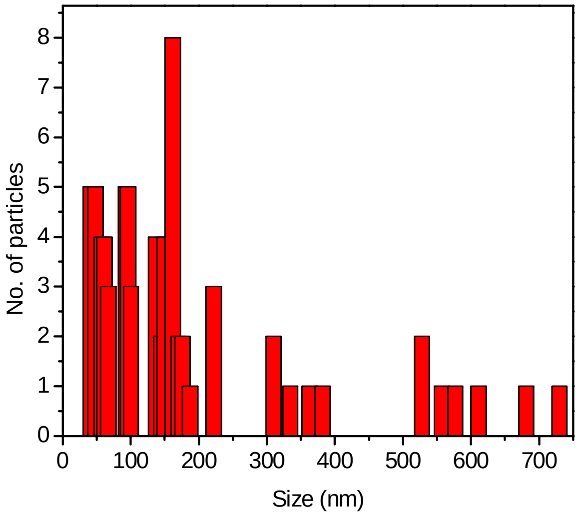

Figure3.10. - Size distribution plot of the particles synthesized using OA alone

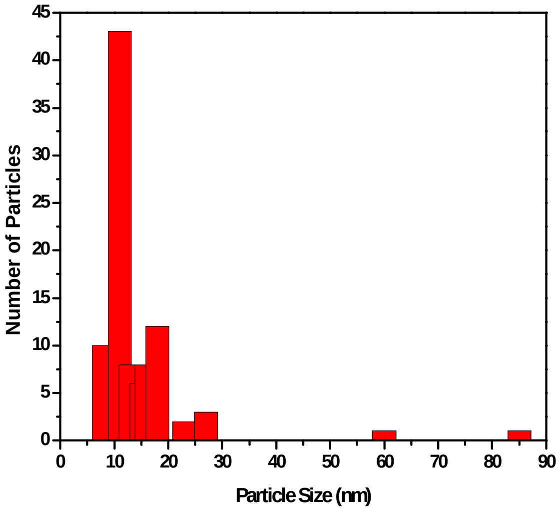

Figure 3.11 - Size distribution plot of the synthesized using OA and PEG

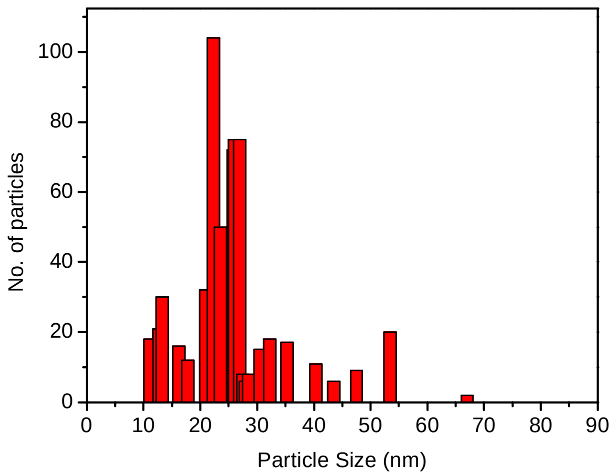

Figure 3.12 - Size distribution plot of the particles synthesized at pH=4.2

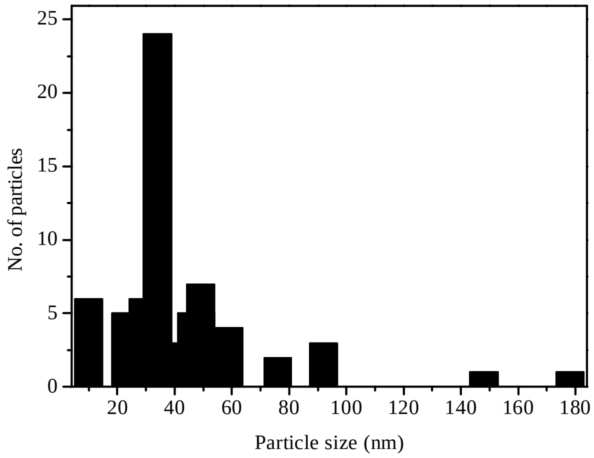

Figure 3.13 - Size distribution plot of the particles synthesized with lanthanum carbonate and HF

3.4 Dynamic Light Scattering (DLS)

Colloidal solutions were prepared by taking 5 mg of the synthesized powder samples and dispersed in 5 ml of DM water, ultrasonicated for about 30 min. This colloidal solution was used for particle size measurements using DLS technique. In case of DLS measurement, the particle size is calculated taking the motion of the particle and light scattering by it. In the case of acidic synthesis, as-prepared samples were taken for dispersion. Figure 3.14 (a & b) show the size distribution of the of oleic acid coated LaF_3:Ce particles. Majority of the particles were between 5 and 350 nm and the rest particles were of bigger sizes ranging from 300 to 750 nm. Figure 3.15 (a & b) show the size distribution of the particles synthesized using OA and PEG. Almost all the particles were between 150-225 nm and the majority were 200 nm sized. This clearly brings out the fact that combination of surfactants has really resulted in nano sized particles as observed earlier with the FESEM. Figure 3.16-3.19 show the size distribution plot of the colloidal samples from the as-prepared samples synthesized at various pH conditions 4.2, 4.6, 5.6 and in HF method respectively. With pH 4.2, majority of the particles were between 20 and 30 nm and the range was 10-55 nm. In case of pH 4.6, majority of the particles were between 30 and 40 nm with the range of 10-140 nm and for pH 5.6, majority of the particles were between 30 and 40 nm with the range of 25-200 nm. This shows that as the pH increases, the size of the particles as well as the distribution also tend to increase. Figure 3.19 shows the size distribution of the sample synthesized using lanthanum carbonate with hydrofluoric acid. It is clear from the figure that majority of the particles have 215 nm and have a range between 190-480 nm. The heavy agglomeration might be due to the DM water medium supporting agglomeration. The DLS measurement indicates that combination of Oleic acid and PEG results in small size and narrow size distribution which can also be obtained without any coating in the acidic environment with a low pH and is represented in the figure 3.20.

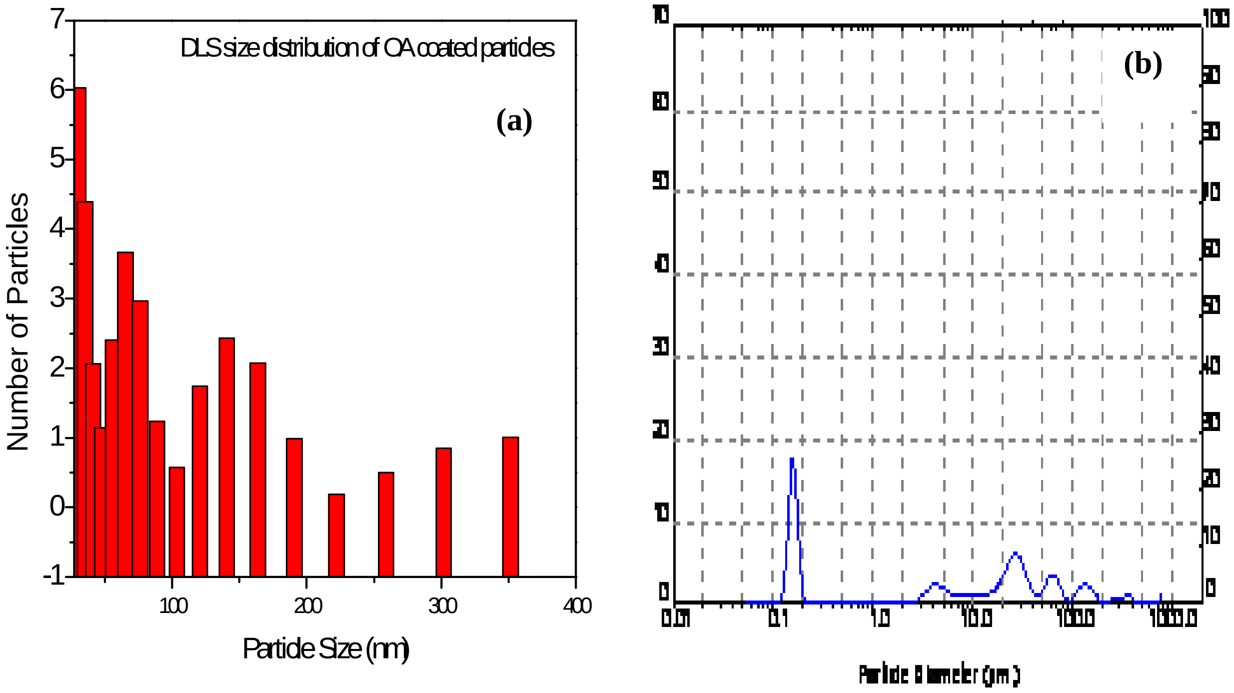

Figure 3.14 (a) Size distribution (b) histogram plot of the $La_{0.95}F_3$:$Ce_{0.05}$particles synthesized using OA coating

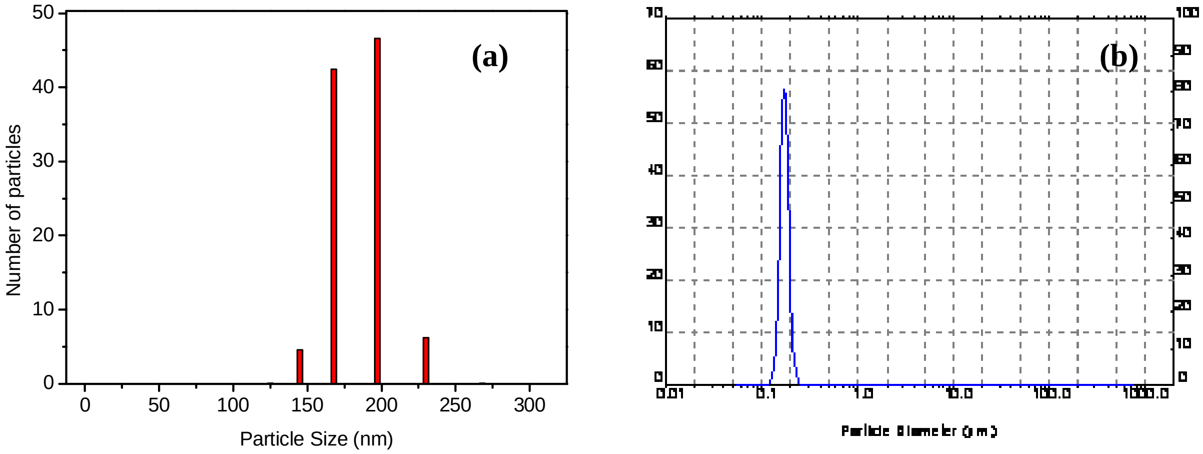

Figure 3.15. (a) Histogram plot of the $La_{0.95}F_3$:$Ce_{0.05}$ particles synthesized using OA and PEG ; (b) Size distribution plot obtained from the instrument

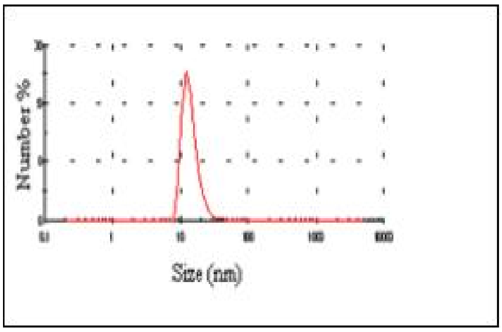

Figure 3.16 Size distribution plot of uncoated LaF_3:Ce particles synthesized at pH=4.2

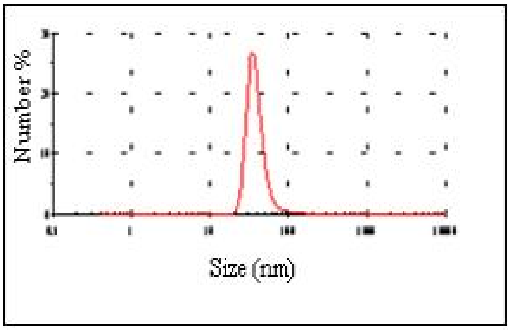

Figure 3.17 Size distribution plot of uncoated LaF_3:Ce particles synthesized at pH=4.6

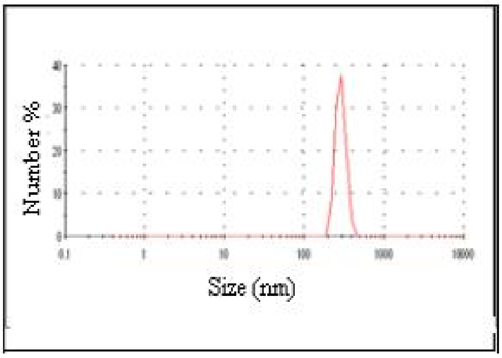

Figure 3.18 Size distribution plot of uncoated LaF_3:Ce particles synthesized at pH=5.6

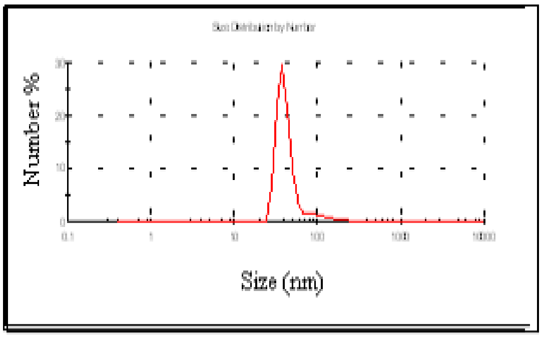

Figure 3.19 Size distribution plot of uncoated LaF_3:Ce particles synthesized with lanthanum carbonate and hydrofluoric acid

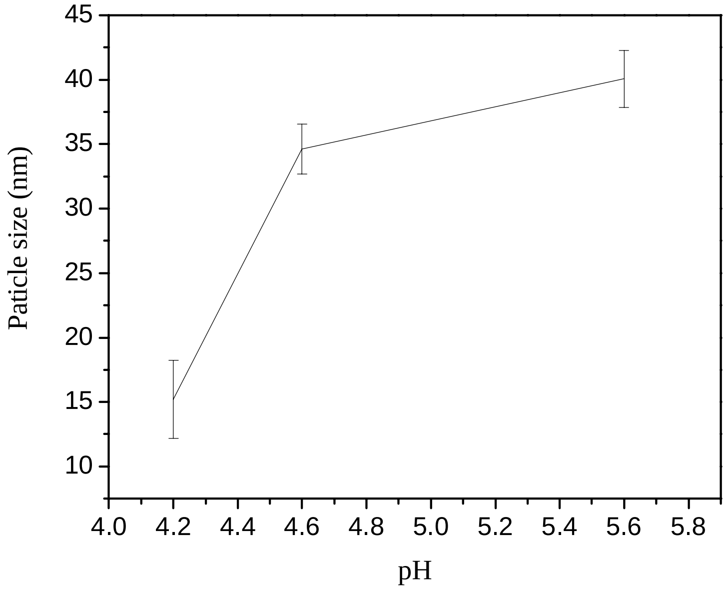

Figure 3.20 pH vs particle size of uncoated LaF_3:Ce particles

3.5 FTIR

Figure 3.21 shows the FTIR spectra of pure oleic acid (a), (b) oleic acid coated LaF_3:Ce nano particles, (c) pure PEG and (d) OA plus PEG coated LaF_3:Ce . In curve (a) the two peaks at 2841 and 2754 cm^{-1} correspond to CH_2 asymmetric and symmetric stretching vibration frequency of Oleic acid. Presence of both these peaks in the curve (b) for oleic acid coated LaF_3 indicates the presence of the organic surfactant Oleic acid on the surface of LaF_3:Ce nano particle. A similar observation was also made by N.Wu et al 2004 [14]. In the curve (b) the peak for carboxyl group at 1708 cm^{-1} (for C=O) observed for Oleic acid (a) is absent. Instead, two new bands at 1582 and 1453 cm^{-1} are observed and these can be assigned to asymmetric (COO^-) and symmetric (COO^-) stretch of the carboxylate formed on the nano LaF_3:Ce surface. In curve (c) the 1090 cm^{-1} strech is due to the C-O-C and 2872 cm^{-1} due to $-CH_2$ stretchings. These groups are attached to the nanosized LaF_3:Ce nano along with Oleic acid coating. Due to this C-O-C addition, the $-CH_2$ peaks are slightly shifted towards higher wave number. This is in confirmation with the observations made by J.Zhou et al., 2001[6], and Joanne Manson et al., [27]. The disappearance of C=O stretching vibration and presence of two COO^- stretching confirms that Oleic acid is not physically adsorbed on the surface of LaF_3:Ce nano particle rather it is coordinated through carboxylate group with nano particle. These results confirm that Oleic acid as well as PEG molecules were chemisorbed on nano LaF_3:Ce particles (Jianshe wang et al., 2007)[7].

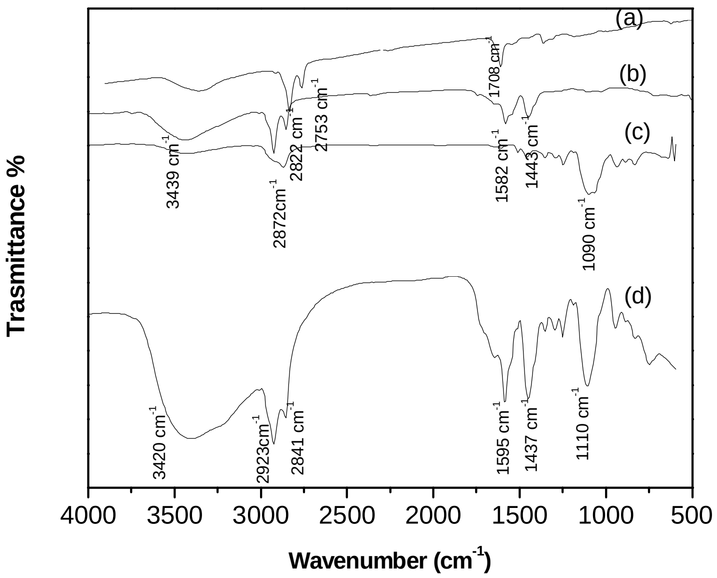

Figure 3.21 FTIR spectra of (a) Oleic acid; (b) Oleic acid coated LaF_3:Ce nanoparticles (c) PEG; (d) Oleic acid and PEG coated LaF_3:Ce nanoparticles

Figure 3.22, shows the FTIR spectra of (a) pure lanthanum carbonate, curve (b) as-prepared LaF_3:Ce and (c) annealed product at 900˚C. In curve (a) the intense peaks at 1450 cm^{-1} and 1388 cm^{-1} are attributed to the vibration modes of $(CO_3)_2$ group. The observed split in the band might be due to the carbonates in different crystallographic location (non-equivalent site) [15]. The absorption peak at 3500 cm^{-1} is attributed to the stretching vibration of the O–H bond [12-16]. In curve (b), the product LaF_3 seems to posses certain amount of impurity (unreacted components). The peaks at 1052 cm^{-1}, 846 cm^{-1} and 700 cm^{-1} can be ascribed to the symmetric stretching modes of $(CO_3)_2$ groups of rare earth carbonates [13, 17]. In curve (c), the absence of carbonate signatures are clearly seen which is due to the decomposition of carbonates at 900°C releasing CO_2 gas which leaves the product matrix.

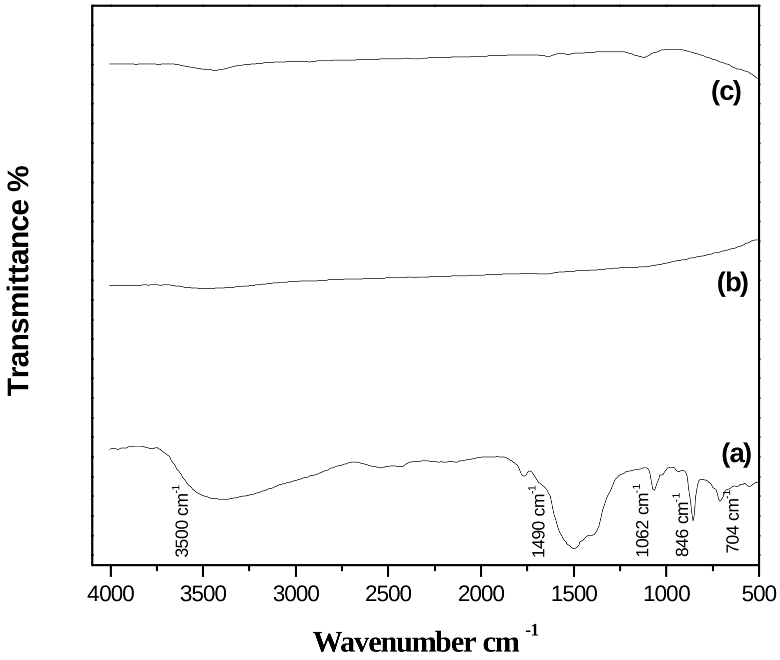

Figure 3.22 FTIR of (a) pure La_2CO_3; (b) as-prepared LaF_3:Ce; (c) annealed LaF_3:Ce at 900 °C

3.6 Optical Characterization

3.6.1 UV-Vis absorption

The colloidal solution sample (prepared as described earlier) was used for UV-Visible absorption measurements. Figures 3.23-3.27 show the UV-Visible absorption spectra of the samples $La_{1-x}F_3:Ce_x$. Figure 3.23 shows the Ce^{3+} absorption spectrum of OA coated $La_{1-x}F_3:Ce_x$ (x=0.05). The weak absorption peaks at 208, 225 and 250 nm are clearly seen. Figure 3.24 show curves (a) DM water blank and (b) OA with PEG coated $La_{1-x}F_3:Ce_x$ (x=0.05). Curve (b) shows absorption at 218, 234 and 250 nm with a better clarity compared to the OA coated LaF_3:Ce.

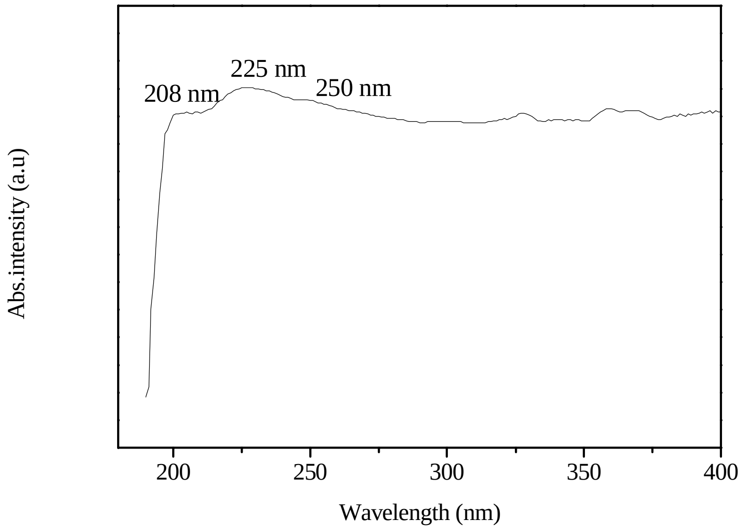

Figure 3.23 UV-Vis absorption spectra of $La_{0.95}F_3$:$Ce_{0.05}$, coated with OA

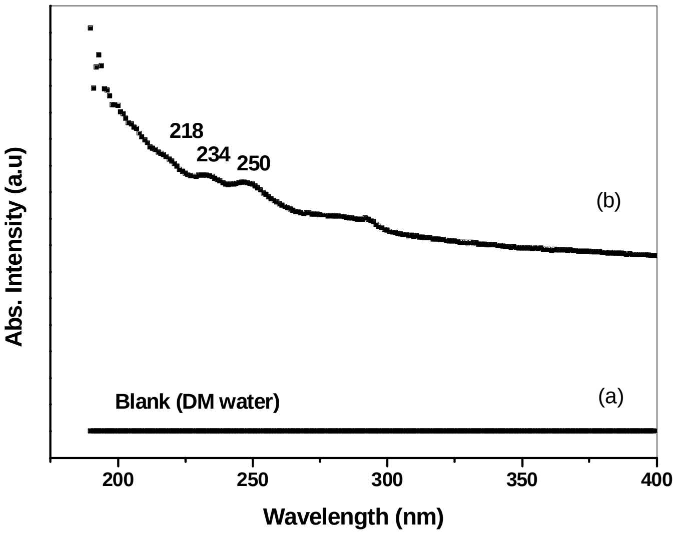

Figure 3.24 UV-Vis absorption spectra of $La_{0.95}F_3$:$Ce_{0.05}$, coated with OA and PEG

Figure 3.25 shows the absorption spectra of the as-prepared colloidal solution sample containing uncoated $La_{0.95}F_3$:$Ce_{0.05}$ obtained through the acidic route. In figure 3.25 curves (a), (b) and (c) represent samples synthesized at pH of 4.2, 4.6 and 5.6 respectively. All the curves show absorption at 200, 217, 231 and 247 nm. However the peaks are not well resolved. Moreover, it was further observed that there was a minute shift in the 244 nm absorption towards the blue region in the sample synthesized at pH 4.2 compared to samples prepared at higher pH. This is probably due to smaller particle (12 nm) as mentioned earlier as smaller particles are expected to increase the band gap. Figure 3.26 show the absorption curves (a) showing five distinct, clearly resolved absorption peaks (a) at wavelengths 198, 205, 218, 234 and 247 nm.

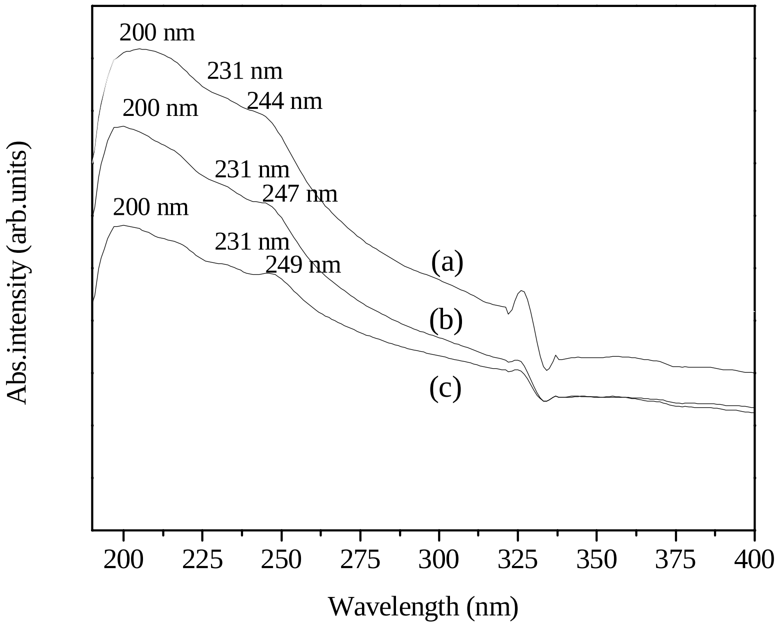

Figure 3.25 UV-Vis absorption spectra of the uncoated $La_{0.95}F_3$:$Ce_{0.05}$ obtained at different pH (a) 4.2; (b) 4.6; (c) 5.6

Figure 3.26 shows the absorption peaks of the uncoated $La_{1-x}F_3$:Ce_x samples synthesized at pH 4.6 In figure 3.26 curves (a) represent the DM water blank ;(b) x=0.01;(c) x=0.03;(d) x=0.05;(e) x=0.10 and (f) x=0.2. It is clear that as cerium concentration increases the peaks become distinct as absorption depends on the concentration.

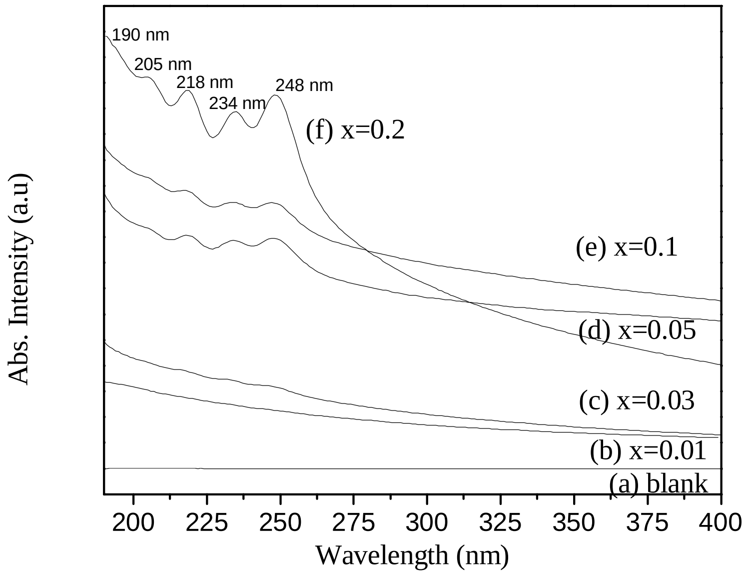

Figure 3.26 UV-Vis absorption spectra of the uncoated samples of $La_{1-x}F_3:Ce_x$ (a) blank DM water ;(b) x=0.01;(c) x=0.03;(d) x=0.05;(e) x=0.10 and (f) x=0.2.

Figure 3.27 shows the absorption peaks of the uncoated $La_{1-x}F_3:Ce_x$ sample synthesized by reacting Hydrofluoric acid and Lanthanum carbonate. In figure 3.27 curves (a) represent the DM water blank and curve (b) $La_{0.95}F_3:Ce_{0.05}$ respectively. The absorption peaks are clear similar to the absorption curves in figure 3.26.

Figure 3.28 show the absorption of (a) DM water blank (b) undoped LaF_3 (c) cerium chloride solution and (d) $La_{0.95}F_3:Ce_{0.05}$. There is no significant absorption by plain LaF_3 in the 220-250 nm range, but absorbs significantly at wavelengths less than 220 nm. The reason for absorption is not clear but might be due to impurities or defect present in the matrix [13]. Plain cerium chloride (bulk) solution shows (curve c) absorption at 298 nm and has flat region in the 190-250 nm range. Curve (d) shows all the five energy levels distinctly in the 190 -250 nm range moreover the absorption of $CeCl_3$ at 298 nm disappears. This clearly demonstrates that the added cerium present in the lattice of nano sized LaF_3 host. The absorption wavelengths correspond to the lower energy levels of Ce^{3+} as shown in figure 3.29 (P.Dorenbos (2000) & L.R.Elias) [18 and 19] and are consistence with observations made by Heaps et. al., (1973) & Coutts et al., (2004) [20 and 21].

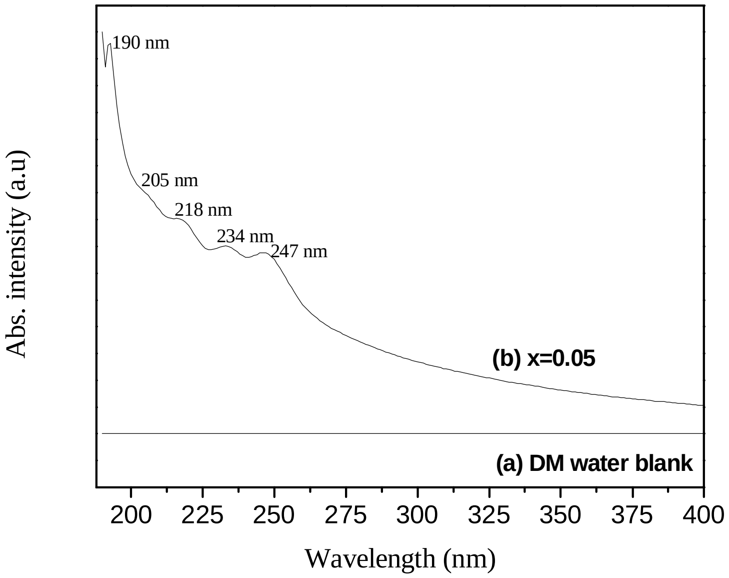

Figure 3.27 UV-Vis absorption spectra of the uncoated samples of $La_{1-x}F_3:Ce_x$ prepared using HF method (a) blank DM water and (b) x=0.05

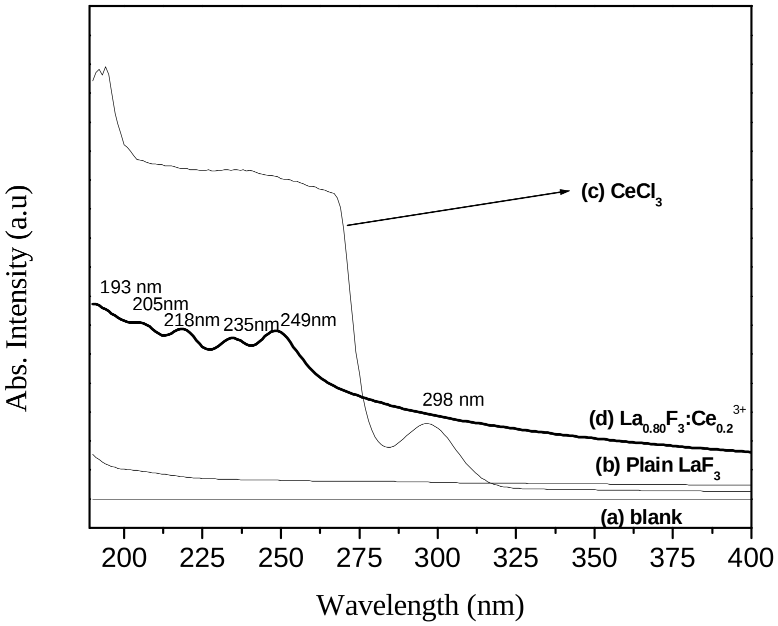

Figure 3.28 UV-Vis absorption spectra of (a) blank DM water; (b) Plain LaF_3 ; (c) $CeCl_3$ and (d) $La_{0.80}F_3:Ce_{0.2}$

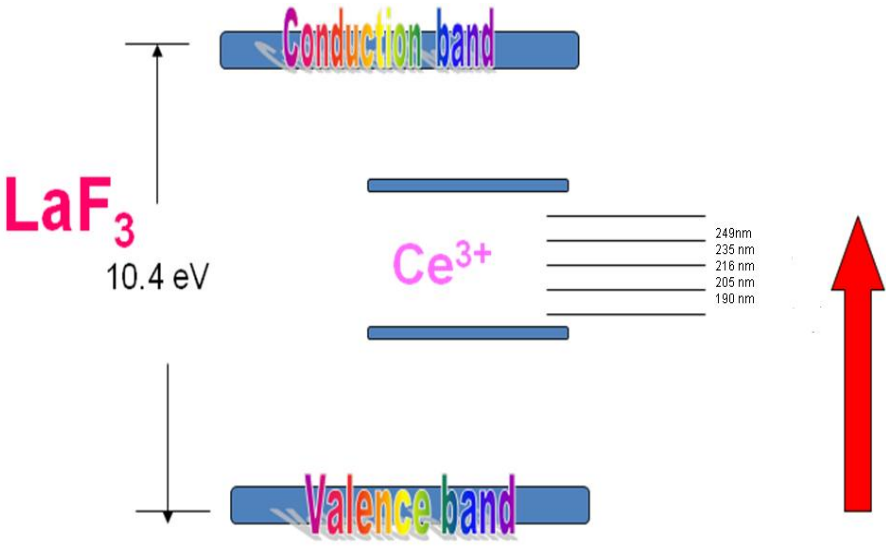

Figure 3.29 Energy level explanations

3.6.2 Study on the settlement of the suspended nanoparicles in DM water

The settling of the particles in a nano colloidal suspension of OA, OA with PEG and Uncoated coated LaF_3:Ce was studied by observing the UV-Vis absorption periodically for 10 days. About 2.3 mg of the nano powder was dispersed well in 100 ml of DM water by ultrasonicating for 30 minutes. These solutions were kept undisturbed in three beakers. The sample for UV-Vis absorption measurements was taken from the top surface of the liquid.The results of the experiment are provided graphically in figures 3.30, 3.31 and 3.32 corresponding to OA ,OA with PEG and uncoated respectively. It is clear that absorption decreases with increase in time. The decrease in the absorption was about 40 (OA), 66 (OA+PEG) and 42% (uncoated) loss, which indicates that rest of particles, has settled. The result shows that uncoated and OA coated appears to have better suspendabilty.

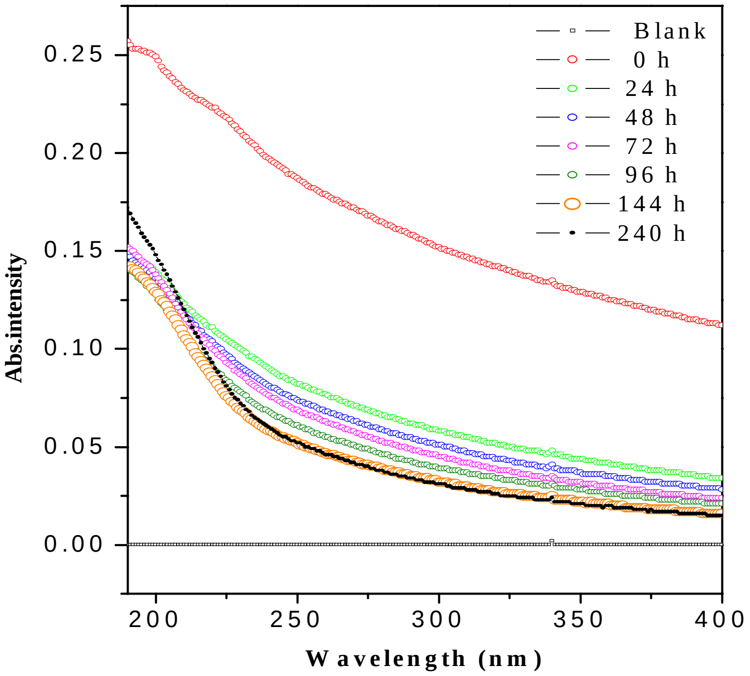

Figure 3.30 UV-Vis absorption of OA coated $La_{0.95}F_3$:$Ce_{0.05}$

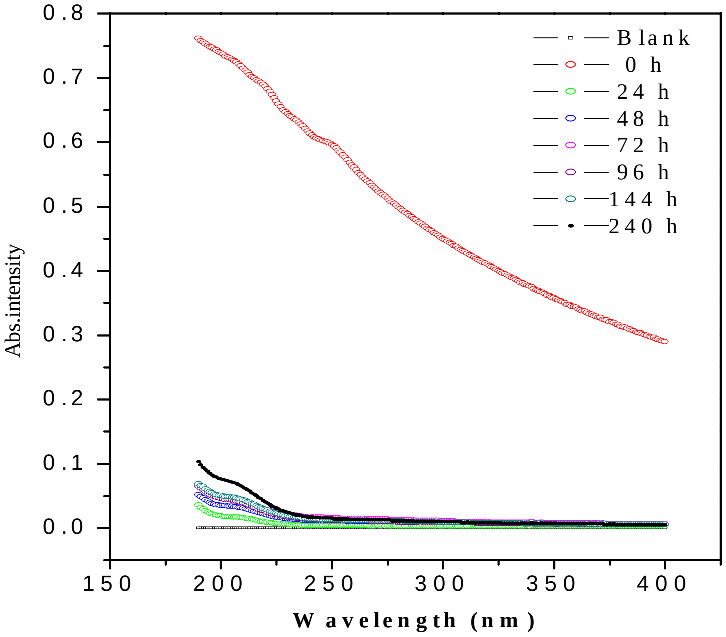

Figure 3.31 UV-Vis absorption of OA and PEG coated $La_{0.95}F_3$:$Ce_{0.05}$

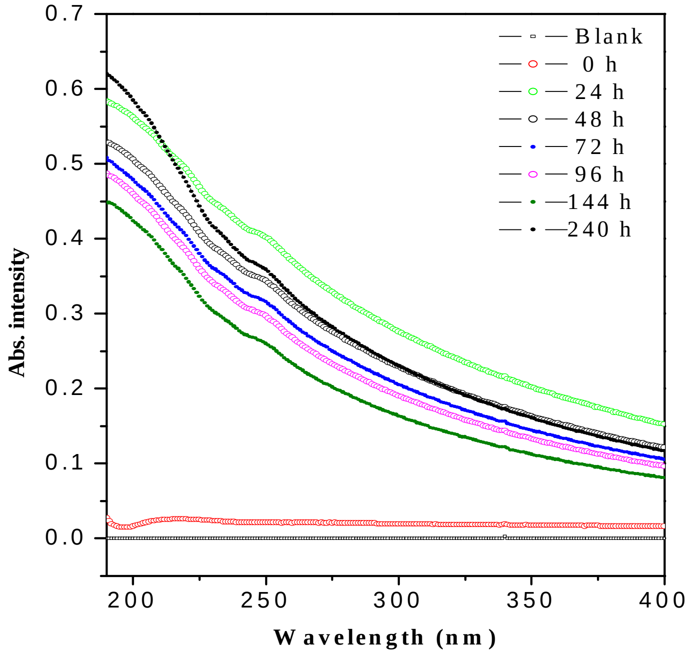

Figure 3.32 UV-Vis absorption of uncoated $La_{0.95}F_3:Ce_{0.05}$

3.7 Photoluminescent characterization

3.7.1 PL of OA coated $La_{0.95}F_3:Ce_{0.05}$

Figures 3.33 (A) and 3.33 (B) represent the PL spectra of Oleic acid coated $La_{0.95}F_3:Ce_{0.05}$ powder pellet. In figure 3.33(A) the 311 nm emission was obtained when the sample was exited at 251nm wavelength. The spectrum was recorded with slit width of 1.5 nm. The excitation and emission spectra shown are in agreement with that reported in literature [N.J.Withers et al., 2009] [22]. Moreover, with OA coated $LaF_3:Ce$, another emission peaking at 361 nm was observed corresponding to the 251 nm excitation as shown in figure 3.33 (B). In order to find out the individual PL contribution, around 1 mg of cerium chloride powder was added to 5 ml of oleic acid ultrasonicated well to get an uniform solution, for the PL measurement. Similarly 1 mg of plain powder LaF_3 (undoped) was added and shaken well. Figure 3.34 shows the PL spectra of pure oleic acid curves (a & b), oleic acid with cerium chloride salt curves (c & d)) and oleic acid with Plain LaF_3 curves (e & f). It is clear that some slight signature of Ce^{3+} emission with poor intensity in the oleic acid and Cerium chloride solution curves (c & d). It is also evident that the contribution of 361 nm peak, which has a corresponding UV absorption at 220 nm arises from the combination of oleic acid and plain LaF_3 matrix. The PL intensity of 361 nm decreases as the excitation wavelength increases towards 270 nm. The predominate 361 nm emission was observed in the OA and PEG coated LaF_3:Ce as shown in figure 3.34. All the samples synthesized with organic coating displayed this 361 nm emission, whereas this was absent in the uncoated samples as it is evident from figure 3.35. However this emission requires further investigations.

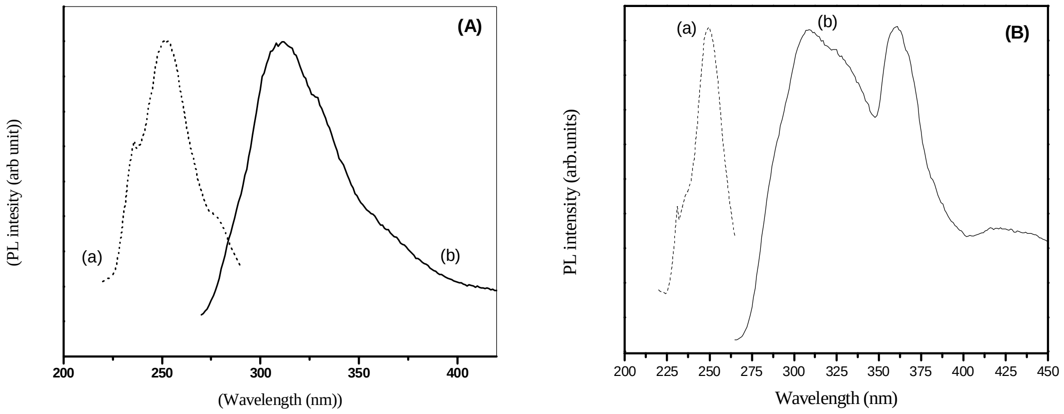

Figure 3.33(A) & 3.33(B) PL spectra of Oleic acid coated $La_{0.95}F_3:Ce_{0.05}$ curve (a) Ex=251 nm;(b) Em=308 nm slit width=1.5 nm

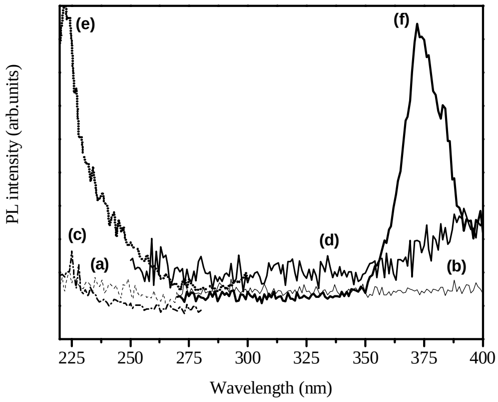

Figure 3.34 PL excitation curves (a) (Oleic acid), (c) (Oleic acid and Cerium chloride); (e) (Oleic acid and Plain LaF_3) for (λ_{Em}=361 nm) and emission curves (b) Oleic acid. (d)

Oleic acid and Cerium chloride for (λ_{Ex}=251 nm); (f) Oleic acid and Plain LaF_3 for (λ_{Ex}=220 nm)

3.7.2 PL of OA and PEG coated LaF_3:Ce

Figure 3.35 shows the PL spectra of Oleic acid with PEG $La_{1-x}F_3:Ce_x$ powder pellet with various x values (x=0.005, 0.01 and 0.05). In figure 3.35 curves (a, c, e) represent the excitation (λ_{emi}=305 nm) spectra and (b, d, f) the corresponding emission (λ_{exi}=250 nm) spectra respectively. There are two excitation maximas one at λ_{exi}=225 nm and another at 250 nm for λ_{emi}=305 nm. The emission at 368 nm might arise from the surfactant combination with host material as seen in the figure 3.34 but slightly right shifted. From this figure it is clear that photo luminescence intensity decreased with the increase in the cerium concentration. The decrease in PL intensity might be due to concentration quenching phenomenon and also due to the increase in the surface defects. Table 3.6 shows the calculated Stokes shift.

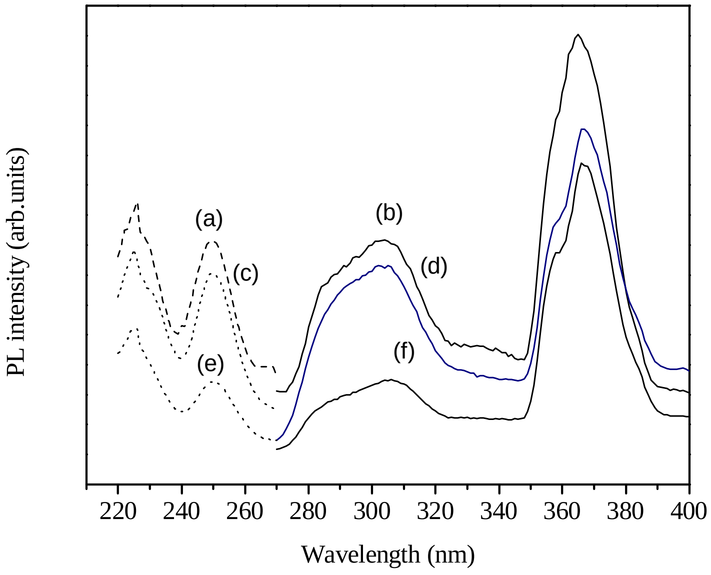

Figure 3.35 Photo luminescent spectra of Oleic acid and PEG coated $La_{1-x}F_3:Ce_x$ pellet with x = 0.005 (a, b), x=0.01 (c, d) and x=0.05 (e, f) where a, c and e are excitation spectra recorded at λ_{emi}= 305 nm and b, d and f are emission spectra for λ_{exi} =250 nm at slit width of 3nm each.

Table 3.6 Stokes shift of LaF_3:Ce (OA and PEG coated)

S.No	X=	λ_{Exi} wavelength (nm)	λ_{Em} Wavelength (nm)	Stokes shift (nm)/ Energy (J)	Peak centroid
1	0.005	249.68	301.77	52.08 (0.152 J)	301.77
2	1	249.97	301.76	51.73 (0.152 J)	301.76
3	3	252.7	313.46	60.67 (0.158 J)	313.46
5	5	250.6	306.42	55.82 (0.154 J)	306.5

3.7.3 PL of uncoated LaF_3:Ce synthesized in acidic environment

Figure 3.36 shows the PL spectra of $La_{1-x}F_3:Ce_x$ (x=0.01, 0.03, 0.05, 0.10 and 0.20) synthesized through the acidic route at pH=4.6. In figure 3.36, curve (a; x=0.01), (c; x=0.03), (e; x =0.05), (g; x=0.1) and (I; x=0.2) and b, d, f, h and j are the corresponding excitation and emission spectra respectively. Increase in the Cerium concentration resulted in increased luminescence as shown in figure 3.36. Curves (a) and (b) show the excitation spectrum for λ_{emi}= 303 nm and emission for λ_{exi}= 250 nm respectively for x=0.01. Curves (c) & (e) show the excitation spectra of x=0.03 and x=0.05 for λ_{emi}= 305 nm respectively and the corresponding emission spectra for λ_{exi}= 253 nm are shown in (d) & (f). Similarly, (g) & (i) show the excitation for λ_{emi}= 310 nm of x=0.10 and x=20 respectively whereas (h) & (j) show the corresponding emission for λ_{exi}= 258 nm. All the spectra were recorded at slit width of 1.5 nm. The peak maxima of both excitation and emission spectra are red shifted slightly as observed above. Generally in case of nano particles, wavelength shift is observed towards lower wavelength or higher energy compared to that of the bulk material as decrease in size increases the band gap. However in this case, all the samples are nano sized particles and are expected to be close to each other with respect to size as all these are prepared under similar experimental conditions. The only other possible reason for the observed shift (figure 3.36) can be the extent of

Cerium doping that can cause perturbed cerium energy levels in the lattice. The results observed here are in consistence with that reported by N. J. Withers et. al, [22]. Figure 3.37 shows PL intensity Vs Cerium mol plot indicating the PL intensity tending towards saturation. It is observed that as the extent of doping has increased, the magnitude of the shift also has increased. XRD data did not reveal any information with respect to the doping indicating that there is probably no change in the structure at macro level. However, the doping could have changed the microstructure due to the presence of defects [17] resulting in the observed wavelength shift. More studies are required to confirm it.

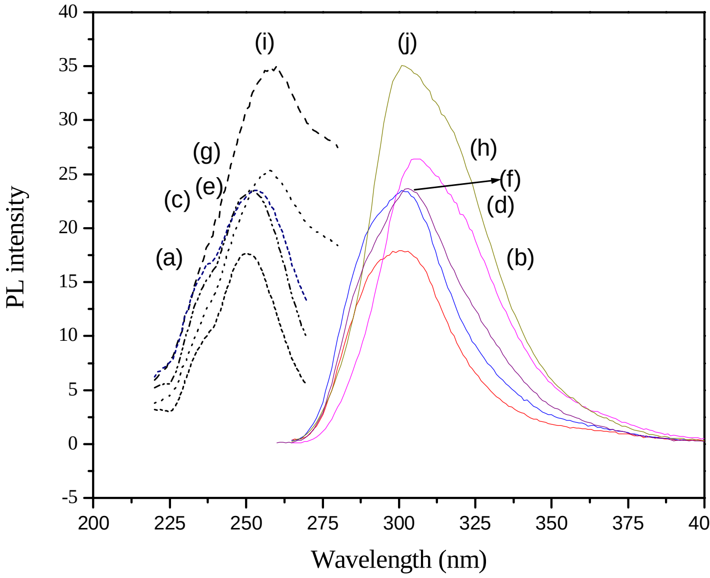

Figure 3.36 PL spectra of the $La_{1-x}F_3:Ce_x$; x=0.01(a, b), x=0.03 (c, d), x=0.05 (e, f), x=0.10 (g, h) and x=0.20 (I, j). Excitation curve (a) for λ_{Em}= 303 nm and Emission curve (b) for λ_{Exi}= 250 nm; curves c & e for λ_{Em}= 305 nm; curves d & e for λ_{Exi}= 253 nm; curves g & i for λ_{Em}= 310 nm; curves h & j for λ_{Exi}= 258 nm. Slit width= 1.5 nm.

Table 3.7 Stokes shift of uncoated La $_{1-x}$ F_3:Ce_x; x=0.01(a, b), x=0.03 (c, d), x=0.05 (e, f), x=0.10 (g, h) and x=0.20 (I, j). (uncoated; through acidic route)

Ce X=	**λ_{Exi} (nm)**	**Intensity**	**Pk.Width**	**λ_{Em} (nm)**	**Intensity**	**Pk.Width**	**Stoke's Shift(nm) /Energy (J)**
0.01	250.08	908.72	30.398	303.4	896.53	34.602	53.32 (0.0266 J)
0.03	250.82	1640.3	39.252	301.35	1439.5	36.3	50.53 (0.0256 J)
0.05	251.81	2234	50.44	305.05	1503.6	38.42	53.1 (0.0267J)
0.10	260.56	4610.8	73.128	311.7	1876.5	41.682	51.14 (0.0254 J)
0.20	261.65	7207.6	80.052	308.84	2489.3	41.352	47.1 (0.0241 J)

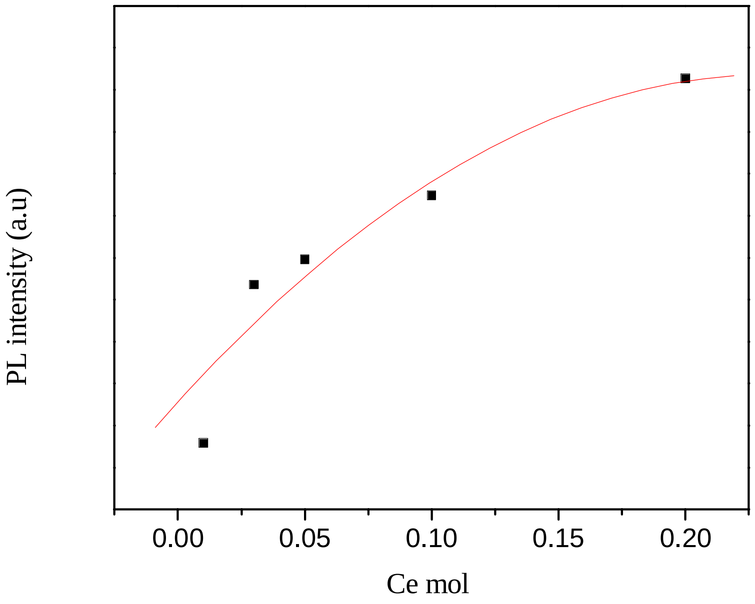

Figure 3.37 PL intensity vs Ce mol

Figure 3.38 shows the PL spectra of uncoated La_{1-x} F_3:Ce $_x$ (x=0.05) as-prepared colloidal solution samples synthesized at various pH 4.2, 4,6 and 5.6. The difference in the PL intensity might be due to the difference in the particle sizes [P..H.Borse. et al (2005) [9]. The relation between the particle size and the pH is shown graphically in figure 3.39, indicating increase in the PL intensity as the particle size decreases. Table 3.6 shows the Stokes shift particulars of the synthesized uncoated LaF_3:Ce. it is clear from the table that at higher dopant concentration, Stokes shift decreases and subsequently leading to decreased energy loss which shows the improved fluorescence properties. Table 3.7 shows the calculated Stokes shift.

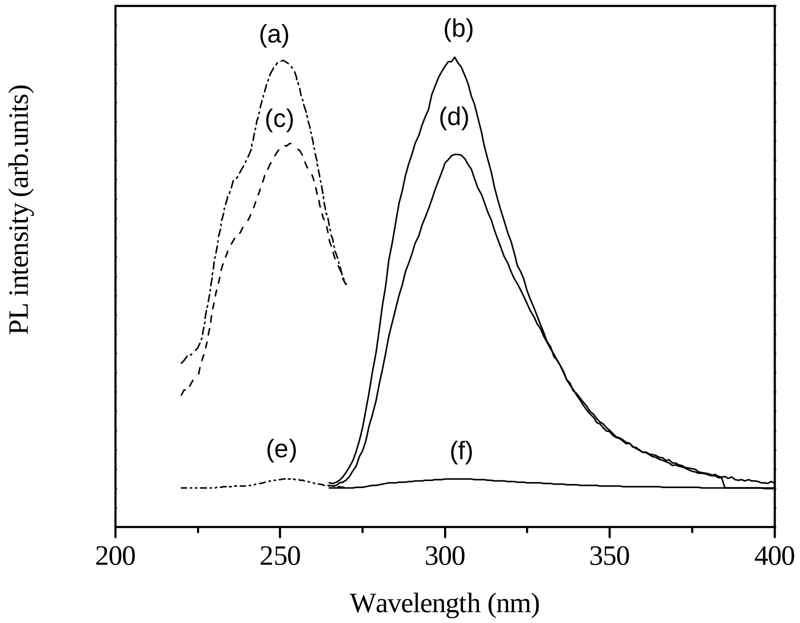

Figure 3.38 PL spectra of the colloidal sample containing nano sized LaF_3:Ce particles pH = 4.2 (curves a & b), pH = 4.6 curves (c & d), pH = 5.6 curves (e & f). All the excitation and emission spectra were recorded at λ_{emi}=305 nm and λ_{exi} =250 nm respectively with slit width of 1.5 nm.

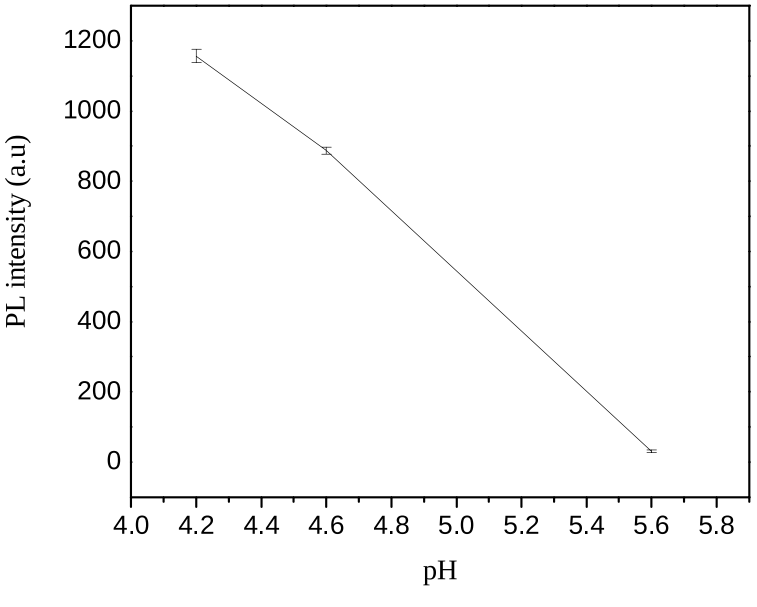

Figure 3.39 pH vs PL intensity

3.7.4 STE from OA and PEG and Uncoated LaF_3:Ce

Figure 3.40 shows the PL spectra of the Oleic acid and PEG coated powder samples recorded at the excitation wavelength of 380 nm with slit width 3 nm. Similarly, Figure 3.41 shows emission of uncoated powder sample recorded at excitation wavelength of 380 nm with slit width 1.5 nm. Both the samples exhibited emission peak at 453 nm. The luminescence intensity of the uncoated sample was very high and was beyond the recording range at 3 nm slit width. Hence this sample was recorded at slit width of 1.5 nm. Compared to the intensity obtained at 3 nm slit width, the intensity obtained at 1.5 nm is nearly 10 times less. In figure 3.41 curves (a and c) and (b and d) represent excitation and corresponding emission of the uncoated particles synthesized in acidic different environment. The particle sizes were 24 nm (a & b) and 164 nm (c & d) as obtained from the DLS result. It is clear that the intensity of the emission of small sized particle is more than that of the bigger particle.

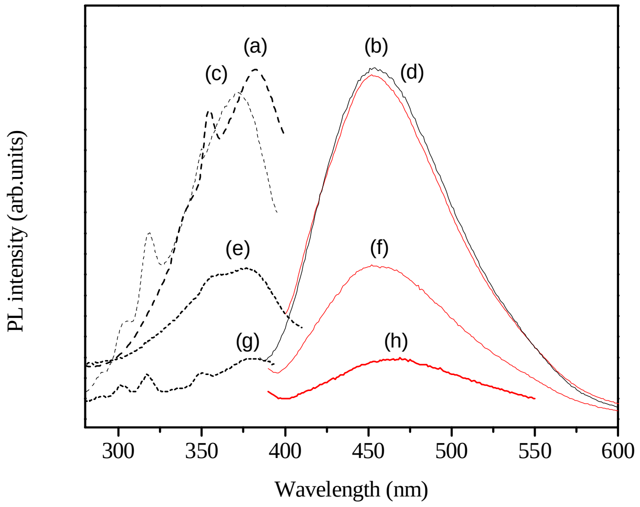

Figure 3.40 PL spectra showing the STE emission from OA and PEG coated $La_{1-x}F_3$:Ce_x samples with x = 0.005 (a, b);x=0.0 1(c, d);x=0.03(e, f) and x=0.05 (g, h) where a, c, e and g are excitation spectra recorded at λ_{emi}=453 nm and b, d, f and h are emission spectra for λ_{exi} =380 nm at slit width of 3 nm each.

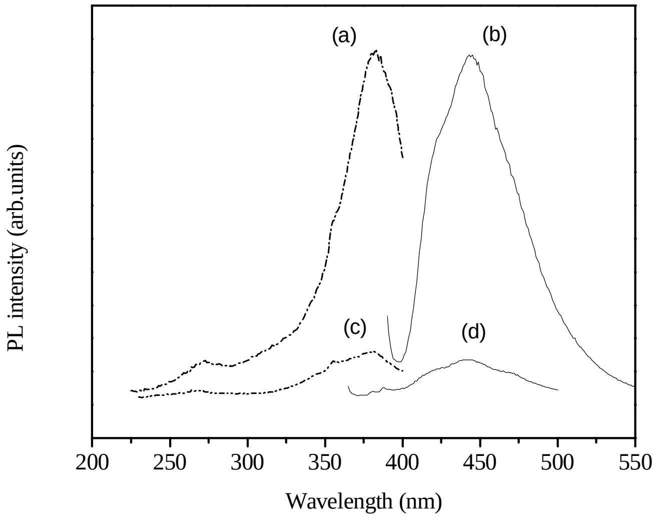

Figure 3.41 PL spectra of the $La_{0.95}F_3:Ce_{0.05}$ samples of particle size 24 nm for curves (a & b) and 164 nm for curves (c, d) where (a) and (c) are Excitation for (λ_{emi}=453 nm) and emission curves (b) and (d) at (λ_{exi} =380 nm).

Figure 3.42 curves [a-h] also show PL spectra of uncoated $La_{1-x}F_3:Ce_x$ powder samples recorded at excitation wavelength of 380 nm with slit width 1.5 nm. Curves (a, c, e, g) and (b, d, f, h) represent excitation and corresponding emission for various x=0.01, 0.03, 0.10 and 0.20 Ce respectively. This emission (Fig 3.40 -3.42) may be attributed to the surface trapped exiton emission (STE). The STE arises when an electron is bound to a V_k centre which has a hole trapped by two fluorine ions. This is similar to a vacancy defect which migrates through the crystal at room temperature [23,24&25]. The STE emission intensity from the synthesized material was significant and varied with Cerium concentration. This might be due to the difference in the number of traps available which in turn may depend on the Cerium concentration though observed PL intensity was not consistent with Cerium concentration. It is also possible that these emission and excitations were due to the perturbed cerium that are possible due to the defects generated at higher Cerium concentrations [17]. More studies are required to confirm the exact mechanism which is beyond the scope of the present study.

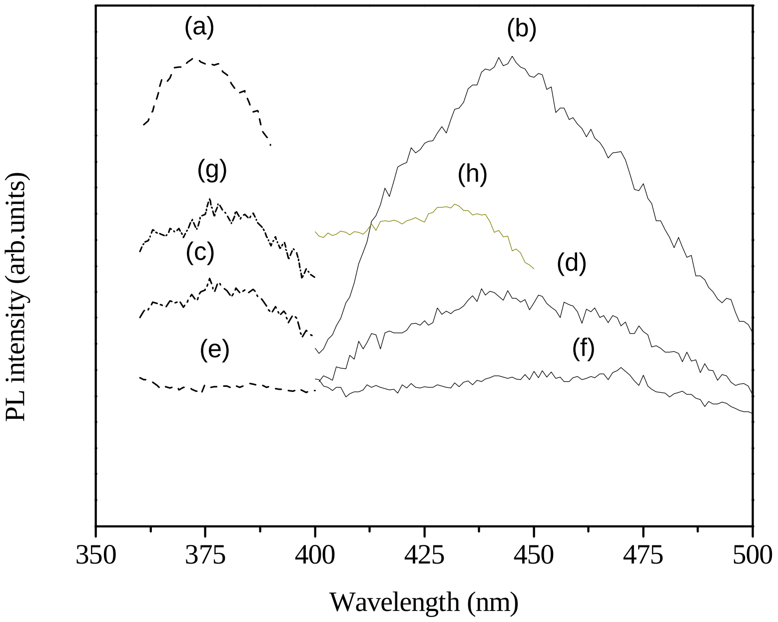

Figure 3.42 Curves a (x=0.01),c (x=0.03),e (x=0.10) and g (x=0.20) are Excitation for λ_{emi}= 453 nm and Curves (b),(d),(f) and (h) are emission for λ_{exi}=380 nm ; recorded at Slit width= 1.5 nm.

3.7.5 PL spectra of Uncoated LaF_3:Ce obtained through HF method

Figure 3.43 shows the excitation and emission spectrum of $La_{1-x}F_3:Ce_x$ nano-crystal pellet obtained by reacting Lanthanum carbonate and hydrofluoric acid. In figure 3.43 curves (a), (c) and (e) represent excitation for λ_{emi}= 304 and 327 nm for x=0.05, x= 0.01 and x=0.20 respectively. Curves (b), (d) and (f) represent the emission when exited at λ_{exi}= 262 and 287 nm respectively. The intensity was significant for x=0.10 and decreased for x=0.20, this might be due to the concentration quenching as well as the unreacted carbonate impurities present. Moreover, there was a significant red shift of the peak at x=0.20 which might be due to the higher molar doping.

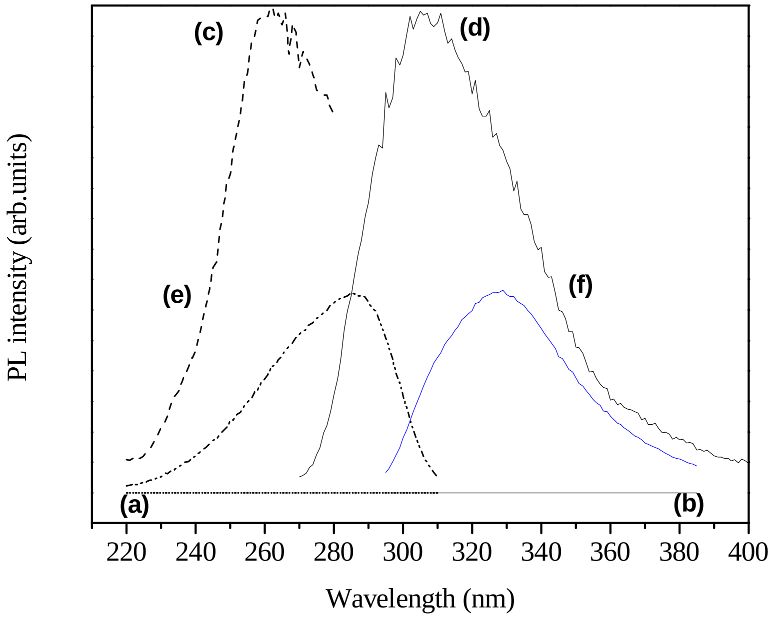

Figure 3.43 PL spectra of the $La_{1-x}F_3:Ce_x$ sample Excitation curve (a) x=0.05 ; (c) x=0.10 for λ_{Em}= 304nm ; (e) x=0.20 for λ_{Em}= 327 nm ;; Emission curves (b) and (d) at λ_{Exi}= 262 nm ;(f) λ_{Exi}= 287 nm

3.8 Life time

Figures 3.44, 3.45 and 3.46 show the exponentially fitted PL lifetime recorded with 280 nm wavelength excitation from a pulsed diode source for the colloidal solutions prepared with OA+PEG, uncoated samples through acidic route and through HF route respectively. The LaF_3:Ce has a prompt decay time of 3 ns and delayed life time of 25 ns, which are consistent with the values obtained by L.R.Elias. et al.,[19,20 & 25]. The Oleic acid and PEG coated sample posses a faster PL time when compared to that reported in prompt decay time [26]. No significant changes were observed in the life time of the uncoated and the coated lifetimes indicating that the positions of Ce^{3+} occupied in the LaF_3 in both the cases are similar. Moreover, no significant change was observed with the change in cerium concentration.

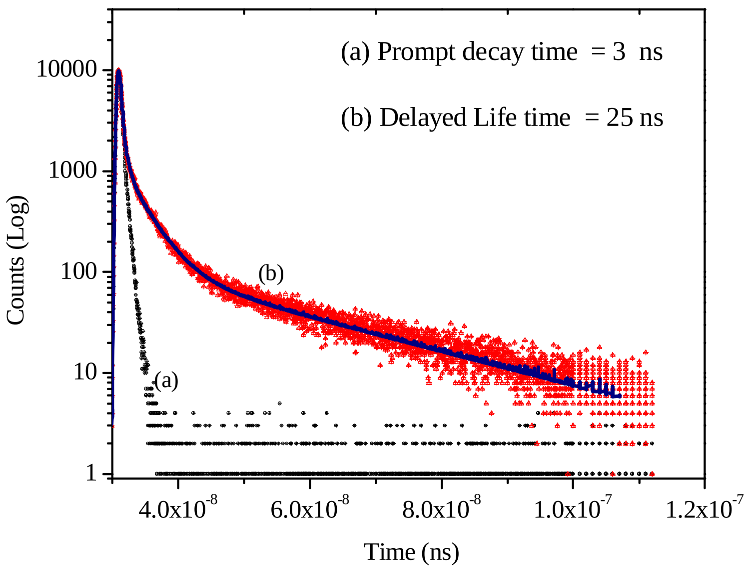

Figure 3.44 Life time spectra of Oleic acid and PEG coated $La_{0.95}F_3:Ce_{0.05}$particles

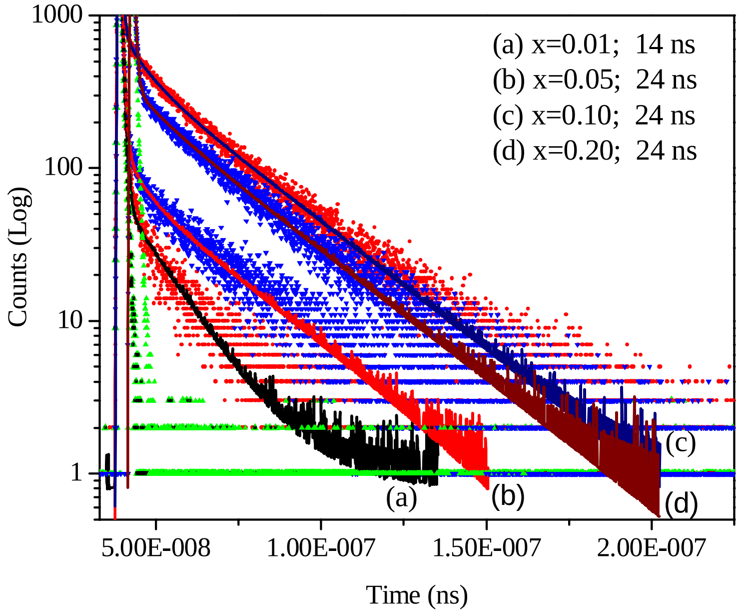

Figure 3.45 PL lifetime of uncoated $La_{1-x}F_3:Ce_x$ synthesized through acidic route (a)x=0.01;(b) x=0.05;(c) x=0.1 and (d) x=0.2

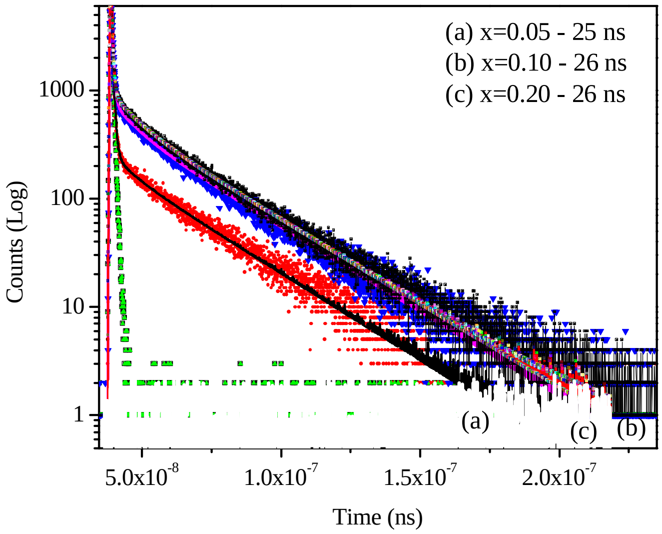

Figure 3.46 Lifetime of uncoated $La_{1-x}F_3:Ce_x$ synthesized through HF route (a)x=5;(b) x=0.10 and (c) x=0.20

3.9 LaF_3:Ce with co-doping

The emission of LaF_3 :Ce is in the UV region. In order to convert the UV to visible emission, a suitable codopant is required which should effectively receive the excitation energy from the Ce^{3+} activator (donor) in the matrix to it (acceptor). Such a conversion may find application in high energy counting techniques as the Photo Multiplier Tubes generally have higher sensitivity for the visible emission. However, the codopant should not quench or aid the non-radiative path within Ce^{3+} itself. Moreover, earlier studies indicate that Ce^{3+} among all the lanthanide ions, owing to its allowed absorption and board emission band can effectively overlap the acceptors like Tb^{3+} absorption energy bands and facilitate the excitation energy transfer. Therefore, Tb^{3+} and Eu^{3+} were codoped along with Ce^{3+} in LaF_3 and $LaF_3:Ce^{3+},Tb^{3+}$ and $LaF_3:Ce^{3+},Eu^{3+}$ were prepared for exploring the energy transfer between Ce^{3+}-$Tb^{3+}$and Ce^{3+}-Eu^{3+} in LaF_3 matrix. Samples were synthesized by adopting the solution co-precipitation route in an acidic environment (at pH=4.6) and their structural and Optical characterization are presented below.

Fig. 3.47 shows the XRD patterns of the $La_{0.95}F_3:Tb^{3+}_{0.05}$ and $La_{0.90}F_3:Ce^{3+}_{0.05},Tb^{3+}_{0.05}$ nanoparticles represented by the curves (a) and (b). The XRD pattern exhibits prominent peaks that match well with JCPDS standard (32-0483) of the hexagonal LaF_3 crystal. The slight shift towards higher angels may be due to the lesser atomic radius of Terbium (175 pm) dopant compared to Lanthanum (270 pm). No detectable signals of any impurity phase were observed. Lattice parameter calculated is shown in Table 3.8.

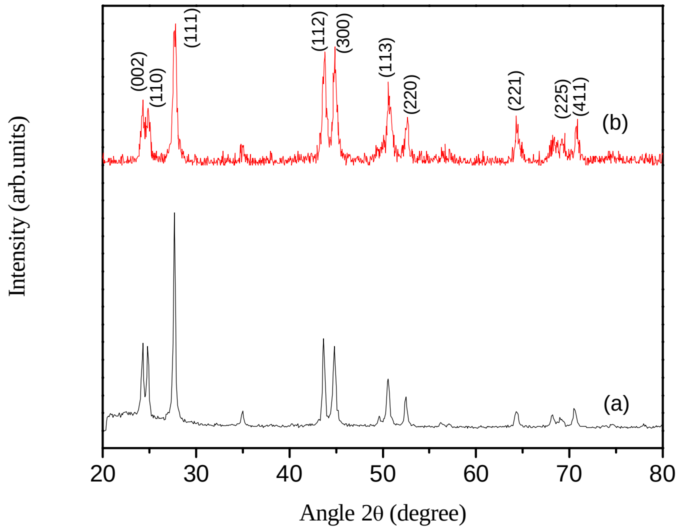

Figure 3.47 XRD pattern of (a) LaF_3:Tb ; (b) LaF_3:Ce,Tb synthesized at pH=4.6

Table 3.8 Lattice parameters of LaF_3:Tb and LaF_3: Ce,Tb

Sample	**a Å**	**c Å**
LaF_3: Tb	7.166 (2)	7.330 (3)
LaF_3: Ce,Tb	7.161 (4)	7.336 (6)

3.10 Energy Transfer mechanisms

While exploring the energy transfer probability between the donor and acceptor, it is imperative to find out the overlap between the donor emission and acceptor excitation. A good overlap indicates that there is a possibility of energy transfer between the two. Though overlap alone does not guarantee the energy transfer, absence of overlap indicates that there is no possibility of energy transfer. Figure 3.48 shows the emission of Ce^{3+} (b) and excitation of Tb^{3+} (a) in LaF_3. The $Ce^{3+}$was recorded by setting the excitation monochromator at 250 nm and the Tb^{3+}excitation was recorded by setting the emission monochromator at 544 nm emission. Both excitation and emission were recorded at 1.5nm slit width. It is obvious from the figure that there is a good overlap between the emission of Ce^{3+} and excitation of Tb^{3+}.

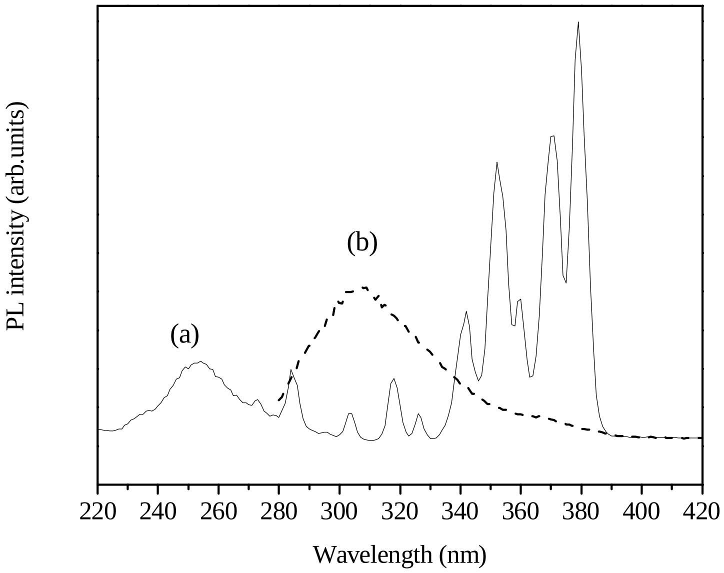

Figure.3.48 Overlap of (b) emission spectrum of Ce^{3+} in $La_{1-x}F_3$:$Ce_{x=0.05}$ and (a) excitation spectrum f-f transitions of Tb^{3+} in $La_{1-x}F_3$:$Tb_{x=0.05}$

Therefore, the preliminary requirement of overlap for the possible energy transfer between Ce^{3+} and Tb^{3+} is satisfied. Fig.3.49 shows the excitation spectra of Tb^{3+}, (a) Ce^{3+},Tb^{3+} and (b) Tb^{3+}in LaF_3. Both the excitation spectra were recorded by monitoring the emission at 544 nm which is the characteristic emission peak of Tb^{3+}. It is obvious from the figure that all the excitation peak intensities of both Tb^{3+} and Tb^{3+}, Ce^{3+} are comparable except the intensities of peaks around 250 nm which is the characteristic excitation peak of Ce^{3+}. The excitation and emission spectra of LaF_3:Ce^{3+} is shown in Figure 3.50 The excitation peak seen for LaF_3:Ce^{3+} is around 250 nm.

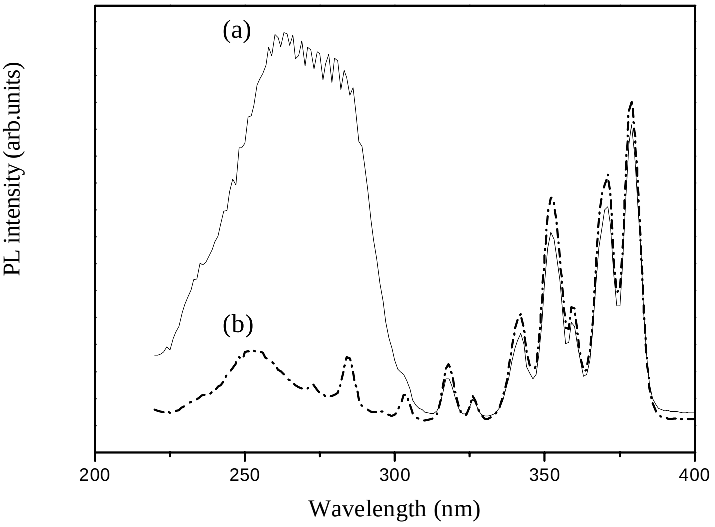

Figure.3.49 Excitation spectra of (a) $La_{1-2x}F_3:Ce^{3+}{}_{x=0.05},Tb^{3+}{}_{x=0.05}$ (solid line) and (b) $La_{1-x}F_3:Tb^{3+}{}_{x=0.05}$(dotted line), λ_{emi}=544 nm, slit width=1.5 nm each.

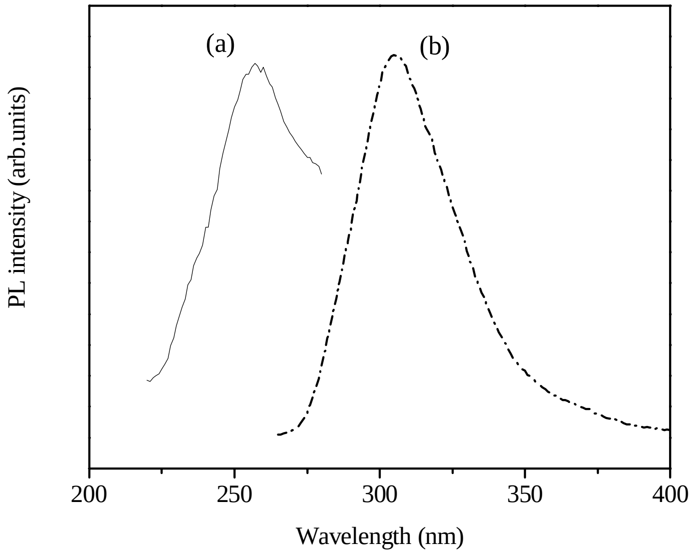

Figure 3.50 Excitation spectrum of (a) $La_{1-x}F_3:Ce^{3+}{}_{x=0.05}$ (solid line) λ_{emi}=305 nm and emission spectrum of (b) $La_{1-x}F_3:Ce^{3+}{}_{x=0.05}$ (dotted line), λ_{exi}=250 nm, slit width=1.5 nm each.

In presence of Ce^{3+}, a broad intense excitation peak for Tb^{3+} is seen from LaF:Ce^{3+},Tb^{3+} which matches well with the excitation peak of Ce^{3+}. This further indicates towards the energy transfer from Ce^{3+} to Tb^{3+} in this matrix. Figure 3.51 shows the emission spectra of $La_{1-x}F_3:Ce^{3+}_{x=0.05}$ and $La_{1-2x}F_3:Ce^{3+}_{x=0.05},Tb^{3+}_{x=0.05}$ upon excitation at 250 nm. The enhancement in the fluorescence intensity of Tb^{3+} is around two times in presence of Ce^{3+} compared to that of in absence of Ce^{3+}. Therefore, the observations made above with respect to the figures 3.48 to 3.51 presented here clearly prove that there is energy transfer from Ce^{3+} to Tb^{3+} in LaF_3.

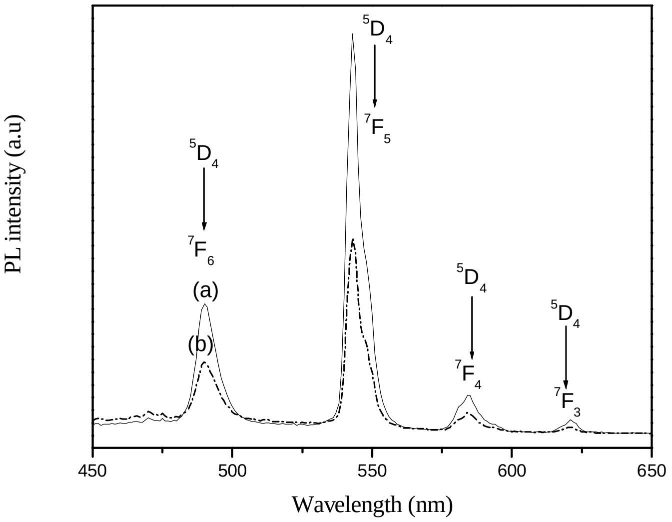

Figure 3.51 Emission spectrum of (a) $La_{1-2x}F_3:Ce^{3+}_{x=0.05},Tb^{3+}_{x=0.05}$ (solid line), λ_{exi}=250 nm and (b) $La_{1-x}F_3:Tb^{3+}_{x=0.05}$ (dotted line), λ_{exi}=250 nm, slit width=1.5nm each.

Doping of Tb^{3+} along with Ce^{3+} in LaF_3 can bring the luminescence in to the visible range but the emission is only in the green range of visible spectrum as Tb^{3+} predominantly emits in the green region. Therefore, Eu^{3+} was also codoped with Ce^{3+} in LaF_3 to bring the emission in to the red region of the visible spectrum as Eu^{3+} predominantly emits in the red region. To bring the emission in to the red region, doping of Eu^{3+} would suffice but if there can be an energy transfer between Ce^{3+} and Eu^{3+} , as seen in case of Ce^{3+} and Tb^{3+}, then the luminescence efficiency in the visible range can be efficient.

Fig.3.52 shows the overlap spectra of Ce^{3+} emission and Eu^{3+} excitation. It is obvious from this figure that there is an overlap between the two. However, compared to the extent of overlap between Ce^{3+} and Tb^{3+}, the same between Ce^{3+} and Eu^{3+} is significantly low.

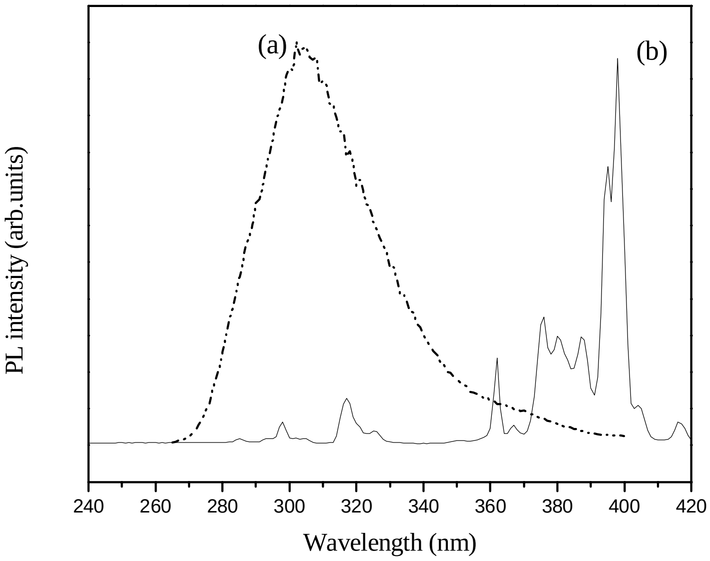

Figure 3.52 Overlap of (a) emission spectrum of Ce^{3+} in $La_{1-x}F_3:Ce_{x=0.05}$ and excitation spectrum of Eu^{3+} in $La_{1-2x}F_3:Ce_x,Eu_x^{3+}$.

Fig.3.53 shows the emission of Eu^{3+} from $LaF_3:Ce^{3+}$, Eu^{3+} upon excitation at 250 nm (1.5 nm slit width for both excitation and emission monochromators). This clearly indicates that at 250 nm excitation, there is no significant emission from Eu^{3+} implying that there is no significant energy transfer from Ce^{3+} to Eu^{3+} in LaF_3 host. This is in agreement with the fact that an overlap of the emission spectrum of the donor and the excitation spectrum of acceptor does not necessarily mean that there has to be an energy transfer though it is a precondition for the energy transfer. Probably, in case of $LaF_3:Ce^{3+}$, Eu^{3+}, the non-radiative decay path is quite significant at excitation of 250 nm and coupled with the fact that the overlap is significantly low; the energy transfer could not be observed under the experimental conditions employed here.

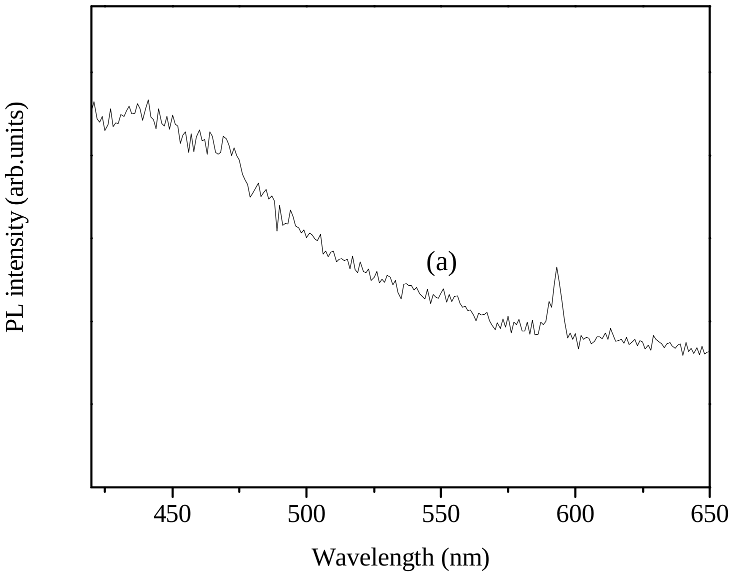

Figure 3.53 Emission spectrum of (a) Eu^{3+} in $La_{1-2x}F_3$:$Ce_{x=0.05}$,$Eu_{x=0.05}$ at λ_{exi}=250 nm, slit width=1.5 nm.

3.11 Conclusion

Oleic acid, Oleic acid plus PEG coated and uncoated LaF_3:Ce^{3+} particles prepared were of nano size. The samples synthesized through all the routes studied were nano crystalline in nature. XRD pattern of uncoated samples indicated that these were of high crystalline nature. The size distribution was a bit narrower in the case of OA plus PEG combination. Agglomeration was minimum with OA plus PEG coated and the uncoated LaF_3:Ce particles as is evident from the results of FESEM and DLS. The absorption measurements of OA and OA plus PEG coated particles exhibited only 200, 234 and 250 nm wavelengths whereas uncoated particles showed five distinct, clearly resolved absorption peaks at wavelengths 198, 205, 218, 234 and 247 nm. In one of the uncoated sample, the particle size was so small that a marginal shift of the UV-Vis absorption was observed. The result of the UV-Vis absorption study (to know the settling rate) showed that uncoated and OA coated appears to have better suspendabilty in DM water.

It is known that the particle size has a direct effect on the PL intensity as the smaller is the size, more is the luminescence. The photoluminescence intensity of Oleic acid coated particle was higher when compared to that of the OA+PEG coated particles. However, the uncoated samples compared to Oleic acid or Oleic acid plus PEG coated samples, yielded yet smaller particles exhibiting higher PL intensity. The STE emission intensity also increases with decrease in the particle size though no significant change in the PL life time was observed. In this host, the energy transfer between the Ce^{3+} and Tb^{3+} was observed with a significant overlap between the emission spectrum of Ce^{3+} and the excitation spectrum of Tb^{3+}. However, no energy transfer between Ce^{3+} and Eu^{3+} could be observed in this host.

References

[1] K. Sattler, Charpter-2 *www*.phys.hawaii.edu/~sattler/Publications/pdf

[2] C. Wena, L. Sun, J. Yan, Y. Liu, J.S.Y Zhang, H.L.Z Kang, J. Colloid Interf. Sci., 357 (2011) 116.

[3] J.W. Stouwdam, G.A. Hebbink, J. Huskens, F.C.J.M. van Veggel, Chem. Mater., 15 (2003) 4604.

[4] E. Beaurepaire, V. Buissette, M.P. Sauviat, D. Giaume, K. Lahlil, A. Mercuri, D. Casanova, A. Huignard, J.L. Martin, T. Gacoin, J.P. Boilot, A. Alexandrou, *NanoLetters* 4 (2004) 2079.

[5] H. Deng, S. Yang, S. Xiao, H.M. Gong, Q.Q. Wang, J. Am. Chem. Soc., 130 (2008) 2032

[6] J. Zhou, Z. Wu, Z. Zhang, W. Liu, H. Dang, Wear (2001) 249-333.

[7] J. Wang, J. Hu, D. Tang, X. Liu, Z. Zhen , J. Mater.Chem., 17 **(**2007) 1597.

[8] R.N. Bhargava, D. Gallagher, X. Hong, A. Nurmikko, Phy. Rev. Letters., 72, (1994) 416.

[9] P.H. Borse, W. Vogel, S.K. Kulkarni, J. Colloid. Interf. Sci. 293 (2006) 437.

[10] A. Chatterjee, A. Priyam, S.C. Bhattacharya, A. Saha, Colloids. Surf. A: Physicochem. Eng. Aspects 297 (2007) 258.

[11] W. Schärtl, R. Xie, T. Ren, M. Sejfic, G. Wenz, R. Heisel, C. Scherer, M. Maskos, K. Fischer, T. Basché, J. Luminescence 129 (2009) 1428.

[12] F. Wang, Y. Zhang, X. Fan, M. Wang, J. Mater. Chem., 16 (2006) 1031.

[13] J.W. Stouwdam, F.C.J.M. van Veggel, Nano Lett. 2 (2002) 733.

[14] N. Wu, L. Fu, M. Su, M. Aslam, K.C. Wong, P.V. Dravid, Nano Letters 4 (2004) 383.

[15] G.S. Yi, G.M. J. Matter. Chem., 15 (2005) 4460.

[16] R.E. Kroon , H.C. Swart, O.M. Ntwaeaborwa, H.A.A. SeedAhmed, Physica B , doi.org/10.1016/j.physb.2013.10.054

[17] P.S. Peijzel, R.T. Wegh, A. Meijerink, J. Hölsä, R. Lamminmäki, J. Opt. Commun. 204 (2002) 195.

[18] P. Dorenbos, Phys. Rev. B., 62 (2000) 15640.

[19] L.R. Elias,W. Heaps, W.M. Yen, Phys. Rev. 8 (1993) 11.

[20] S. Heaps, L. R. Elias, L. M. Yen. Phys. Rev. B., 13 (1976) 94.

[21] D.W. Coutts, A.J.S. McGonigle, Quantum Electronics 40 (2004) 1430.

[22] N. J. Withers, K. Sankar, T.A. Memon, B.A. Akins, J.J. Gu, T.Y. Gu, G. Smolyakov, M. Osinski, 28th Annual Conference on Lasers and Electro-Optics CLEO (2008), San Jose, California.

[23] W.W. Moses, S.E. Derenzo, M.J. Weber, A.K. Ray-Chaudhuri, F. Cerrina, J. Lumin. 59 (1994) 89.

[24] C. Pedrini, B. Moine, D. Bouttet, A.N. Belsky, V.V. Mikhailin, A.N. Vasil'ev, E.I. Zinin, Chem. Phys. Letters 206 (1993) 470-474.

[25] L.G. Jacobsohn, A. Toncelli, K.B. Sprinkle, C.J. Kucera, J. Ballato, J. Appl. Phys.

111 (2012) 074315

[26] J.C. Boyer, F. Vetrone, L.A. Cuccia, J.A. Capobianco, J. Am. Chem. Soc. 128 (2006) 7444.

[27] J. Manson, J. Manson, D. Kumar, Brian J. Meenan and Dorian, DOI 10.1007/s13404-011-0015-8.

Chapter 4

Synthesis and Characterization of $La_{0.4}F_3$:$Ce_{0.45}$,$Tb_{0.15}$ (Core)/ TiO_2 (Shell) Structure and Non-Stoichiometric in LaF_3:Ce

4.1 Introduction to core shell structure

Light amplification by another shell structure over the nano phosphor surface is being studied by many researchers. The shell material for LaF_3:Ln^{3+} [Ln = Ce or Eu)] (core) is either particles of a semiconducting oxide or plain undoped same core material. Unlike bulk energy states, nanomaterial surface states originate from the discontinuous lattice periodicity and broken chemical bonds. These states provide radiationless pathways. Surface coating stabilizes these states by providing charges [1 & 2], thereby reduce radiationless pathways. The surface modification while inducing nonradioactive pathways also ensures more effective energy transfer to the luminescent activator.

During the past decade there have been a significant number of reports on shelling of LaF_3-core leading to enhanced light output. In their interesting work, MengYinXie.et al 2009 [2] reported a very good enhancement in the PL intensity of LaF_3:Ln^{3+}(Core)/LaF_3 (Shell) material codoped with various lanthanides vizCe ,Tb and Nd. Of the shell materials attempted, SiO_2 [3] was found to be the most effective in enhancing the photoluminescence properties of LaF_3.

QiangWanga et al (2010) [4] have studied the $La_{0.8}F_3$:$Ce_{0.15}$,$Tb_{0.05}$ and $La_{0.4}F_3$:$Ce_{0.45}$,$Tb_{0.15}$ as core compositions. In their study, the luminescence properties of lanthanum fluoride nanocrystals produced using the hydrothermal method with varying amounts of Ce and Tb. The quantum yield of the synthesized $La_{0.4}F_3$:$Ce_{0.45}$,$Tb_{0.15}$ material was 55%. In another interesting core/shell work reported by H.Kim et al., (2009) [5] TeO_2 (core)/ TiO_2 (shell) was synthesized using MOCVD process and demonstrated that the PL emission intensity can be increased or the wavelength of the emission can be controlled by selecting a proper coating material and a proper coating layer thickness. Apart from surface modification studies, another interesting field of non-stoichiometric Lanthanum fluoride behavior on the cerium emission is also discussed here.

Crystals with desired luminescence properties can be obtained by controlling the defects during synthesis. Defects in a material can be created in many ways such as temperature annealing, impurity addition or by varying the nominal chemical composition. Non-stoichiometric substancesviolate the law of definite proportionsas theirelemental composition cannot be represented by a ratio of well-defined natural numbers. Non-stoichiometricsolids contain crystallographic point defects, interstitial atoms and vacancies, which result in excess or deficiency of an element, respectively. Crystal structure investigations are important for strongly non-stoichiometric phases, regardless of the chemical type of compounds. The data on the defect character of nonstoichiometric crystals at the atomic level may be useful in preparation of materials with desired properties. Experiments were carried out to study the effect of non-stoichiometry on luminescence and quantum efficiency of cerium ions which is known [6,7] to vary depending on the strength of the crystal field due to surrounding ions in host system.

In this work, LaF_3:Cecore structure with a cerium concentration of 0.45 mol was chosen to be codoped with Terbium (0.15 mol). We report here the successful synthesis of $La_{0.4}F_3:Ce_{0.45},Tb_{0.15}$-core / TiO_2 shell nano particles for the first time. The structure and effects of the TiO_2 shell layer thickness on the photoluminescence properties of $La_{0.55}F_3:Ce_{0.45}{}^{3+}$, $La_{0.85}F_3:Tb_{0.15}{}^{3+}$ and $La_{0.4}F_3:Ce_{0.45},Tb_{0.15}$ were reported. {This work presents for the first time a detailed study on nonstoiciometric synthesis and optical characterstiation of $LaF_3:Ce^{3+}$ nanoparticles prepared at our laboratory through a wet chemical co-precipitation technique}.

4.2 Experimental

4.2.1 Synthesis of $La_{0.40}F_3$:$Ce_{0.45}$,$Tb_{0.15}$ / TiO_2 Core/Shell nanoparticles

Nano sized crystals of $La_{0.55}F_3$:$Ce_{0.45}^{3+}$,$La_{0.85}F_3$:$Tb_{0.15}^{3+}$ and $La_{0.4}F_3$:$Ce_{0.45}$,$Tb_{0.15}$ were synthesized at pH=4.6 by following the procedure as mentioned in chapter 3. TiO_2 powder was prepared using the procedure adopted by Rajini. P et. al. [8]. Nano sized TiO_2 (2-5 nm)[8] --- 2% wt of the $La_{0.4}F_3$:$Ce_{0.45}$,$Tb_{0.15}$) powder was disbursed in methanol by ultra sonicating for 30 mins (solution-1). Around 0.5 g of the $La_{0.4}F_3$:$Ce_{0.45}$,$Tb_{0.15}$powder was disbursed in methanol separately for about 30mins to obtain a uniform colloidal mixture (solution-2). Then the well disbursed solution-1 was added drop by drop to solution-2 and the mixture was stirred thoroughly for 24h. Likewise in order to vary the coating thickness, another sample was synthesized by stirring for 52h.

4.2.2 Synthesis of Stoichiometric and Non-stoichiometric $La_{0.95}F_3$:$Ce_{0.05}$

LaF_3:Ce^{3+} was synthesized in both stoichiometric and non-ichiometric ratios. The compound LaF_3 was prepared with lanthanum and fluoride molar variations to study the non-stiochiometric effects. Firstly, the amount of lanthanum was varied by keeping the fluorine amount constant. Then the amount of fluorine was varied by keeping lanthanum constant. Stock solutions were prepared and used to avoid preparation errors. From the study of effect of concentration, we found that the optimum concentration of cerium was 0.05 mol. The nanoparticles synthesized in this manner have hexagonal structure and exhibited intense photoluminescence. Rare earth halides are conveniently synthesized from mixtures of the respective binary halides as starting materials. Since the hygroscopicity of such compounds strongly increases from chlorides to iodides, their preparation needs special precautions to avoid oxide contamination. The dopant was also in halide form. The powder products from the reactant liquid was difficult to separate even at 10,000 rpm in the case of La/F ratios 0.41 and 0.39, as it led to a very fine colloidal formation. The colloidal solution were dried and transferred to a filter paper and washed thoroughly with DM water to remove the unreated chlorides. The filtered water was checked for the presence of chloride by adding $AgNO_3$ solution. The filter paper containing the precipitate was removed from the filtering setup and was dried in vacuum oven at 85°C for 2 h. similar procedure was adopted in the stoichiometric synthesis of LaF_3.

XRD,TEM,FTIR,UV-Visabsorption, Photoluminescence, Life time characterization as well as XRFelemental analysis were carried out. X-ray diffractometer (APD 2000PRO) with $Cu_{K\alpha}$ line wavelength 1.5406 Å, Transmission Electron Microscope (TEM) micrographs were recorded using FEI CM200 TEM that operates at 200 kV using a pettier cooled TVIPS 2k X 2k CCD camera. FTIR spectra were recorded using HORIZON MB3000 ABB spectrophotometer, UV-Vis absorption measurements were carried out using SHIMADZU (UV1800). Photoluminescence were carried out using a SHIMADZU spectrophotometer [RF-5301PC] in the range of 200 – 700 nm at 1.5 & 3 nm slit widths. “Horiba”spectrophotometer was used to for life time measurements at SAIF, IIT Chennai. XRF elemental analysis was carried out using EX-6600SDD Xenemetrix instrument. Scintillation under X-ray excitation was observed using Avantes 2010 fiber Optic spectrometer.

4.3 Structural Characterization

4.3.1 XRD

Figure 4.1 shows XRD pattern of (a) $La_{0.4}F_3$:$Ce_{0.45}$,$Tb_{0.15}$; (b)TiO_2 surface modified $La_{0.4}F_3$:$Ce_{0.45}$,$Tb_{0.15}$ and (c) $La_{0.55}F_3$:$Ce_{0.45}$ samples matches with the JCPDS data of LaF_3 (32-0483). It is clear that $La_{0.4}F_3$:$Ce_{0.45}$,$Tb_{0.15}$ sample had single phase and well formed. The fluoride products such as LaF_3 and CeF_3 easily crystallize with a hexagonal-phase structure, which is determined by the intrinsic crystalline structure of lanthanide fluoride

[9]. It is evident that there was no shift even with 0.45 mol of Ce (curve c). However there is a peak shift towards higher angels which indicate the substitution of La^{3+} ions by smaller Tb^{3+} ions in the lattice structure at certain sites which results in changes in the lattice parameter and homogenous dispersal of Ce^{3+} and Tb^{3+} ions in the lattice [10]. The crystallite size is estimated from the Scherrer equation, $D=0.90\lambda/\beta \cos \theta$, where D is the grain size, λ is the X-ray wavelength (0.15405 nm), and θ and β are the diffraction angle and full-width at half-maximum of an observed peak, respectively. The dominant peaks viz [002], [110], [111], [300], [133] and [302] at 2θ=24.49, 25.07, 27.84°, 44.06, 45.23 and 51.01 respectively were used to calculate the average crystallite size (D) of these nanoparticles.The estimated average crystallite sizes of uncoated,TiO_2 coated $La_{0.4}F_3$:$Ce_{0.45}$,$Tb_{0.15}$ and $La_{0.55}F_3$:$Ce_{0.45}$ were around 20, 21and 23 nm.

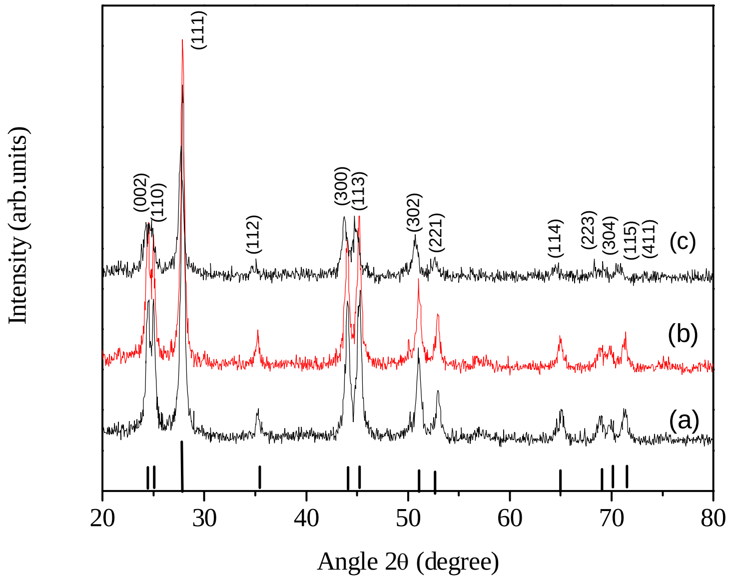

Figure 4.1 XRD spectra of (a) $La_{0.4}F_3$:$Ce_{0.45}$,$Tb_{0.15}$ (b) $La_{0.4}F_3$:$Ce_{0.45}$,$Tb_{0.15}$/TiO_2 (Core/shell) and (c) $La_{0.55}F_3$:$Ce_{0.45}$

4.3.2 TEM

Figures 4.2, 4.4 and 4.6 show the TEM image of the uncoated, thinly and thickly TiO_2 coated particles of $La_{0.4}F_3$:$Ce_{0.45}$,$Tb_{0.15}$ with inset showing the diffracted pattern. The inset image displaying SAED (selective area electron diffraction) pattern taken from an individual nano crystal indicates a single crystalline phase. From figure 4.2, it is clear that particles are agglomerated; the average size of the particle was 26 nm. Moreover the ‘d’ (d - inter lattice planar distance) spacing of the lattice parameter was obtained by considering the first five rings of the diffraction pattern using the Image J software, which closely matched with ‘d’ planes: d=3.584Å (110); d=3.115 Å (111); d=2.061 Å (300); d=1.858 Å (002) and d=1.751 Å (221) indicated in the JCPDS (32-0843) data of LaF_3. The calculated ‘d’ values of the particular five orientations were compared with the standard TiO_2. The ‘d’ values did not match with the obtained result indicating absence of TiO_2 in the uncoated sample. Similarly, the results of the ‘d’ spacing comparison obtained from the diffraction pattern of figures 4.4 and 4.6 closely matched with the lattice orientations of LaF_3 (002) d=3.891 Å ; d= 2.544 Å (112);d= 2.267 Å (211) and TiO_2 of anatase structure d=3.52 Å (101), d=1.89 Å (200) as well. Figures 4.4 and 4.6 indicate that the coated particle appears to be spherical in shape with average of 16.06 and 16.6 ± 5 nm size as obtained from the size distribution analysis. The particle sizes obtained are less than the sizes reported in the Meng-Yin et. al. [1] and A. Khorsand Zak et al., [20], which may be due to the effect of acidic environment adopted here during synthesis. This demonstrates the effectiveness of acidic environment to synthesize surfactant-free nano materials. In TEM images, contrast depends on the electron scattering power of the object forming the images. The particle size was calculated using Image J software. The EDS (Energy Dispersion Spectroscopy) spectrum shows that no impurities are present in the sample except Cu, which was used as the fine grid for holding the sample. The contrast region is utilized in estimating the coating thickness. Using the Image J software the thickness of the coating was estimated. The shell thickness were 1.6–2 nm and 4-6 nm for thinly and thickly coated $La_{0.4}F_3:Ce_{0.45},Tb_{0.15}$ nanoparticles.

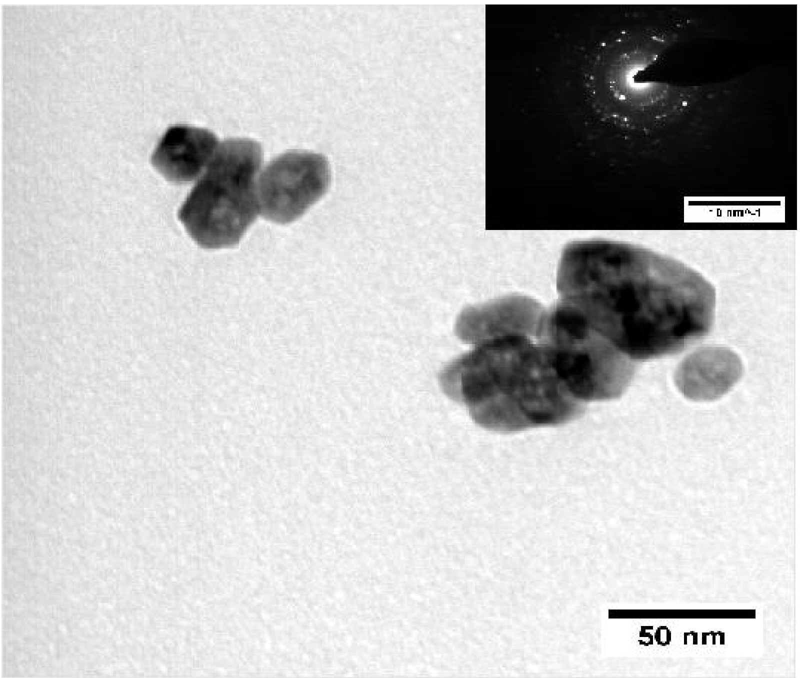

Figure 4.2TEM image uncoated $La_{0.4}F_3:Ce_{0.45},Tb_{0.15}$with insert showing the diffraction pattern

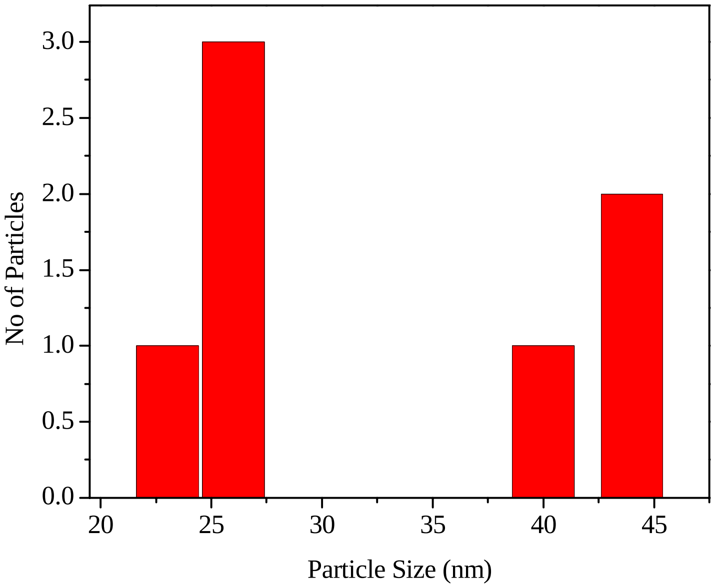

Figure 4.3 Size distribution of uncoated $La_{0.4}F_3:Ce_{0.45},Tb_{0.15}$

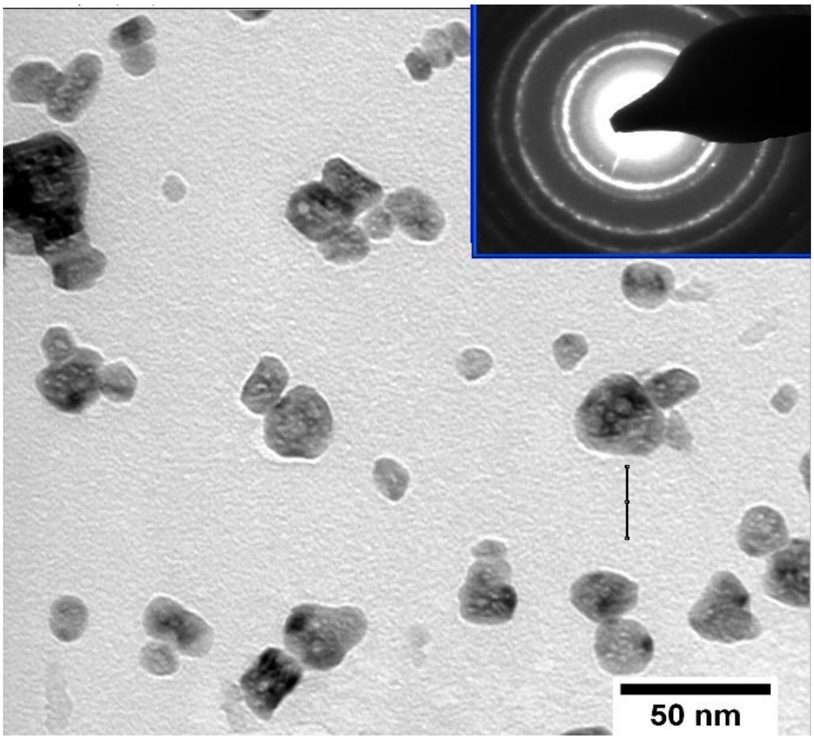

Figure 4.4TEM image of thinly (TiO_2) Coated $La_{0.4}F_3$:$Ce_{0.45}$,$Tb_{0.15}$with insert showing the diffraction pattern

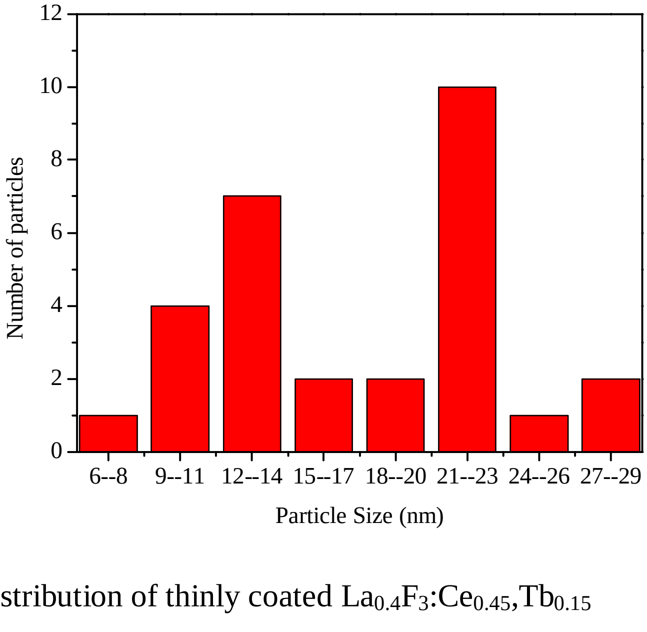

Figure 4.5 Size distribution of thinly coated $La_{0.4}F_3$:$Ce_{0.45}$,$Tb_{0.15}$

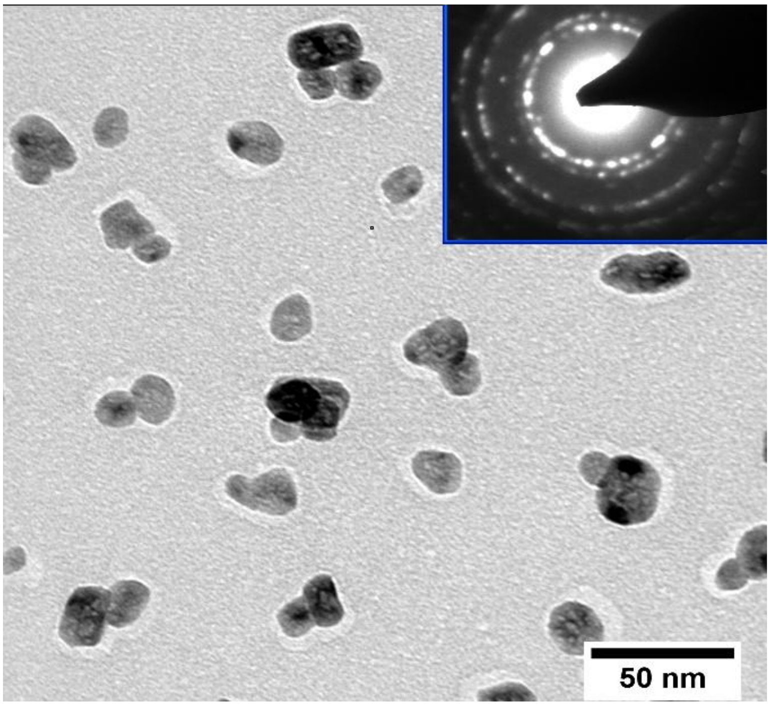

Figure 4.6TEM image of thickly coated $La_{0.4}F_3$:$Ce_{0.45}$,$Tb_{0.15}$ with insert shows the diffraction pattern

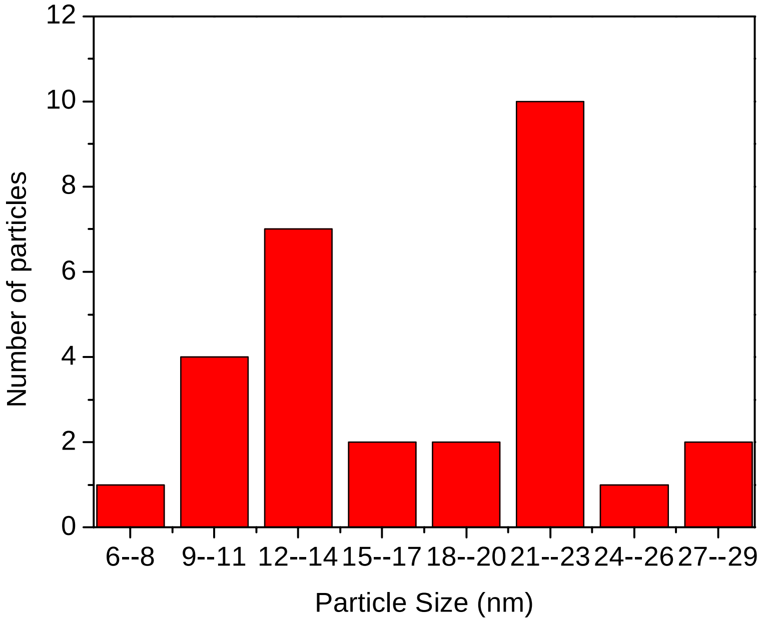

Figure 4.7 Size distribution of thickly coated$La_{0.4}F_3$:$Ce_{0.45}$,$Tb_{0.15}$

Figures 4.8, 4.9 and 4.10 show the chemical composition spectra of the uncoated, thinly and thickly TiO_2 coated $La_{0.4}F_3$:$Ce_{0.45}$,$Tb_{0.15}$ nanoparticles respectively. The EDAX chemical compositional analysis of the uncoated particles as in provided in the figure 4.8 revealed the presence of lanthanum, Fluorine, cerium and terbium only. From figures 4.9 and 4.10 which represent the TiO_2 coated $La_{0.4}F_3$:$Ce_{0.45}$,$Tb_{0.15}$ the presence of Ti along with other constituents is revealed.These data clearly confirm that the products are $La_{0.4}F_3$:$Ce_{0.45}$,$Tb_{0.15}$- TiO_2 composite nanoparticles. The elemental analysis revealed the entire elements present (as shown in tables 4.1-4.3). This technique is only qualitative. The presence of Ti in TiO_2 coated $La_{0.4}F_3$:$Ce_{0.45}$,$Tb_{0.15}$ which is about 0.17 and 0.81wt%.

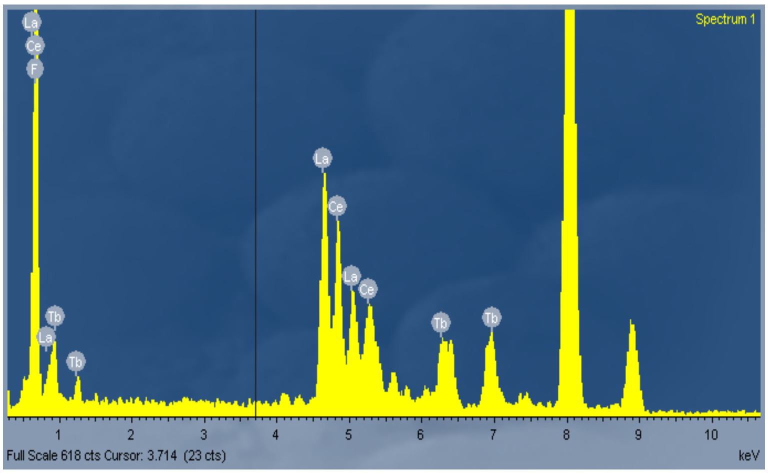

Figure4.8EDS spectra of Uncoated$La_{0.4}F_3$:$Ce_{0.45}$,$Tb_{0.15}$ sample

Table 4.1 Uncoated elemental composition of $La_{0.4}F_3$:$Ce_{0.45}$,$Tb_{0.15}$

Element	**PK.Area**	**Area sigma**	**K Factor**	**Abs. corn.**	**Weight %**	**Weight % sigma**	**Atomic %**
O K	95	39	1.871	1.000	0.49	0.20	1.82
F K	2981	117	1.752	1.000	14.51	0.54	45.10
Cu K	8904	152	1.393	1.000	34,45	0.67	32.02
La L	4302	167	2.019	1.000	24.13	0.79	10.26
Ce L	3516	166	2.020	1.000	19.73	0.80	8.32
Tb L	1103	111	2.180	1.000	6.68	0.63	2.48

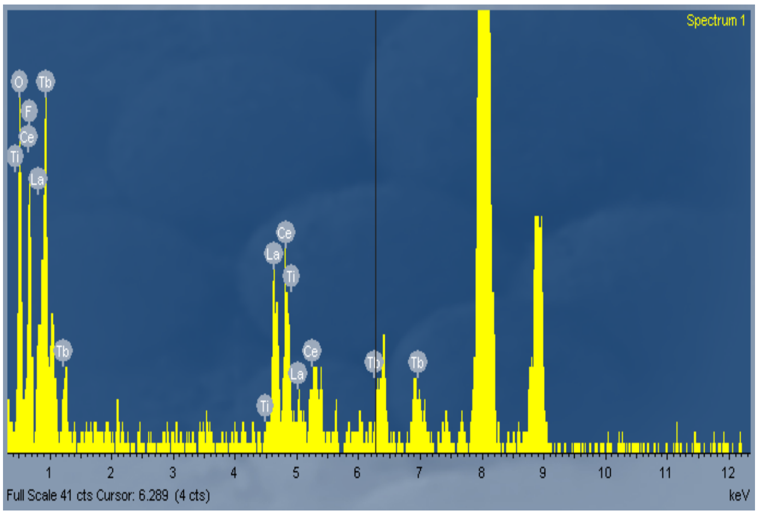

Figure 4.9 EDS spectra of Thinly coated $La_{0.4}F_3$:$Ce_{0.45}$,$Tb_{0.15}$ (core/shell)

Table 4.2 Chemical composition of thinly coated $La_{0.4}F_3$:$Ce_{0.45}$,$Tb_{0.15}$ (core/shell)

Element	**PK.Area**	**Area sigma**	**K Factor**	**Abs. corn.**	**Weight %**	**Weright % sigma**	**Atomic %**
O K	119	22	1.871	1.000	7.29	1.30	25.34
FK	58	30	1.752	1.000	3.31	1.65	9.68
Ti k	5	17	1.069	1.000	0.17	0.59	0.20
Cu K	1341	60	1.393	1.000	61.26	3.01	53.63
La L	204	41	2.019	1.000	13.54	2.43	5.42
Ce L	218	35	2.020	1.000	14.41	2.11	5.73
Tb L	0	25	2.180	1.000	0.01	1.81	0.00

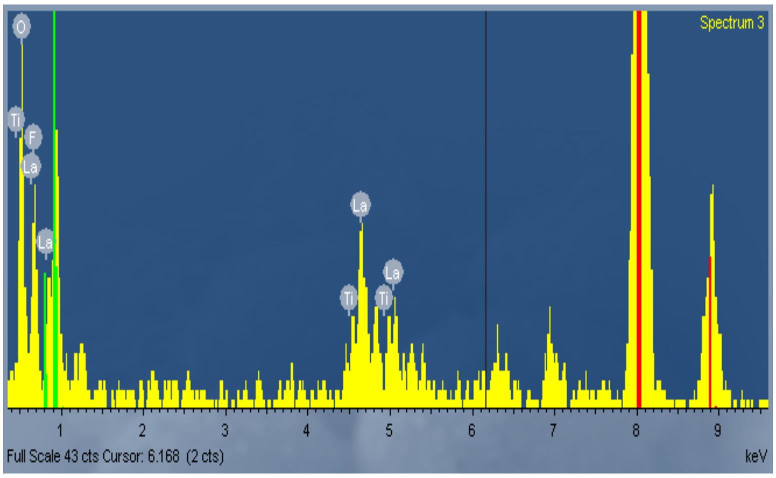

Figure 4.10 EDS spectra of thickly coated $La_{0.4}F_3$:$Ce_{0.45}$,$Tb_{0.15}$ (core/shell)

Table 4.3 Chemical composition of thickly coated $La_{0.4}F_3$:$Ce_{0.45}$,$Tb_{0.15}$ (core/shell)

Element	**PK.Area**	**Area sigma**	**K Factor**	**Abs. corn.**	**Weight %**	**Weright % sigma**	**Atomic %**
O K	123	23	1.871	1.000	9.58	1.73	28.59
F K	67	18	1.752	1.000	4.88	1.29	12.26
Cu K	1236	56	1.393	1.000	71.68	3.32	53.85
La L	155	41	2.019	1.000	13.05	3.27	4.48
Ce L	3516	166	2.020	1.000	19.73	0.80	8.32
Ti L	18	22	1.069	1.000	0.81	0.98	0.81

4.4 FTIR

Figure 4.11 shows the FTIR spectra of (a) Uncoated, (b) Plain TiO_2 and (c) TiO_2 coated$La_{0.4}F_3$:$Ce_{0.45}$,$Tb_{0.15}$. In curve (b), the 3340 cm^{-1} and 492 cm^{-1} wave numbers are attributed to the OH and Ti-O stretching [11,12]. The band at 1618 cm^{-1} is attributed to the bending vibration of H–O–H bonds [12]. In curve (c), the 3406 cm^{-1}, 1450 cm^{-1} and 492 cm^{-1} wave numbers are of OH, Ti-O-Ti [11] and Ti-O stretching indicate the presence of TiO_2 on the surface.

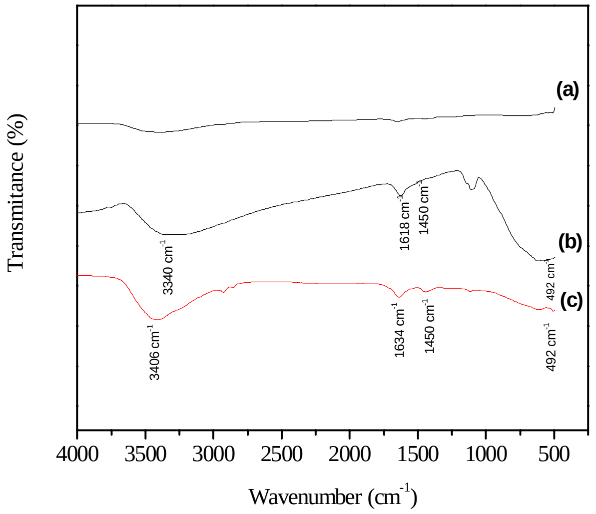

Figure 4.11FTIR of the curves (a)Uncoated;(b) Plain $TiO_2$and (c) TiO_2 Coated $La_{0.4}F_3$:$Ce_{0.45}$,$Tb_{0.15}$

4.5 Optical Characterization

4.5.1 UV-Vis absorption

Figure 4.12 represents the UV-Vis absorption spectra of TiO_2 coated and uncoated $La_{0.4}F_3:Ce_{0.45},Tb_{0.15}$ colloidal solutions obtained by dispersing 10 mg of powder in 5 ml of DM water and ultrasonicated for 30 minutes. Curves a and b represent the absorption of the uncoated $La_{0.4}F_3:Ce_{0.45},Tb_{0.15}$ and $La_{0.4}F_3:Ce_{0.45},Tb_{0.15}$ / TiO_2 coated samples respectively. The five absorptions of Ce^{3+} are distinctly clear and it is consistent with that reported by L.R.Elias and P. Dorenbos [14,15& 16]. It is observed that the Ce^{3+} absorption in the TiO_2 coated material was less compared to that of the uncoated sample. The presence of TiO_2 around $La_{0.4}F_3:Ce_{0.45},Tb_{0.15}$ probably has decreased the absorption of the light by Ce^{3+}.

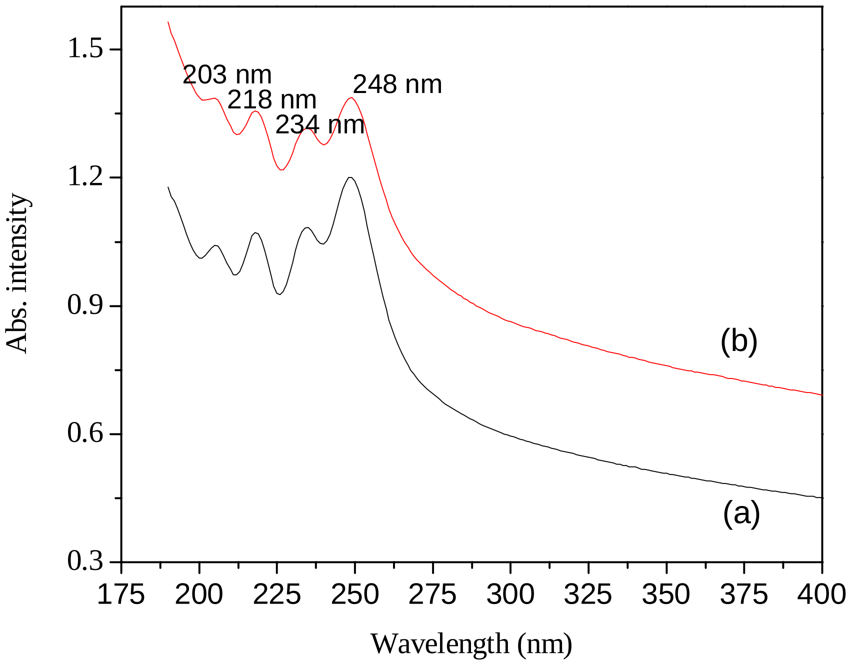

Figure 4.12 UV-Vis absorption of (a) $La_{0.4}F_3:Ce_{0.45},Tb_{0.15}$and(b) $La_{0.4}F_3:Ce_{0.45},Tb_{0.15}/TiO_2$ (Core/shell)

4.5.2Photoluminescent Spectroscopy

4.5.2.1 Tb^{3+} emission from $La_{0.4}F_3$:$Ce_{0.45}$,$Tb_{0.15}$

Figure 4.13 shows the PL spectra of the as-prepared uncoated $La_{0.4}F_3$:$Ce_{0.45}$,$Tb_{0.15}$(core) powder sample synthesized at pH 4.6. The spectrum was recorded by exiting the samples at 262 nm. The emission spectrum agrees well with the Tb^{3+} emission spectrum as discussed in [16]. The excitation spectrum also agrees well with the Tb^{3+} excitation spectrum in presence of Ce^{3+} reflecting the energy transfer from $Ce^{3+}$to Tb^{3+}.

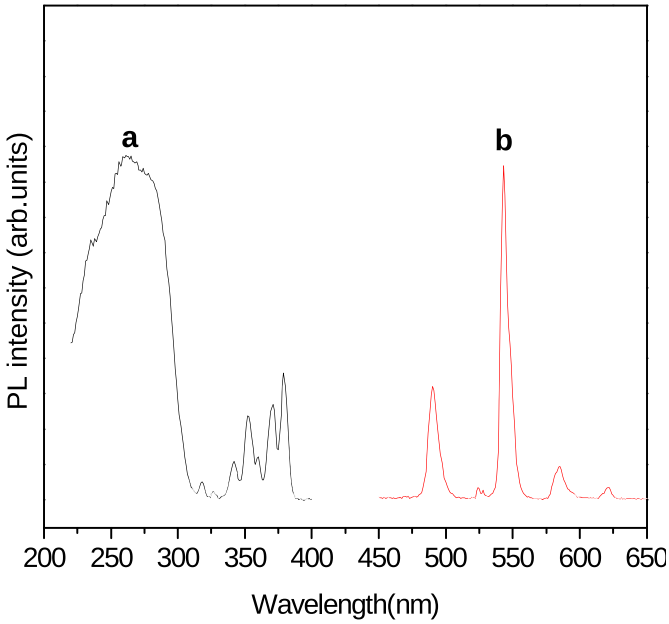

Figure 4.13PL spectra of uncoated $La_{0.4}F_3$:$Ce_{0.45}$,$Tb_{0.15}$synthesized at pH=4.6; (a) Excitation spectrum λ_{em}=543nm (b) Emission spectrum λ_{ex}=262 nm; slit width=1.5nm.

4.5.2.2 Effect of coating on Ce^{3+} emission

In figure 4.14 presents the Ce^{3+} excitation and emission spectra of $La_{0.4}F_3$:$Ce_{0.45}$,$Tb_{0.15}$ core and $La_{0.4}F_3$:$Ce_{0.45}$,$Tb_{0.15}$ core/TiO_2 shell luminescent materials On comparing the core and core/shell spectra provided in the figure, it is obvious that, TiO_2 shell of thickness 1.6-2 nm of lanthanum fluoride phosphor reduces the cerium photoluminescence intensity by 2.5 times. The cerium emission intensity further decreased with the increase in the shell thickness (4-6 nm). As discussed previously in Figure (4.12), the presence of TiO_2 shell decreased the absorbance too. Therefore, decrease in absorption led to decrease in the emission from cerium.

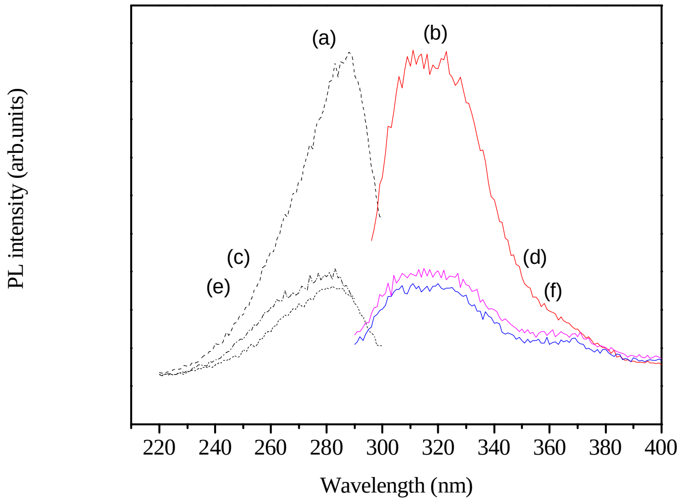

Figure 4.14 Uncoated (core) excitation curve (a) for λ_{emi} =325 nm ; emission curve (b) for λ_{exi} = 292 nm ;; TiO_2 coated $La_{0.4}F_3:Ce_{0.45},Tb_{0.15}$ excitation curves (c)with coating thickness 1.6-2 nm; (e) with coating thickness 4-6 nm for λ_{emi} =325 nm;; Emission curves (d)with coating thickness 1.6-2 nm ; (f) with coating thickness 4-6 nm λ_{exi} =292 nm.

4.5.2.3 Effect of coating on Tb^{3+} emission from $La_{0.4}F_3:Ce_{0.45},Tb_{0.15}$ / TiO_2

Figure 4.15 represents the PL spectra of core and core shell structures of $La_{0.4}F_3:Ce_{0.45},Tb_{0.15}$ with different shell thickness. The PL excitation and emission intensity for shell thickness (1.6-2nm) has decreased slightly compared to $La_{0.4}F_3:Ce_{0.45},Tb_{0.15}$ core. However, upon increasing the shell thickness to 4- 6 nm, there is a significant enhancement in the green emission from $^5D_4$ energy level (544 nm). At this shell thickness, the intensity was enhanced by 1.76 times compared to that from core nano particles. The probable process involved in this interesting observation is discussed as follows. J.K Han et.al [14], have studied the SiO_2 as the shell around $Y_2SiO_5:Ce^{3+},Tb^{3+}$ which increased light output of this nano phosphor. According to them, the surface defects present invariably in nanomaterials are quenched in presence of shell structures. The surface defects are known to increase the non-radiative decay of the excitation energy. Therefore, the reduction in the surface defects may result in minimizing the non-radiative decay process and thereby enhancing the luminescence. In the presence study, significant enhancement of luminescence is observed for 4-6 nm TiO_2 thickness whereas marginal quenching of luminescence was observed for 1.6-2 nm thickness. This indicates probably an optimum coating thickness is required for observing enhancement in luminescence. However, more studies are required to understand the surface modification process and its effect on luminescence

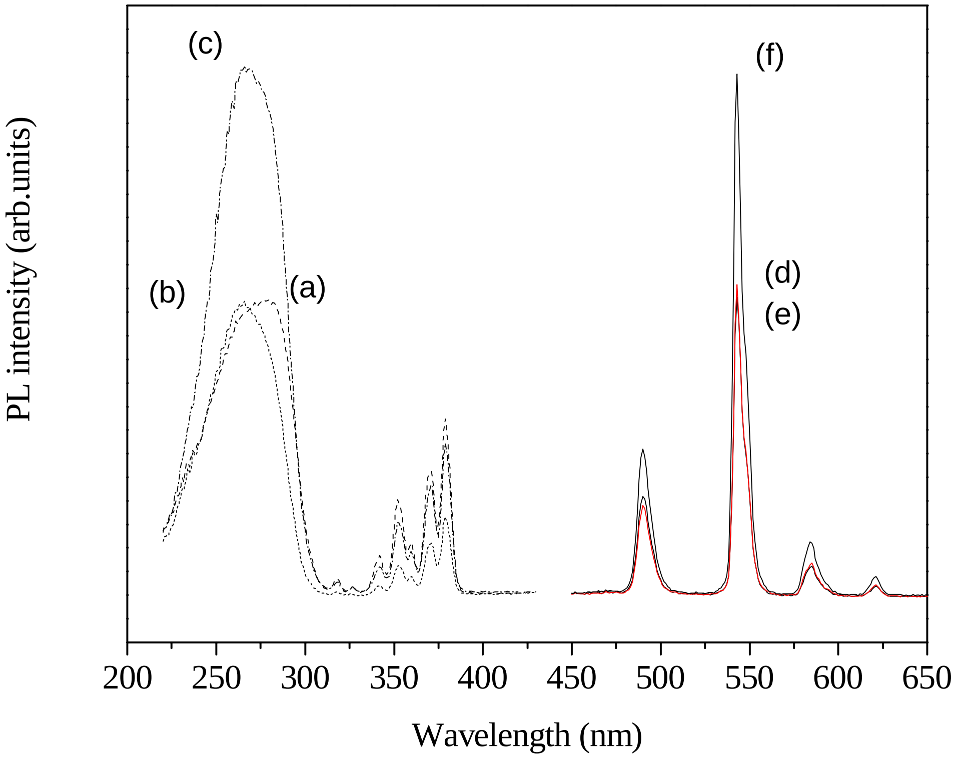

Figure 4.15 PL. spectra of $La_{0.4}F_3$:$Ce_{0.45}$,$Tb_{0.15}$ excitation curves of (a) uncoated (core) ;; (b) thinly and (c) thickly TiO_2 coated $La_{0.4}F_3$:$Ce_{0.45}$,$Tb_{0.15}$ (core/shell) for λ_{em}=543 nm ; emission curves (d) uncoated for λ_{ex} = 283 nm;(e) thinly (1.6-2 nm) and (f) thickly (4-6 nm) TiO_2 coated for λ_{ex} = 268 nm

4.5.2.4 Effect of coating on Tb^{3+} emission from $La_{0.85}F_3$:$Tb_{0.15}$ (core/shell)

In figure 4.16, curves a ,c represent the Tb^{3+} excitation for 543 nm emission and curves b,d represent emission of the uncoated (core) and the TiO_2 coated $La_{0.85}F_3$:Tb $_{0.15}$ (core/shell) samples with 379 nm excitation wavelength. It is evident that the 543 nm emission of the uncoated is higher than the coated, which might be due to prevention of the excitation UV photons from reaching the Tb^{3+} centers by TiO_2. With thin coating the PL intensity is decreased which might due to the coating paving ways for the increased radiationless transfer.

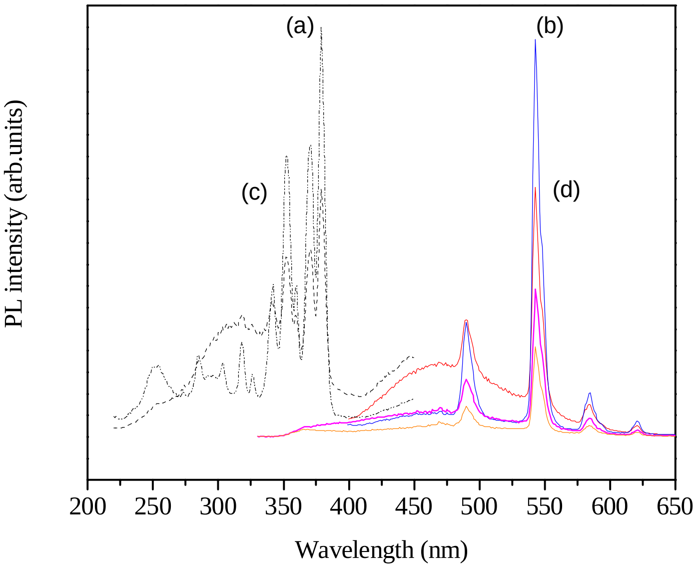

Figure 4.16PL. spectra of $La_{0.4}F_3$:$Ce_{0.45}$,$Tb_{0.15}$; Exitation curves (a) uncoated (core);(c) TiO_2 coated $La_{0.4}F_3$:$Ce_{0.45}$,$Tb_{0.15}$ (core/shell) for λ_{em}= 543 nm; Emission curves (b) uncoated ;(d) TiO_2 coated λ_{exi}=379 nm

4.6 PL Life time

Figures 4.17 and 4.18show the PL, emission lifetime of Ce^{3+} and Tb^{3+} from uncoated and TiO_2 coated $La_{0.4}F_3$:$Ce_{0.45}$,$Tb_{0.15}$colloidal samples exited with 280 nm wavelengths. The obtained data were fitted with third order exponential which shows that the TiO_2 coated Ce^{3+} emission decays marginally faster thanthe uncoated. The life time of the Ce^{3+} in coated and uncoated were 13.6 and 12.9 ns, which is also evident from the decrease in the Ce^{3+} emission intensity from the coated sample (figure 4.14). In the case of the Tb^{3+} emission, the uncoated and coated decay times were 19.17 and 21.05 µs respectively. This clearly demonstrates that shelling increases the luminescence decay time of Tb^{3+}; the result is in consistence with Tb^{3+} lifetime reported in the [3,17].

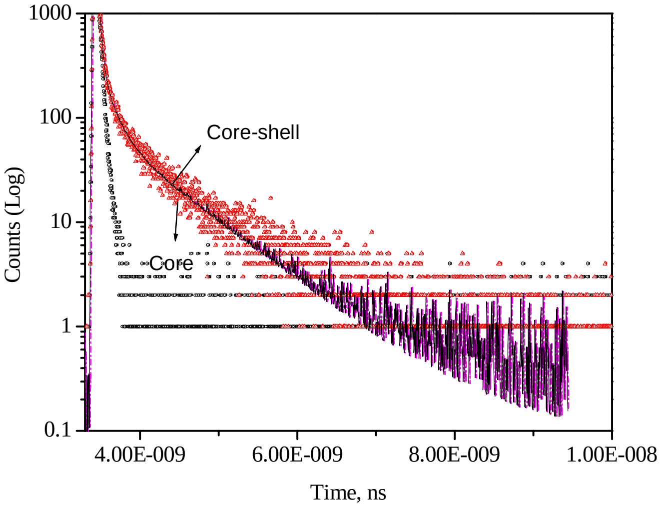

Figure 4.17 Time-resolved luminescence intensity decay curves of Ce^{3+} in the $La_{0.4}F_3$:$Ce_{0.45}$,$Tb_{0.15}$ (Core) and $La_{0.4}F_3$:$Ce_{0.45}$,$Tb_{0.15}$ / TiO_2 (Core/shell) nanocrystals

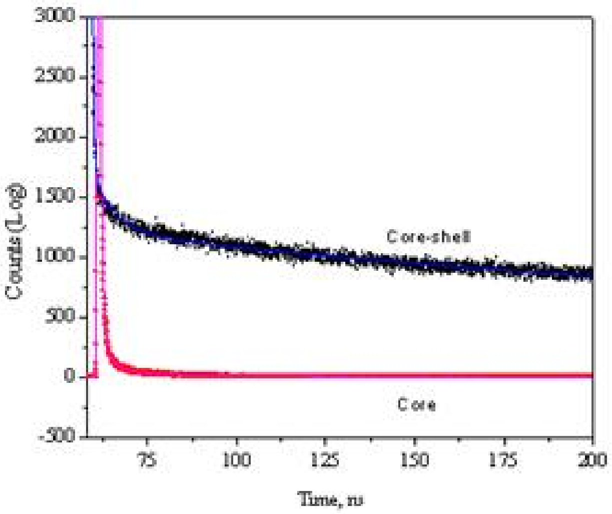

Figure 4.18 Time-resolved luminescence intensity decay curves of Tb^{3+} in the $La_{0.4}F_3$:$Ce_{0.45}$,$Tb_{0.15}$(Core) and $La_{0.4}F_3$:$Ce_{0.45}$,$Tb_{0.15}$ / TiO_2 (Core/shell) nanocrystals

4.7 Scintillation under X-ray excitation

The powder samples were kept in a dark plastic container at 10 cm away from the X-ray tube. The fiber optic cable probe for collecting the light emitted was fixed tightly to a stand and kept at 1cm away from the powder sample a bit inclined so as not to prevent the X-rays, which is connected to CCD based spectrometer (Avantes 2010). The spectrometer is operated through a laptop connected to it using inbuilt software. Figures 4.19, 4.20 and 4.21 show the experimental setup, scintillation spectra from uncoated and TiO_2 coated $La_{0.4}F_3:Ce_{0.45},Tb_{0.15}$ materials, obtained by irradiating the powder sample with X-rays. The X-ray tube was operated at 110 kV and 12 mA for 30 seconds. There are many emission lines in the figure due to the stray background light in the X-ray chamber. The scintillation intensity was a bit less in the uncoated sample compared to the coated sample. This indicates that $La_{0.4}F_3:Ce_{0.45},Tb_{0.15}/TiO_2$ (core-shell) marginally improves the scintillation output in this study that agrees well with data reported in [13].

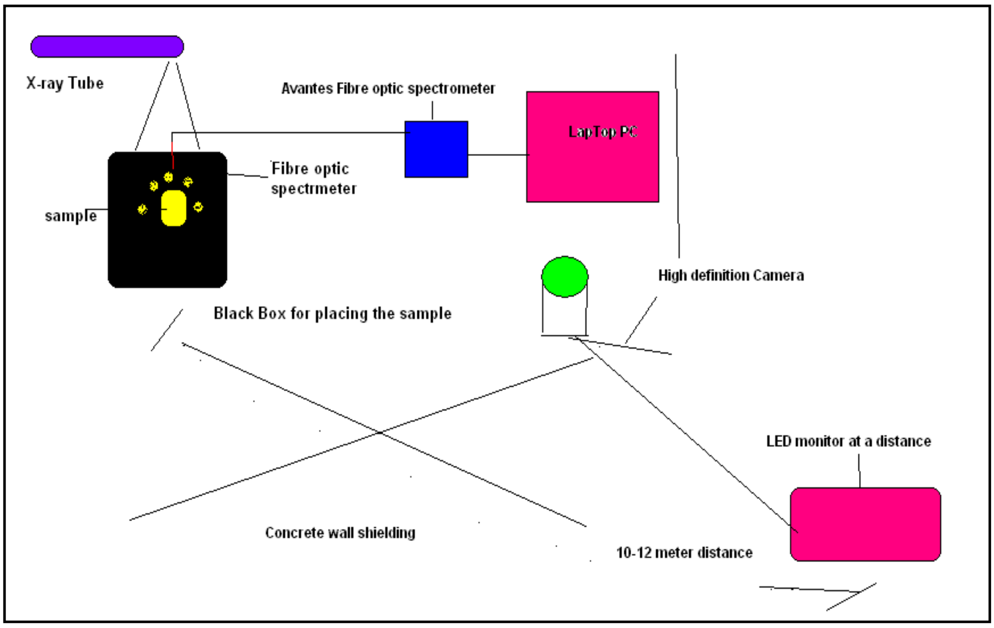

Figure 4.19 Experimental setup for scintillation experiment

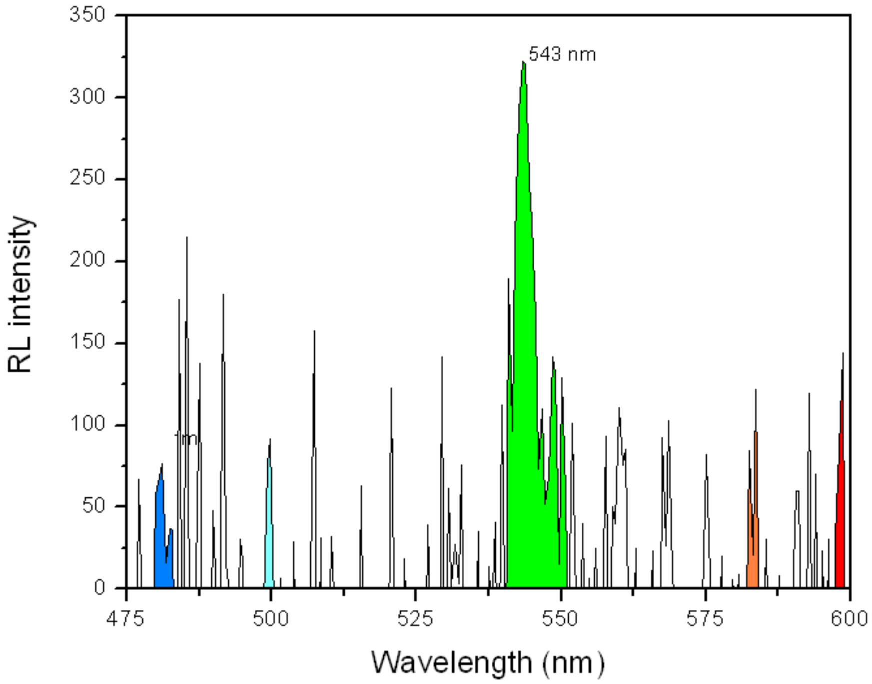

Figure 4.20 Scintillation spectra of uncoated $La_{0.4}F_3$:$Ce_{0.45}$,$Tb_{0.15}$ under X-ray excitation

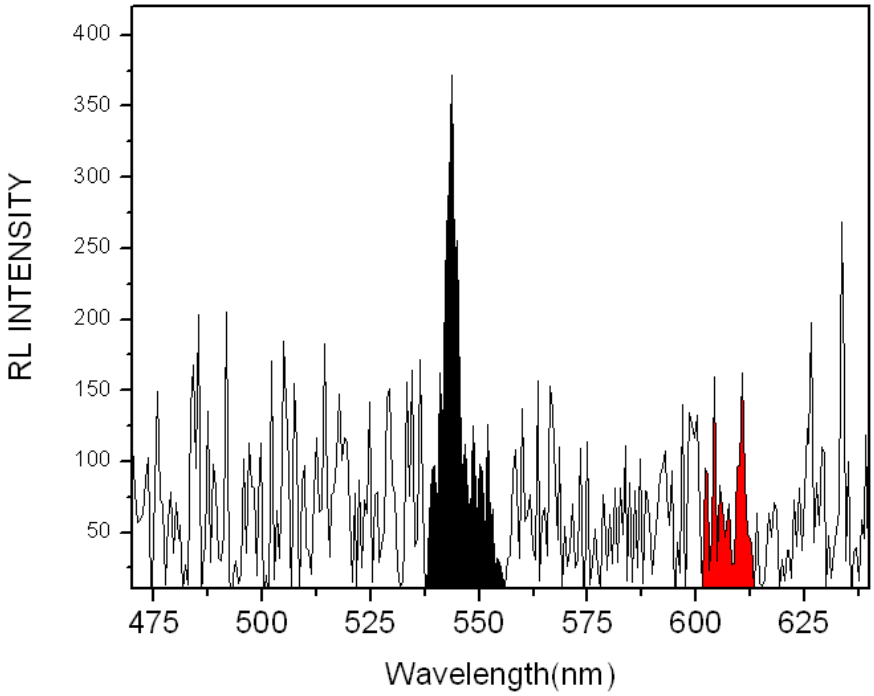

Figure 4.21 Scintillation spectra of TiO_2 coated $La_{0.4}F_3$:$Ce_{0.45}$,$Tb_{0.15}$under X-ray excitation

4.8 Experimental

4.8.1 Synthesis of non-stoichiometric LaF_3:Ce

$LaF_3:Ce^{3+}$ was synthesized in both stoichiometric (nominal composition) and non-stoichiometric ratios by adopting co-precipitation technique as discussed in chapter-3. The compound LaF_3 was prepared with various lanthanum and fluoridemolar ratios to studyeffect of nonstiocimetriy on PL. Firstly the amount of lanthanum was varied by keeping the fluorine amount constant. Then the amount of fluorine was varied by keeping lanthanum constant. In this experiment the molar ratio of La to F was maintained at 0.30, 0.28, 0.26; 0.37, 0.39 and 0.40. From the study of effect of concentration we found that the optimum concentration of cerium was 0.05 mol. The nanoparticles synthesized in this manner have hexagonal structure and exhibited intense photoluminescence. In order to avoid oxygen contamination halide compounds were chosen as the precursor materials. Moreover, stock solutions were also prepared to avoid any error during synthesis. The precipitate from the reactant liquid was difficult to separate even at 10,000 rpm in the case of La/F ratios 0.41 and 0.39, as variation in the fluorine compositing lead to a very fine colloidal formation. The colloidal solution was dried and transferred to a filter paper and washed thoroughly with DM water to remove the unreacted chlorides. The filtered water was checked for the presence of chlorine by adding $AgNO_3$ solution for white precipitate formation. The filter paper containing the precipitate was removed from the filtering setup and was dried in vacuum oven at 85°C for 2 h. similar procedure was adopted in the stoichiometric synthesis of LaF_3. Characterizations of the samples were performed at room temperature. X-ray diffractometer (GNR APD 2000 PRO) with $Cu_{K\alpha}$ line wavelength 1.5406 Å was used to analyze the structure. The room temperature PL spectra were recorded with a Flourimeter (RF5401PC) equipped with 150 W of Xenon lamp as excitation source. XRF analysis was also carried out to estimate Lanthanum and cerium composition.

4.8.2 XRD investigations

XRD is the preferred method for examining the formation of the crystalline materials. In our experiments, the samples prepared by varying the stoichiometry of lanthanum and fluoride were subjected to XRD investigations. In this experiment the molar ratio of La to F was maintained at 0.30, 0.28, 0.26; 0.37, 0.39 and 0.40. X-ray diffraction pattern of LaF_3:$Ce^{3+}$is presented in the figure.4.22 (curves a-f). It is clear from figure 4.22 that all samples show the sharp peaks of reflection indicating the high crystallanity of nano crystals irrespective of lanthanum to fluoride molar ratio.

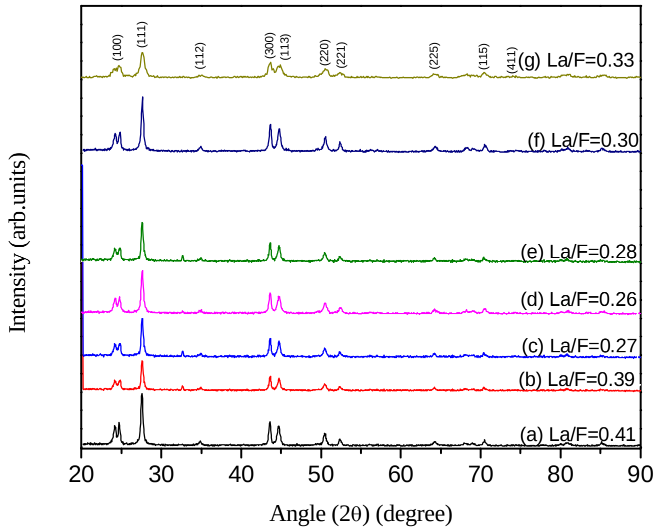

Figure 4.22 XRD patterns of LaF_3:Ce for various La and F molar ratios

All dominant positions of stoichiometry as well as non nonstoichiometric samples are closely matching with data reported in value of JCPDS [32-0483] of pure hexagonal LaF_3 crystal structure. The crystallite (coherently scattering domains) sizes of the nanocrystals are calculated from the XRD patterns using Williamson Hall plot method.The lattice parameters of all the samples were estimated using “STOE WINXPOW” (a XRD pattern analyzing software that takes into account the all the peaks in the XRD pattern).

As per the calculated lattice parameters and the obtained hexagonal structure nature for all the samples, it is obvious that there was no effect on the lattice even in the case of deliberately created non stoichiometry during synthesis. However, in case of samples aimed for non-stoichiometry, slight peak shifting towards higher angles was observed in (f) La/F= 0.30 and (e) La/F=0.28. In the case of fluorine deficient samples impurity contributions from chlorine peak was observed. However there was no change in the lattice parameter *a* and*c* values.

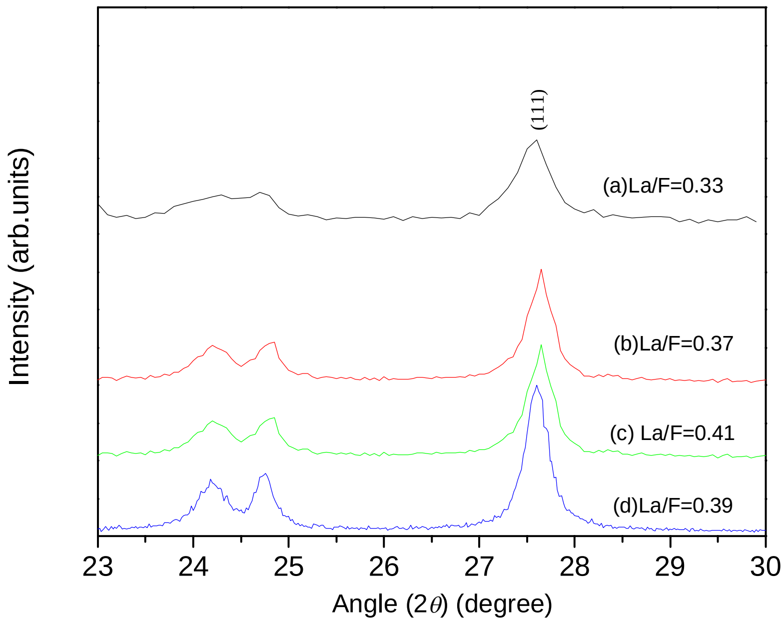

Figure 4.23XRD profiles of LaF_3 nano particles with different La/F molar ratio

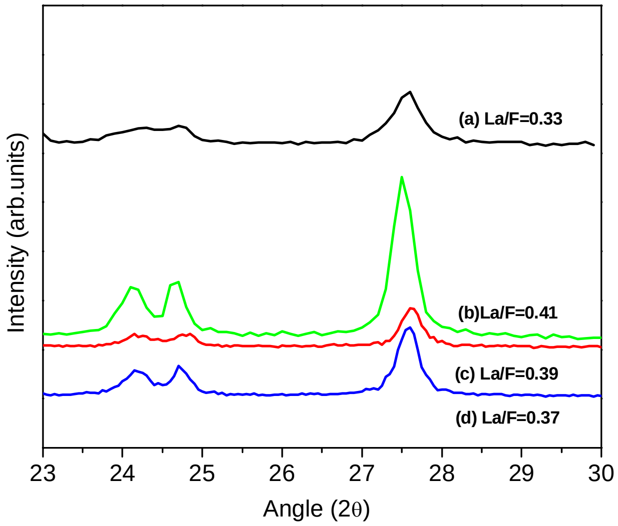

Figure 4.24XRD profiles of LaF_3 nano particles with different La/F molar ratio

From figures 4.23 and 4.24 one can see that the FWHM of (111) line is slightly narrowing with decrease in La^{3+} as well as F- molar ratios as suggesting the crystallinity of the sample is improved. Furthermore, it is commonly admitted that the domain size of sample is inversely proportional to the FWHM of its XRD lines, so it can be inferred that the domain size of sample become larger with the decrease in the La^{3+} as well as F^- (Table 4.4). Good cyrstallinity is important for phosphors, because high crystallinity and large grain size always means less intrinsic defects and more effective luminescence centers, which really lead to stronger luminescence [18]. Nano phosphor prepared from exact stoichiometry LaF_3 (1:3) ratio possess the average crystallite size of 22 nm whereas the size of lanthanum and fluoride deficient samples are varied from 20 nm to 45 nm. Very small size is attained when the fluorine concentration was the least. This shows that the particle size has direct dependence on the cation / anion charges present in the precursor solution. The non variation in the lattice parameters implies that there was no change in the structure (hexagonal) or lattice is strained deliberately created non stoichiometry during synthesis. XRD results clearly reveal that variation in concentration of either lanthanum or fluoride does not change the crystal structure significantly. The calculated cell parameters, the average crystallite size are provided in Table.4.4.

Table 4.4 Lattice parameter and particle size

S.No	**Composition**	**Molar ratio (La:F)**	**Average Particle size** (nm)	**Lattice parameters (Å)**
1	Stochiometry (LaF_3)	0.33	22	a=7.179 (2) c=7.337 (4)
2	$LaF_{2.7}$	0.37	20	a=7.182 (2) c=7.348 (2)
3	$LaF_{2.55}$	0.39	39	a=7.172 (4) c=7.331 (4)
4	$LaF_{2.44}$	0.41	38	a=7.175 (2) c=7.336 (4)
5	$La_{0.9}F_3$	0.30	39	a=7.180 (4) c=7.348 (2)
6	$La_{0.85}F_3$	0.28	30	a=7.178 (2) c=7.347 (6)
7	$La_{0.8}F_3$	0.26	45	a=7.176 (4) c=7.334 (2)

4.9 UV-Vis absorption

The colloidal solution sample (prepared as described earlier) was taken for UV-Visible absorption studies. Figure 4.25 shows the UV-Vis absorption spectra of the samples non-stiochiometric(a) La/F=0.30 (b) La/F=0.28 (c) La/F =0.26(d) La/F =0.37(e) La/F=0.39 and (f)La/F=0.41. $La_{1-x}F_3:Ce_{x=0.05}$ samples. The absorption spectra show five distinct, clearly resolved absorption peaks at wavelengths 198, 205, 218, 234 and 247 nm. These wavelengths correspond to the lower energy levels of Ce^{3+} as made by

Dorenbos2000[14]and Heaps [16&23]. There were no new absorptions wavelengths observed and the absorption intensity is less in the case of samples formed with La/F= 0.26 and La/F=0.41 molar ratios.

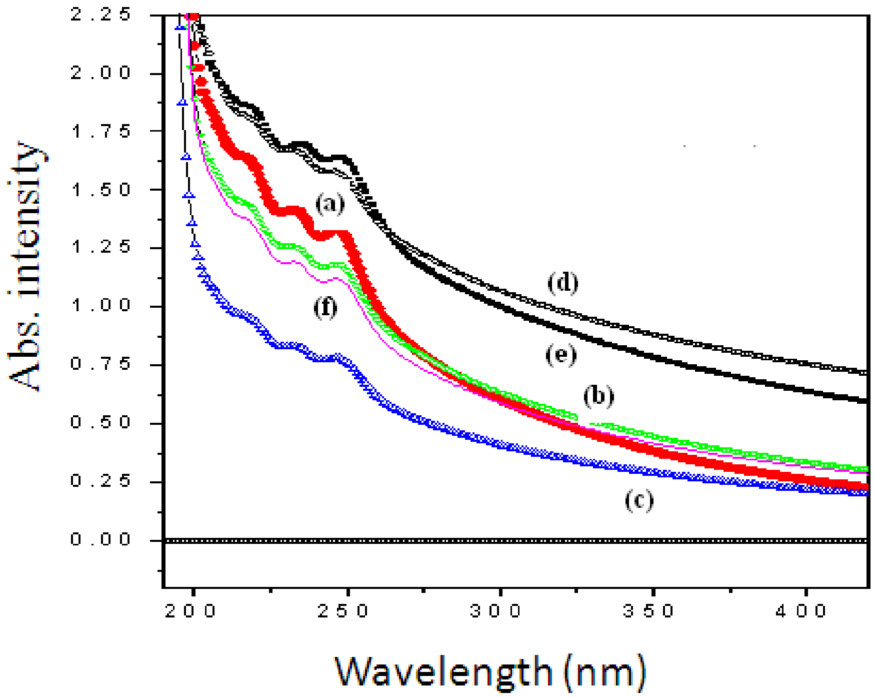

Figure 4.25 UV-Vis absorption spectra of non-stoiciometric samples Curve (a) La/F=0.30 (b) La/F=0.28 (c) La/F =0.26(d) La/F =0.37(e) La/F=0.39 and (f)La/F=0.41.

4.10 Effect of non-stoichiometry on photoluminescence of LaF_3:Ce

4.10.1 Effect of lanthanum Variation on PL spectra of $LaF_3:Ce^{3+}$nano particles

Figure.4.26shows the room temperature photoluminescence spectraof $LaF_3:Ce^{3+}$nano particles in different La/F molar ratio. Curves a(La/F=0.33),b(La/F=0.3),c(La/F=0.28),d (La/F=0.26) e (La/F=0.26) and a’b’c’d’e’ represent the excitation and emission profiles respectively.The excitation and emission profiles are exhibited at 250 nm and at 303 nm respectively. It has been well established that, these broad excitation and emission bands are due to 5d-4f transitions from Ce^{3+}. In our studies, among all the samples that we investigated the sample with proper stoichiometry ratio (La/F=0.33)(curves a & a’) has shown maximum PL intensity.

Conversely, the samples with decreasing lanthanum concentration the photoluminescence intensity of cerium decreased marginally and it reduced significantly for the sample with non-stoichiometry wherein the La/F ratio is 0.30. This reduction is probably due to the presence of unreacted impurity phases (not evident from XRD) which provide non radiative pathways of relaxation for cerium and thereby quench emission. It has been reported that, the multiphonon relaxation of the excited state of rare-earth ions doped can be faster[20] which is true our case also, the effect of change in stoichiometry indeed enhanced the multiphonon relaxation from cerium. With La/F=0.30 and La/F=0.28, there are no significant change in the observed profile of excitation and emission spectra suggesting that there is no perceptible change in crystal field experienced by cerium ion in this host. But at La/F= 0.26, there are excitation maximas appearing at 248 and 260 nm with corresponding 304 and 346 nm emission respectively. In many hosts, cerium exhibits single emission peak if spin orbit coupling is low. Whereas in our case these nanoparticles present two luminescence bands at 304 and 346 nm attributed to Ce^{3+} transitions from the perturbed 5*d* level of Ce^{3+} ions located nearby defect centers [6,22] de-excited to two 4*f* ground levels $^2F_{5/2}$ and $^2F_{7/2}$ formed due to the changes in the crystal field [15].

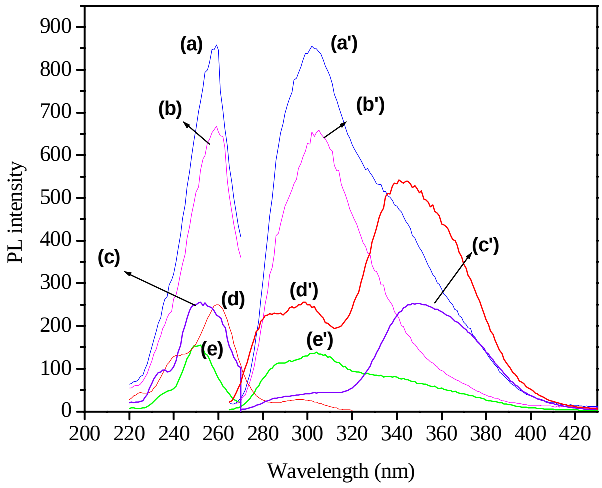

Figure 4.26PL excitation and emission spectra of LaF_3:Ce Stoichiometric (La/F=0.33); (a) λ_{emi} =301,(a')λ_{exi} = 259 nmand Non-stoichiometric(b) (La/F =0.30) ;λ_{emi} =304nm ;(b')λ_{exi} = 259 nm ;(c) (La/F =0.30) ; λ_{emi}=304nm; (c') λ_{exi} = 260 nm ;(d) (La/F =0.28) ; λ_{emi} =346nm ; (d') λ_{exi} = 251 nm ;(e) (La/F=0.26) ;λ_{emi} =303 nm ; (e') λ_{exi} = 260 nm

4.10.2 Effect of fluorine on the PL spectra of LaF_3:$Ce3^+$nano particles

Figure 4.27 (a)presents the excitation profiles of fluorine deficient LaF_3:Ce^{3+}nano particles with decreasing molar % from La/F= 0.37, La/F= 0.39 to La/F= 0.40 respectively. Curve $A_{ex,}$ having peak maximum at 258 nm represents the molar ratio La/F= 0.33 (stoichiometric), curve $B_{ex}$and C_{ex} with peak maxima at 259 and 275nm represent the molar ratio La/F= 0.37; Both $D_{ex}$and E_{ex} represent the molar ratio La/F= 0.39and F_{ex} represents the molar ratio La/F= 0.40. At molar ratio La/F=0.37 for Curve B_{ex}, the intensity is bit less though it almost follows the stoichiometric curve A_{ex}. Curve C_{ex} possesses a shoulder at 259nm with less intensity and a peak at 275 nm. C_{ex} also seems to have a peak around 318nm. The intensity of 275nm peak is slightly higher than the stoichiometric curve $A_{ex.}$ At molar ratio La/F=0.39, Curves $D_{ex}$and E_{ex} with their peak maxima at 252 and 262nm possess less intensity compared to A_{ex}. At molar ratio La/F=0.40, Curve F_{ex}having peak maxima at 260 and 317 nm possessed slightly higher intensity than the stoichiometric curve A_{ex}. This curve has also exhibited shoulders around 226 and 240 nm. The appearance of a peak around 317 nm is interesting.

Figure 4.27 (b)presents the corresponding emission profiles of Fluorine deficient LaF_3:Ce^{3+}nano particles with decreasing molar La/F ratios 0.37, 0.39 and 0.40 respectively. Curve $A_{em,}$ having peak maxima at 303 nmrepresents the molar ratio La/F=0.33 (stoichiometric); curve $B_{em}$and C_{em} peaking at 304 and 344nm represent the molar ratio La/F=0.37. D_{em} and E_{em} representing the molar ratio La/F=0.39 have peaks around 286,306,343 nm. F_{em} representing the molar ratio of La/F=0.40 has peaks around

303, 340 and 364nm. The overall consideration of the excitation and emission spectra of these Fluorine deficient samples show that the emission characteristic of such samples can be different depending on the extent of the Fluorine deficiency. This could have been due to the location of the Ce^{3+} in different environment experiencing a different electrostatic interactive forces resulting in shifting of the excitation and emission characteristics. This indicates towards a possibility of introducing tunability by changing the stoichiometry.

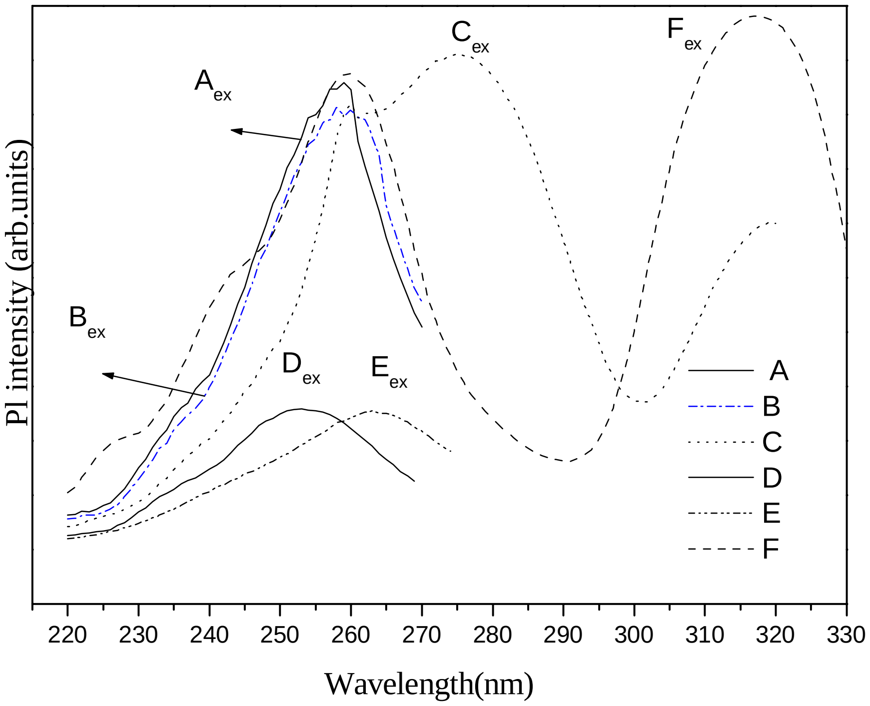

Figure 4.27 (a) PL spectra of stoichiometric LaF_3:Ce^{3+} Excitation curve $A_{ex}\lambda_{em}$ =304;Non-stoichiometric La/F=0.37 Excitation curves $B_{ex}\lambda_{em}$ =302 nm; $C_{ex}\lambda_{em}$ = 346nm ; La/F=0.39 Excitation curves D_{ex} = λ_{em} =304nm; $E_{ex}\lambda_{em}$ =346nm ;La/F=0.40 Excitation curves $F_{ex}\lambda_{em}$ =346 and 375nm

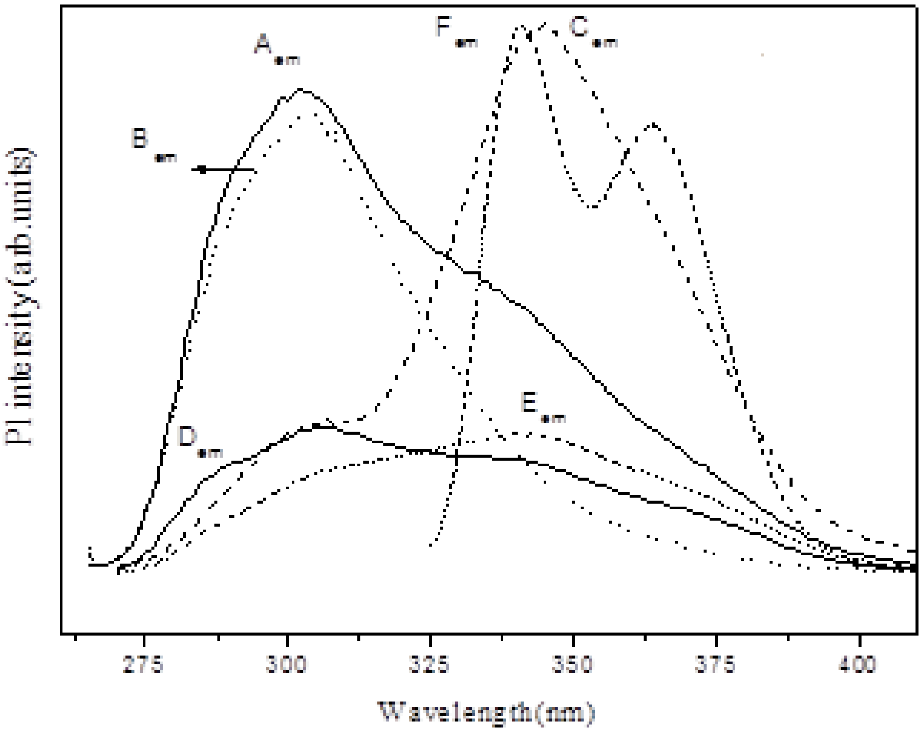

Figure 4.27 (b) PL emission spectra of stoicimetric LaF_3:Ce Emission curve $A_{em}\lambda_{ex}$ =251nm;Non-stoiciometric Emission curves La/F=0.37 ; $B_{em}\lambda_{ex}$ =231nm; $C_{ex}\lambda_{ex}$ = 275nm ; La/F=0.39 $D_{em}\lambda_{ex}$ =243nm; $E_{em}\lambda_{ex}$ =265nm ; La/F=0.40 $F_{em}\lambda_{ex}$ =251nm

Moreover, there was not much difference in the Stokes shift with La/F=0.3 molar ratio when compared to the stoichiometric (1:3) sample. As we further decrease the La concentration stokes's shift decreases initially implying decrease in energy loss and considering 346 nm emission with La/F=0.26 ,there is a considerable increase in the shift implying ,increased loss of energy which might arise due to the variation in the crystal field.Unlike the case lanthanum, when the fluorine concentration decreases the Stokes shift increases for all the ratios implying higher energy loss. At La/F=0.40 molar ratio, with 375nm emission the shift was the maximum. Table 4.5 shows the calculate Stoke's shift parameters.

It is obvious from the Stokes shift observation, that the variation of anion (fluorine) causes more Stokes shift than the Lanthanum variation (cation), implying anionic deficiency (defects) has more bearing or (distorts more) influence on the emission spectra a in the ionic based host matrices.

Table 4.5 Stokes shift: Stoichiometric and Non stoichiometricLaF_3:Ce

S.No	**Excitation wavelength (nm)**	**Emission wavelength (nm)**	**Stoke's shift (nm) (Energy in Joules)**
La/F= 0.33stoi	258	301	42 (0.0261)
La/F=0.3	251	303	52 (0.0262)
La/F=0.28	258	304	46 (0.0231)
La/F=0.26	260	288,304,346	86 (0.014,0.022,0.0432)
	251	346	95 (0.0478)
La/F=0.37	231	302	71 (0.0357)
	275	346	71 (0.0357)
La/F=0.39	243	304	61 (0.0307)
	265	346	81 (0.0407)
La/F=0.40	251	346;375	95;124 (0.0478; 0.0624)

4.11Conclusion

After being doped with Ce^{3+} and Tb^{3+} no significant change in the crystal structure of LaF_3 was observed though a slight decrease in the lattice parameter was observed with a heavy dopant concentration. The estimated average crystallite size of $La_{0.4}F_3$:$Ce_{0.45}$,$Tb_{0.15}$and TiO_2 coated $La_{0.4}F_3$:$Ce_{0.45}$,$Tb_{0.15}$ nanoparticles were around 21 and 22 nm respectively. TEM images & the associated diffraction pattern and the EDAX confirmed the formation of the $La_{0.4}F_3$:$Ce_{0.45}$,$Tb_{0.15}$–core and TiO_2 shell structure. FTIR spectra also corroborated the presence of TiO_2 on the $La_{0.4}F_3$:$Ce_{0.45}$,$Tb_{0.15}$surface. The coating thickness was around 1.6-2 and 4-6 nm in two different samples. The particles sizes as per the TEM image were 16.1 ± 5 nm. With TiO_2 coating/shelling, the cerium luminescence was observed to be quenched. However, in case of terbium, the green emission was enhanced 1.76 times. The scintillation under X-ray excitation of the coated and uncoated samples was recorded. The scintillation intensity of the TiO_2 coated sample was marginally higher than the coated sample. Non-stoichoimetic LaF_3:Ce was studied by varying the lanthanum and fluorine nominal composition. XRD results clearly reveal that variation in concentration of either lanthanum or fluoride does not change the crystal structure significantly. Nano phosphor prepared from exact stoichiometry LaF_3 (1:3) ratio possess the average crystallite size of 22 nm whereas the size of lanthanum and fluoride deficient samples are varied from 20 nm to 45 nm. Very small size is attained when the fluorine concentration was the least. This shows that the particle size has direct dependence on the cation / anion charges present in the precursor solution.In both the cases, despite a better crystallnitythere was a decrease in PL intensity and slight changes in the peak excitation and emissions at La/F= 0.26,0.28,0.37,0.39 and 0.40 molar ratios arising out of crystal field perturbations. Stokes shift observation indicates that the variation of anion (fluorine) causes more Stokes shift than the Lanthanum variation (cation), implying anionic deficiency (defects) has more bearing or (distorts more) influence on the emission spectra a in the ionic based host matrices.

References

[1] M. Rosff, “Nano Surface Chemistry” BOOK, Publisher: Marcel Dekker inc. (2001).

[2] M.Y. Xie, Y. Liao, H. Hui, Y. Xue-Feng, J. Solid State Chem.182 (2009) 597.

[3] C. Kai, G. Chao, P. Bo, W. Wei, J. Nanomater. 2010 (2010), http:// dx.doi.org /10.1155/ 2010/238792

[4] Q. Wanga, Y.You, R. Ludescher , Y. Ju , J. Lum. 130 (2010) 1076.

[5] H. Kim, C. Jin, S. Park, C. Lee, *ICCM* /Proceedings /data/3.../P3.../P3-30-IK0214.pdf, 18^{TH} International conference on composite materials.

[6] Moses, J E Derenzo, M J Weber, F Cerrina, A Ray Chaudri, J. Lumin. 59 (1994) 89.

[7] C. Pedrini, M. Moing, D. Bontes, V.V BelskyAnMiKhailin, A N Visler, E Zialin, Chem. Phys. Letters 206 (1993) 490.

[8] R. P. Antony , T. Mathews , A. Dasgupta, S. Dash, A.K.Tyagi, Baldev Raj, J. Solid State Chem. 184 (2011) 624.

[9] C.H. Kam, S. Buddhudu, Physica B 337 (2003) 237.

[10] B. Liu, M. Gu, X. Liu, C. Ni, D. Wang, L. Xiao, R. Zhang, J. Alloys Compd. 440 (2007) 341.

[11] C.X. Li, X.M. Liu, P.P. Yang, C.M. Zhang, H.Z. Lian, J. Lin, J. Phys. Chem. C. 112 (2008) 2904.

[12] J. Yu, X. Zhao, J. Yu, G. Zhong, J. Han, Q. Zhao, J. Mater. Sci. Lett. 20 (2001) 1745.

[13]K.Thangavelu , R. Annamalai, D. Arulnandhi,Int. J. Emerg. Technol. Adv. Engin., 3 (2013) 1.

[14] P.Dorenbos, Phys. Rev. B62 (2000) 15640.

[15] J.K. Han, G.A. Hirata, J.B. Talbot, J. McKittrick., Mater. Sci. Eng., 176 (2011) 436.

[16] S.Heaps, L. R. Elias, L. M. Yen., Phys. Rev. B., 13 (1976) 94.

[17] A.L.N. Stevels, J. Lumin., 17 (1978) 121.

[18] Y. Liu, W. Chen, S.Wang, A.G. Joly, S. Westcott., J. Appl. Phys. 103 (2008) doi: 10.1063/1.2890148

[19] F. Wang, Y. Zhang, X. Fan, M. Wang, J. Mater. Chem. 16 (2006) 1031.

[20] l. A. Risebergt and h. W. Moos, Phys. Rev. 174 (1968) 10.

[21] A. Khorsand Zak, W.H. Abd. Majid, M.E. Abrishami, RaminYousefi, Solid State Sci. 13 (2011) 251.

[22] C. Pedrini, M. Moing, D. Bontes, V.V BelskyAnMiKhailin, A N Visler, E Zialin, Chem. Phys. Letters 206 (1993) 490.

[23] L.R. Elias,W. Heaps, W.M.Yen, Phys. Rev., 8 (1973) 11.

Chapter 5

Gamma Irradiation Effect on Photoluminescence from Functionalized LaF_3:Ce Nanoparticles

5.1 Introduction

One of the proposed major applications of cerium-doped lanthanum halide nano crystals could be radiation detection [1]; hence it is important to test the radiation stability of the material. Prolonged exposure to high-energy radiation can easily degrade most of the crystalline material by creating vacancies and defects, leading ultimately to poor luminescent intensity. However, a review of literature reveals scant data on the degradation effects of organic coated lanthanide-halide nano crystals exposed to gamma irradiation. Hence it is important to study their radiation stability (hardness). Electron *(e)*–hole *(h)* pairs would be created in the crystal when irradiated by gamma rays. These *e–h* pairs get captured by various lattice defects during the process of their transport in the crystal lattice, and results in formation of different color centers. Degradation of nano crystals is evaluated based on the measured room temperature PL intensity following the irradiation dose. Preliminary radiation hardness studies in terms of PL intensity degradation with gamma exposure with the LaF_3:Ce nano composite materials have indicated that nano crystalline (NCs) exhibited excellent radiation hardness after an extended exposure dose of about 24 kRads [2]. Bangaru et al., (2011) [3] reported that in single crystals of KBr:Ce^{3+} and KCl:Ce^{3+} luminescent material the formation Ce^{2+} from Ce^{3+} due to gamma irradiation yields emission bands above 390 nm. Themoluminescence is also one of the tools with its own limitation to assess the true characterization of the defect nature.

Though in one way the material's PL performance degrades due to defect formation with irradiation, the other luminescent property (thermoluminescent) of the same material can be applied to assess the radiation dose. LaF_3 is a simple ionic crystal (La^+; F^-) belonging to the family of alkali/ alkaline fluorides wherein self traps (V_k holes) persist due to the unstable exited states against localized lattice distortion. Self trapped ions have strong influence on ion transport and radiation damage [4]. As the radiation interacts with the crystal, it causes electrons in the crystal atoms to jump to higher energy states, where they stay trapped due to defects/impurities present. Thermoluminescence (TL) is a powerful technique used for estimations of doses of high-energy ionizing radiations as the energy absorbed during irradiation and the TL intensity on stimulation (heating) is proportional to the radiation doses. Thermoluminescent (TL) technique is being used for radiation assessing the dose received by the personnel working radiological areas (Nuclear reactors) and in environmental dose assessment. The present work is also a small step taken forward in the same direction for a search of an ideal TL phosphor, though the material studied in this work is not a tissue equivalent material and is thus not recommended for medical dosimetry. In this connection, interest is shown in nanosized phosphors since some data point to their better radiation resistance [5]. Recent studies on different luminescent nanomaterials have showed that they have a potential application in dosimetry of ionizing radiations for the measurements of high doses using the TL technique, where the conventional microcrystalline phosphors exhibit saturation. This saturation occurs due to the ionized zones overlapping each other in the micromaterial at higher doses. However, with the use of very tiny particles such as nanoscale TLD materials, the problem of saturation is overcome to a major extent. The TL results of the reported nanomaterials have revealed very imperative characteristics such as high sensitivity and saturation at very high doses. This has encouraged us to further study the TL of nanocrystalline LaF_3:Ce for measuring the high γ ray exposures. Of late, interest of researchers towards nanomaterials has increased because of their countless advantages over the bulk materials for various applications including TL. Recent TL studies, report that nanophosphors are more suitable compared to their corresponding conventional microphosphors for accurately measuring high doses of ionizing electromagnetic as well as particulate radiation [6-11]. One of the interesting nanophosphors that have been reported is magnesium borate activated by dysprosium [11]. This material in its conventional microcrystalline form is well suited for measuring doses of only up to 10 Gy of gamma rays. However, its nanocrystalline form can be used for accurately measuring doses of up to 5 kGy. Such characteristic is also observed in case of another nanophosphor $Ba_{0.97}Ca_{0.03}SO_4$:Eu. Here too, the conventional microphosphor $Ba_{0.97}Ca_{0.03}SO_4$:Eu [9] has a linear response to gamma radiation only in the range 0.1–50 Gy, whereas the corresponding nanophosphor exhibits a linear response in the range 1–20 kGy. In a recent study on $K_2Ca_2(SO_4)_3$:Eu nanophosphor ,with particle size of 26 nm prepared by the ball-milling method has a high TL sensitivity at low doses of gamma radiation and continues to have a linear TL response over a very wide range of gamma doses (1 Gy to 1 kGy) with less fading[11].

A number of commercially available thermoluminescent dosimeters (TLD) are available for this purpose. However, efforts are still on to improve the TL properties of these materials by preparing them using different techniques. Recent studies on different luminescent nanomaterials have showed that they have a potential application in dosimetry of ionizing radiations for the measurement of high doses using the TL technique, where the conventional microcrystalline phosphors saturate. In the case of LaF_3, the easy formation of anion vacancies and a high equilibrium vacancy concentration are of interest in optical studies of the defect properties.

In this work, a simple co-precipitation synthesis route was adopted to synthesize uncoated and oleic acid coated LaF_3:Ce nanoparticles (as described in chapter 3).

Nanoparticles were characterized on their crystal structure, functional group, and optical properties by means of X-ray diffraction (XRD), Transmission electron microscope (TEM), FTIR, UV-Vis and Photoluminescence respectively. The particle size was estimated from the XRD pattern and also by measuring the particle size of the TEM images using the software Image J. FTIR, UV-Vis and Photo luminescent measurements were carried out before and after the irradiation with Cobalt-60 gamma ray photons, for various doses up to 6.19 kGy. Thermolumniscence measurements were carried out using annealed LaF_3:Ce.

5.2 Experimental details

X-ray diffraction measurements were done using a Shimadzu (XRD-6000) diffractometer with a Cu K_α (1.5406 Å) X-ray source. The presence of oleic acid coating was confirmed by FTIR using HORIZON MB3000 ABB spectrophotometer and from the TEM image. Gamma irradiation was done inside a gamma chamber (GC 5000, BRIT) containing 4.8 TBq activity of Cobalt-60 radioisotope and providing an exposure rate of 2.69 kGy/h. The samples were characterized with LIBRA 200FE (Carl Zeiss) high resolution transmission electron microscope operated at 200 kV equipped with energy dispersive X-ray spectroscopic (EDS) analysis, scanning transmission electron microscopy (STEM) and in-column energy filter. The information limit of the microscope is 0.13 nm. UV-Vis absorption measurements were carried out with samples unirradiated and irradiated for 0, 140 Gy, 350 Gy and 6.1 kGy dose. Photoluminescence (PL) measurements on the discs were carried out using a SHIMADZU spectrophotometer (RF-5301PC).

5.3 Results and discussions

5.3.1 XRD

Figure 5.1 shows the XRD pattern of oleic acid coated and uncoated nanoparticles. The peak positions and intensities agree well with the data reported in the JCPDS standard card (32-0483) for hexagonal LaF_3:Ce crystals. The diffraction peaks were with large width, which is an indication of the nanosize of the particles. The structure was determined to be hexagonal with a= 7.187 ;c=7.35 Å ;; *a*= 7.18*; c*=7.35 Å of oleic acid coated and uncoated respectively. The sizes of the nanoparticles were calculated from the XRD data based on the Debye–Scherer formula. The results showed that the oleic coated and uncoated nano crystallite sizes were 10 nm and 18 nm respectively.

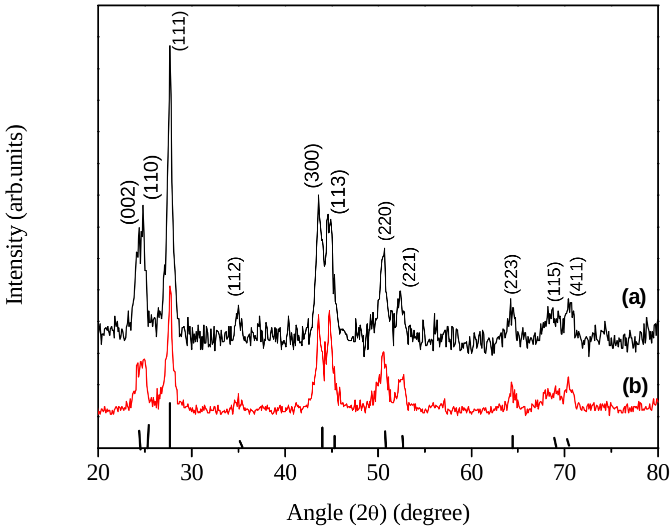

Figure 5.1 XRD pattern of (a) oleic acid coated and (b) uncoated nanoparticles of LaF_3:Ce

5.3.2 TEM

Figures 5.2, 5.5 and 5.4, 5.7 show the transmission electron microscope (TEM) images of the LaF_3:Ce nanoparticles before and after the gamma irradiation respectively. Figure 5.2 with insert showing the HRTEM image of an individual particle, represent oleic acid coated particle before gamma irradiation. In figure 5.2, the as prepared particles were in spherical and slightly oblong shape with some agglomeration. Particles size were also measured using TEM images with the help of Image J software. The mean size of the oleic acid coated nanoparticles was found to be 7.6 nm, with a 3.9 nm standard deviation (from a statistical sample size of 138 nanoparticles from different images). Figure 5.3 shows the particle size distribution. Figure 5.4 shows the oleic acid coated particles after gamma irradiation upto a dose of 6.19 kGy. After gamma irradiation, particle shape appears to be non spherical, irregular and with clearly distinct edges, which might be due to the damage of the oleic acid on surface as well as the on LaF_3:Ce crystal by gamma photons.

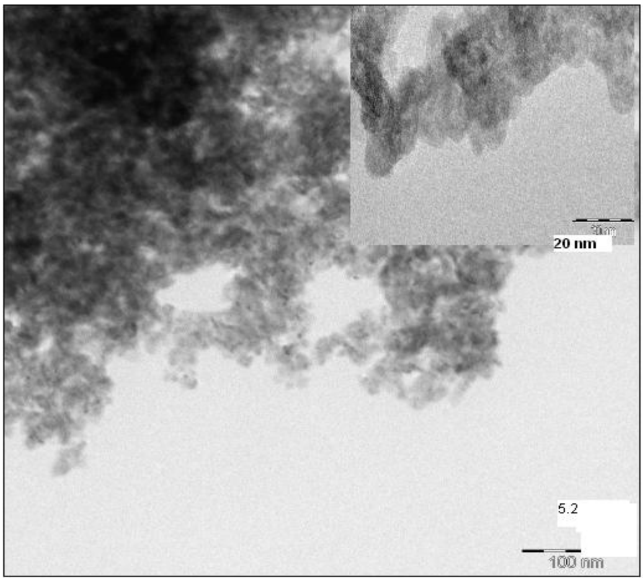

Figure 5.2 TEM image of Oleic acid coated LaF_3:Ce nanopraticles before irradiation (Inset image show the HRTEM image)

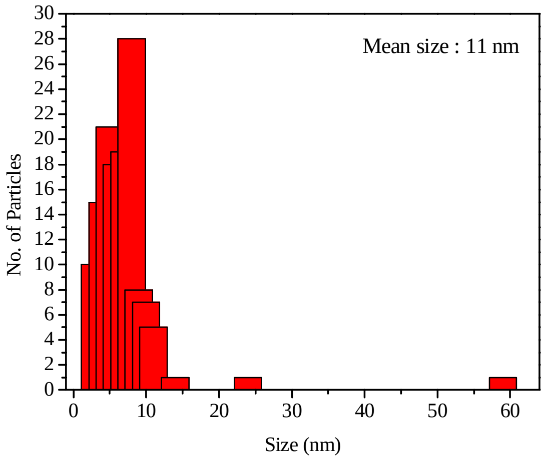

Figures 5.3 Size distribution of the particles Oleic acid coated particles before gamma irradiation.

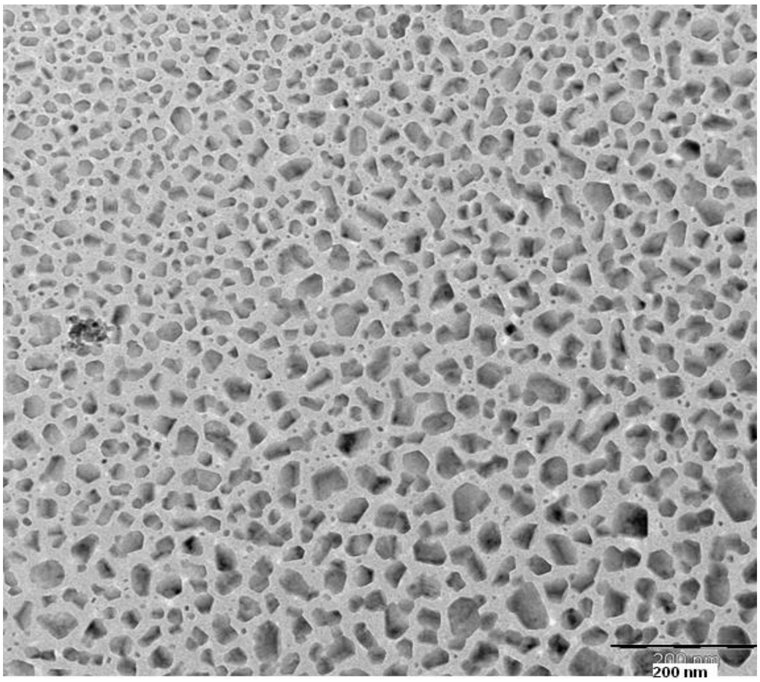

Figure 5.4 HRTEM image of the OA coated LaF_3:Ce after gamma irradiation.

Figure 5.5 with inset show of the HRTEM image of an uncoated particles before irradiation and figure 5.7 show TEM image of the uncoated particles after gamma irradiation to a dose of 6.1 kGy respectively. From figure 5.4 it is obvious that the as prepared uncoated particles were spherical and with uniform microstructure, with less agglomeration present. The mean size of the uncoated particles was 20.7 nm with a 7.7 nm standard deviation (from a statistical sample size of 171 nanoparticles from different images). Figure 5.6 shows the particle distribution plot. The statistics of the particle size are in close agreement with the estimated size values through XRD route. After gamma irradiation, the uncoated particles appear to be in spherical shape but with a bigger size and close packing.

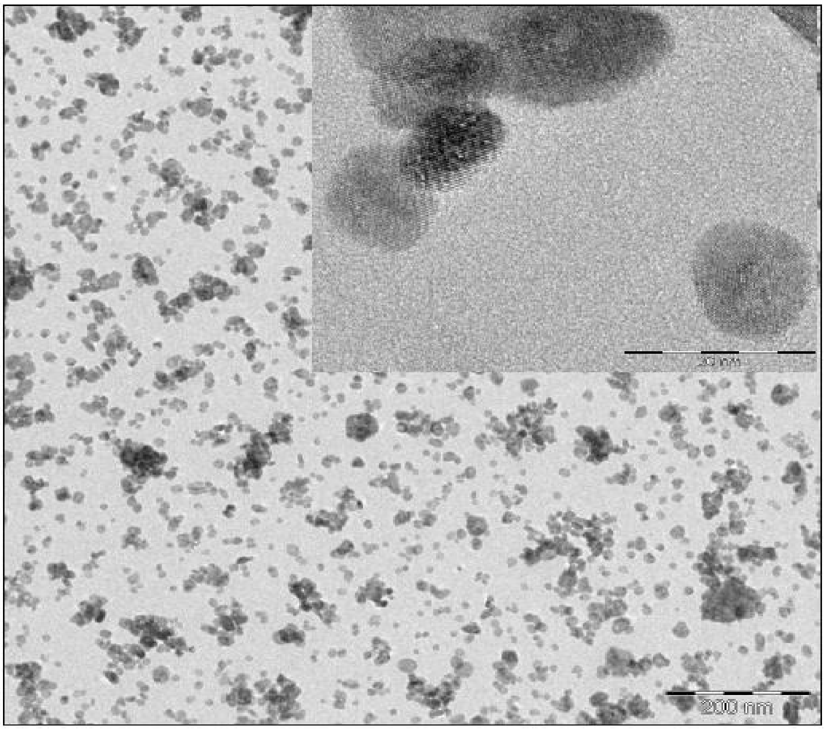

Figures 5.5 TEM image of uncoated nano size LaF_3:Ce particles before irradiation. (Inset image HRTEM image)

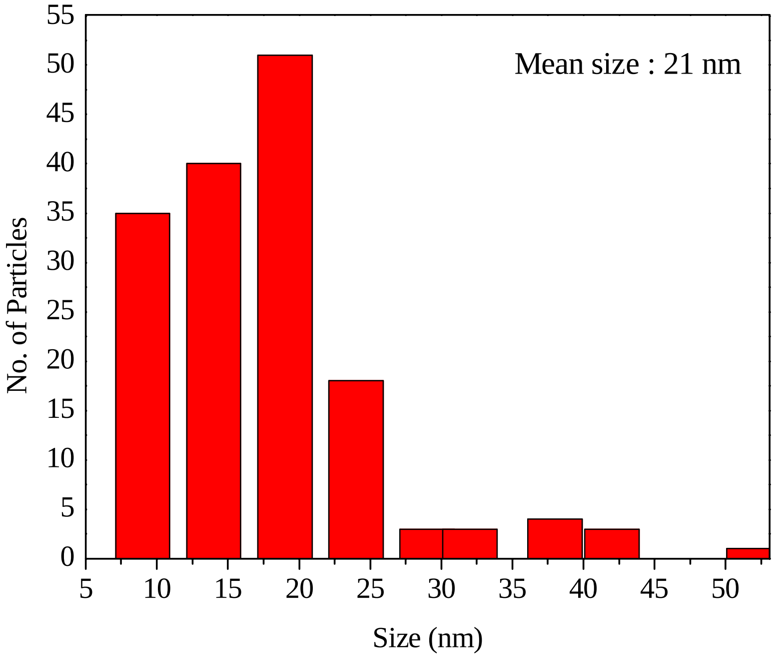

Figures 5.6 Size distribution of the uncoated particles before gamma irradiation.

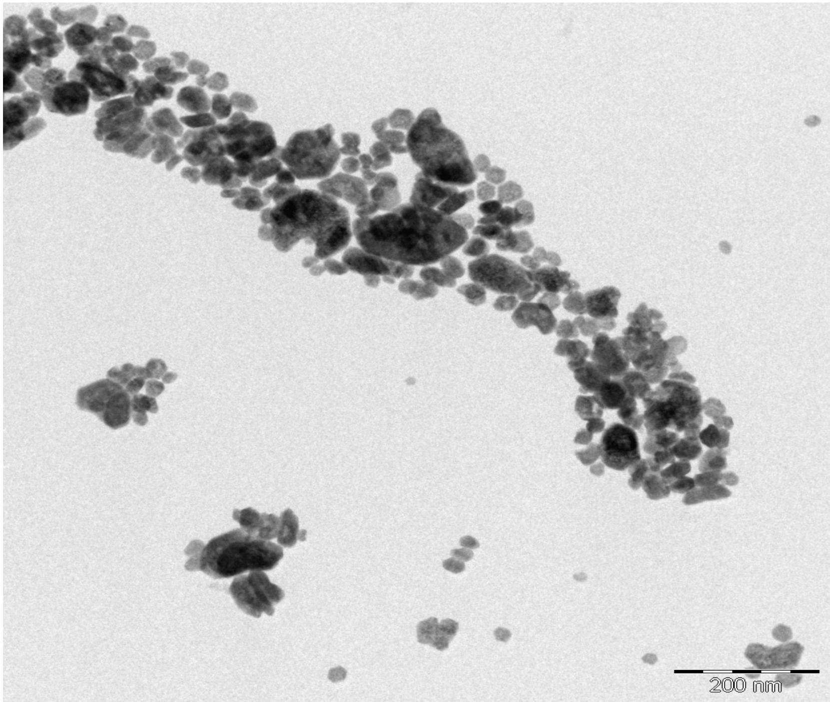

Figure 5.7 TEM images of the uncoated LaF_3:Ce particles after gamma irradiation.

5.4 FTIR

Figure 5.8 shows the FTIR spectra of both pure oleic acid (curve a), oleic acid coated LaF_3:Ce nanoparticles (curve b) before and after gamma irradiation (curve c) oleic acid coated LaF_3:Ce nanoparticles (curve c). In curve (a) the broad feature between 3500 and 2500 cm^{-1} is due to the O-H stretch of the carboxylic acid. The 2924 and 2854 cm^{-1} are attributed to the asymmetric and symmetric stretch of CH_2. The peak at 1713 cm^{-1} is a signature of C=O stretch and the band at 1285 cm^{-1} exhibited the presence of the C-O stretch. In curve (b) with the surfactant, the asymmetric and the symmetric CH_2 stretch are found to occur at 2908 and 2852 cm^{-1} respectively in consistence with those of pure oleic acid. In curve (a) strong peak at 1713 cm^{-1} attributed to stretching vibration of C=O group. When compared to curve (a) in curve (b) the reduction peak intensity of 1713 cm^{-1} C=O stretching vibration and appearance of two new absorption peaks at 1566 and 1450 cm^{-1} are due to carboxylate formation on the nano LaF_3:Ce surface, which are attributed to the characteristics of the asymmetric and symmetric stretch of (COO-) Wang et al. (2007)

[12]. The disappearance of C=O stretching vibration and presence of two (COO-) stretching confirms that oleic acid is chemisorbed on the surface of LaF_3:Ce nano particle, coordinated through carboxylate group. In order to compare the changes in the surface groups the FTIR spectra was obtained with the same quantity of unirradiated and irradiated powders. The new peak at 1640 cm^{-1}, absence of 1566 cm^{-1} and 1450 cm^{-1} peak absorption in the curve (c) clearly indicates the damage / breach in oleic acid cover (caroxylate formation) at the surface.

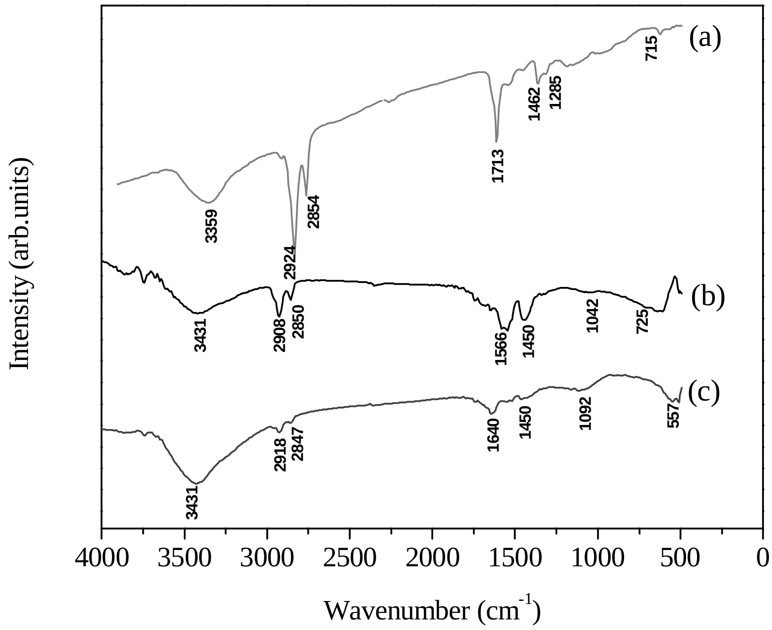

Figure 5.8 shows the FTIR spectra of (a) Oleic acid alone (b) OA coated LaF_3:Ce before irradiation(c) OA coated LaF_3:Ce after irradiation

5.5 UV-Vis absorption

Figures 5.9 and 5.10 show the UV-Vis absorption spectra of the uncoated (curves a-d) and oleic acid coated LaF_3:Ce nanoparticles (curves a-d) before and after gamma irradiation for various 0,140 Gy, 350 Gy and 6.1kGy doses. The inserts in the figures display the difference of spectra illustrating the net changes in absorption. From figure 5.8 it is very clear that uncoated particles show significant absorption at 190 and 250 nm than that of oleic acid coated particles, which confirms the cerium energy levels Dorenbos

(2000) [13]. It is also obvious from curves (b), (c) and (d) irradiated to various doses of 140 Gy, 350 Gy and 6.1 kGy that the absorption decreases with increase in gamma dose, which indicates the possibility of Ce^{3+} conversion to Ce^{4+} during irradiation. This was corroborated by the PL spectra (Figures 5.11 & 5.12) wherein the effect of gamma radiation reduced the PL intensity. In figure 5.9, one of the oleic acid coated samples, irradiated at 350 Gy as represented by curve (c) showed some increased absorption in the above said region than the un-irradiated sample, which might be due to the higher absorption changes in the organic groups at the surface. This increasing trend at 350 Gy dose was not observed in the Photo luminescence behavior. It is also evident from the absorption spectra that there were no new absorption levels are formed.

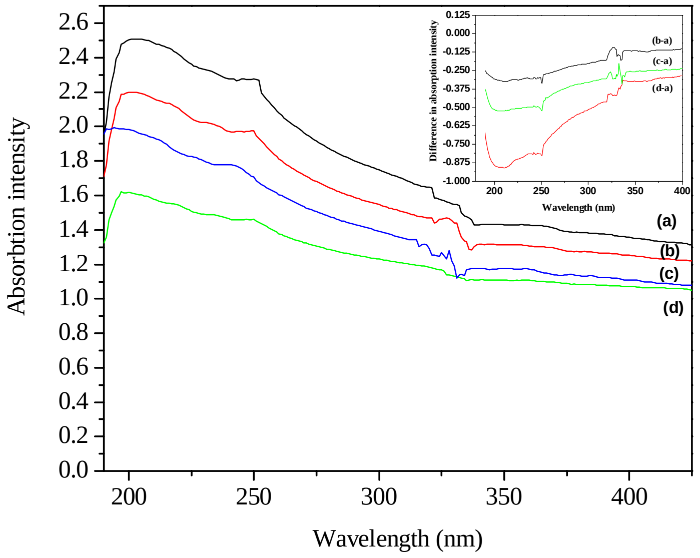

Figure 5.9 UV-Vis absorption spectra of the uncoated unirradiated (a) and gamma irradiated curves (b) 140 Gy;(c) 350 Gy and (d) 6.1 kGy of nano sized $LaF_3:Ce^{3+}$; with insert showing the difference spectra.

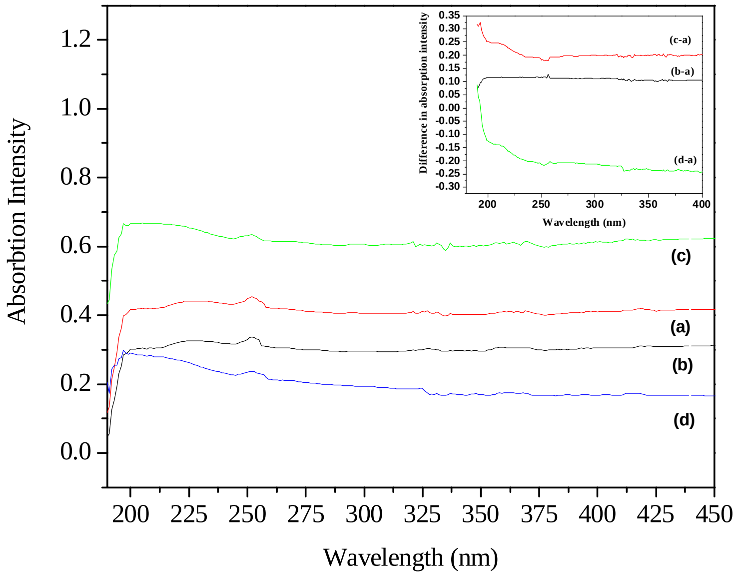

Figure 5.10 UV-Vis absorption spectra of the oleic acid coated unirradiated (a) and gamma irradiated curves (b) 140 Gy;(c) 350 Gy and (d) 6.1kGy of nano sized $LaF_3:Ce^{3+}$; With insert showing the difference spectra

5.6 Photoluminescence

Figure 5.11 shows the excitation and emission spectra of uncoated & unirradiated nanoparticle pellets (curves a and b) and those after gamma ray irradiation to different doses (curves c to l). Curves c, e, g, i, and k are excitation curves for (Em=305 nm) and curves d, f, h, j, l are the emission curves for (Ex=250 nm) spectra for various doses, recorded in low sensitivity mode. The excitation spectrum was recorded for the sample by scanning the excitation wavelength from 200 nm to 265 nm, while the emission monochromator was fixed at 305 nm. The excitation peaks were found to be at 237 and 250 nm (curve a), which agrees with the lower energy levels on (4f to 5d, {5.9 and 4.96 eV}) of cerium ions Dorenbos (2000) [13]. Emission spectrum was obtained by exciting the sample with 250 nm wavelength with 3 nm spectral band-pass and the recording in the region 265 nm to 450 nm with a similar spectral band pass of 3 nm slit widths, in low sensitivity mode. The emission peak was found at 305 nm (curve b), which is attributed to 5d to 4f transitions of Ce^{3+} emission. One can see that the emission of the unirradiated pellet is intense. The PL intensity was found to decrease with increase in the gamma dose, this might be due to defects formed in the host material which interferes in the excitation energy transfer process to cerium, and also due to Ce^{3+} conversion to Ce^{4+} due to hole trapping, which act as quenching centers Dubios et al. (1986) [14]. Around 68 % of intensity loss of 305 nm peak was observed for a dose of 348 Gy. The higher percentage fall in intensity as compared to that reported by Sankar et.al (2009) [2] might be due to the use of higher energy photons with a higher dose rate. A slight shift in peak towards lower wavelength was also observed. The shape of the spectra did not change with gamma dose and also no signature of Ce^{2+} absorption (at 240 nm) / emissions beyond 390 nm were observed even at high doses. Non formation of Ce^{2+} might be due to the rigid bonding of cerium with fluorine, in lattice forming cerium tri-fluoride bond at certain locations, unlike in KCl:Ce / KBr: Ce were cerium atoms physically held in the lattice. This shows the radiation hardness of the material unlike other alkali earth halides. However with regar to Ce^{2+} formation, more experiments are needed.

Figure 5.12 shows the results of another experiment, excitation and emission spectra of unirradiated (curves a and b) and gamma irradiated oleic acid coated LaF_3:Ce nano paarticle pellets. Curves c, e, g, i, k represent the excitation for (Em=308 nm) and curves d, f, h, j, l are the emission (Exi=252 nm) spectra for various gamma irradiation doses. The excitation and emission spectra of the coated pellet were recorded with 3 nm slit width in the high sensitivity mode, as the intensity was less as compared to the uncoated pellet due to the presence of –OH and $-CH_2$ groups at the surface which act as quenchers.

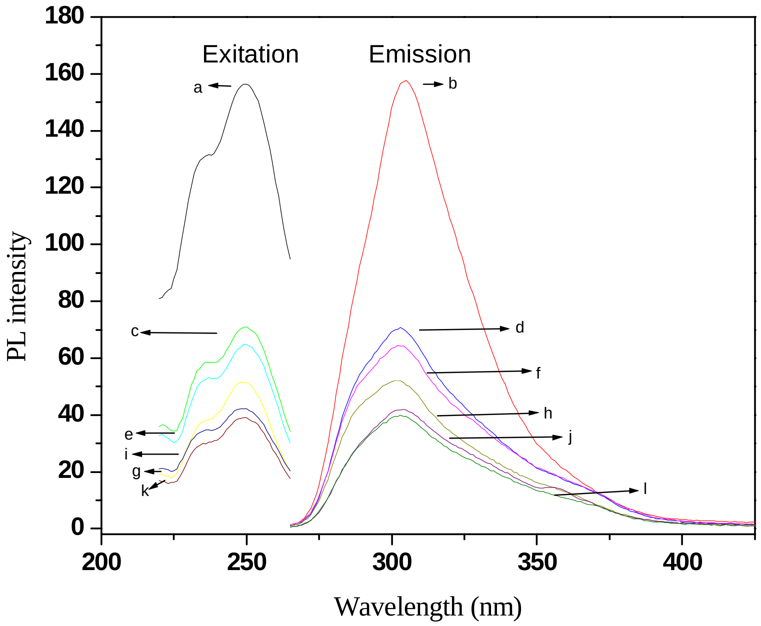

Figure 5.11 PL excitation (curves a, c, e, g, i, and k) (Em=305 nm) and emission (curves b, d, f, h, j and l) (Ex=250 nm) spectra of uncoated LaF_3: Ce^{3+} nanoparticle pellets for 0, 10, 24.8, 50, 198.7 and 348 Gy respectively.

The excitation spectra contain peaks at 231 and 252 nm. The emission spectra contained two peaks viz 308 and 361 nm obtained when exited with 252 nm wavelengths. It is further to be emphasized that in presence of oleic acid the 305 nm peak was slightly shifted to 308 nm, in addition to the appearance of a peak at 361 nm.

A decrease in the photo luminescence intensity was observed with increase in the gamma dose. The loss in luminescence intensity could be due to cleavage in the surface groups and creation of defects in the host material, which may act as quenching centers. Ce^{4+} formation by capturing a hole created in the valence state of anions due to irradiation might also contribute to the fall in intensity. An intensity loss of 69% was observed at a dose of 348 Gy similar to the pellet of uncoated particles. This shows the insignificant effect of surface defect at organic cover on 308 nm peak. Around 77 and 86% of intensity loss for 308 and 361 nm peaks respectively for a dose of 6.19 kGy were observed. The drastic reduction in 361 nm peak might be due to the defects formed in the LaF_3 as well as breach in the oleic acid. This shows that the organic layer at the surface is vulnerable to Compton electrons. The bump between 400 and 450 nm also decreases with dose. The spectral shape was very stable even at a very high dose and no Ce^{2+} absorption / emission were observed unlike in KBr:Ce crystals as reported by Bangaru et al., (2011) [3] . There was a slight shift in both the excitation and emission peaks towards lower wavelength due to the irradiation. Figure 5.13 shows the variation of PL intensity as a function of dose in log scale (curve a- coated, b-uncoated). The rate of fall in the 308 nm peak intensity is similar for both the pellets. Therefore, nanoparticle LaF_3:Ce system has better radiation hardness, unlike other bulk alkali halides.

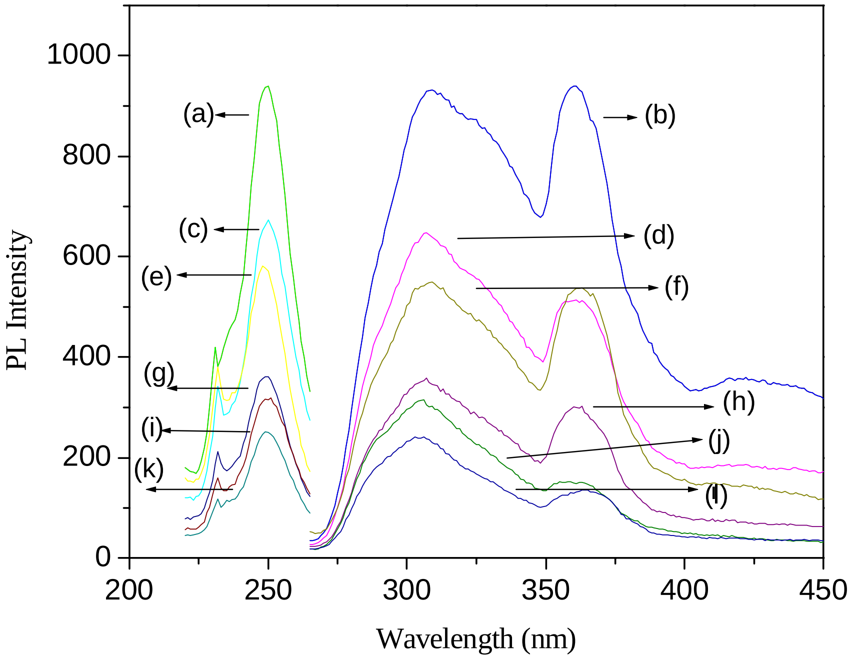

Figure 5.12 PL excitation (curves a, c, e, g, i, and k) (λ_{Em}=308 nm) and emission (curves b, d, f, h, j and l) (λ_{Ex}=252 nm) spectra of Oleic acid coated LaF_3: Ce nanoparticlie pellets 0, 50, 99.4, 198.7, 348 Gy and 6.19 kGy respectively.

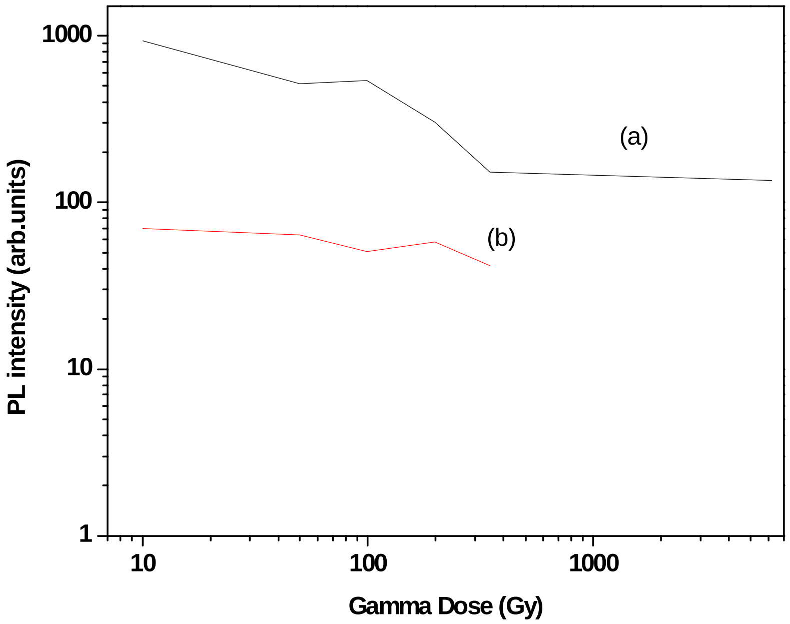

Figure 5.13 Dose vs PL intensity

5.7 Thermoluminescent properties of the nano sized LaF_3:Ce

5.7.1 Experimental

The synthesized nano sized Oleic acid coated LaF_3:Ce powder was annealed at 1300 °C by placing the pellet in alumina boat which is kept at the centre of the tubular furnace, under argon atmosphere for 3 h for dopoant diffusion and also to remove the organic cover. FTIR of the annealed Oleic acid coated samples were carried out to check the presence of the coating. PL spectra of the annealed samples were also recorded. Gamma irradiation at different doses was done in Gamma Chamber (BRIT, BARC) providing a dose rate of 2.2 kGy/h. Samples were irradiated at various doses upto 2 kGy. TL glow curves were recorded using Risoe TL/OSL reader- DA 20.

5.7.2 FTIR

Figure 5.14 shows the IR spectra of both), Oleic acid coated LaF_3:Ce nanoparticless curve (a) and nanoparticles after heating at 1300 °C (curve b) In curve (b), the formation of two new absorption peaks at 1546 and 1450 cm^{-1} occurs which are due to the carboxylate formation onto the nano LaF_3:Ce surface and are attributed to the characteristic of the asymmetric (COO-) stretch and the symmetric (COO-) stretch. Further the 2924 and 2854 cm^{-1} bond also appear which are attributed to the asymmetric and symmetric stretch of CH_2. In the adsorbed state, molecules experience the field of the solid surface, as a result the characteristic bands get shifted to a lower frequency region to 2908 and 2852 cm^{-1} [15]. The 3428 Cm^{-1} is due to the –OH streching. The result indicates that the nano LaF_3:Ce particles is surrounded by hydrocarbon chains. In curve (b) the absorption peak intensity in the regions 1546 and 1450 cm^{-1}is insignificantly less, which shows that the absence of the organic layer over the surface.

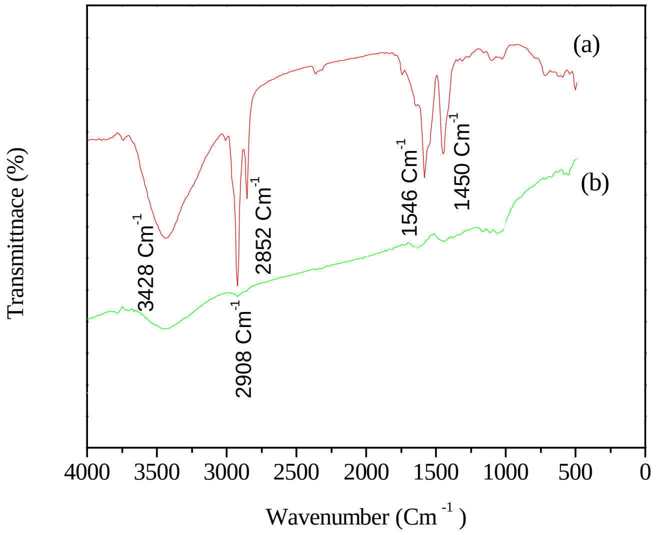

Figure 5.14 FTIR of (a) OA coated LaF_3:Ce before annealing ; (b) $La_{0.95}F$:$Ce_{0.05}$ after annealing 1300 ℃

5.7.3 PL after annealing at 1300 ℃

Figure 5.15 represents the Pl spectra of the as prepared (curves a & b) and annealed (curves c & d) samples. Curves a, c represent the excitation (Em=308 nm) and b, d are the emission (Ex=252 nm) spectra. It is clear that PL intensity decreases to half of the as prepared sample intensity after annealing in argon atmosphere for 1300˚C. This might be due to the diffusion of surface Ce^{3+} ions into the matrix as well as the conversion of Ce^{3+} to Ce^{4+} as argon gas contains some oxygen impurity. There is no change in the spectral peak positions. The kink at 361 nm which might be due to the effect of the Oleic acid and cerium shows some slight left shift.

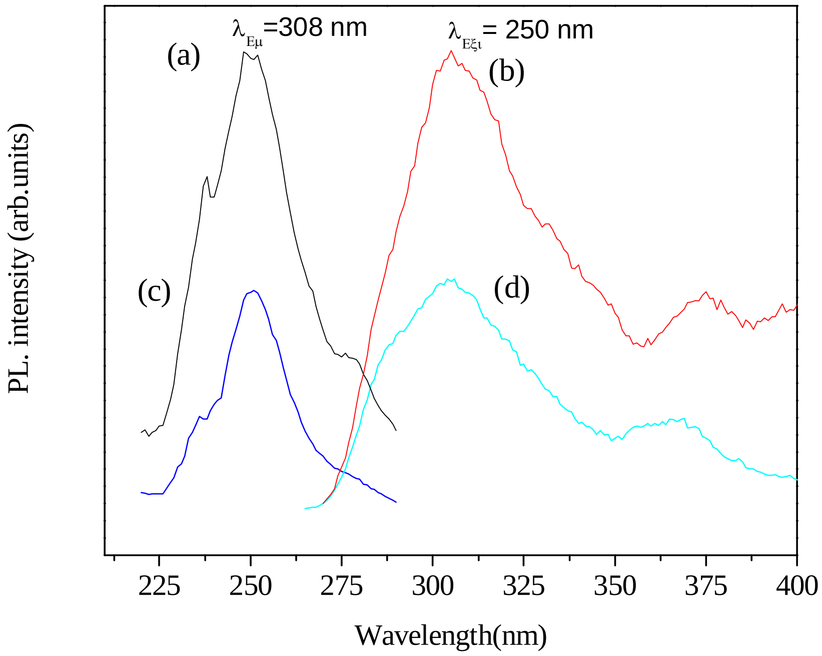

Figure 5.15 PL spectra of as prepared Curve (a); annealed (c) Excitation (λ_{Em}=308 nm) and Emission as prepared (b) ;annealed (d) (λ_{Ex}=250 nm) of $La_{0.95}F:Ce_{0.05}$

5.7.4 TSL investigations of $LaF_3:Ce^{3+}$

Figure 5.16 shows the TL response of the $La_{0.95}F_3:Ce^{3+}{}_{0.05}$ nano particle sample annealed at 1300 ° C and irradiated for various doses upto 2 kGy. In figure 5.16, curves represent TL output for doses (a) 65 Gy;(b)159 Gy;(c) 717 Gy; (d) 1.28 kGy and (e) 2.0 kGy. The TL glow curve appears at 409 ° K (136°C), which is very intense. Subsequently TSL was recorded at the heating rate of 5 °C s^{-1}. The profile of TSL glow curve indicates that the main peak appearing at 136 °C (409 K) is dosimetrically useful peak.

Further, the dosimetric characteristics of TL materials mainly depend on the kinetic parameters quantitatively describing the trapping emitting centers responsible for the TL emission [16]. The TSL parameters such as activation energy (E_t) and trap density

(n_o) were calculated by using Chen's equation [17& 18]. The peak shape method depends on the certain characteristics of single glow peak. Chen's equation is represented as $E= k\ [2.52\ k\ T_m^2\ /\ \omega\ -\ 2\ k\ T_m]$ and the symmetry factor $\mu = \omega/\delta$, where k is Boltzmann constant, T_m is glow peak temperature, τ is the low-temperature half-width, ω is the full-width at half-maximum of the peak ($\delta + \tau$), δ is high temperature half width. Trap density is calculated based on the following empirical equation, $n_o = I_m/\{b\ [2.52+10.2\ (\mu_g–0.42)]\}$, b is the order of kinetics. Figure 5.17 shows the curve with geometrical parameters of the TL glow curve.

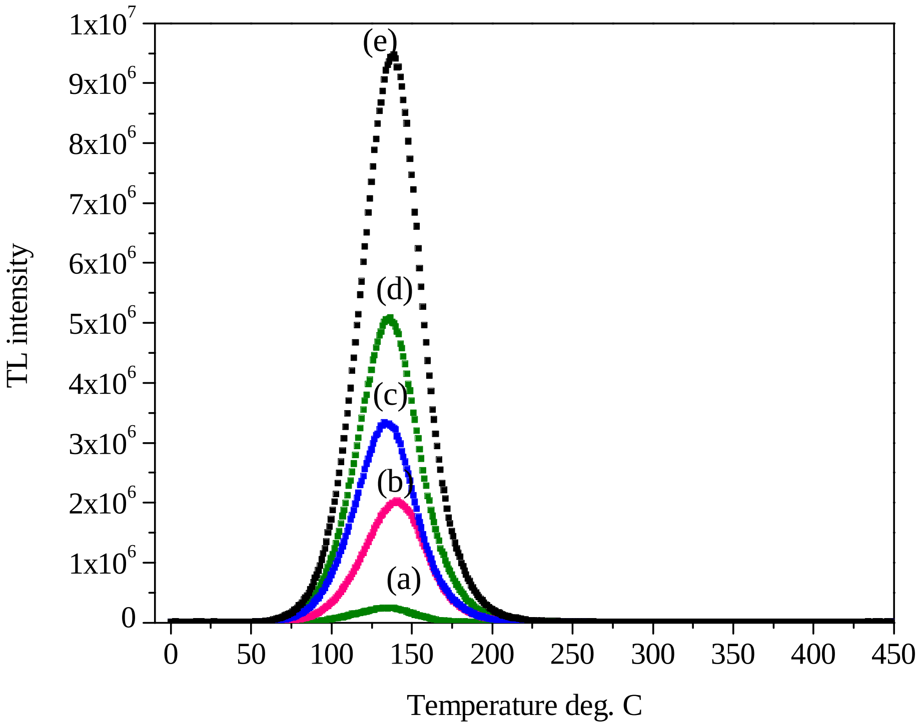

Figure.5.16 Thermally stimulated luminescence glow curve from $LaF_3:Ce^{3+}$ nano particles (a) 65 Gy;(b)159 Gy;(c) 717 Gy ; (d) 1.28 kGY and (e) 2 kGy

Table 5.1 TSL parameters of $LaF_3:Ce^{3+}$ nanoparticles

Sample	Glow peak Temp T_m (K)	Glow peak shape parameters				TSL parameters	
		δ (K)	τ (K)	ω (K)	μ (K)	E_t (eV)	n_o (cm^{-3})
$LaF_3:Ce^{3+}$	409	21	17	38	0.55	0.57	2.3 E5

Table 5.1 shows the glow peak shape parameters and TSL parameters of $LaF_3:Ce^{3+}$ nanoparticles. The trap depth calculated for the main peak at 409 K using Chen's equation [17] is 0.57 eV. These parameters are considered to be finger prints of any TSL materials. The value of symmetry factor μ =0.55 suggests that, the kinetics of this thermo luminescence decay follows second order, indicting perfect trap formation to trap more ions, which recombine to give more light. Moreover, the γ value (γ= δ/τ) is 1.25 which also confirms the second order kinetics of the TSL glow curve [19]. Figure 5.18 shows the TL intensity with gamma dose. The TL response was found to be linear from 40 Gy to 2 kGy.

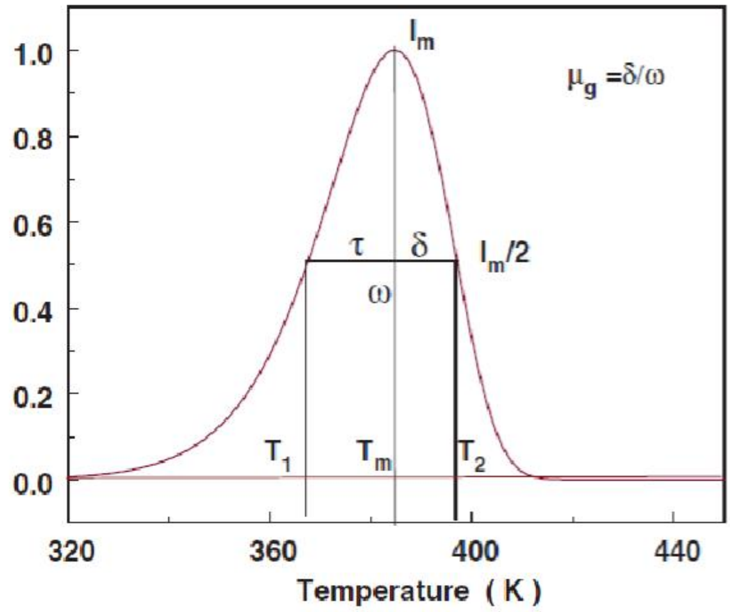

Figure 5.17 Geometrical characteristics of a single glow-peak (Adopted from Ref 18).

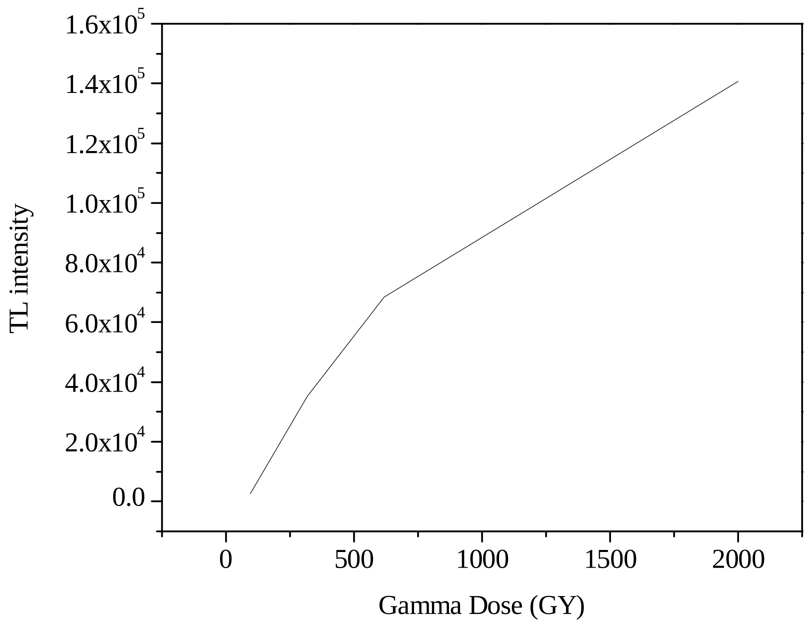

Figure 5.18 Gamma dose vs TL glow curve intensity of $La_{0.95}F_3:Ce_{0.05}$ sample**.**

5.8 Conclusion

Oleic acid coated and uncoated LaF_3:Ce nanoparticles were synthesized by adopting the co-precipitation technique. The sizes of coated and uncoated particles were around 10 and 18 nm respectively. The particle sizes measured using the TEM images showed a mean size of the oleic acid coated nanoparticles arround 7.6 nm, with a 3.9 nm standard deviation and the mean size of the uncoated particles was 20.7 nm with a 7.7 nm standard deviation. After gamma irradiation the oleic acid coated particles shape appears to be non spherical, irregular and with distinct edges, which might be due to the damage of the oleic acid on surface of the particle by gamma photons. The uncoated particles after gamma irradiation appear to be in spherical shape but with a bigger size and closely packed. These nanoparticles were gamma irradiated for various doses up to 6.19 kGy. The UV-Vis absorption spectra of the oleic acid coated and the uncoated sample exhibited decrease in absorption intensity with increase in dose. FTIR spectra obtained before and after irradiation of the coated show the reduction in the IR absorption intensity due to the damage of the oleic acid surface capping. The PL intensity degradation was similar in both systems. The coated sample showed an 86% loss of the original PL intensity of un-irradiated sample at a dose of 6.19 kGy. The 361 nm peak drastically decreased as compared to 308 nm peak with increase in the dose. No Ce^{2+} emission was observed and the spectral shape was unchanged. The PL intensity is found to saturate at higher doses. Thus LaF_3:Ce nanoparticles are found to be radiation harder than other alkaline halide systems. TL glow peak appears at 409° K (136 °C), whose kinetics of the decay follows second order. The perfect Gaussian peak indicates perfect trap formation to trap more ions, which recombine to give more light. The trap depth calculated for the main peak at 409° K using Chen's equation is 0.57 eV. The dose response was found to be linear from 40 Gy to 2 kGy.

References

[1] E.A. McKinney, R.E. Del Sesto, L.G. Jacobsohn, P.A. Santi, Muenchausen. K.C, Ott, T. Mark McCleskey, B.L. Bennett,J.F. Smith, D. Wayne Cooke, 2001, Nucl. Instrum. Methods in Phys. Res. A 579, 15.

[2] K. Sankar, J. B. Plumley, B. A. Akins, T. A. Memon, N. J. Withers, G. A. Smolyakov, M.Osiński., Proc. of SPIE Vol. 7189 71890911,(2009).

[3] Bangaru.S 2011. Physica B 406 159–1641 2

[4] K.S. Song, R.T. Williams, Self-Trapped Excitons,Springer Series in S.S.Sci. 105, Springer, Berlin (1993).

[5] V.S. Kortov, Radiation Measurements 45 (2010) 512–515

[6] N. Salah, P.D. Sahare, S.P. Lochab, P. Kumar, Radiat. Meas. 4 (2006) 40.

[7] N. Salah, P.D. Sahare, A.A. Rupasov, J. Lumin. 124 (2006) 357.

[8] P.D. Sahare, R. Ranjan, N. Salah, S.P. Lochab, J. Phys. D 40 (2007) 759.

[9] S.P. Lochab, P.D. Sahare, R.S. Chauhan, N. Salah, A. Pandey, J. Phys. D 40 (2007) 1343.

[10] S.P. Lochab, A. Pandey, P.D. Sahare, R.S. Chauhan, N. Salah, R. Ranjan, Phys. Stat. Sol. A 204 (2007) 2416.

[11] N. Salah , P. D. Sahare , S. Nawaz, S. P. Lochab, Radiation Effects and Defects in Solids, 159, 5, 2004

[12] J. Wang, J. Hu, D. Tang, X. Liu, Zhen, J. Mater. Chem., 17 (2007)1597.

[13] P. Dorenbos, Phys. Rev. B 62 (2000) 15640.

[14] Dubois L.H, Zegarski. B, Nuzzo. R.G. J.Langmuir 2 (1986) 412.

[15] Wu, L. Fu, M. Su, M. Aslam, K. Chun Wong, P.V. Dravid, Nano Letters 4 (2004) 383.

[16] C. Furetta, G. Kitis, C. H. Kuo, Nucl. Instrum. Methods Phys. Res., Sect. B 160 (2000) 65.

[17] R. Chen, Y. Krish, Analysis for Thermally Stimulated Process, Pergamon, Oxford,(1981) 159

[18] Chen, S.W.S. Mckeever, Thermoluminescence and Related Phenomena, World Scientific Publishing Co., Singapore (1997).

[19] M. Barlin, J. Therm An., 17 (1979) 319.

Chapter 6

Synthesis and Characterization of Luminescent Polymer Nanocomposites

6.1 Current studies on Luminescent polymer nanocomposites

In the quest for new luminescent material, embedded polymer nanocomposites (PNC) are currently being explored. PNC materials have demonstrated their radiation sensing abilities. Hypothetically “nanocrystals,” of certain inorganic scintillator of size 2–5 nm in diameter packed densely in plastic or inorganic solutions, can absorb most of the X-ray and gamma-ray energies, thus perform like the large crystals. The choice of polymers is based on its refractive index and transparency. Luminescent PNC materials are inexpensive and can be synthesized in different shapes and sizes, easily but the high vibration energies of polymers interact with the rare-earth ion transitions limiting their application in the area of optics. Generally, so far studied matrices are polycarbonate, polystyrene, polymethylmethacrylate (PMMA) and polyacrylamide (PAM). Moreover, the smaller the particles leading to better transparent PNC material. In the brief history of PNC material, initially compound semiconductors were incorporated in transparent polymer matrices. Klausch.a et al., [1] successfully prepared ZnS:Cu embedded in highly transparent acrylate based composite materials. They demonstrated that with 2 % doping the PL intensity was very high. Kalima et al.,[2] in the year 2009, demonstrated the UV curing abilities of commercially available OROCOMP polymer by adding nano sized ZnS particles. In another simple synthesis method demonstrated by Y.Chen et al.,[3] in the year 2002, uniformly distributed CdS nanoparticles with very narrow size distribution was taken in acrylyic based polymer. In another work, Perda et al.,[4] in the year 2006, demonstrated the intense green emission form the synthesis of PbI_2 embedded polyacrylamide by exiting it at wavelengths less than 350 nm. Zhang et al.,[5] have demonstrated the improved optical properties of ZnO embedded PMMA by adopting free radical copolymerization synthesis method Ivano et al., [6] in the year demonstrated the increase in the thermal stability of silver doped polycarbonate material with good transparency.

In this context, rare-earth doped nanophosphors embedded in transparent polymer composites are being studied by many groups. Luminescent enhancement of Terbium co-doped Sammarium in PMMA, was demonstrated by Jiu. H et al.,[7] in the year 2009 due to the intermolecular energy transfer. The branch of Polymer nano composites not only stopped with luminescent materials but also improved the thermal as well as electrical conductivity of the polymers. Kyle Gibson et al., [8]& [13] have demonstrated the performance of ligand capped Terbium doped LaF_3 embedded in PMMA in this regard. Of all the PNC material in study, PMMA based composite material seems to be a suitable matrix for nanomaterialas to sense high energy X-ray and gamma radiation. The utility of LaF_3:Ce embedded polymer nanocomposites for sensing X- ray and γ-ray photons and neutrons also reported by Del Sesto et al.,[9], Paul Guss et al.,[10]. Del sesto et al., in the year 2007 demonstrated the Cs-137 gamma radiation sensing capacity of LaF_3:Ce embedded polymer. The particle size was < 10 nm in the matrix with 30 weight % loading. TEM image of the particle inside the matrix showed uniform dispersibility.

In the year 2013 Paul Guss et al., have demonstrated the viability of the spectral application of nano structured LaF_3 for Co-60 gamma radiation sensing. They say that these materials have an intrinsic response to nuclear radiation that may be correlated to the energy of the incident radiation. PNC studies also insist the particles uniform distribution in the monomer is a vital parameter that decides the transparency and the performance of the composite. The heavy inorganic particles owing to their weight tend to sink and settle at the bottom of the container. To achieve good dispersibility is to modify the surface of luminescent nanoparticle with functional groups, whereby the forces of interaction prevent sinking and disburse the dopant uniformly in the transparent polymer hosts. One of the methods to prepare PNC materials is to synthesize nanoparticles first and then blend into the required matrices through intimate mixing of nanoparticles with monomer solution and subsequent immobilization through polymerization. Lin Zhang et al.,[13& 14] demonstrated the optical properties of ZnO embedded PMMA by a simple synthesis method.

In this work, we report the synthesis of Oleic acid coated and uncoated LaF_3:Ce nanoparticles embedded in polyacrylamide. Also, uncoated and TiO_2 coated $La_{0.4}F_3$:$Ce_{0.45}$,$Tb_{0.15}$ particles were embedded in PMMA through insitu polymerization. The surface views of the prepared discs were observed under optical transmission microscopy and FESEM. Their photo luminescence characteristics are presented. The TiO_2 coated $La_{0.4}F_3$:$Ce_{0.45}$,$Tb_{0.15}$ embedded in PMMA discwas exited by X-ray tostudythescintillation.

6.2 Experimental

6.2.1 Material and methods

Polyacrylamide powder, Methylmethacryalte (MMA) monomersolution and 2-2-Dimethyl-propiono-phenol solution were used as purchased. Oleic acid coated and uncoated $La_{0.95}F_3$:$Ce_{0.05}$as well as uncoated and TiO_2 coated $La_{0.4}F_3$:$Ce_{0.45}$,$Tb_{0.15}$nano sized particles which were synthesized here (in 3rd and 4th chapters) were used to prepare the composite material. Gamma irradiation assisted polymerization was carried out inside a gamma chamber (GC 5000, BRIT) containing 4.8 TBq activity of Cobalt-60 radioisotope and providing an exposure rate of 2.69 as well as 5.0 kGy/h. XRD was also carried out using XRD 6000. The prepared discs were observed using an optical microscope (ZEISS Jenoptix).Photoluminescence (PL) measurement of discs was carried out using a

SHIMADZU spectrophotometer (RF-5301PC). Scintillation measurements were carried out using Avatnes fiber optic spectrometer under X-ray excitation.

6.2.2Synthesis of LaF_3:Ce embedded in polyaryl amide using Oleic acid coated powder

LaF_3:Ce embedded polyacrylamide (PAM) disc was prepared using the nano sized Oleic acid coated LaF_3:Ce powder (discussed in the third chapter). The particle sizes were in the range of 9-850 nm. Theparticles were embedded inside PAM disc using a slightly different procedure. A solution containing 8 g of arylamide in 10 g of DM water was prepared. LaF_3:Ce embedded discs were synthesized using the acrylamide solution with two different nano-powder concentration of 16.6 and 1.75 mg/ml. The mixtures were thoroughly stirred for 30 minutes and placed in an ultrasonic water bath for 20 minutes for the gas bubbles, if any, to escape. Then the mixture was transferred to a glass beaker and polymerized in a gamma chamber (GC 5000) containing 4.8 TBq activity of Cobalt-60 radioisotope by irradiating for four minutes to a gamma dose of 221 Gy. The polymerized samples were dried in a vacuum oven at 90˚C for 4 h. The discs were circular in shape with 2 cm diameter and 1 cm thickness. The weight percent of the nano powder in the polymer composites were 1.634% (termed as NG1) and 0.1664% (termed as NG2) respectively.

6.2.3 Synthesis LaF_3:Ce embedded polyacrylamide using uncoated powder

Polyacrylamide nanocomposite (PNC1) disc was fabricated using the colloidal product solution obtained in the acidic synthesis as mentioned earlier in chapter 3 by adopting the procedure followed in the earlier preparation. The particle size was around 12.5 nm. About 4g of acrylamide monomer powder was added to 5 ml of the obtained as prepared colloidal solution of LaF_3:Ce with a concentration of 1150 µg/ml. The weight % was 0.143. It was observed that mixture did not polymerize at a dose of 221 Gy as observed with earlier sample; so was irradiated for more time. As the colloidal sample was bit acidic, it was observed to polymerize at about 350 Gy dose. The polymerized samples were taken, dried in a vacuum oven at 85°C for 4h. The disc had similar dimension of the earlier disc.

6.2.4Synthesis of uncoated and TiO_2 coated $La_{0.4}F_3$:$Ce_{0.45}$,$Tb_{0.15}$ particles embedded in PMMA

About 4 ml of monomer methylmethacrylate (MMA) was taken in a glass bottle having dimensions of 15 cm height and 2 cm diaand ultrasonicated for 15 min to get rid of gases if any. Three wt% of HDPA (2-hydroxy-2 methyl propiono phenol) - a polymerization imitator solution was added and ultrasonicated for about 30 minutes [12].About 1 wt % (0.04g) of the powder particle sized 16nm with respect to the monomer was taken and dispersed in 6ml methanol to get fine colloidal solution after ultrasonication for about 30min. Thiscolloidal solution in methanol was added to this monomer solution and the mixture was further ultrasonicated for about 30 min. The mixture was kept inside the gamma chamber for polymerization for about 38h at a dose rate of about 4.78 kGy/h. The polymerized disc(PM1) was then taken out. Similar procedure was adopted to embed TiO_2 coated $La_{0.4}F_3$:$Ce_{0.45}$,$Tb_{0.15}$ nano particle to from a transparent PMMA disc (PM2).

6.3Results and Discussion

6.3.1 XRD

Figure 6.1 illustrates the formation of an humpy region between 10 °- 23 ° angle in curve (a), indicating the presence of amorphous polymer (PMMA) and other orientations are visible but with poor intensity. The poor intensity is due to the less amount (1 wt% ` 0.040g) of nano powder in the matrix. Curve (a) shows the diffraction pattern of the synthesized powder $La_{0.4}F_3$:$Ce_{0.45}$,$Tb_{0.15.}$

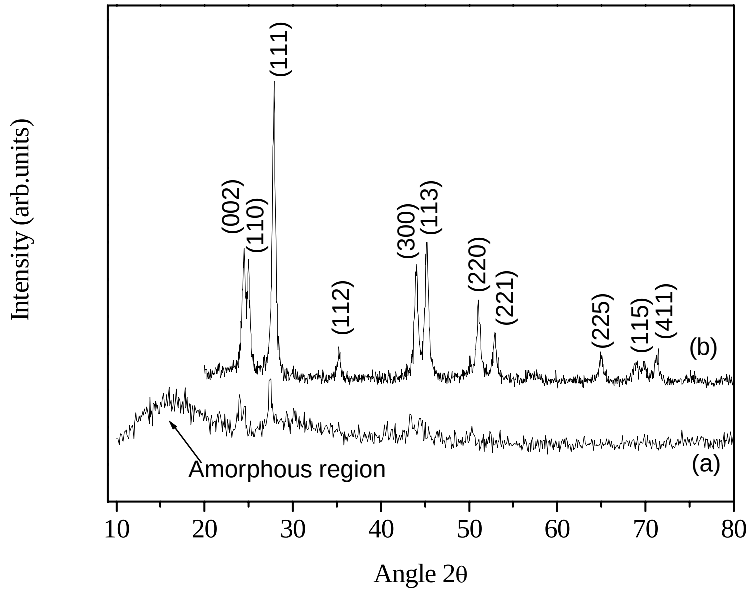

Figure 6.1 XRD of (a) PNC (PAM) nano composite; (b) uncoated $La_{0.4}F_3$:$Ce_{0.45}$,$Tb_{0.15}$

6.3.2 Polyacrylamide based disc appearance and Optical transmission Microscopy

Figures6.2,6.4. 6.6 and 6.8show the digital photographs obtained using Sony digital camera of plain polyacrylamide disc, NG1 and NG2 discs.It is clear from the photographs that transparency comes down with increase in dopant weight %. Moreover the PNC (PAM) disc prepared with uncoated LaF_3:Ce nano particle has the best transparency.

Figures 6.3,6.5 and 6.7 show thesurface of the Plain PAM,NG1and NG2discs at 40X magnification.In figure 6.3, the contrast spots and the lines like appearance might be due to the scratches or driedregions on the surface.The uniform bright region throughout the disc shows the transmitted lightthrough the disc.From 6.5 and 6.7,it is clear that NG2 disc is more transparent than NG1 disc due to higher % loading in NG1. The magnified image shows bright regions which are due to the transmitted light whereas the dark regions are due to the shielding effect of the embedded particles. The particles appear to get agglomerated and also form some irregular shaped network structure leading to non uniform distribution. Moreover, the oleic acid on the LaF_3:Ce surface might also reflect the incident light leading to a dark image.

Figure6.8show a clear smooth disc with bettertransparencyas compared to the earlier discs. It is also evident from themagnifiedmicroscope images figure 6.9(a) at 5X &6.9(b)at 40X . Figure 6.9(a) shows an uniform distribution of white and dark linear regions. Figure 6.9(b) shows some uniform distribution of irregular shaped network structure which is due to the agglomerated particles.The dimension of agglomerated region was in the range of 10-100 μm. This demonstrates the uniform distribution of uncoated particles in a PAM matrix, which was probably possible due to very small sized particles yielded through the acidic synthesis.

The polyacrylamide disc is hydro gel based disc which continuously throws out water and gets dried up. Due to this, some severe white patches are seen over the disc leading to a lesser transparency over time.These PAM discs have to be properly preserved in polythene covers to prevent excess water loss over a period of time.

Figure 6.2 Photographic picture of Plain PAM disc

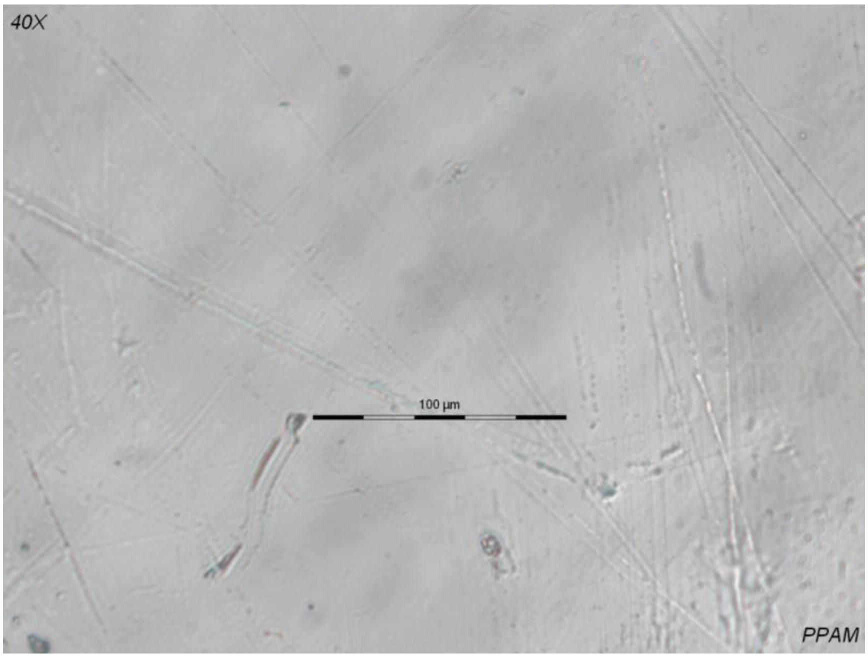

Figure 6.3 Transmission Microscopy image at 40 X magnification of plain PAM

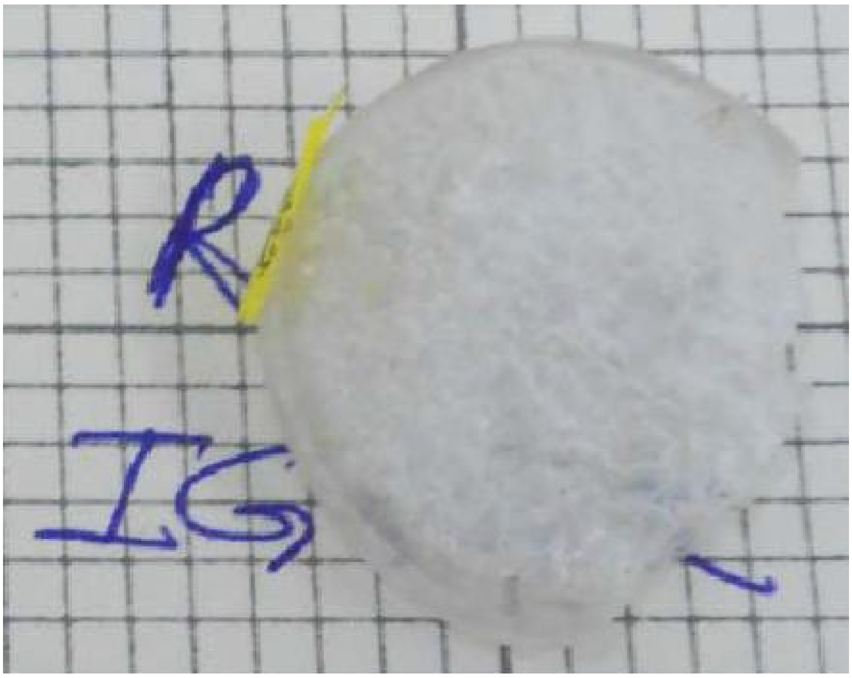

Figure 6.4 Photographic picture of NG1 PNC disc

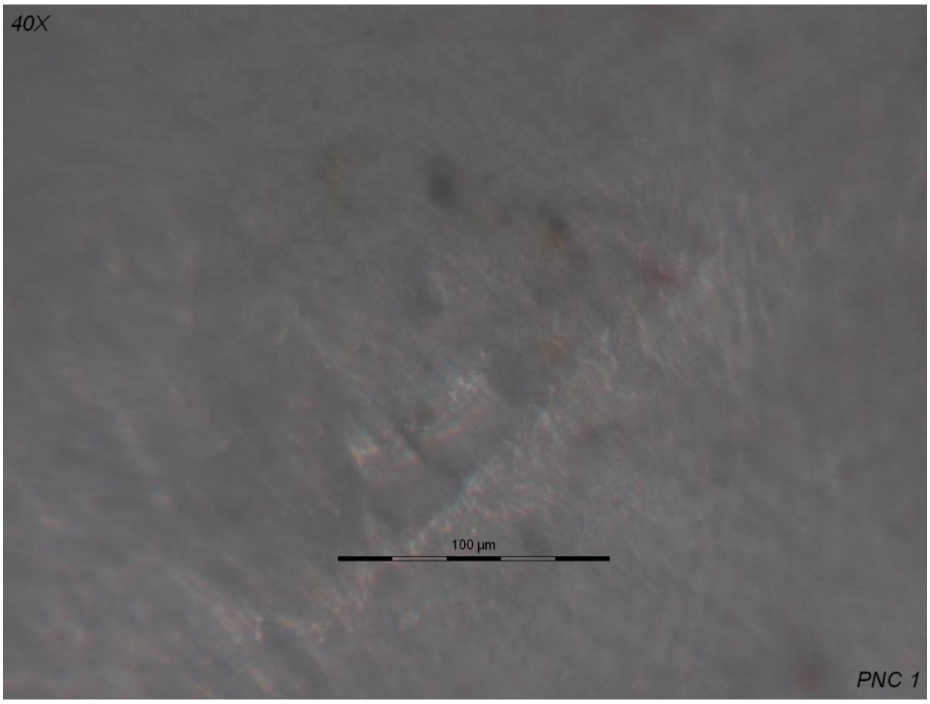

Figure 6.5 Transmission Microscopy image at 40x magnification of PAM disc NG1

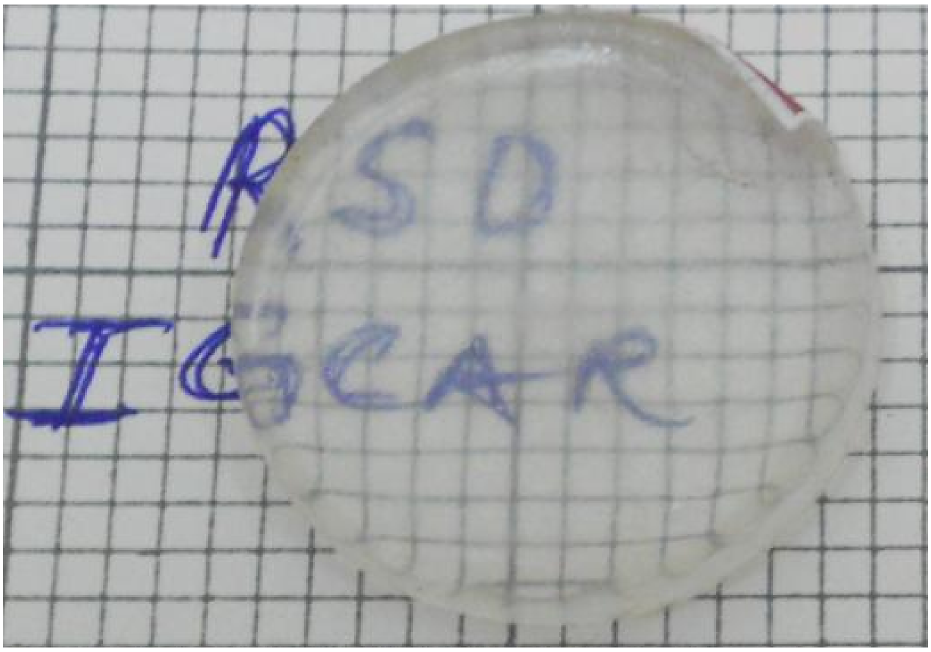

Figure 6.6 Photographic picture of NG2 disc

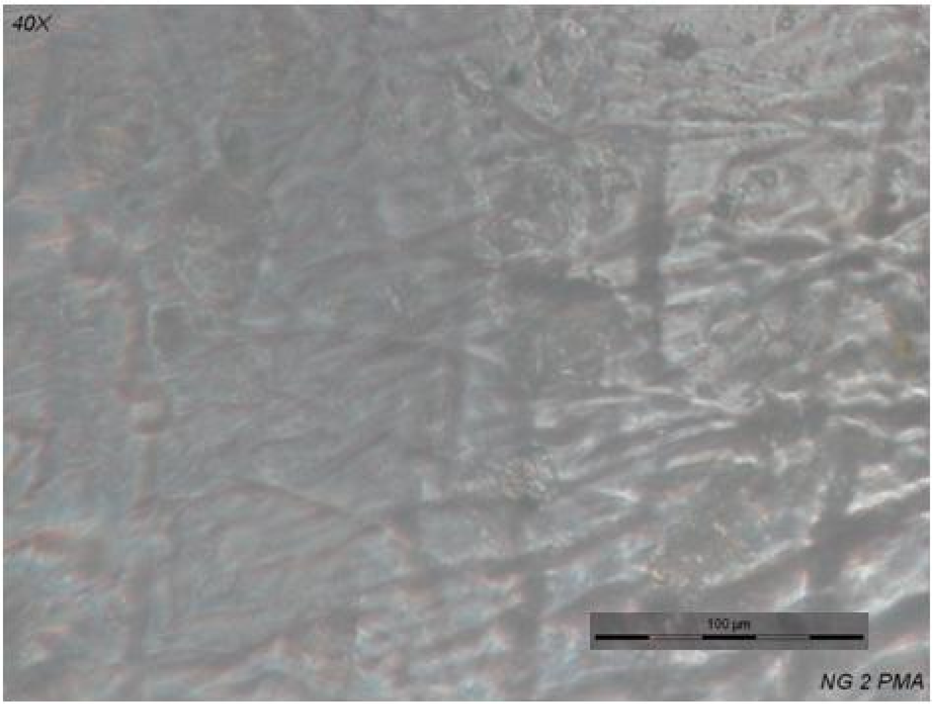

Figure 6.7 Transmission Microscopy image at 40x magnification of NG2

Figure 6.8 Photographic picture of PNC1 pam disc

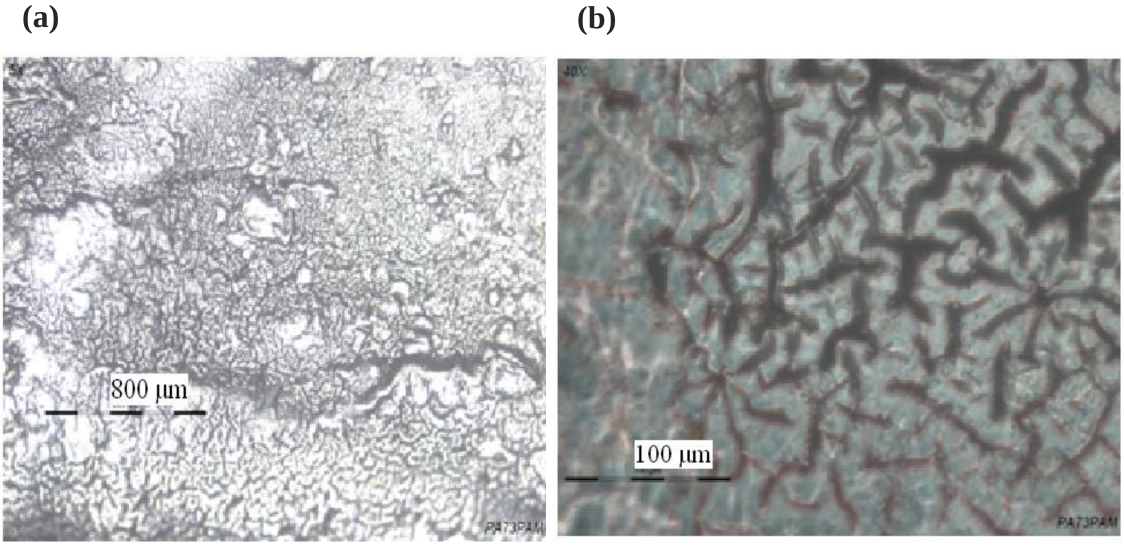

Figure 6.9 Transmission Microscopy image at Uncoated$La_{0.95}F_3$:$Ce_{0.5}$ loaded PNC 1 disc at (a)5X and (b) 40X magnification

6.3.3 Polymethylmethacyrlate based disc appearance and Optical transmission Microscopy

Figures 6.10, 6.12 and 6.14 show the photographs of the plain PMMA, disc,uncoated $La_{0.4}F_3$:$Ce_{0.45}$,$Tb_{0.15}$embedded PMMA disc (PM1) and TiO_2 coated$La_{0.4}F_3$:$Ce_{0.45}$,$Tb_{0.15}$ PMMA disc (PM2) respectively. It is clear that the transparency is bit less in the loaded discs when compared to the empty disc. Figure6.11 shows the photograph of the disc taken under magnification of 40X.Figures 6.13 (a & b) and 6.15 (a & b) show the photographs of the discs taken under magnification of 5X and 40X respectively. The plain PMMA disc has a smooth surface, where as the PM1 surface show linearhair like structures which are due to the particles embedded. The PM2 surface show a circular flower like agglomerated structures which are due to the particles embedded. The uniform distributions of the bright and dark spots indirectly convey that the particle distribution is uniform. The dimension of the dark regions was in the range of <5-20 μm. The PMMA disc has better transparency, hardness and environmental stability. PMMA has a refractive index of 1.54 [15] which is quite near to the refractive index of LaF_3: Ce (1.64).PM1 and PM2 discsappear to possesreasonably uniform distribution with slight aggregatedpatches leading to the hair like structures of fewµm which is consistent with the pictures reported by Ivan Moreno et al., [6].In the case of TiO_2embedding the aggregations are linear hair like structures; this might be due to the effect of surface titania during polymerization.

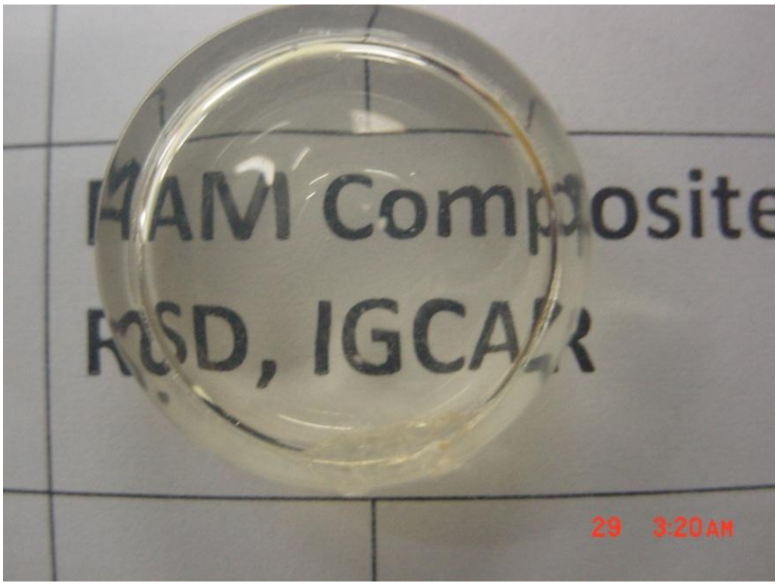

Figure 6.10 Photographic picture of Plain PMMA disc

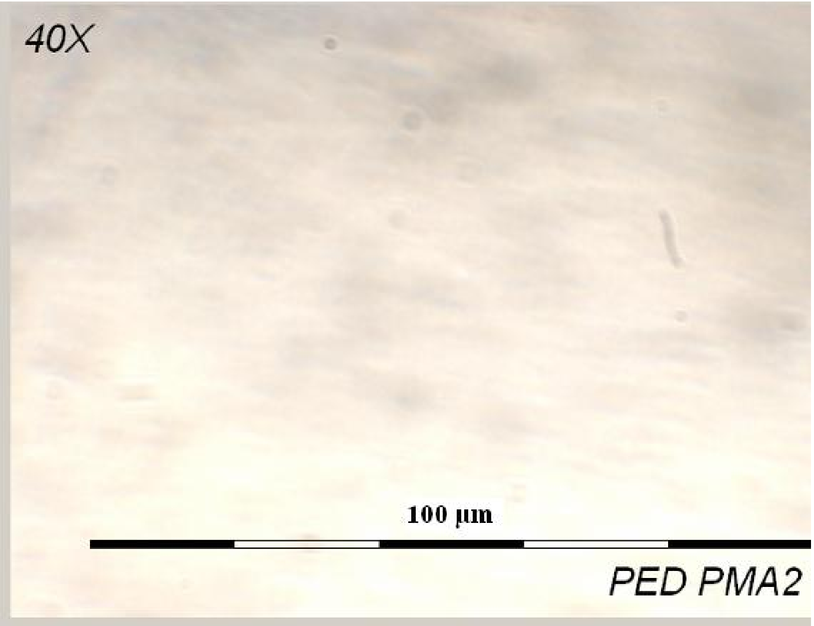

Figure 6.11 TransmissionMicroscopy image at 40x magnification of plain PMMA disc

Figure 6.12 Photograph of the uncoated $La_{0.4}F_3$:$Ce_{0.45}$,$Tb_{0.15}$ loaded PM1disc

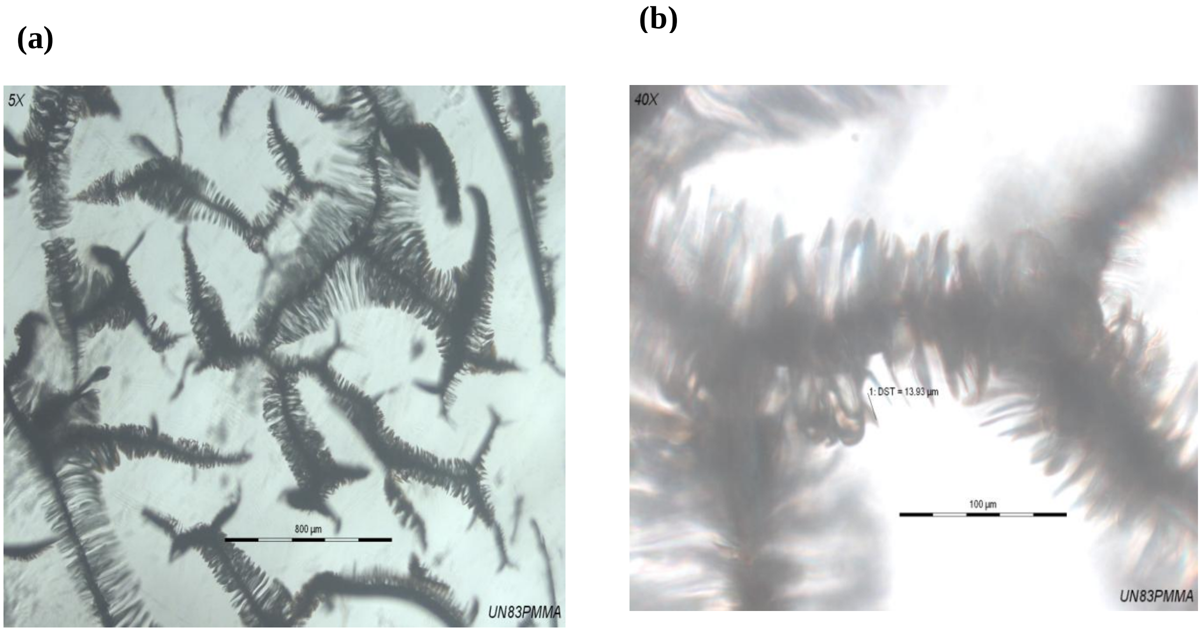

Figure 6.13 Transmission Microscopy image of Uncoated$La_{0.4}F_3$:$Ce_{0.45}$,$Tb_{0.15}$ loaded PM1 nanocomposite at (a)5X and (b) 40X magnification

Figure 6.14 Photograph of the TiO_2 coated $La_{0.4}F_3$:$Ce_{0.45}$,$Tb_{0.15}$ loaded PM2disc

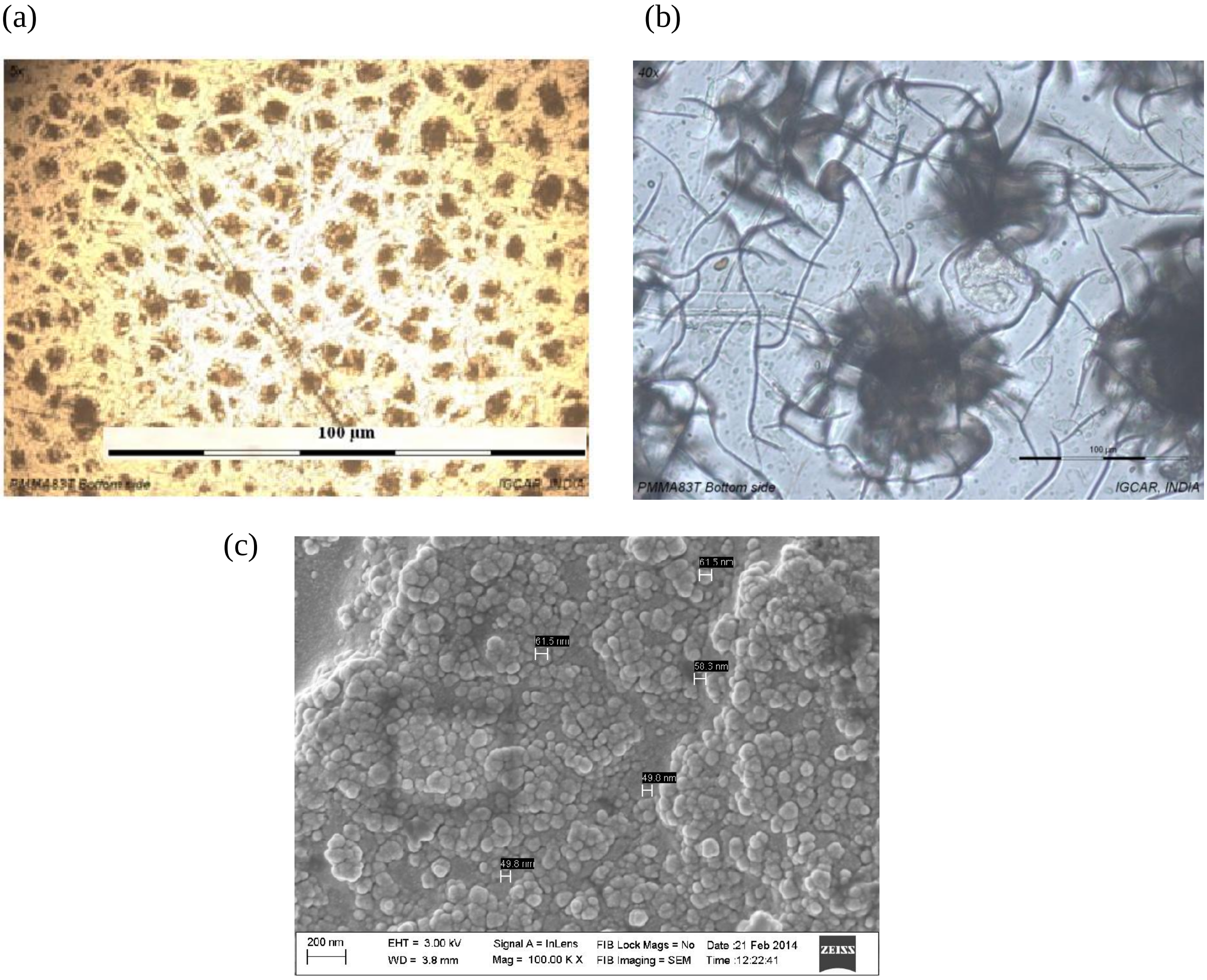

Figure 6.15 Transmission Microscopy image of TiO_2 coated $La_{0.4}F_3$:$Ce_{0.45}$,$Tb_{0.15}$ loaded PM2 nanocomposite at (a)5X and (b) 40X magnification(c)FESEM micrograph of the PM2 disc

6.3.4 FESEM micrograph of PM2 disc

Figure 6.15 (c) shows the FESEM micrograph of the PM2 disc. It is clear from the figure that the particles were spherical in shape with uniform microstructure. The particle sizes were in the range 49-61 nm. However some bigger particles are also present.

6.3.5Photoluminescence spectroscopy

6.3.5.1 PL spectra of Polyacrylamide based PNC disc

Figure 6.16 shows the excitation and emission spectrum of the 0.05 mol Ce-doped LaF_3nanoparticle pellet, where the 306nm emission from the pellet is intense. Figure 6.17 shows the excitation and emission spectra of the blank-PAM, LaF_3:Ceembedded PAM (NG1) and NG2 discs. The spectra of blank-PAM and nanocomposite materials were recorded in the region 220 - 400 nm. Curves a and b respectively correspond to the excitation and emission of blank-PAM disc. The emission peak at 370 nm corresponds to the 253 nm absorption of blank-PAM. Curves c (NG2), e (NG1) belong to the excitation and d (NG2), f (NG1) correspond to the emission spectra of doped-PAM discs. One can see that the emission spectra of the composite exhibit two peaks, one at 308 nm and the other at 370 nm. The spectral positions slightly shift towards the blue region as compared to that of pure LaF_3:Cenano-powder pellet. It is important to point out that the 253 nm excitation of the nanocomposite gives much lower intensity of the 370 nm emission compared to that of blank-PAM. This suggests that doping the PAM matrix by the nanoparticles causes suppression of the photoluminescent emission from the polymer host. The 370 nm PL emission of the host matrix is further suppressed when the doping concentration is increased (curve f). Thus, the present results suggest that only the nano-particles are selectively excited while the host excitation is probably transferred to the nanoparticles. This property may be useful where interference from the host is to be avoided. Lower intensity of the 308 nm emission from the nanocomposite disc NG1 might be due to less wt% doping and larger opacity. This suggests that low-doped NG2 translucent composites can be used as efficient intrinsic PL emission materials with reduced interference from the host.

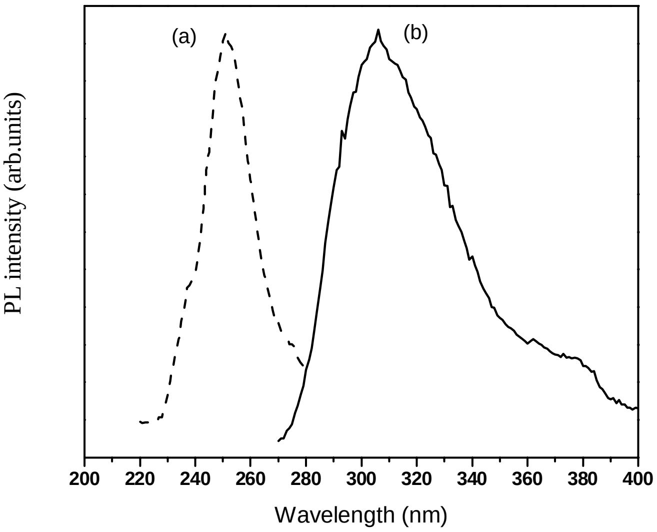

Figure 6.16 PL excitation and emission spectra of oleic acid coated $La_{0.95}F_3$:$Ce_{0.05}$ doped LaF_3 nanoparticle pellets (a) Excitation (λ_{em} = 306 nm); (b) Emission (λ_{ex} = 251 nm).

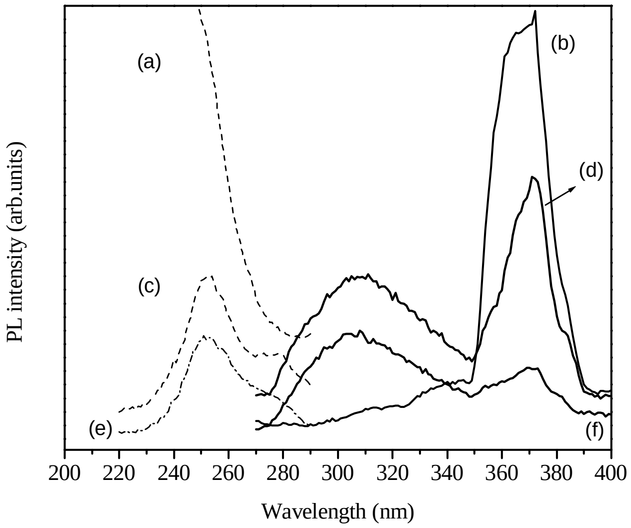

Figure 6.17 Excitation and emission spectra of blank PAM and LaF_3:Ce^{3+} embedded PAM discs. (a) Blank PAM excitation (λ_{em} = 370 nm); (b) Blank PAM emission (λ_{ex} = 253 nm); (c and e) NG2 and NG1 excitation (λ_{em} = 308 nm); (d and f) NG2 and NG1 emission (λ_{ex} = 253 nm) slit width 1.5 nm at high sensitivity

Figure 6.18 shows the PL spectra of the LaF_3:Ce(0.05mol) embedded disc (PNC1) prepared using the as prepared colloidal solution(cs) obtained through the acidic route. The spectrum was obtained at slit width 1.5 nm. Curves (a,b), (c,d)and (e,f) represent the excitation and emission of as prepared colloidal solution, colloidal solution embedded PAM composite and Plain PAM disc respectively. On comparing the PL intensity of the NG1 disc PNC1 disc seems to have better intensity. This might be due to the difference in the particle size as well as without any organic coating.The lesser intensity of PAM composite might also be due to the mismatch in the refractive index of PAM(1.34) and LaF_3(1.6). The emission at 372 nm whose intensity is comparable to the cerium emission at 305nm might be due the host polyarylamide emission. No significant shift in peak was observed.

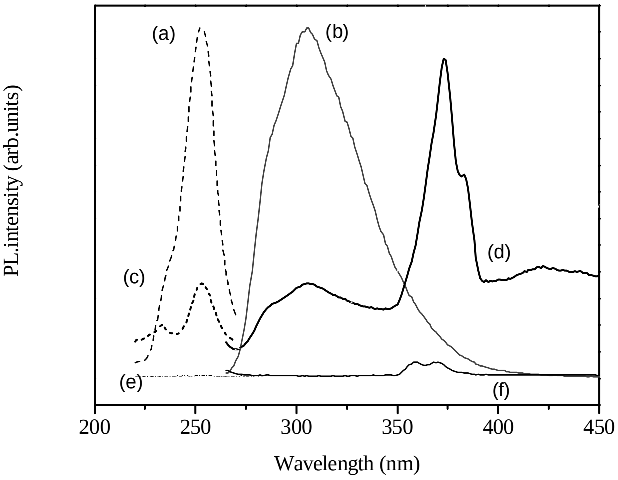

Figure 6.18PL spectra of colloidal solution (a,b),LaF_3:Ce^{3+} embedded PNC1 disc (c,d) and blank PAM (e,f). Excitation Curves (a) =(c) =(e) for (λ_{em} =305nm); Emission curves (b)=(d)=(f) for λ_{ex}=250nm; slit width 1.5 nm at high sensitivity

6.3.5.2 PL spectra of Polymethylmethacrylate based PNC discs

Figure 6.19shows the PL spectra of the cerium emission from the PM1 and PM2 discs. The discs exhibited 305 nm emission when exited with 254nm. In figures 6.18 curves a,c represent excitation and b,d represent emission in respectively. The PM2 discembedded shows a better intensity which might arise due to the (i) TiO_2 shell effect (ii) a more uniform distribution leading to a higher quantum light output (iii) also be due to the suppression of radiationless transfer by the polymer environmentas reported by Kyle Gipson[8]. The 372 nm peak might be due to PMMA host emission like the polyacrylamide composite..

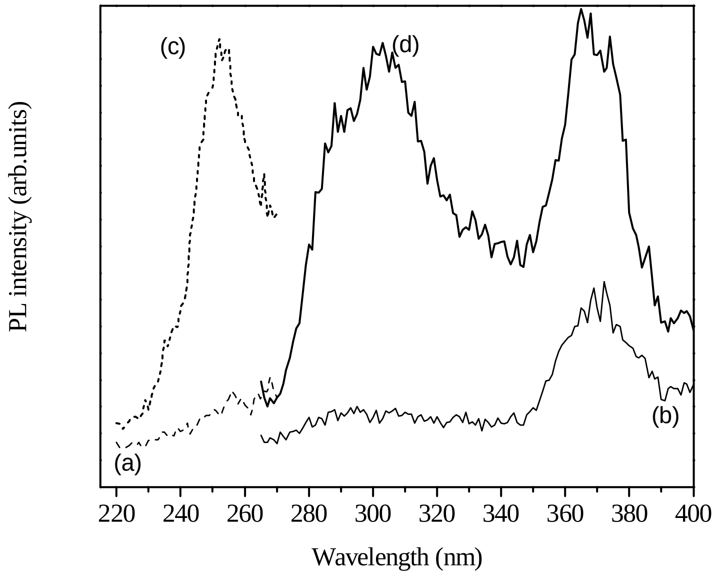

Figure 6.19PL spectra of PM1 disc (containing uncoated particles)&PM2 disc (containing TiO_2 coated particles). Excitation Curves (a)uncoated $La_{0.4}F_3$:$Ce_{0.45}$,$Tb_{0.15}$and (c)TiO_2 coated ($La_{0.4}F_3$:$Ce_{0.45}$,$Tb_{0.15}$) λ_{em} =305nm; Emission curves (b) uncoated $La_{0.4}F_3$:$Ce_{0.45}$,$Tb_{0.15}$=(d) TiO_2 coated ($La_{0.4}F_3$:$Ce_{0.45}$,$Tb_{0.15}$) λ_{ex}=254nm; slit width 1.5 nm at high sensitivity

Figure 6.20 shows the PL spectra of the STE emission due to cerium from the PM1 and PM2 discs. The discs exhibited 450 nmemissions when exited with 380nm. In figures 6.19 curves a,c represent excitation and b,d represent emission respectively. The spectra were similar to that observed(Figure 3.41, Chapter 3) with the powder sample but with moderately higher intensity.

Figure 6.21 shows the PL spectra of the Terbium emission from the PM1 and PM2 discs. The discs exhibited 543 nm emission when exited with 249nm. In figures

6.21curves a,c represent excitation for (λ_{em} =543) nm and b,d represent emission at (λ_{exi} =249 nm) in respectively. The spectra were similar to that observed (Figure 4.13, chapter 4)with the powder sample but with moderately higher intensity than the curve (d).

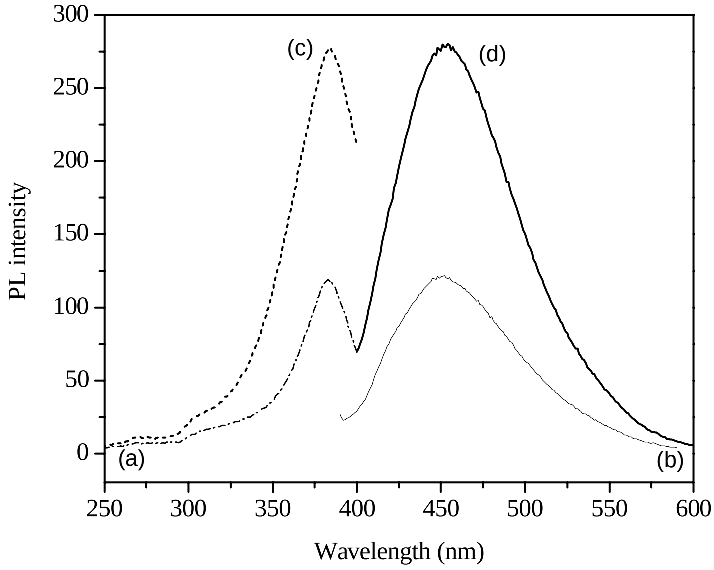

Figure 6.20PL spectra of PM1 & PM2 disc.Excitation curves (a) uncoated $La_{0.4}F_3$:$Ce_{0.45}$,$Tb_{0.15}$and (c)TiO_2 coated ($La_{0.4}F_3$:$Ce_{0.45}$,$Tb_{0.15}$) λ_{em} =450 nm Emissioncurves (b) uncoated $La_{0.4}F_3$:$Ce_{0.45}$,$Tb_{0.15}$and (d)TiO_2 coated $La_{0.4}F_3$:$Ce_{0.45}$,$Tb_{0.15}$$\lambda_{ex}$=380nm; slit width 1.5 nm at high sensitivity

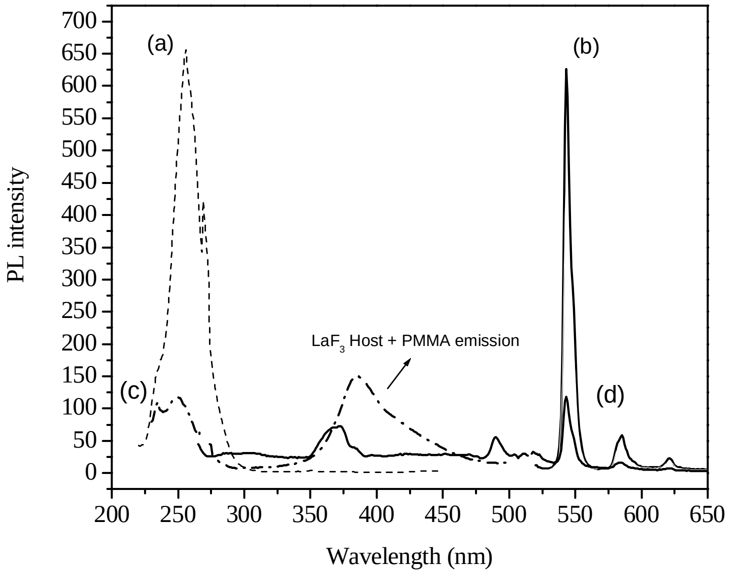

Figure 6.21PL spectra of PM1&PM2 disc. Excitationcurves (a)TiO_2 coated

($La_{0.4}F_3$:$Ce_{0.45}$,$Tb_{0.15}$) and (c) uncoated $La_{0.4}F_3$:$Ce_{0.45}$,$Tb_{0.15}$$\lambda_{em}$=543 nm / Emission curve (b) TiO_2 coated $La_{0.4}F_3$:$Ce_{0.45}$,$Tb_{0.15}$and (d) uncoated $La_{0.4}F_3$:$Ce_{0.45}$,$Tb_{0.15}$$\lambda_{ex}$=249nm

6.3.6Scintillation of PMMA composite under X-ray excitation

Radiolunmiscence experiment was carried out within the X-ray chamber. The PMMA composite containing TiO_2 coated powder was kept at a distance of 7cm from the X-ray tube.The X-ray machine was operated at 110kV and 10mA current.The light from the sample was collected using the fiber optic probe connected to the spectrometer (Avantes) the radioluminescence intensity is displayed in the LapTop computer connected. Figure6.22 shows the radioluminescence from the TiO_2 coated powder embedded in PMMA composite. The other emission lines are due to the stray background light.

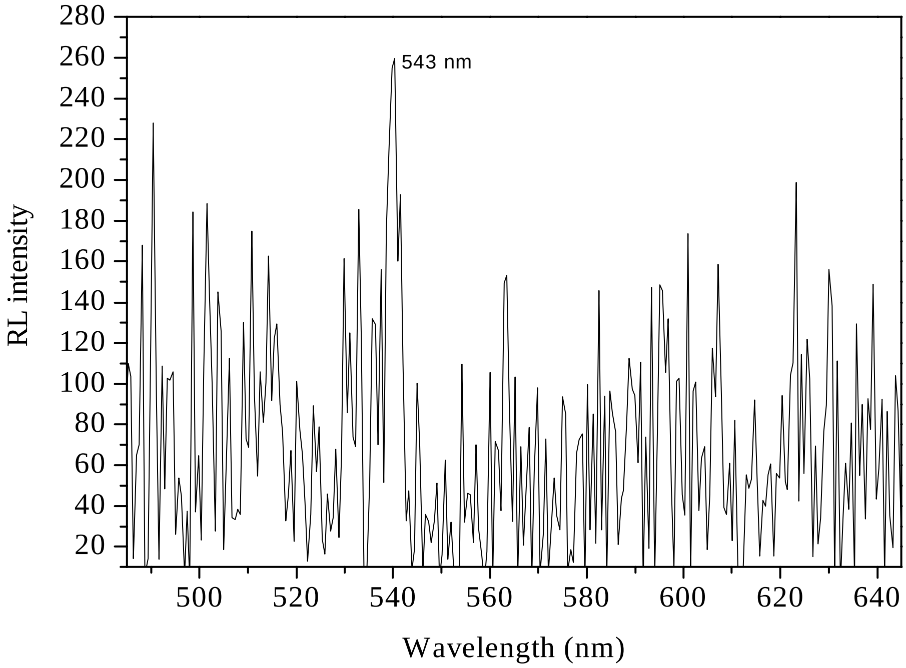

Figure 6.22 Radioluminescencespectra from the TiO_2 coated powder embedded in PM2 disc

6.4 Conclusion

LaF_3:Ce embedded in polyacrylamide discs were synthesized for both the Oleic acid coated powder and as prepared uncoated colloidal solution by a simple radiation assisted polymerization method. The photoluminescent study confirmed the presence of the nano-phosphor in the organic matrix. Although LaF_3:Ce nanoparticles and PAM exhibit characteristic PL emission at 308 and 370 nm respectively, both these materials have excitation peaks at 253 nm. The nanocomposite is found to have reduced emission from the host matrix as compared to pure PAM disc, suggesting selective excitation of the nanoparticles and suppression of the PL from the matrix. Out of the three polyacrylamide discs discussed, uncoated particles synthesized in the acidic environment leads to a better transparencyand PLintensity. Nano sized uncoated and TiO_2 coated $La_{0.4}F_3:Ce_{0.45},Tb_{0.15}$particles were embedded in PMMA matrices using the colloidal route. The colloidal route using the powder synthesized through the acidic route leads to better uniform distribution of the particles in the polymer disc. The PM2 disc shows a better PLintensity and uniform distribution of particles embedded.Scintillation (Tb^{3+} emission) from the PM2 disc was observed at 543nm under X-ray excitation.

References

[1] A.Klausch, H.Althues, C.Schrage, P.Simon, A.Szatkowski, M.Bredol, D.Adame, S.Kaskel, J. Lumin., 130 (2010) 692.

[2] V.Kalima, I.Vartiainen, T.Saastamoinen, M.Suvanto, M.Kuittinen and T.T.Pakkanen, Opt. Mater.,31(2009) 1540.

[3] Y.Chen, X.Ji, Q.Sun, S.Jiang and B.Jiang, J. Non-Crystalline Solids,311(2002)314.

[4] N. Preda, l. Mihut, I. Baltog, T. Velula, V. Teodorescu, J. Optoelectron. Adv. Mater., 8 (2006) 909.

[5] L. Zhang, F. Li, Y. Chen, X. Wang, J.Lumin., 131 (2011) 1701.

[6] I. Moreno,N. Navascues, M. Arruebo, S. Irusta,J. Santamaria, Nanotechnology, 24 (2013) 275603.

[7] H. Jiu, L. Zhang, G. Liu, T. Fan, J. Lumin., 129 (2009) 317.

[8] K. Gipson, B. Ellerbrock, K. Stevens, P. Brown, J. Ballato, J. Nanotechnology, (2011) 2011 Article ID 386503, 8 pages .

[9] R.E. Del Sesto, E.A. McKigney, D.W. Cooke, R.E. Muenchausen, K.C. Ott, R.D. Gilbertson,T.M. McCleskey, M. Bacrania, L.G. Jacobsohn, A.K. Burrell1, B.L. Bennett, S.C. Sitarz3, J.F. Smith,http://www.lanl.gov/orgs/mpa/LALP-07-030/Spring 2007

[10] P. Guss, R. Guise, D. Yuan, S. Mukhopadhyay, R.O'Brien, J. Appl. Phys., 113 (2013) 064303.

[11]] Lin Zhang, FanLi. YiwangChen, XiaofengWang, J. Lumin. 131 (2011) 1701–1706

[12] R.APyles,Bethel Park, R.C. Hedden, D.M.Lentz ,US Patent 0077038 AI, March-2012.

[13] J. Franklin, Z.Y. Wang , Chinese J. Polymer Science V 21, 5 (200) 533.

[14] B. Kulyka, V. Kapustianyka, V. Tsybulskyya, O. Krupkab, B. Sahraouic ,Shevchenko National University, 60 Volodymyrska Str., Kyiv, Ukraine c Institute of sciences

[15] http://microchem.com/pdf/PMMA_Data_Sheet.pdf

Chapter 7

Summary and Future Scope

7.1 Summary

Nano sized Lanthanum Fluoride doped with cerium has been successfully synthesized by adopting co-precipitation technique through four different synthesis routes: with Oleic acid coating, with Oleic acid plus PEG coating and uncoated $LaF_3:Ce^{3+}$ using conc.HCL and HF. The samples synthesized through all the routes were nano crystalline in nature. XRD pattern of OA and OA- PEG coated samples exhibited a high background effect due to the presence of organic material at the surface. XRD pattern of uncoated sample indicated that samples were in high crystalline nature. Uncoated samples were synthesized by varying cerium concentration (0.01, 03, 05, 0.1, 0.2 and 0.45 mol) at pH=4.6. Even with 45 mol% of Cerium in the LaF_3 lattice, no signigicant changes in the lattice parameters could be observed. These samples displayed high intensity fluorescence emissions at 305 and 453 nm when exited at 250 and 380 nm respectively. In the $La_{0.55}F_3:Ce_{0.45}^{3+}$ sample there was a red shift in the PL spectra. In one of the samples (5 mol%), the elemental presence of Lanthanum (95%) and Cerium (05%) were confirmed through the XRF experiment. FESEM results showed that OA coated particles appeared to be flattened and not of spherical size and also were of irregular shapes. The size of the particles was ranging between 12 and 790 nm. Agglomeration of particles was clearly evident. SEM micrograph shows that OA - PEG coated particles were of spherical or slightly oblonged in shape with the diameter ranging between 8 and 36 nm. However, some agglomeration of particles leading to bigger sized particles was also observed. The modified approach with the combination of OA and PEG yielded particles of smaller size compared to Oleic acid alone. SEM micrographs of uncoated particles appeared spherical with uniform microstructure. The image indicated absence of any bigger agglomerates.

The particle size of samples, (through DLS) prepared through different synthesis routes were observed to be in the range of 6-800 nm in the case of OA coated, 6-90 nm with OA-PEG combination, 6-30 nm obtained with pH 4.2 and 190-480 nm with HF method. The size distribution was a bit narrower in the case of OA+PEG combination. The FESEM as well as the DLS measurement indicated that agglomeration was the minimum with OA plus PEG coated and the uncoated LaF_3:Ce particles. A novel method of synthesis in acidic environment was successful in yielding small particles with narrow size distribution and high light output. The particle size decreases as the pH decreases (acidic). FTIR measurements of the samples with organic surfactants showed the presence of COO- (OA) and C-O-C (carboxyl) stretching coordinated through carboxylate group with $LaF_3:Ce^{3+}$ nano particle. The OA and OA- PEG coated samples showed weak absorption at 208, 225 and 250 nm. The feeble absorption might be due to the scattering of the light at OA as well as OA - PEG cover. Uncoated samples showed five distinct, clearly resolved absorption peaks at wavelengths 198, 205, 218, 234 and 247 nm. In one of the preparations, the particle size was so small that a slight shift of the UV-Vis absorption was seen. The result of the UV-Vis absorption follow up study (to know the settling rate) indicated that uncoated and OA coated LaF_3:Ce particles appear to have better suspendabilty in DM water.

The PL spectra of Oleic acid coated LaF_3:Ce samples displayed the 311 nm emission when exited at 251 nm wavelength. The PL spectra of OA plus PEG coated samples displayed emissions at 288 and 307 nm when exited at 250 nm. The excitation spectra for 307 nm wavelength emission consisted of two peaks one at 235 and the other at 250 nm wavelength. It was also evident that the photoluminescence intensity decreased with the increase in the cerium concentration. The decrease in PL intensity might be due to concentration quenching phenomenon. In the case of uncoated $LaF_3:Ce^{3+}$ samples displayed an emission at 310 nm emission when exited at 258 nm wavelength. A red shift in the emission was observed as the Cerium % was increased. It is also observed that, the magnitude of the shift also increased with the extent of doping. The PL intensity from the uncoated samples was very high. The PL output of uncoated was the best, when compared to OA and OA-PEG coated. The photoluminescence intensity of Oleic acid coated was higher when compared to that of the OA+PEG coated particles. Though OA+ PEG combination yielded very small particles with narrow size distribution, the PL output was very less which is due to the surface groups aiding the radiation less transfer as well as prevent the UV light from reaching the Ce^{3+}.

It is reestablished that the particle size has a direct effect on the PL intensity as the smaller is the size, more is the luminescence. However, the uncoated samples compared to Oleic acid or Oleic acid plus PEG coated samples, yielded comparitively smaller particles exhibiting higher PL intensity. The STE emission intensity also increases with decrease in the particle size though no significant change in the PL life time was observed.

In this host, the energy transfer between the Ce^{3+} and Tb^{3+} was observed with a significant overlap between the emission spectrum of Ce^{3+} and the excitation spectrum of Tb^{3+}. $LaF_3:Ce^{3+}$ showed emission at 305 nm when exited with 250 nm wavelength. $La_{0.4}F_3:Ce_{0.45},Tb_{0.15}$ showed emission at 305, 490,543,585 and 615 nm when exited with 268 nm wavelength indicates energy transfer from cerium to terbium. However, no energy transfer between Ce^{3+} and Eu^{3+} could be observed in this host. The potential application of nano sized phosphors embedded in transparent polymer composite for X-ray radiation detection is demonstrated.

For the first time, TiO_2 coated $La_{0.4}F_3:Ce_{0.45},Tb_{0.15}$ is synthesized an its PL characteristics are reported. TEM images confirm the core-shell formation and good crystallinity of the nanocrystals. EDS (Energy Dispersion Spectroscopy) confirms the elemental composition. FTIR measurements of TiO_2 coated $La_{0.4}F_3$:$Ce_{0.45}$,$Tb_{0.15}$ also indicated the presence of TiO_2 Scintillation under X-ray excitation was observed with uncoated and TiO_2 coated powder products. A significant increase in the 543 nm emission intensity and its corresponding excitation at 283 nm of the TiO_2 coated was observed. As coating thickness increases to 4-6 nm, the PL intensity was about 1.76 times increased in the 543 nm emission compared with that of the uncoated. The enhancement in the spectral intensity might be due to the prevention of the radiation less transfer via surface effects by the TiO_2. A decrease in Ce^{3+} as well as Tb^{3+}excitation and emission was observed in the uncoated and the TiO_2 coated La $_{0.55}F_3$:Ce $_{0.45}$ and La $_{0.85}F_3$: Tb $_{0.15}$ samples where the coating thickness was 2-4 nm. It is evident that the 325 and 563 nm emissions of the uncoated is higher than the coated, which might be due to prevention of the excitation UV photons from reaching the Ce^{3+} centers. It was observed that there was about 2.2 times decrease in the 325 nm emission from the TiO_2 coated sample. The PL intensity is very less which might due to the coating obstructing the reach of exiting photons. TiO_2 coated samples decays marginally slower than the uncoated; the result is in consistence with Tb^{3+} lifetime.

It is demonstrated that there is a possibility of introducing short tunability by changing the stoichiometry. XRD results clearly reveal that variation in concentration of either lanthanum or fluoride does not change the crystal structure. Nano phosphor prepared from exact stoichiometry LaF_3 (1:3) ratio possess the average crystallite size of 22 nm whereas the size of lanthanum and fluoride deficient samples ranged from 20 nm to 45 nm. Very small size is attained when the fluoride concentration was the least. This shows that the particle size has direct dependence on the cation / anion charges present in the precursor solution in this synthesis method. In both the cases, though there was better crystallnity there was a decrease in PL intensity and slight changes in the peak excitation and emissions at 0.8 mol% arising out of crystal field perturbations. The study indicates towards a possibility of introducing tunability by changing the stoichiometry.

Even after gamma radiation exposure using Cobalt-60 gamma rays upto a dose of 6.1kGy, the PL profile remained unchanged demonstrating the radiation stability of $LaF_3:Ce^{3+}$. During gamma irradiation, a breach in the Oleic acid coating was observed in the OA coated material. After gamma irradiation OA coated particles shapes and appearance changed to an irregular and with clearly distinct edges, which might be due to the damage of the Oleic acid on surface of the particle by gamma photons. After gamma irradiation, the uncoated particles appear to be in spherical shape but with a bigger size and closely packed. The UV absorption as well as the PL intensity decreased with increase in the gamma dose. The TL trap depth calculated for the main peak at 409 ° K using Chen's equation is 0.55 eV. The results are highly promising towards using these crystals for radiation dosimetry.

LaF_3:Ce embedded in polyacrylamide discs were synthesized using oleic acid coated powder and as prepared uncoated colloidal solution by a simple radiation assisted polymerization method. Although LaF_3:Ce nanoparticles and PAM exhibit characteristic PL emission at 308 and 370 nm respectively, both these materials have excitation peaks at 253 nm. Out of three polyacrylamide discs discussed, uncoated particles synthesized in acidic environment leads to a better transparency and PL intensity. Nano sized uncoated and TiO_2 coated $La_{0.4}F_3:Ce_{0.45},Tb_{0.15}$ were embedded in PMMA matrices using the colloidal route. The colloidal route using powder synthesized through acidic route leads to a uniform distribution of particles in the sample. The PM2 disc shows a better intensity and uniform distribution as well as light output. Moreover PMMA disc is thermally, mechanically and environmentally more stable than hydrogel based composites. Scintillation (Tb^{3+} ems.) from PM2 disc was observed at 543 nm under X-ray excitation.

7.2 Future Scope

Further studies are currently underway to investigate scintillation properties of LaF_3:Ce nanocrystals under γ and X-rays. Moreover, attempts will be made to improve the scintillation and study of the PNC materials under neutron irradiation. Prior to these studies, a full fledged electronic system should be designed to capture the scintillation emission and convert to an electronic signal for further process and display the conventional count rate. Preliminary Liquid scintillation studies with tritiated (H^3) water have been carried out and the results indicate that the colloidal solution of $La_{0.4}F_3$:$Ce_{0.45}$,$Tb_{0.15}$ scintillates and will be further investigated. Scintillation of the nano sized $La_{0.4}F_3$:$Ce_{0.45}$,$Tb_{0.15}$ under the hard beta irradiation will also be carried out. .In order to increase the light output further, a new material capping will also be attempted. The PNC material doping % will also be varied without affecting the transparency significantly will also be studied. PL as well as radiolimniscence studies will be carried out in the same LaF_3 matrix but with other suitable dopants. The TL behavior also will be investigated at lower as well as higher doses.

Functionalised LaF_3 with suitable dopants may be used as bio dosimetric labels. In the case of nuclear establishments where high radiation exposure accidents caused by natural disaster, terrorism or war, precise dose estimation is the important requirement for saving the victim as the, body-worn dosimetry equipment such as film badge is not useful beyond a certain dose .Moreover public personnel don't put on these dose measuring devices on their body. Biological dosimetry (biodosimetry) is a suitable way for this purpose and cytological biodosimetry methodology is most popular and has been used for long time. Nano luminescent materials attached to the di-centrics or any other radiation induced chromosome aberrations glow under UV lamp facilitating easy and fast scoring applied for the high dose emergency radiation exposures.

Publications

Journal Publications

1. **T.K. Srinivasan**, B. Venkatraman, D.Ponraju and A.K.Arora, “Photo luminescent characteristics of oleic acid coated LaF_3:Ce embedded in Polyarylamide”, **World Journal of Nano Science and Engineering. 2 (2012) 201.**

2. **T.K. Srinivasan**, B.S. Panigrahi, A.K. Arora, B. Venkatraman and D.Ponraju, “Gamma irradiation effect on Photoluminescence from functionalized LaF_3:Ce nanoparticles”, Radiation Physics and Chemistry 99 (2014) 92–96

3. **T.K. Srinivasan**, B.S. Panigrahi, N. Suryamurthy and B.Venkatraman, “Enhanced green emitting $La_{0.4}F_3$:$Ce_{0.45}$,$Tb_{0.15}$ /TiO_2 -core/shell structure”, Accepted in J.Rare Earths in May 18th -2014

2. **T.K. Srinivasan**, B.S. Panigrahi, and B. Venkatraman, “Novel synthesis and characterization of nano sized LaF_3 :Ce^{3+} and its polymer nanocomposites”, (Manuscript ready for submission)

3. **T.K. Srinivasan,** B.S. Panigrahi, N. Surya Murthy, and B. Venkatraman , “ Effect of non-stoichiometry on the photo luminescent of LaF_3:Ce” (Manuscript ready for submission).

4. **T.K. Srinivasan**, B.S. Panigrahi and B. Venkatraman, “Synthesis and characterization of LaF_3:Ce using Lanthanum carbonate” (Manuscript ready for submission).

International/National Conferences

1. **T.K. Srinivasan**, D. Ponraju, B. Venkatraman and A.K. Arora, “Effect of gamma irradiation on Oleic acid coated LaF_3: Ce on nano phosphor” National Symposium on

Radiation Physics and Nanomaterials (NSRPN), p 187, (2011) at Patiala, Punjab, INDIA.

2. **T.K. Srinivasan**, D. Ponraju, M. Kamarudin, B. Venkatraman and A.K. Arora, “Synthesis and characterization of surface modified LaF_3:Cenano particles, IEEE Xplore digital library; International Conference on Nanoscience Engineering and technology (ICONSET), p 528, (2012) Chennai, TN, INDIA.
3. **T.K. Srinivasan**, M.T. Jose, B. Venkatraman and A.K. Arora, ”Luminescence characteristics of Oleic acid coated LaF_3:Ce,Tb” at 4th Interdisciplinary Chemistry and Materials Science” (ISMC) p300, (2012) at BARC, Mumbai Maharashtra, INDIA
4. **T.K. Srinivasan**, M.T. Jose, B. Venkatraman and A.K. Arora, “Luminescence properties of nano sized LaF_3:Ce,” National Symposium of Radiation Physics (NSRP19) proceedings p 285, (2012) at IGCAR, Kalpakkam, TN, INDIA.
5. **T.K. Srinivasan**, B.S. Panigrahi and B. Venkatraman “Optical Properties of LaF_3:Ce and LaF_3:Ce,Tb embedded PMMA composite” Recent trends in Material chemistry (RMTC) p 101, (2013) at VIT Vellore., TN, INDIA.